North Carolina Department of Transportation Project No. 2008-13

Final Report

Field Verification of Undercut Criteria and Alternatives for Subgrade Stabilization – Coastal Plain

by
Timothy D. Cowell, E.I
Sang Chul Pyo
M. A. Gabr, Ph.D., P.E.
Roy H. Borden, Ph.D., P.E.

Department of Civil, Construction, and Environmental Engineering
North Carolina State University

In Cooperation with
The North Carolina Department of Transportation

Raleigh, North Carolina
June 2012

1. Report No. **FHWA/NC/2008-13**	2. Government Accession No.	3. Recipient's Catalog No.
4. Title and Subtitle Field Verification of Undercut Criteria and Alternatives for Subgrade Stabilization – Coastal Plain		5. Report Date June 2012 6. Performing Organization Code
7. Author(s) Timothy D. Cowell, E.I. Sang Chul Pyo Mohammed A. Gabr, Ph.D, P.E. Roy H. Borden, Ph.D, P.E.		8. Performing Organization Report No.
9. Performing Organization Name and Address Department of Civil, Construction, and Environmental Engineering North Carolina State University Campus Box 7908 Raleigh, NC 27695		10. Work Unit No. (TRAIS) 11. Contract or Grant No.
12. Sponsoring Agency Name and Address North Carolina Department of Transportation Research and Analysis Group Raney Building, 104 Fayetteville Street Raleigh, North Carolina 27601		13. Type of Report and Period Covered Final Report August 2010 – June 2012 14. Sponsoring Agency Code 2008-13
Supplementary Notes:		

16. Abstract

The North Carolina Department of Transportation (NCDOT) is progressing toward developing quantitative and systematic criteria that address the implementation of undercutting as a subgrade stabilization measure. As part of this effort, a laboratory study and numerical analysis were performed from 2008 to 2010 with the results providing proposed criteria for undercutting under various roadway site conditions and the adequacy of stabilization measures typically employed if undercut was deemed necessary. These criteria provide provisions for discerning possible rutting and pumping of the subgrade under construction loading, and provide response and subgrade stiffness under repeated loading of 10,000 cycles. The work in this report is focused on performing full-scale testing in the field on instrumented unpaved roadway sections to collect data for the validation of guidelines developed from the laboratory and modeling study. Four 16 feet wide by 50 feet long stabilized test sections were built on poor subgrade soils encountered in the Coastal Plain region of North Carolina. One test section encompassed undercutting and replacement with select material (Class II), the second and third test sections included reinforcement using a geogrid and geotextile, respectively, in conjunction with undercutting and replacement with ABC (Class IV), and a fourth test section included cement treatment of the soft subgrade soil. Full-scale testing was conducted on the test pad by applying 1000 consecutive truck passes using a fully loaded tandem-axle dump truck over a period of four days. During this time visual observations were noted and measurements were collected regarding rut depth, vertical stress increase at the base/subgrade interface, and subgrade moisture content with truck passes. Once trafficking was completed, the test pad was re-graded and proof roll testing was performed to look for signs of pumping and rutting. Based on the field results, the proposed undercut criteria are evaluated in regards to the ability to discern the need for undercutting as well as predict the performance of the stabilized test sections. Finally, a performance cost analysis is conducted to illustrate the relative cost of each stabilization measure in relation to the measured performance (rutting) such that an informed decision on cost-effective subgrade stabilization can be made.

17. Key Words *Full-scale testing, undercut, geosynthetics, cement stabilization, earth pressure cells, LiDAR, performance cost*	18. Distribution Statement		
19. Security Classif. (of this report) Unclassified	20. Security Classif. (of this page) Unclassified	21. No. of Pages 229	22. Price

Form DOT F 1700.7 (8-72) Reproduction of completed page authorized

DISCLAIMER

The contents of this report reflect the views of the authors, who are responsible for the fact and accuracy of the data presented herein. The contents do not necessarily reflect the official views or policies of the North Carolina Department of Transportation. This report does not constitute a standard, specification or regulation.

ACKNOWLEDGEMENTS

The authors would like to thank the members of the NCDOT Geotechnical, Materials, and Construction divisions who worked on this project. The time, expertise and guidance of NCDOT engineers were invaluable to this project. Special thanks are due to the members of the steering committee:

Njoroge W. Wainaina, P.E.
Medhi Haeri
Kyung J. Kim, Ph.D, P.E.
Chris Kreider, P.E.
John L. Pilipchuk, P.E., L.G.
Mrinmay Biswas, Ph.D., P.E.
Dean Hardister, P.E.
Chun Kun Su
Ernest Morrison, P.E.

TABLE OF CONTENTS

LIST OF FIGURES

LIST OF TABLES

EXECUTIVE SUMMARY

The North Carolina Department of Transportation (NCDOT) is progressing toward developing quantitative and systematic criteria that address the implementation of undercutting as a subgrade stabilization measure. As part of this effort, a laboratory study and numerical analysis were performed from 2008 to 2010 with the results providing proposed criteria for undercutting under various roadway site conditions and the adequacy of stabilization measures typically employed if undercut was deemed necessary. These criteria provide provisions for discerning possible rutting and pumping of the subgrade under construction loading, and provide response and subgrade stiffness under repeated loading of 10,000 cycles. The work in this report is focused on performing full-scale testing in the field on instrumented unpaved roadway sections to collect data for the validation of guidelines developed from the laboratory and modeling study.

Four 16 feet wide by 50 feet long stabilized test sections were built on poor subgrade soils encountered in the Coastal Plain region of North Carolina. One test section encompassed undercutting and replacement with select material (Class II), the second and third test sections included reinforcement using a geogrid and geotextile, respectively, in conjunction with undercutting and replacement with ABC (Class IV), and a fourth test section included cement treatment of the soft subgrade soil. Dynamic cone penetrometer (DCP), soil stiffness gauge (SSG), and falling weight deflectometer (FWD) tests were performed on the test pad at various stages of the project to obtain strength and stiffness data in situ for both the subgrade and base layer materials. Full-scale testing was conducted on the test pad by applying 1000 consecutive truck passes using a fully loaded tandem-axle dump truck over a period of four days. During this time visual observations were noted and measurements were collected regarding rut depth, vertical stress increase at the base/subgrade interface, and subgrade moisture content with truck passes. Once trafficking was completed, the test pad was re-graded and proof roll testing was performed to look for signs of pumping and rutting.

Based on the field results, the proposed undercut criteria are evaluated in regards to the ability to discern the need for undercutting as well as predict the performance of the stabilized test sections. Finally, a performance cost analysis is conducted to illustrate the relative cost of each stabilization measure in relation to the measured performance (rutting) such that an informed decision on cost-effective subgrade stabilization can be made.

CHAPTER 1: INTRODUCTION

The presence of soft subgrade soils during new roadway construction is a common occurrence in the state of North Carolina. This is especially true in the lowland areas of the Coastal Plain region where the combination of a high groundwater table and large quantities of organic material can create an unsuitable platform to build on. Aside from the long-term stability that is essential for many years of successful pavement performance, subgrade soils must be able to provide short-term stability during construction operations where heavy equipment is routinely traversing the site. If not properly addressed, soft subgrade soils can lead to undesirable consequences in the form of unexpected cost overruns and construction schedule delays. As a result, stabilization of the soft subgrade layer generally is required. Typical stabilization methods consist of the removal of the unsuitable subgrade soil and its replacement with select backfill material, such as stiff granular soil, an aggregate base course (ABC), geosynthetics, or a combination of these materials. The stabilization procedure generally is termed "undercut" in the field. Another stabilization method is to treat the unsuitable subgrade soils with chemical additives such as lime and/or cement which reduces the subgrade water content and creates cementitious bonds between the soil particles. Soft subgrade soils are typically detected during the initial site investigation so that the associated costs of stabilization can be anticipated prior to construction. Once construction begins, the stability of the subgrade soil is evaluated by subjectively observing a proof rolling process to identify areas of excessive pumping and/or rutting. The magnitude of pumping and/or rutting that is considered "excessive", however, is at the discretion of the proof roll inspector. In light of this fact, the North Carolina Department of Transportation (NCDOT) has sought out to develop a systematic approach for determining whether or not undercutting is necessary, and to investigate the adequacy of stabilization measures typically employed if undercutting is deemed necessary.

Background

This study is a part of an effort by the NCDOT to develop undercut criteria, including systematic short-term criteria for expected construction loading and long-term criteria that establish the subgrade strength and stiffness for the design of the pavement layers. The overall research effort encompasses four phases. Phases I, II, and III were covered under research project 2008-07. Phase I focused on characterizing soils that are typically encountered in undercut situations in

North Carolina, including their engineering characteristics and resilient modulus degradation with accumulated strain under repeated loading. Phase II included 22 large-scale tests to develop a systematic approach of using in situ methods for discerning the need for undercutting, and to provide data to assist in estimating the depth of undercut. Data from Phase II were also used to evaluate improvements in subgrade properties with the implementation of chemical and geosynthetic stabilization techniques, and to develop cost equivalency factors. Phase III consisted of numerical modeling of subgrade sections to investigate the response of four field configurations with undercutting as a stabilization measure and investigate associated levels of deformation and plastic strain under loading.

The laboratory testing and numerical modeling work performed under research project 2008-07 culminated in proposed systematic criteria for undercutting and alternative stabilization measures under various roadway site conditions. These criteria provide provisions for discerning possible rutting and pumping of the subgrade under construction loading based on strength and modulus data obtained for the subgrade soils. Guidelines were also provided for specifying various stabilization measures to achieve adequate subgrade support. These measures included the use of select material, an aggregate base course (ABC), geogrids with ABC, geotextiles with ABC, and lime stabilization. Finally, a comparative cost analysis was also presented to illustrate the relative cost of each stabilization measure in relation to performance.

Problem Statement

Although laboratory testing and numerical modeling can provide valuable information regarding the behavior of roadway systems, there are limitations in their ability to accurately represent actual field conditions. Laboratory testing allows for a high degree of quality control, however, the results can be hampered due to boundary effects and the inability to simulate live loading conditions. Numerical modeling is cost-effective and allows the modeler to exercise complete control over the system. However, it is based on idealized constitutive models that may or may not accurately represent field situations. To this extent, field testing under actual field conditions is a critical component of any research program to validate guidelines developed from laboratory testing and numerical modeling.

Objectives

The main objective of this research report is to present the results of field testing on instrumented roadway sections (Phase IV) to validate undercut criteria as developed from the laboratory testing and numerical modeling study (Phases I, II, and III). Specifically, the objectives of this research project are to:

i. Identify a test site for implementation of alternative or supplemental approaches to undercut, including the use of geosynthetics and/or chemical stabilization.
ii. Instrument four test sections at the identified site and monitor the performance in terms of induced rutting and stress distribution under repeated truck loading.
iii. Perform field testing using a Dynamic Cone Penetrometer (DCP), Soil Stiffness Gauge (SSG), and Falling Weight Deflectometer (FWD) to collect information on soil properties using in situ techniques.
iv. Use the field data to validate the proposed undercut evaluation criteria as developed from the laboratory and modeling study.
v. Use the field data to calibrate the comparative cost analysis based on results from the laboratory study, and illustrate the relative cost of each measure such that an informed decision on cost-effective subgrade stabilization can be made.

Scope of Work

The scope of this research project included the construction and instrumentation of four 16 feet wide by 50 feet long test sections on poor subgrade soils encountered in the Coastal Plain region of North Carolina. One test section encompassed undercutting and replacement with select material (Class II), the second and third test sections included reinforcement using a geogrid and geotextile, respectively, in conjunction with undercutting and replacement with ABC (Class IV), and a fourth test section included cement treatment of the soft subgrade soil. Field instrumentation of the test pad was performed with each test section instrumented with four earth pressure cells (EPCs) and two soil moisture sensors. Full-scale field testing consisted of 1,000 consecutive passes of a fully loaded tandem axle dump truck. All 1,000 passes were conducted within approximately the same wheel path. The EPCs were installed within the wheel path of the loaded truck at a depth of three to six inches below the base/subgrade interface. Profile

surveying was performed at periodic intervals to provide permanent deformation (rutting) with increasing number of truck passes. Instrumentation was used to measure the peak vertical stress in the subgrade with traffic and monitor the moisture conditions of the subgrade soil.

DCP, SSG, and FWD tests were performed on the test pad at various stages of the project to obtain strength and stiffness data in situ for both the subgrade and base layer materials. This data was then used to explain full-scale testing results and investigate the validity of the proposed undercut criteria for defining the depth of undercut and predicting the performance of the replacement layer.

Report Layout

The Scope of Work (described above) was performed from March 2011 to August 2011. As mentioned earlier, this study is supplemental to the three phases covered under research project 2008-07. This report is organized into eight chapters. They are divided as follows:

Chapter 2. Reviews appropriate studies from the literature that were not covered in the FHWA/NC 2008-07 report.

Chapter 3. Presents the details of the field testing including site information, relevant soil and material properties, instrumentation, the process of constructing the test pad, and the test procedures for quality control, in situ testing, and full-scale testing.

Chapter 4. Presents the results of quality control and in situ field tests performed at various stages of the project.

Chapter 5. Presents the results of full-scale testing including field observations, rut development, subgrade stresses, soil moisture, and proof roll testing.

Chapter 6. Evaluates the proposed undercut criteria based on a combination of laboratory determined and DCP correlated soil properties.

Chapter 7. Presents a cost analysis of the various stabilization measures investigated and compares the results to that obtained from the laboratory study (Phase II).

Chapter 8. Presents a summary of the research, draws conclusions from the results, and suggests directions for future research.

Terminology

Before proceeding, it is important to establish the terminology of the various pavement layers that will be discussed within this report. Shown in Figure 1-1 is the roadway profile during full-scale field testing (a) and after the final pavement layer (b). Typically, when subgrade stabilization is required the mechanically or chemically stabilized layer is referred to as "subbase". For simplicity, this layer will be referred to as "base" within this study to differentiate between the non-stabilized and stabilized subgrade layer. However, this is not meant to be confused with the upper five inch base layer that was placed months after full-scale testing was completed.

Also, note that throughout the report the term "test pad" will be used to identify the complete 200 feet of instrumented roadway, whereas the term "test section" will be used to identify a particular 50 foot mechanically or chemically stabilized portion of the test pad.

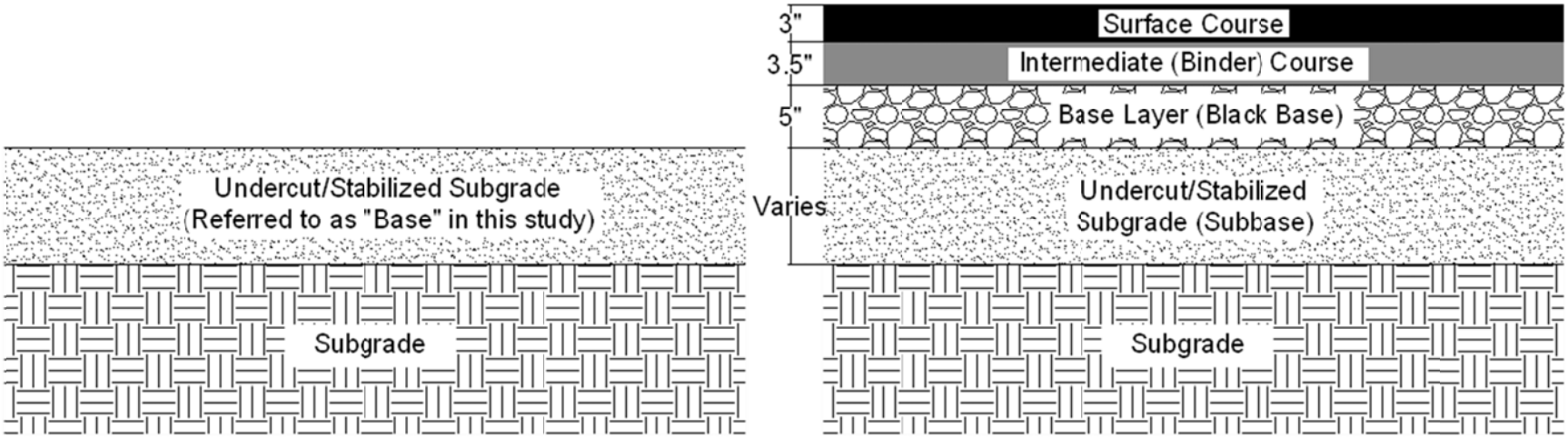

(a) **(b)**

Figure 1-1: Roadway profile (a) during field project, (b) after the final pavement layer

CHAPTER 2: LITERATURE REVIEW

An extensive review of the current state of practice for several topics relevant to this report can be found in the literature reviews conducted by Cote (2009) and Borden *et al.* (2010). These topics include roadway subgrades, mechanical stabilization using granular layers, and mechanical stabilization using geosynthetics. This review summarizes the current state of practice and recent findings in regards to cement stabilization and full-scale roadway testing.

Cement Stabilization

The increased costs associated with replacing soft soils with high quality fill has forced transportation agencies to look at treating rather than removing the existing soils on highway construction projects. A number of chemicals including cement, lime, fly ash, and polymer fibers have been successfully used as additives to stabilize soft subgrade soils and provide a stable platform for the design life of the pavement structure. The focus of this literature review will be on cement because it was used to stabilize a portion of the roadway subgrade during full-scale field testing reported in this study. It is important to note that this discussion is meant to serve as a highlight of some of the important factors associated with cement stabilization. Current research in areas such as additional additives (e.g. air entrainment), and innovative test methods will not be discussed in this review.

Background

The first known use of Portland cement to stabilize soft subgrades was in the early 1930's during a study performed by the South Carolina Department of Transportation (SCDOT). In this study, the SCDOT looked at low-cost solutions for roadway construction and found that that process of mixing cement into the existing soils was a viable method to stabilize the subgrade. Since then, the Portland Cement Association (PCA) has worked to establish testing standards for soil-cement (Scullion *et al.* 2005). These standards were later adopted by the American Society of Testing and Materials (ASTM) in 1944 and the American Association of State Highway Officials (AASHTO) in 1945.

Design

Currently, state agencies typically rely on compressive strength as the sole indicator of the cement content needed for a particular project. The US Army uses Table 2-1 as an initial estimate of the cement content based on the soils classification.

Table 2-1: Estimated cement requirements for various soils (US Army, 1994)

Soil Classification	*Initial Estimated Cement Content, percent dry weight*
GW, SW	5
GP, GW-GC, GW-GM, SW-SC, SW-SM	6
GC, GM, GP-GC, GP-GM, GM-GC	7
SC, SM, SP-SC, SP-SM, SM-SC, SP	7
CL, ML, MH	9
CH	11

After making an initial estimate, the US Army then recommends preparing triplicate samples at: i) the estimated cement content, ii) 2% below the estimated cement content, and iii) 2% above the estimated cement content. After allowing the specimens to cure for seven days, they are tested using the unconfined compression test. Based on the result, the lowest cement content that meets the required compressive strength is used at the design cement content. Shown in Table 2-2 are the minimum UCS requirements for the US Army.

It is important to note that the selection of cement content is a balancing act where adding too little or too much cement can be detrimental to the final product. Too little cement will under-stabilize the subgrade and potentially shorten the design life of the roadway. However, too much cement can lead to shrinkage cracking which creates openings for moisture to enter. Overtime, the moisture accelerates the degradation of the soil-cement and decreases the strength and stiffness of the overall roadway (Guthrie & Rogers, 2010). In addition, while higher cement content provides a higher strength, too much cement can cause the structure to become brittle, causing rapid failure at relatively low levels of strain (Sariosseiri & Muhunthan, 2009).

Table 2-2: Minimum UCS for cement stabilized soils (US Army, 1994)

	Minimum Unconfined Compressive Strength, psi	
Stabilized Soil Layer	*Flexible Pavement*	*Rigid Pavement*
Base	750	500
Subbase course, select material, or subgrade	250	200

Construction

Cement stabilization is usually performed in six steps: 1) preparing the subgrade, 2) scarifying the subgrade, 3) spreading the cement, 4) mixing the cement into the soil, 5) compacting the soil-cement mixture, 6) finishing the surface. During the preparation and scarifying phases, the subgrade is wetted down to reach the optimum moisture content and loosened up to aid in the mixing process. Dry cement is typically applied using a mechanical spreader attached to the rear of a tanker truck filled with bulk cement. It is important to note that cement should not be applied during excessively windy days. The wind can carry off the dry cement, reducing the amount of cement mixed into the subgrade and potentially damaging the exterior of nearby vehicles and/or buildings (Boswell, 2000). After the cement has been applied, a soil stabilizer is used to pulverize and mix the cement into the soil to the specified depth automatically set by the driver. This is usually done over a number of passes to ensure the cement has been mixed thoroughly into the soil and to the design depth. Once the roadway inspector believes the cement has been uniformly mixed and the moisture content has been verified to be within the specified tolerances, typical compaction equipment (i.e. steel drum roller) is used to densify the soil-cement structure. The compacted densities can then be verified using several methods such as the sand-cone, balloon and the nuclear density gauge. Finally, any necessary finishing is performed to shape the soil-cement surface to the correct lines, grades, and cross sections prior to curing.

Quality Control

According to the US Army (1994), special attention should be placed on the following six factors during soil-cement construction:

1. *Pulverization:* As mentioned previously, it is critical that the cement be thoroughly mixed into the soil so that the particles can interact and bond. Thus, it is important that any soil clods be broken down into as fine of a state as possible. Normally this can be verified through observation, however, passing a sample of the material through a #4 sieve and calculating the percent retained can also provide a more quantitative assessment of the degree of pulverization.
2. *Cement content:* During construction, roadway inspectors should be aware of the required cement content and should spot check to verify uniformity. This can be done by laying a canvas over a known area and calculating the weight of cement that is spread on top. The cement should be spread with relative uniformity throughout the entire stabilized area. Any areas that are over or under-stabilized can create problems in the load distribution properties of the layer (Guthrie & Rogers, 2010).
3. *Moisture content:* Prior to construction, the optimum moisture content of the design mixture should be determined in the lab according to ASTM D 558 (2011). During construction, roadways inspectors should verify the moisture content is within the allowable tolerance specified by the state agency. This can be done by sampling the soil-cement mixture and heating it up under a hotplate as specified in ASTM D 4959 (2007). According to the NCDOT *Standard Specifications* (2012), the moisture content of the mixture should be within a range of optimum to optimum plus 2% moisture during compaction. This is imperative not only to ensure density, but also to facilitate hydration in order for soil-cement mixture to gain strength.
4. *Uniformity of mixing:* Visual inspection of the mixtures level of uniformity is important to ensure long-term stability of the structure. As previously stated, any heterogeneity in the mixture can cause problems in the load distribution properties of the layer (Guthrie & Rogers, 2010). To verify uniformity, the soil cement mixture should have the same color throughout as opposed to a streaked appearance indicating a non-uniform mixture (US Army, 1994).

5. *Compaction:* Prior to construction, the maximum dry density of the design mixture should be determined in the lab according to ASTM D 558 (2011). During construction, roadways inspectors should verify that the layer has reached the relative density specified by the state agency. According to the NCDOT *Standard Specifications* (2012), the relative density of the compacted soil-cement layer should be at least 97%.
6. *Curing:* After the soil-cement layer has been constructed, it is imperative that it cure for at least 7 days. To aid in the curing process, an asphalt or sand seal is typically sprayed over top of the stabilized layer within 24 hours of construction. This keeps the layer moist so that the cement can continue to hydrate and gain strength.

Another factor, not mentioned above is the time permitted between mixing and compaction. When the cement is added, it immediately begins to react with the soil particles. After a while, the ability for the particles to reach a denser configuration becomes limited resulting in soil-cement structure less dense than desired. In addition, early cementitious bonds that form between mixing and compaction are broken down during the compaction phase. Although bonding can occur after compaction, it is critical for the soil-cement structure to reach its final state as soon as possible to reach the design strength (Guthrie & Rogers, 2010). According to the NCDOT *Standard Specifications* (2012), final compaction should occur within three hours after water has been added to mixture. The NCDOT also makes a note that cement mixture should not be left undisturbed for more than 30 minutes if it has not been compacted and finished.

Benefits and Drawbacks

The beneficial effects of using Portland cement to stabilize soft subgrades have been well-documented over the years in the literature (Catton, 1939; Roberts, 1986; Fonseca *et al.* 2009). Cement stabilization improves the subgrade by increasing bearing capacity and reducing the plasticity of the existing soils (Sariosseiri & Muhunthan, 2009). This is achieved through hydration and hardening effects within the cement in conjunction with the interaction between the soil particles.

Arguably the biggest advantage of cement stabilization is the upfront cost savings when compared to traditional mechanical stabilization measures. The costs associated with mechanical stabilization including undercutting, transporting, and disposing of existing soils as well as

purchasing, transporting, and backfilling high quality materials is non-existent with chemical stabilization. Although, there are associated costs such as purchasing cement and having to transport and mobilize non-typical construction equipment (i.e. soil stabilizer and cement spreader), the construction costs associated with mechanical stabilization tend to surpass that of cement stabilization.

Cement also has its advantages over other additives used in chemical stabilization, specifically lime. Cement can be used to treat most soil types, whereas, lime is generally limited to high plasticity, fine grained soils. However, there are a few exceptions when cement should be avoided. These include high plasticity clays, organic soils, and poorly reacting sands (ACI, 1990). Another advantage of cement is that it can be compacted immediately after mixing. With lime there is a one to four day time period required to allow the mixture to mellow.

Despite the advantages of cement stabilization, it also has its share of drawbacks. Probably the biggest disadvantage of cement stabilization is the seasonal restrictions that limit when cement stabilization can be performed. Current NCDOT practice states that soil-cement construction cannot be performed when: i) The air temperature is less than 40°F nor when conditions indicate that the temperature may fall below 40°F within 24 hours, or ii) if the cement-treated layer will not be covered with pavement by December 1 of the same year (NCDOT, 2012). These seasonal restrictions are based on the established fact that cement hydration and corresponding strength are significantly reduced when subjected to cold temperatures (DeBlasis, 2008).

Another drawback is the seven day curing time after compaction. With mechanical stabilization, however, the paving process can proceed without interruption. Also, the NCDOT recommends that after curing, completed cement stabilized sections should not be trafficked except when necessary with light weight vehicles (2012). This is to prevent marring and distorting the stabilized surface which can only be repaired by replacing the layer to its full depth. This severely limits the access routes for construction equipment to traverse the site and makes contractors devise alternate routes which presumably take longer time for equipment to get from point “A” to point “B”. With mechanical stabilization, there are no such limitations and equipment is allowed to traffic the stabilized roadway as needed leading up to paving operations.

Full-Scale Roadway Testing

The vast majority of design methods for unreinforced and geosynthetically reinforced roads are derived and/or calibrated based on a combination of numerical models and physical testing. Physical tests can be performed at different scales including small-scale testing, large-scale testing, and full-scale testing. With each scale of test there are both positives and negatives. Shown in Table 2-3 is a comparison of the pros and cons associated with each physical test.

Table 2-3: Comparison of the positives and negatives of the different physical tests

	Level of Quality Control	Ability to Simulate Live Loading Conditions	Relative Ease to Construct and Perform
Small-Scale Testing	Excellent	Fair	Excellent
Large-Scale Testing	Good	Good	Good
Full-Scale Testing	Fair	Excellent	Fair

Small-scale testing usually consists of test models constructed in either small-sized plane strain boxes with maximum dimension of approximately one meter, in modified Proctor or CBR molds, or in triaxial cells. Due to the small sample size, a high degree of quality control can be reached with small-scale tests. In addition, a number of tests can be performed in a short period of time due to the relative ease to construct and perform. However, due to size and boundary effects, small-scale tests typically show large contributions from mechanical reinforcement that does not accurately represent what would be observed in the field (Cote, 2009). Furthermore, the live loading conditions applied by moving tires cannot be simulated on small samples in the lab.

If properly designed, large-scale tests can act as a good alternative to small-scale testing by simulating field conditions without size or boundary effects. In addition, good quality control can usually be maintained during construction due to the controlled environment and relatively relaxed time constraints. However, during large scale testing, loading is usually induced using a stationary rigid circular plate which may not accurately simulate the interface shear stresses, curved loading surface, uneven contact pressures, and soil flow patterns that are generated by

rolling wheels. In addition, the effects of the lateral wander (i.e. lateral distribution of wheel loads), which naturally occur in the field due to driver habits, wind, etc., cannot be simulated using a static plate.

Full-scale field testing is an attractive alternative to large-scale testing because it can mimic the moving wheel loads observed on public and private roadways. These tests, however, are difficult to construct and quality control is hard to maintain due to: i) the large volume of materials used to construct the section, ii) environmental factors such as rain, wind, etc. that cannot be controlled, and iii) unpredictable and non-uniform subgrade soils that are the result of natural deposition over time.

Over the years, a number of full-scale studies have been performed on simulated or actual unpaved roads. Examples include Webster and Watkins (1977), Webster and Alford (1978), De Garbled and Javor (1986), Austin and Coleman (1993), Chaddock (1988), Fannin and Sigurdsson (1996), Tingle and Webster (2003), Hufenus *et al.* (2006), and Tingle and Jersey (2009). This review summarizes the findings of these studies as related to this report. Generally, the experiments encompass sections constructed with either unreinforced or geosynthetic-reinforced aggregate base course (ABC) over soft subgrade. Deflections and stresses are typically measured through various instrumentation arrangements to evaluate the section's behavior before, during, and after trafficking.

Webster and Watkins (1977) were perhaps the first to highlight the benefits of geosynthetic inclusion over soft subgrades for the construction of unpaved roads. Based on unreinforced and geosynthetically reinforced field trials, they concluded that geosynthetics can potentially reduce the design thicknesses of base course layers over soft subgrades. A year later in a follow-up study, **Webster and Alford (1978)** quantified this conclusion, reporting as much as a 50% reduction in the required base course thickness. Since then, the vast majority of research has indicated that geosynthetic inclusion does in fact delay rut formation and helps reduce the amount of granular material needed.

De Garbled and Javor (1986) performed full-scale tests on soft subgrade sections reinforced using three different geotextiles with tensile strength's ranging between 35 and 480 kN/m. Based on their results they found no significant difference in rut development between

geotextiles of varying tensile strength. **Austin and Coleman (1993)** found similar results during a full-scale study using three different geogrids, a geotextile, and a geogrid placed over top a geotextile. In their conclusion they reported, "The performance of polypropylene geogrid reinforced haul roads constructed on soft soils seems to be independent of the tensile strength and the process used to manufacture the products."

Chaddock (1988) reported results from a full-scale field test on unreinforced and geogrid-reinforced test sections built over a soft clay subgrade placed at three different CBR's (.4, 1.6, and 4.9). Crushed limestone was used for the base layer material with a varying thickness that ranged from 23 inches over top the softest subgrade to 6 inches over top the stiffest subgrade. The author concluded that the geogrid sections, on average, supported approximately 3.5 times more traffic than unreinforced sections of equal base thickness. On the softer subgrade sections, it was noted that the geogrid could not prevent base layer contamination. In addition, aggregate interlock was more apparent in the stiffer subgrade section.

Fannin and Sigurdsson (1996) constructed five full-scale test sections overtop an organic clayey silt with high plasticity ($S_U \approx 40$ kPa). One section was unreinforced; three included a geotextile at the subgrade-base interface, and one was reinforced with a high-strength biaxial geogrid at the subgrade-base interface. The base course layer was constructed using sandy gravel with varying thicknesses within each section of 20, 16, 14, 12 and 10 inches. During trafficking measurements were taken in regards to rut depth and geosynthetic strain. Field observations indicated that for thin base course layers, separation appears to dominate performance rather than reinforcement. However, as the thickness of the base course increases, the dominant function shifts to reinforcement. They also note that the benefit of geosynthetic reinforcement tends to increase for thinner base course layers (10-12 inches) and decreases with increasing base course thickness. Fannin and Sigurdsson (1996) also compared their results to the analytical solutions of Giroud and Noiray (1981) and found that the solutions tend to over predict the performance of unpaved roads at small rut depths. They attribute this to the compaction that occurs within the base course layer.

Tingle and Webster (2003) reported the results from full-scale testing on four test sections overtop saturated high plasticity clay (CBR ≈.7). One section was unreinforced with 20 inches of base course material, two sections were reinforced with a woven and non-woven geotextile

with 15 inches of base course material, and a fourth section was reinforced with both a geogrid and a geotextile with 10 inches of base course material. Crushed limestone was used for the base course material on all four sections. Prior to completing construction, all four test sections were trafficked 500 truck passes to simulate construction traffic. Rut depth measurements from this phase were not reported since the focus of the study was on completed unpaved roads. After construction was complete, the test pad was trafficked a total of 2000 truck passes with rut depth measurements taken periodically. Based on the results, the authors reported a potential base aggregated savings of 25% for geotextile-reinforced sections and a 50% for geocomposite reinforced sections (i.e. geotextile and geogrid).

Hufenus et al. (2006) conducted a full-scale field test on a geosynthetics reinforced unpaved road to evaluate the bearing capacity and its performance on soft subgrade soils. Similar to Fannin and Sigurdsson (1996), Hufenus *et al.* reported less benefit in geosythetic reinforcement with increasing base course thickness. Also, they make the recommendation that some amount of trafficking should be performed on reinforced sections prior to completion. This allows the geosynthetic to deform in order to mobilize the tensile forces in the geosynthetics. Hufenus *et al.* also make note that specifying extremely stiff geosynthetics is impractical. This was based on geosynthetic strain measurements that indicated mobilized tensile forces no greater than 6-10 kN/m. This is presumably the reason for why De Garbled and Javor (1986) and Austin and Coleman (1993) did not observe any benefit when using geotextiles and geogrids of varying tensile strength.

Tingle and Jersey (2009) reported the results from a field trial performed under shelter that looked at the effectiveness of geosynthetic reinforcement when used with marginal base course materials. A total of eight test sections were built: four using a high quality crushed limestone (SW-SM), two using a moderate quality crushed chert aggregate (GW), and two sections using a marginal quality clay gravel base (GP-GM). A six inch base course thickness was used to construct all test sections. Reinforced test sections had a polypropylene needle-punched geotextile, a polypropylene geogrid, or a combination of both at the subgrade-aggregate base interface. Three unreinforced control sections were built, each using a different base course material. The test sections were trafficked a total of 10,000 truck passes or until reaching failure at a rut depth of 75 mm (3 inches).

A number of instruments were installed within each test section to measure the system response of each stabilization measure during trafficking. Eight earth pressure cells (EPCs), one per section, were installed along the wheel path at a depth of 50 mm (2 inches) below the subgrade/base layer interface. Single-depth deflectometers were also installed to measure the subgrade surface deflection through tubes buried in the aggregate layer. Time domain reflectometry (TDR) moisture and temperature probes were inserted into the subgrade to measure the environmental response and foil strain gages were attached to the geosynthetics to measure geosynthetic strain. Falling weight deflectometer (FWD) testing was performed before, during, and after trafficking to monitor the deflection basins of each section and backcalculate the subgrade and base layer modulus.

Results showed that for all base course materials, geosynthetic reinforcement delayed rut formation. The best rut resistance was observed in the unreinforced and reinforced test sections built using the clay gravel. Tingle and Jersey (2009) attribute this behavior to the high shear strength of the dry cemented clay particles, however, were quick to point out that the results would likely be much different when exposed to moisture. This is due to clays susceptibility to moisture resulting in a significant decrease in strength and stiffness. In general, the EPCs showed a decrease in vertical stress at the subgrade/base layer interface when using geosynthetic reinforcement. In addition, TDR probes measured little to no change in subgrade moisture and temperature during trafficking. Geosynthetic strains were localized to the loaded wheel paths with higher strains measured in the longitudinal direction (direction of travel) versus the transverse direction. The range of strains measured in the geogrid were significantly lower (.1 to 2.1%) than the strain measured in the geotextile (1 to 4.5%). FWD results on the geosynthetic sections showed a shallower and flatter deflection basin after trafficking indicating a stiffer composite section with a better load distribution ability. Backcalculated moduli confirmed this observation based on a general increase in stiffness with trafficking due to the densification of the base course layer and the mobilization of the geosynthetic reinforcement. The author concluded that different base course materials provide different strength and deformation behavior; however, geosynthetics can be effectively used for reinforcement with both high quality and marginal base course materials.

Summary

In summary, full-scale roadway testing has generally shown that geosynthetic reinforcement in conjunction with granular fill can be used to delay rut formation, and/or reduce the base course thickness. The benefit of geosynthetics is highly dependent on multiple factors including:

- Geosynthetic type and properties
- Strength and stiffness of the subgrade soils
- Base course thickness
- Quality of the base course material

The relative importance of these factors is still up for debate; however, research has shown that with each factor there is a limit to the observed benefit from geosythetic inclusion. The following conclusions, in regards to the factors mentioned above, can be drawn based on this review of full-scale roadway testing on unpaved roads:

- When comparing geosynthetic types, full-scale tests tend to indicate that geotextiles resist rut formation better than geogrids over very soft subgrades. This is principally due to the geotextiles separation, filtration, and drainage functions. However, geogrids have performed well when used over stiff subgrades, principally due to the reinforcing mechanisms that develop from aggregate interlock.
- Research has indicated that it is impractical to specify excessively high strength geosynthetics. This is based on the fact that geosynthetic strains and corresponding stresses that mobilize during trafficking are typically limited due to rutting failure.
- Numerous full-scale studies have shown a decrease in the benefit of using geosynthetics with an increase in base layer thickness.
- Geosynthetics can be used with both high quality and subpar base course materials to mechanically stabilize soft soils.

It is worth noting that, in general, there is a lack of studies available regarding full-scale tests performed on cement stabilized sections. This is presumably due to the fact that cement stabilized sections are not intended to serve as the final surface course for high traffic roadways. As mentioned before, state agencies normally discourage contractors from allowing any traffic on the finished cement-stabilized sections prior to paving.

CHAPTER 3: TESTING PROCEDURE AND MATERIALS

This chapter describes the details of the field testing including site information, soil and relevant material properties, installed instrumentation, and the process of constructing the test pad. Activities performed once the test pad was constructed, including quality control testing and in situ testing, will also be discussed. Finally, the procedures involved with full-scale testing will be summarized.

Site Description

Site Location

The field site was part of a NCDOT widening project (State Project R-3403) located adjacent to the Neuse River on U.S. Highway 17 in Craven County, North Carolina (see Figure 3-2). The project consisted of constructing two additional lanes on new ground and widening the existing highway. The section of U.S. 17 chosen to construct the test pad was located between stations 121+00 and 123+00 in the new southbound right lane.

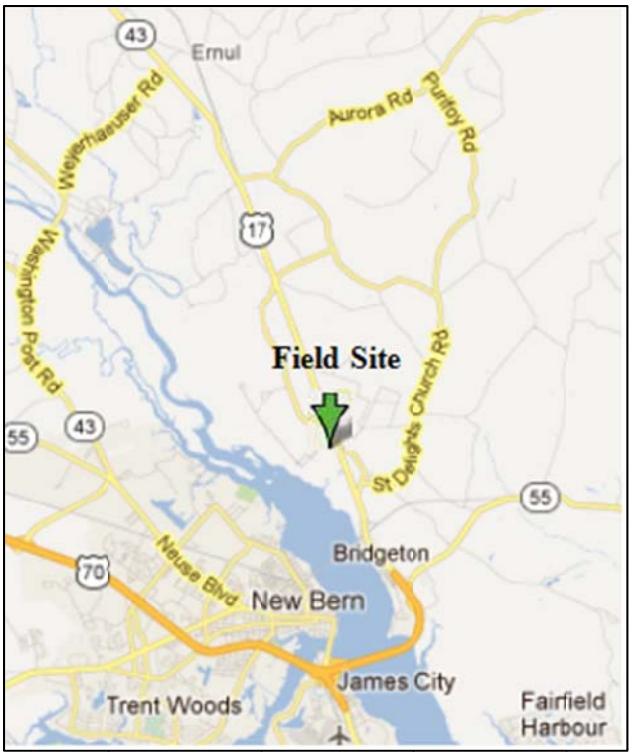

Figure 3-2: Test site location

Physiography & Area Geology

The topography of the site was typical of the Coastal Plain region and was generally flat with poor surface drainage. The elevation of natural ground ranged from 10 to 11 feet with the groundwater table located at an elevation of approximately 3 to 4 feet. The field site geology was made up of Quaternary age fluvial, marine, and eolian type deposits, overlying sedimentary rock of the Yorktown Formation (NCDOT, 2007). A picture of the field site prior to construction is shown in Figure 3-3.

Figure 3-3: Field site prior to construction

Test Pad Configuration

A sketch of full-scale test pad is shown in Figure 3-4. At 200 feet long by 16 feet wide, the test pad was divided into four-50 feet long test sections that were each built using a different subgrade stabilization measure. The four test sections were constructed as follows: i) Test Section 1 consisted of a 31 inch (790 mm) deep undercut backfilled with select material (Class III), ii) Test Section 2 consisted of a 9 inch (230 mm) deep undercut backfilled with ABC stone (Class IV) and a biaxial geogrid, iii) Test Section 3 consisted of a 9 inch (230 mm) deep undercut backfilled with ABC stone (Class IV) and a high strength geotextile, and iv) Test Section 4 consisted of an 8 inch (200 mm) thick layer of cement-stabilized soil constructed in accordance with Section 542 of the NCDOT *Standard Specifications* (2012).

It is worth noting that the original design thickness of the stabilized layer for Test Sections 1, 2, and 3 was 36 inches, 15 inches, and 12 inches, respectively. However, after testing was completed it was realized that based on surveying measurements the contractor failed to undercut to the prescribed depths. As result, all analyses within this study are based on the measured thicknesses of each test section.

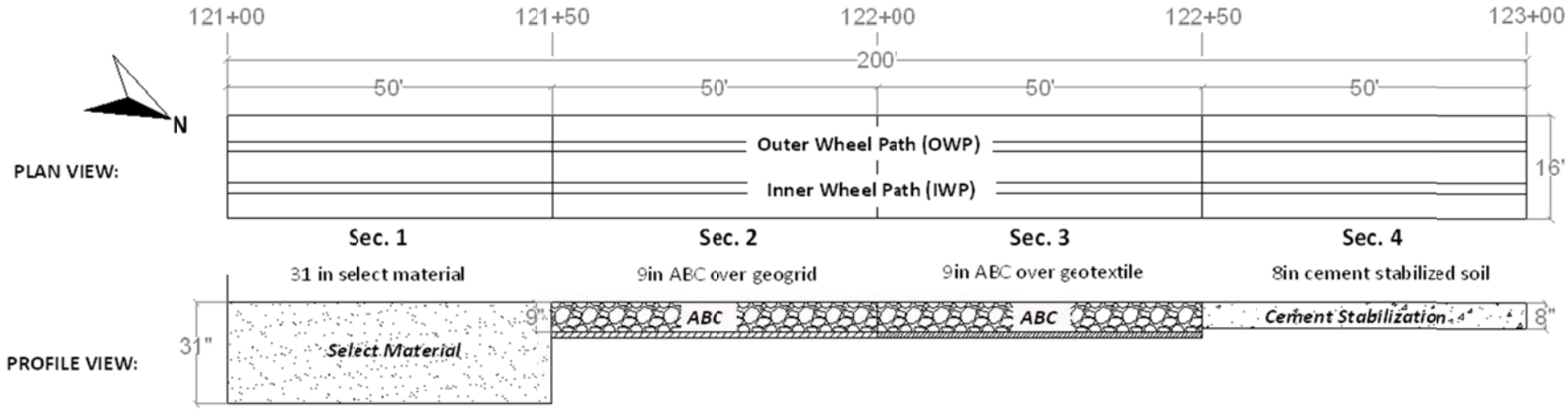

Figure 3-4: Plan and profile views of the full-scale test pad

Materials

This section summarizes the results of small scale laboratory testing to estimate the physical and engineering properties of the subgrade soils encountered at the field site and the base layer materials used stabilize the subgrade. The test soils are divided into four main categories: subgrade soil, select material, aggregate base course (ABC), and cement stabilized soil (CSS). Geotechnical tests were conducted in accordance with ASTM or AASHTO specifications to define the soils' physical and engineering properties. These tests included grain size analysis, Atterberg limits, specific gravity, standard proctor compaction, shear strength, and resilient modulus as appropriate to each soil type.

Subgrade Soil

After Test Sections 1, 2, and 3 had been undercut, seven Shelby tube samples of the subgrade soil were collected from locations throughout the test pad. Due to the granular nature of the subgrade soil the amount of material that remained intact within the tubes varied from 12 to 30 inches. Attempts were made to obtain an eighth Shelby tube sample in Test Section 1, however, the soil failed to remain intact within the tube during its removal. The sample location and depth for each Shelby tube is shown in Figure 3-5.

Basic laboratory index testing was performed on the subgrade soil. The tests included sieve and hydrometer grain size analyses, specific gravity testing, organic content, and Atterberg limits. Table 3-4 presents the index properties from each sample. Gradation curves for all samples are presented in Figure 3-6. The results indicate a relatively narrow range of grain size distribution. According to Unified Soil Classification System the subgrade soils are classified as organic, silty sands (SM) and clayey sands (SC) or A-4(0) according to the AASHTO engineering soil classification system. As shown in Table 3-4, the subgrade soils had little to no plasticity with organic contents that ranged from roughly 3 to 9%.

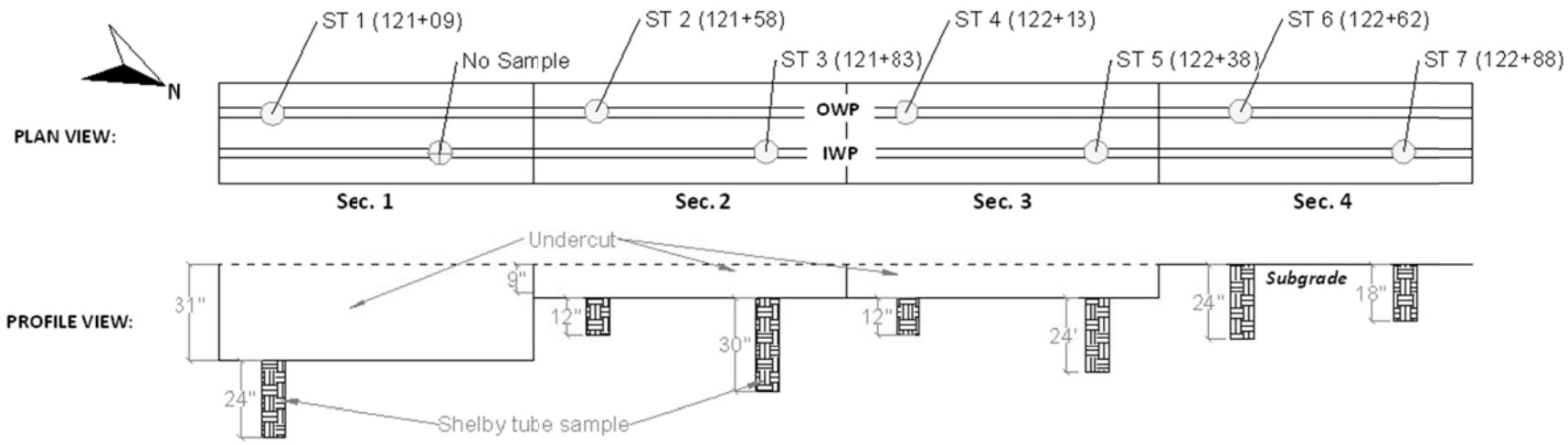

Figure 3-5: Shelby tube sample layout

Table 3-4: Subgrade soil index properties

Soil Sample	LL	PI	G_S	Organic Content (%)	In Situ Bulk Density (pcf)	Natural Water Content (%)	Classification	
							USCS	AASHTO
ST 1	24	NP	2.56	7.5	108.5	31.6	SM	A-4(0)
ST 2	20	NP	-	4.5	113.1	19.7	SM	A-4(0)
ST 3	18	2	2.66	-	129.3	15.9	SC	A-4(0)
ST 4	18	NP	2.63	3.6	119.4	18.1	SM	A-4(0)
ST 5	21	4	-	5.4	112.9	21.8	SC	A-4(0)
ST 6	21	3	2.61	5.4	129.3	14.7	SM	A-4(0)
ST 7	24	3	-	8.8	114.2	26.7	SM	A-4(0)

NOTE: NP = Non Plastic, - = Test not performed

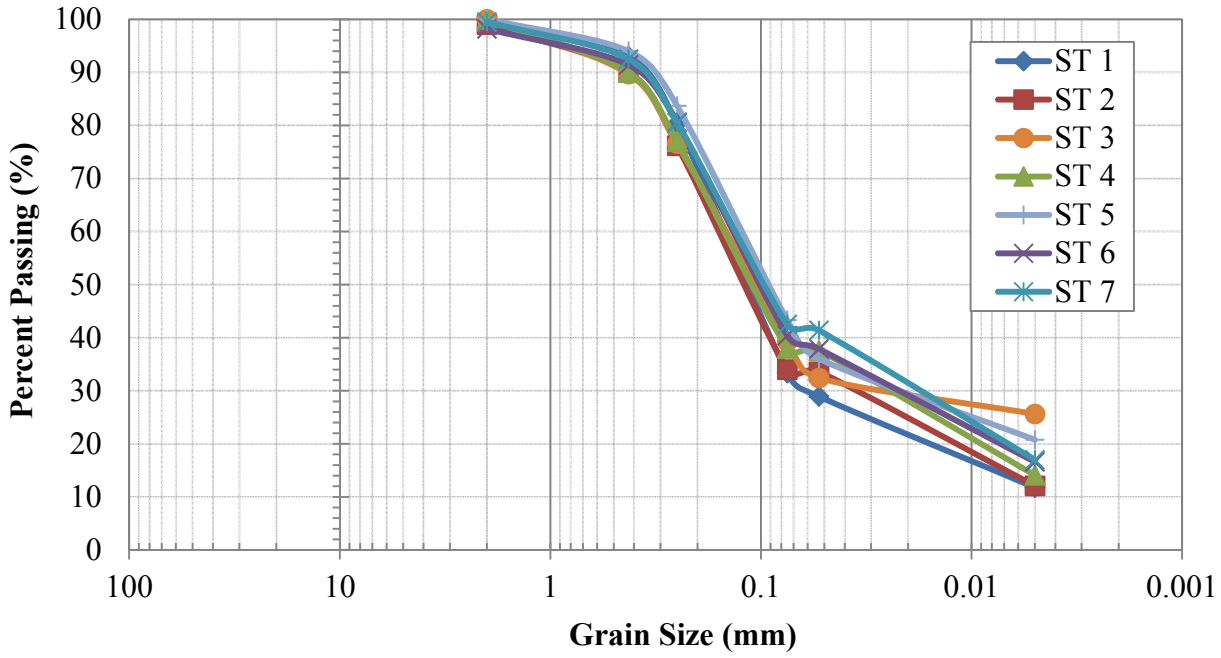

Figure 3-6: Grain size distribution curves for the subgrade samples

Resilient Modulus Testing

Resilient modulus is a measure of the elastic response of a soil under repeated loading. The higher the resilient modulus, the more resistant the soil is to plastic deformation. In recent years the NCDOT has transitioned from using California Bearing Ratio (CBR) to resilient modulus as an indicator of soil subgrade stiffness for pavement design. Thus, laboratory testing primarily focused on evaluating the stiffness of materials using resilient modulus.

Resilient modulus testing on subgrade Shelby tube samples were performed according to AASHTO T-307 by applying five increasing levels of axial stress (2, 4, 6, 8, and 10 psi) at three decreasing levels of confinement (6, 4, and 2 psi) for a total of 15 load sequences. The load sequence for Shelby tube sample 1 is shown in Table 3-5. At each load sequence the axial load was applied in 100 repetitious cycles as a quick load pulse for a 0.1 second in duration; followed by a rest period of 0.9 seconds in duration. The cyclic axial stress is intended to represent the dynamic loading the subgrade soil will be subjected to under traffic conditions. As each load sequence progressed, data was collected in regards to the deformation of the material. Based on the average load-deformation behavior during the last five cycles, the resilient modulus at each load sequence could be determined using the following equation:

$$\mathbf{M_R} = {}^{\sigma_d}/_{\varepsilon_r} \qquad \textbf{Eq. 3-1}$$

Where:

M_R = resilient modulus

σ_d = deviatoric stress

ε_r = recoverable strain.

Table 3-5: Load sequence for resilient modulus tests on the subgrade soil

Sequence No.	Confining Pressure, S_3		Max. Axial Stress, S_{max}		Cyclic Stress, S_{cyclic}		Constant Stress, $.1S_{max}$		No. of Load Applications
	psi	kPa	psi	kPa	psi	kPa	psi	kPa	
1	6	41.4	2.3	15.9	1.8	12.7	0.5	3.1	100
2	6	41.4	4.1	28.2	3.6	25.1	0.5	3.1	100
3	6	41.4	6.0	41.3	5.4	37.3	0.6	3.9	100
4	6	41.4	8.0	55.0	7.2	49.7	0.8	5.3	100
5	6	41.4	10.0	68.8	9.0	62.1	1.0	6.6	100
6	4	27.6	2.3	15.9	1.8	12.4	0.5	3.5	100
7	4	27.6	4.0	27.9	3.5	24.4	0.5	3.5	100
8	4	27.6	6.0	41.0	5.4	37.1	0.6	3.9	100
9	4	27.6	8.0	55.5	7.3	50.2	0.8	5.3	100
10	4	27.6	10.0	69.0	9.0	62.4	1.0	6.6	100
11	2	13.8	2.3	15.9	1.7	11.9	0.6	4.0	100
12	2	13.8	4.0	27.5	3.4	23.6	0.6	3.9	100
13	2	13.8	5.8	39.9	5.2	36.0	0.6	3.9	100
14	2	13.8	7.9	54.5	7.1	49.3	0.8	5.2	100
15	2	13.8	9.9	68.3	9.0	61.7	1.0	6.6	100

The results from resilient modulus testing on the subgrade Shelby tube samples are shown in Figure 3-7. Looking at the results, several trends can be noted. One is that the level of confining stress appears to have a significant effect on the soils resilient modulus. For all tests the resilient modulus increased with an increase in the confining pressure. This behavior is indicative of the stress hardening characteristics typically observed in coarse grained soils. However, at higher confining stresses it becomes apparent that cyclic stress also plays a role in the soils resilient modulus. This behavior suggests the strain-softening characteristics typically seen in fine-grained soils. Rahim and George suggest that this rather mixed behavior is due to the soils moisture ratio (actual moisture content/optimum) and the percentage of fines in the sample (2005). Shown in Figure 3-8 is a plot of the average resilient modulus for each level of confining stress as a function of the samples water content. As expected, the results indicate an increase in moisture content resulted in a decrease in resilient modulus. This type of response has been well documented over the years in the literature (NCHRP, 2008).

Correlated CBR values based on the average resilient modulus at a confining stress of two psi are provided in Figure 3-9. The results indicate a CBR of approximately 1 in Test Section 1 and 2.5 to 4.5 everywhere else in the test pad. This correlation is based on the following AASHTO recommended equation in the 1993 *Guide for design of Pavement Structures*:

Eq. 3-2

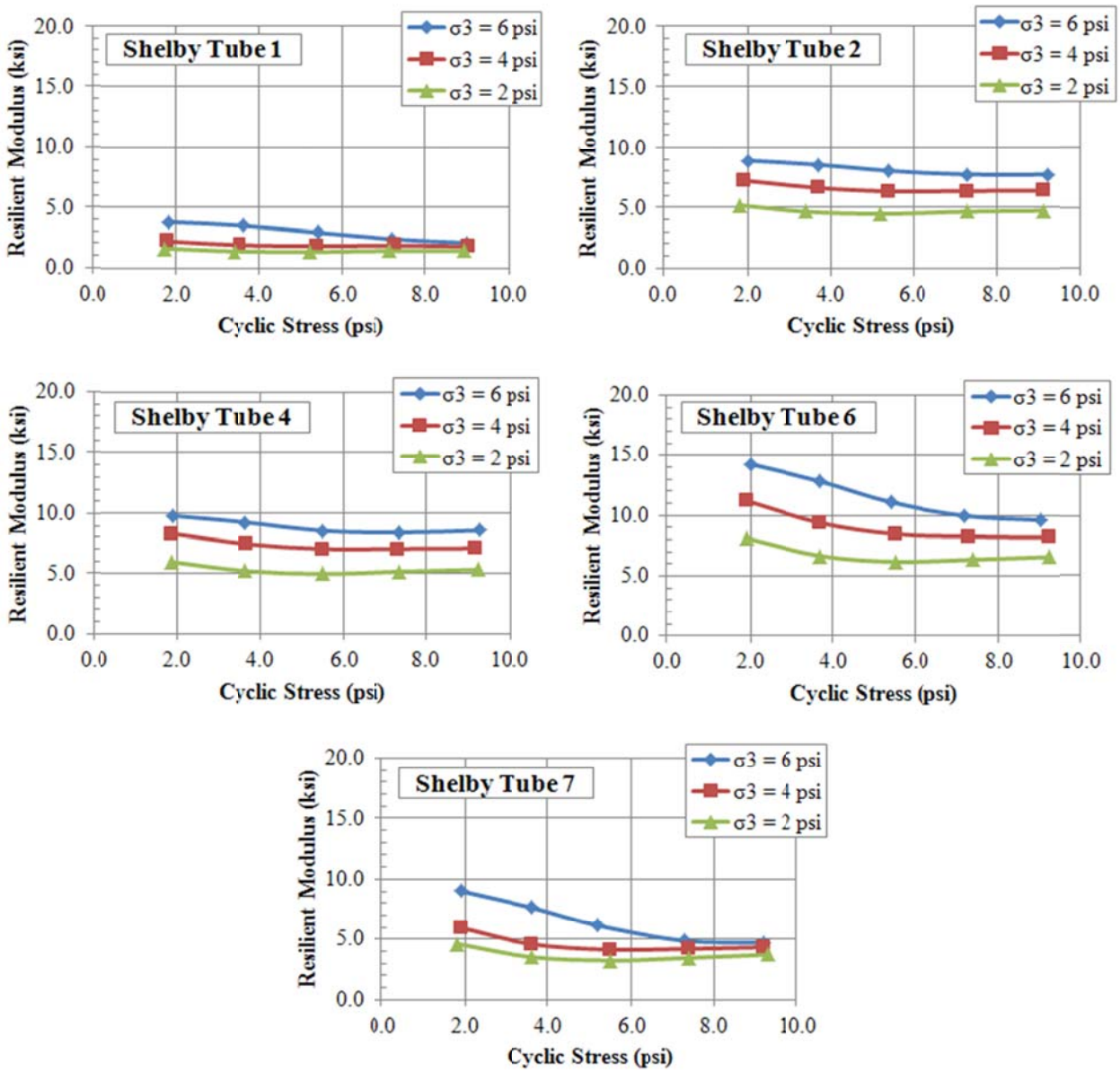

Figure 3-7: Resilient modulus test results on the subgrade Shelby tube samples

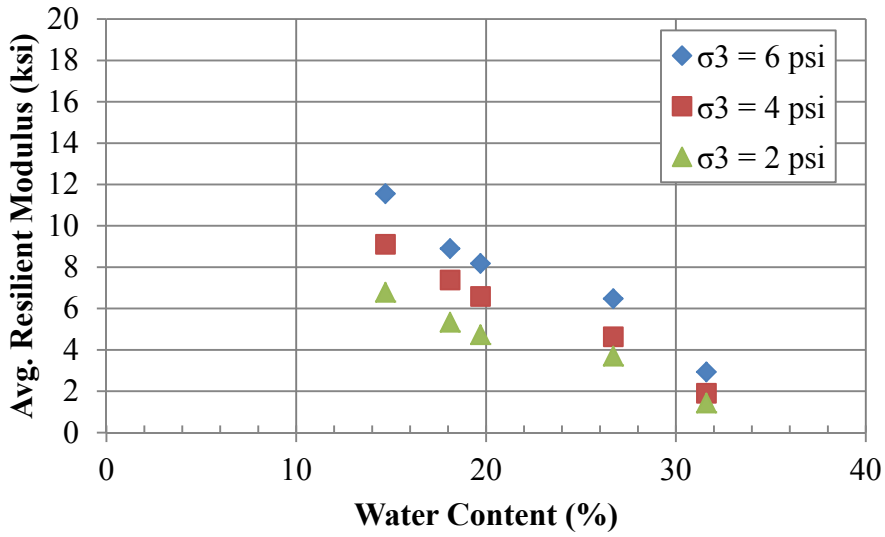

Figure 3-8: Average resilient modulus versus water content at each level of confining stress

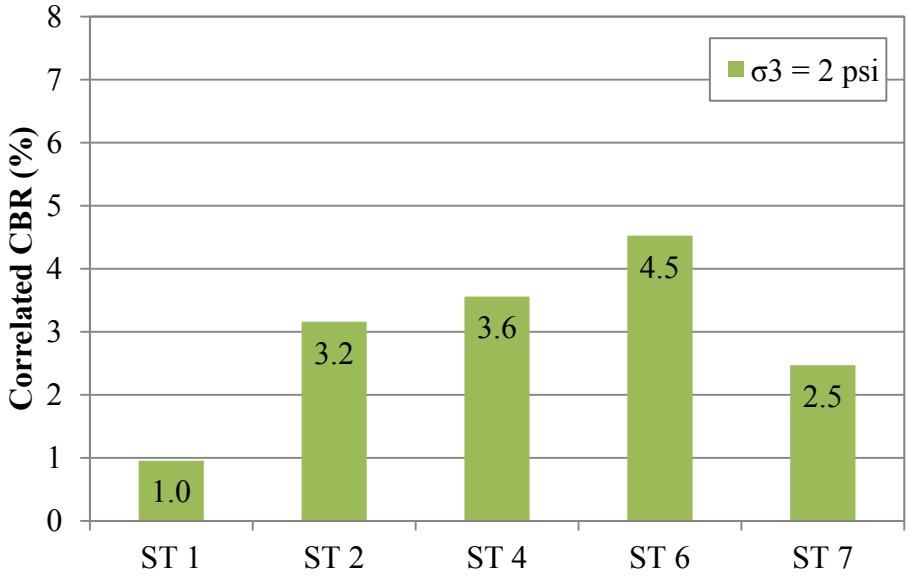

Figure 3-9: Correlated CBR for the subgrade Shelby tube samples

Consolidated Undrained (CU) Triaxial Testing

Two series of consolidated undrained (CU) triaxial tests (ASTM D4767) were performed on subgrade samples collected from Shelby tube 3 in Test Section 2 and Shelby Tube 5 in Test Section 3. A summary of the results are presented in Table 3-6. Strain-stress curves and pore water pressures developed during the shearing stage and Mohr circle charts in terms of both total and effective stresses at the maximum deviator stress criterion are provided in Appendix A.

Table 3-6: Results of CU Triaxial Testing for Subgrade Soil

Soil Sample	Effective Stress		Total Stress		Elastic Modulus (secant; psi)		Undrained Shear Strength, S_U (psi)
	cohesion, c' (psi)	friction angle, Ø' (deg.)	cohesion, c (psi)	friction angle, Ø (deg.)	ε = 1%	ε = 5%	
ST-3	2.4-3.9	30-31	9.5-11.0	16-19	1160-1610	491-619	15.7-19.0
ST-5	1.7	31	5.28	14	1213-1393	302-368	7.5-10.4

Select Material

One of the base course materials used for subgrade stabilization was borrow material taken from the Swift Creek Mine in Craven County, NC. Grain size distribution, Atterberg limits, Standard Proctor, and resilient modulus tests were performed on this soil. Table 3-7 presents the index properties of the borrow material. The gradation curve is presented in Figure 3-10, and standard proctor compaction results are shown in Figure 3-11. Based on grain size and Atterberg limits testing the material met the NCDOT specifications for Class II/Type 2 select material. According to Unified Soil Classification System the select material is classified as silty sand (SM) or A-2-4(0) according to the AASHTO engineering soil classification system.

Table 3-7: Select material index properties

Soil Sample	LL	PI	Maximum Dry Unit Weight, γ_{dmax} (pcf)	Optimum Moisture Content (%)	Classification	
					USCS	AASHTO
select material	17	NP	110.4	12.4	SM	A-2-4(0)

NOTE: NP = Non Plastic

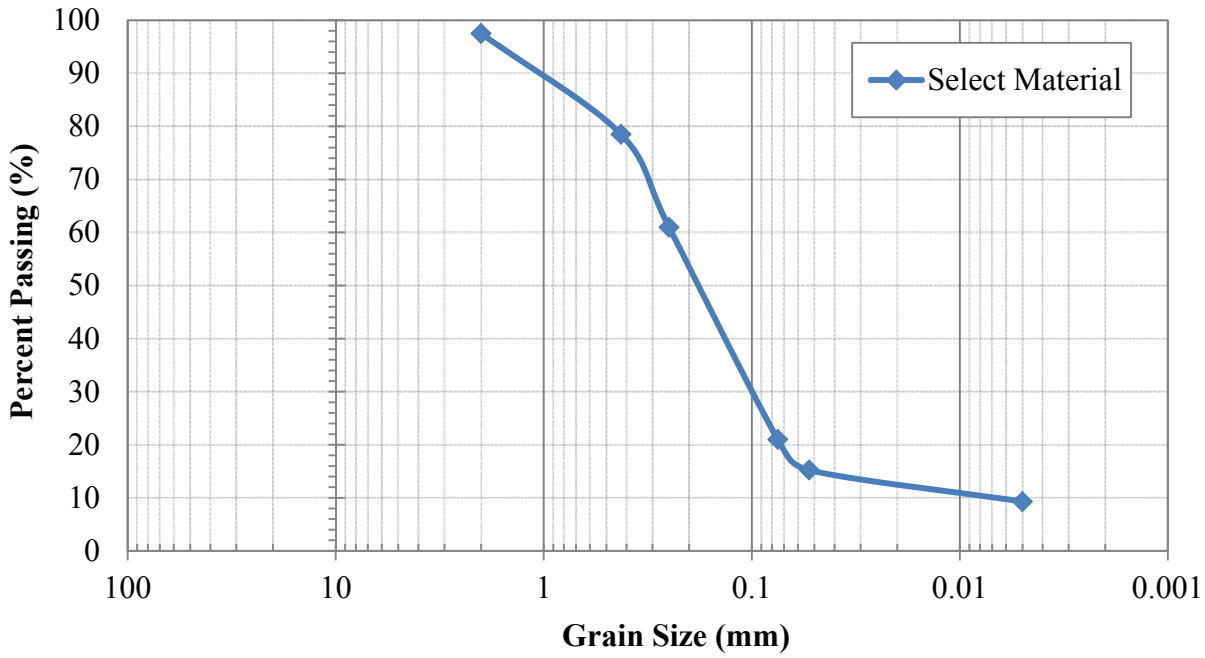

Figure 3-10: Grain size distribution curve for the select material

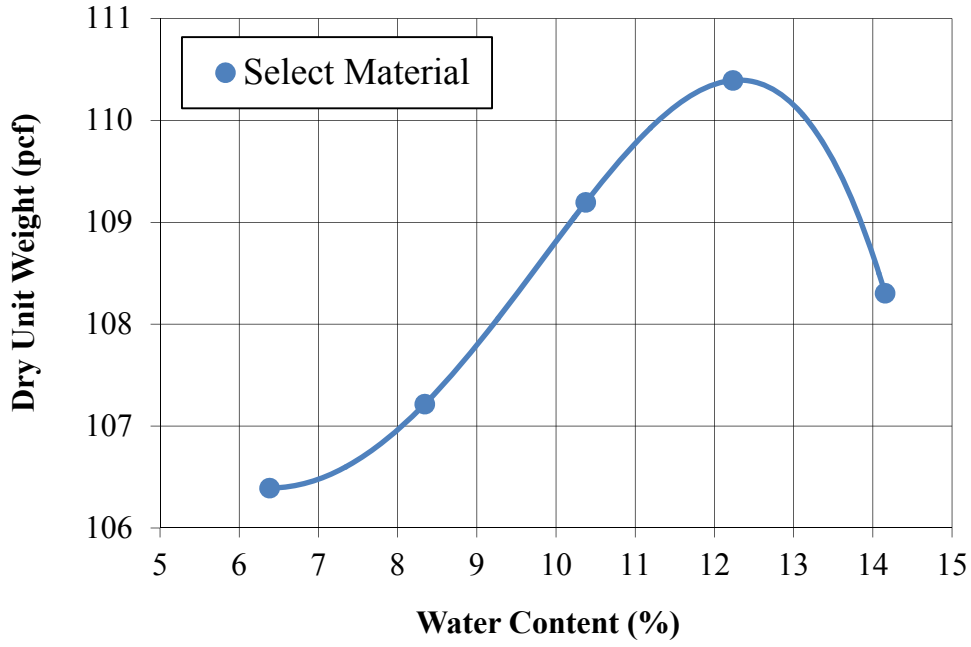

Figure 3-11: Select material standard proctor compaction results

Resilient Modulus Testing

Two resilient modulus tests were performed on the select material according to AASHTO T-307. Both specimens were identical and were compacted in five static lifts to 99% of their standard proctor density. Shown in Table 3-8 is the load sequence for the select material tests as specified by the *Long Term Pavement Performance Protocol P46* (FHWA, 1996). The results are presented in Figure 3-12 as a function of the bulk stress on a log-log plot. Both tests produced identical results that show a clear stress dependency that is typical for granular soils. The simple K- θ equation shown below was used to model the resilient modulus response:

$$\mathbf{M_r = k_1 \times \theta^{k_2}} \qquad \textbf{Eq. 3-3}$$

Where:

θ = bulk stress (psi)

Mr = resilient modulus (ksi)

k_1, k_2 = regression parameters

Table 3-8: Load sequence for resilient modulus tests on the select material

Sequence No.	Confining Pressure, S_3		Max. Axial Stress, S_{max}		Cyclic Stress, S_{cyclic}		Contact Stress, $.1S_{max}$		No. of Load Applications
	psi	kPa	psi	kPa	psi	kPa	psi	kPa	
1	3	20.7	3.3	22.5	2.8	19.1	0.5	3.4	100
2	3	20.7	6.0	41.7	5.5	38.0	0.5	3.6	100
3	3	20.7	9.1	62.6	8.3	57.0	0.8	5.6	100
4	5	34.5	5.0	34.5	4.6	31.8	0.4	2.7	100
5	5	34.5	10.1	69.3	9.2	63.4	0.9	6.0	100
6	5	34.5	15.2	104.6	13.8	95.2	1.4	9.4	100
7	10	68.9	10.0	69.2	9.2	63.5	0.8	5.7	100
8	10	68.9	20.1	138.7	18.3	126.4	1.8	12.3	100
9	10	68.9	30.2	208.3	27.5	189.3	2.8	19.0	100
10	15	103.4	10.1	69.5	9.2	63.7	0.8	5.8	100
11	15	103.4	15.0	103.8	13.8	94.9	1.3	8.8	100
12	15	103.4	30.1	207.7	27.4	189.0	2.7	18.7	100
13	20	137.9	15.0	103.7	13.8	95.0	1.3	8.7	100
14	20	137.9	20.2	139.1	18.4	126.7	1.8	12.3	100
15	20	137.9	36.1	248.9	32.8	226.2	3.3	22.7	100

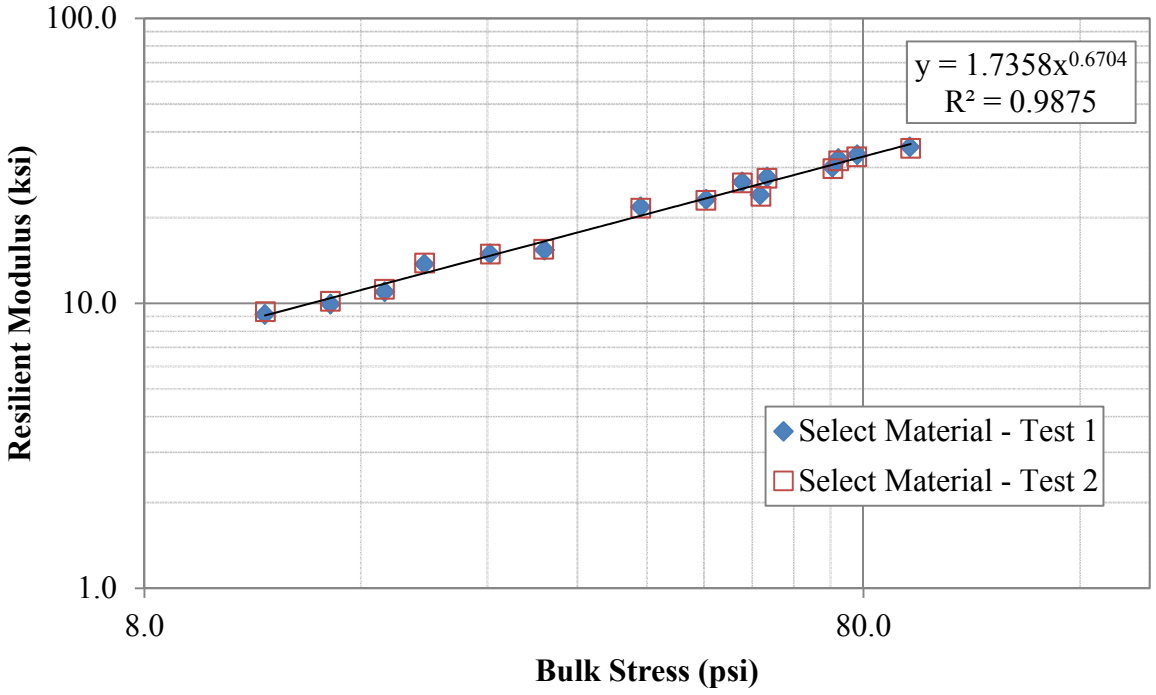

Figure 3-12: Resilient modulus test results on the select material

Aggregate Base Course (ABC)

The aggregate base course (ABC) material used for subgrade stabilization was manufactured by Martin and Marietta out of their Clarks Quarry facility in New Bern, North Carolina. Grain size distribution, Atterberg limits, modified proctor (ASTM D1577), and resilient modulus tests were performed on the ABC material. Table 3-9 presents the index properties of the ABC. The gradation curve is presented in Figure 3-13, and modified proctor compaction results are shown in Figure 3-14. Based on grain size and Atterberg limits testing the ABC material met the NCDOT specifications for aggregate stabilization. According to Unified Soil Classification System the ABC is classified as well-graded gravel with silt and sand (GW-GM) or A-1-a according to the AASHTO engineering soil classification system.

Table 3-9: ABC index properties

Soil Sample	LL	PI	Maximum Dry Unit Weight, γ_{dmax} (pcf)	Optimum Moisture Content (%)	Classification	
					USCS	AASHTO
ABC	15	NP	132.0	8.2	GW-GM	A-1-a

NOTE: NP = Non Plastic

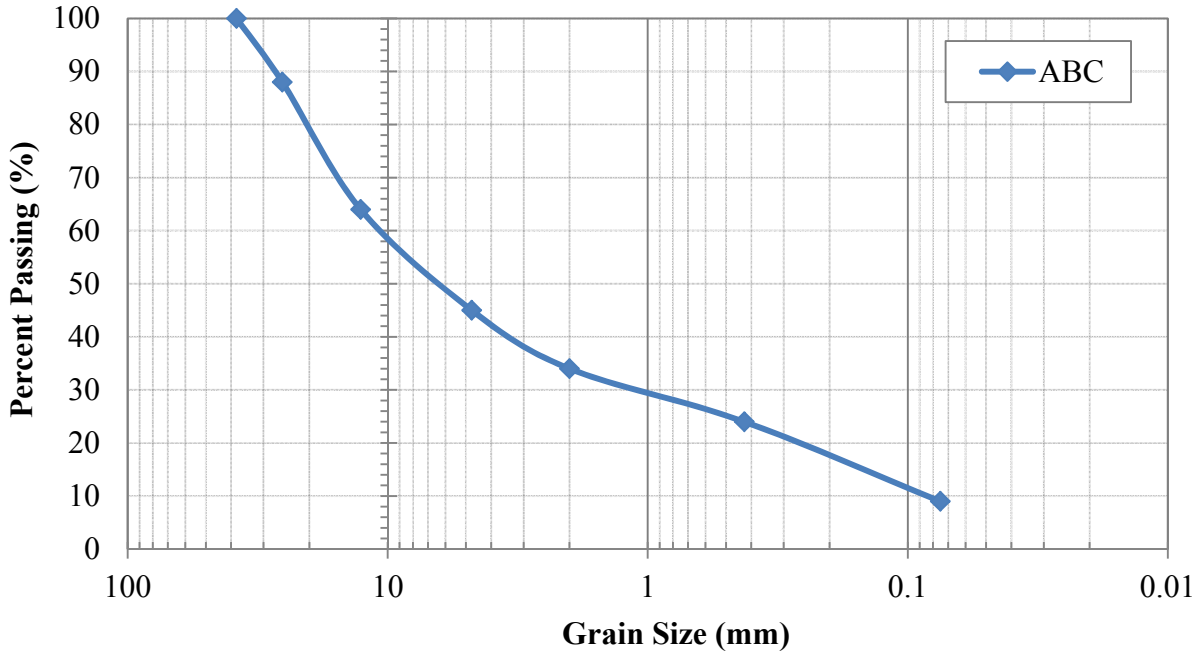

Figure 3-13: Grain size distribution curve for the ABC

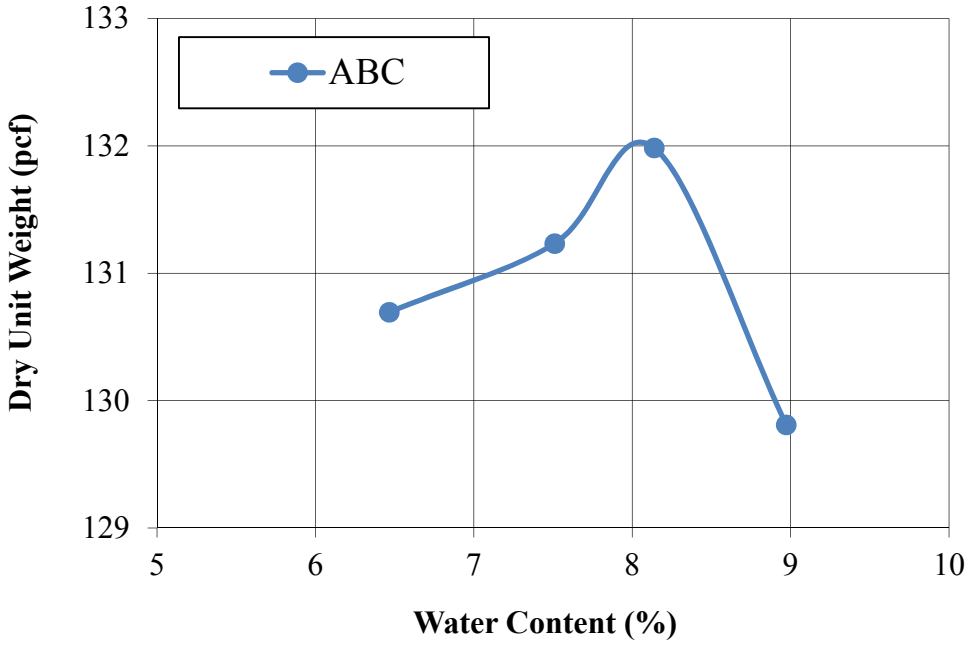

Figure 3-14: ABC modified proctor compaction results

Resilient Modulus Testing

Two resilient modulus tests were performed on the ABC inside a 6 inch by 12 inch chamber using the same load sequence used on the select material (see Table 3-8). Both specimens were compacted in five static lifts at 98% and 95% of the modified proctor compaction, respectively. Shown in Figure 3-15 are the results from the two tests. As expected, the denser specimen exhibited a higher resilient modulus at each load sequence. Once again, the K- θ equation was used to model the resilient modulus's stress dependent response for each of the ABC specimens.

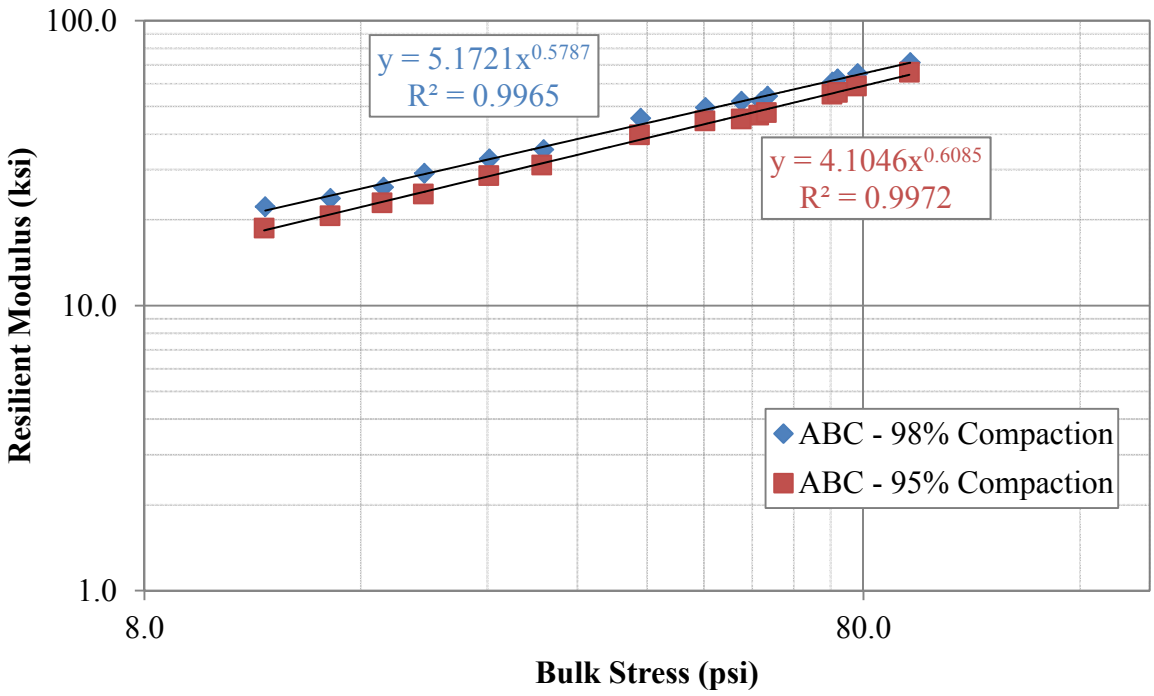

Figure 3-15: Resilient modulus test results on the ABC

Cement Stabilized Soil (CSS)

Standard proctor compaction testing

The moisture-density relationship of the soil-cement mixture was determined by performing standard proctor tests according to ASTM D558. Portland cement type I was added to bulk subgrade samples to simulate the construction of cement stabilized subgrade (CSS) in the field. The subgrade samples were taken from the top 12 inches from grade during a preliminary site visit in March, 2011. First, a single set of standard proctor compaction tests were performed on an untreated sample of the subgrade. Based on a measured maximum dry density of 108 pcf, another round of standard proctor compaction tests were performed, this time adding cement at a dosage rate of 10%. After mixing, the soil-cement mixture was immediately compacted at various water contents to assess the moisture content and dry unit weight relationship. The results are presented in Figure 3-16. Compared with the untreated sample the 10% cement treated sample exhibited a slight increase in optimum moisture content and decrease in maximum dry unit weight. This is consistent with the observations made by Sariosseiri and Muhunthan on cement-treated subgrade soils in Washington state (2009).

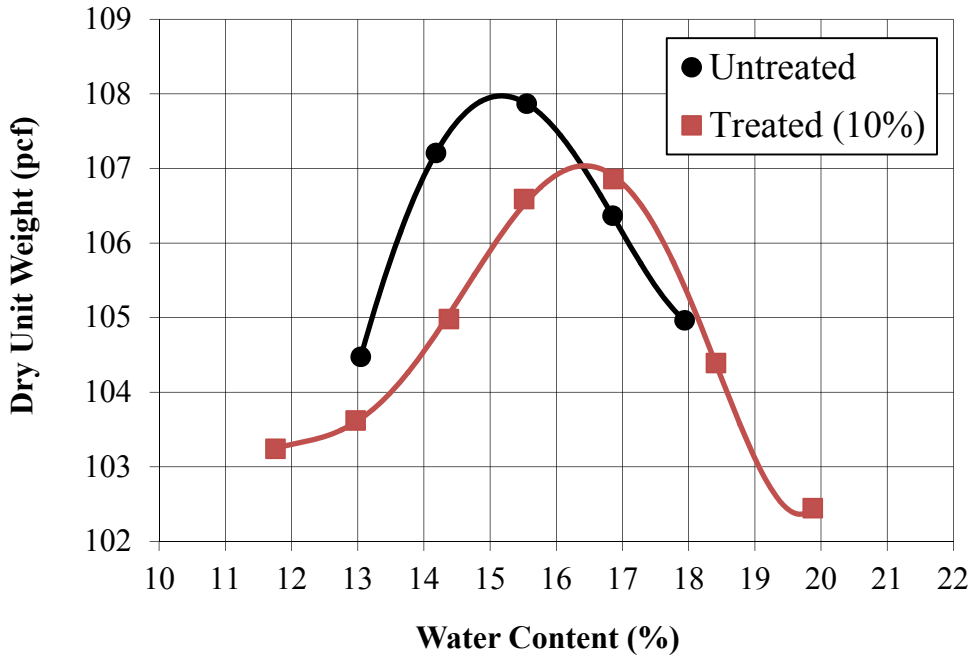

Figure 3-16: Untreated and cement treated subgrade soil standard proctor compaction test results

Unconfined Compressive Strength (UCS) Testing

Six CSS test specimens were prepared at 8, 10, and 12% cement content (2 each) and cured for 7 days for unconfined compressive strength (UCS) testing per ASTM D 2166. The results from UCS testing are shown in Table 3-10.

Table 3-10: UCS test results for cement treated subgrade soils

Cement Content (%)	UCS Test 1 (psi)	UCS Test 2 (psi)	Average UCS (psi)
8	66	74	70
10	91	98	94
12	131	143	137

Despite the relatively high cement contents, the UCS strengths are quite low for typical CSS soils. During the mixing process it was noted that the materials did not appear to mix well resulting in a final product that was somewhat immiscible (Pyo, 2011). This may have been due to the subgrades high organic content which, as mentioned in Chapter 2, is one of the soil types typically avoided with cement stabilization. When organics are present, they tend to be absorbed on the surface of the cement and non-organic soil particles due to their ability to retain high levels of moisture. Consequently, this limits the cement hydration process and hampers the interaction with the soil particles (Chen & Wang, 2006). Regardless of this observation, all test specimens provided an unconfined compressive strength of at least 50 psi, which is the goal of chemical stabilization in NCDOT field practice (Borden *et al.* 2010). To allow for some expected decrease in strength due to the lack of controls in the field versus the lab, a cement content of 12% was chosen by the NCDOT to be used when constructing Test Section 4. This was approximately twice the typical cement content used on previous NCDOT projects according to a 2010 study performed by Daniels et al. However, the projects listed in their study were primarily located in the central part of the state with the closest project being approximately 80 miles away from the field site.

Geosynthetics

One stiff biaxial geogrid and one high strength geotextile conventionally used to reinforce roads were tested at the ABC/subgrade interface. The biaxial geogrid (BX 1500) manufactured by Tensar® is integrally formed out of polypropylene and is used primarily for reinforcement. The geotextile (HP 570) manufactured by TenCate™ is made up of woven polypropylene yarns and is used to provide both reinforcement and separation. Both geosynthetics are within the NCDOT specifications for subgrade stabilization. As previously stated, the geogrid was installed in Test Section 2 and the geotextile was installed in Test Section 3. Appendix B lists the material properties provided by the manufacturers.

Instrumentation

Earth Pressure Cell (EPC)

During the course of field testing the traffic-induced subgrade stresses were recorded using a combination of 4 inch and 9 inch diameter Geokon-Model 3500 earth pressure cells (EPCs). The sensor layout is shown in Figure 3-17. Within each test section a total of four EPCs were installed at the base/subgrade interface. Three 9 inch diameter EPCs and one 4 inch diameter EPC was used in Test Sections 1 and 4 while two 9 inch diameter EPCs and two 4 inch diameter EPCs were used in Test Sections 2 and 3. The capacity of the EPCs varied between 250 kPa (36 psi) to 1000 kPa (145 psi). Refer to Appendix C for a list of the sensor capacities and their corresponding locations within the test pad.

The EPCs used in the field were of the hydraulic type, where two stainless steel plates are welded together around the rim to create a small void in the middle that is filled with de-aired hydraulic oil and connected to a semiconductor-based pressure transducer (see Figure 3-18). When a load is applied the plates compress and induce a hydraulic pressure that is measured by the transducer and converted to a voltage. This voltage can then be converted to a stress using a manufacturer provided calibration factor unique to the transducer's capacity (Geokon, 2007). This calibration factor is typically obtained by applying a known uniform fluid pressure to the EPC and recording the corresponding output. Consequently, by using this calibration factor it is assumed that the contact stress between the soil and EPC will also be uniform. However, in reality the stress is not distributed uniformly through soil (Tergazi, 1943). Rather, based on the distribution of the normal load the EPC may over- or under- register the stress for the same magnitude of applied load. In addition, soil arching can also cause the EPC to over- or under-register due to the stress redistribution that takes place depending on the relative stiffness of the EPC in relation to the surrounding soil (Wachman & Labuz, 2011). To account for these factors, the EPCs were calibrated in the laboratory under soil conditions modeled after the field. A detailed summary of the lab calibration procedure and results is provided in Appendix D.

After EPC installation was complete and the backfilling process had begun (discussed later) the readings from all 16 EPCs became very erratic. After consulting with the manufacturer, the issue appeared to be due to grounding. Based on the National Electric Code, a true earth ground requires a rod to be driven a minimum of 8-feet (Keller, 2008). However, the superintendent on

site informed the NCSU research group that only 6 feet of ground rod was installed for the temporary electrical box being used to power the data acquisition system. As a result, electrical noise coming from the overhead power lines which operate at a 60 Hz frequency intercepted the signals from the EPCs. To combat this issue a filtering option was used within the data acquisition software to filter out frequencies higher than 50 Hz. Prior to construction, it was found that when working properly (no noise) the EPCs consistently operated at a frequency range lower than 50 Hz. As a result, it was concluded that the filtering option would not influence the stress readings from the EPCs.

Before construction traffic testing the reading from EPC #3 (see Appendix C for location in the test pad) became sporadic and was eventually lost. The reason for the loss is unknown but it is believed to be random based on the fact that the 15 other EPCs worked properly throughout the duration of testing.

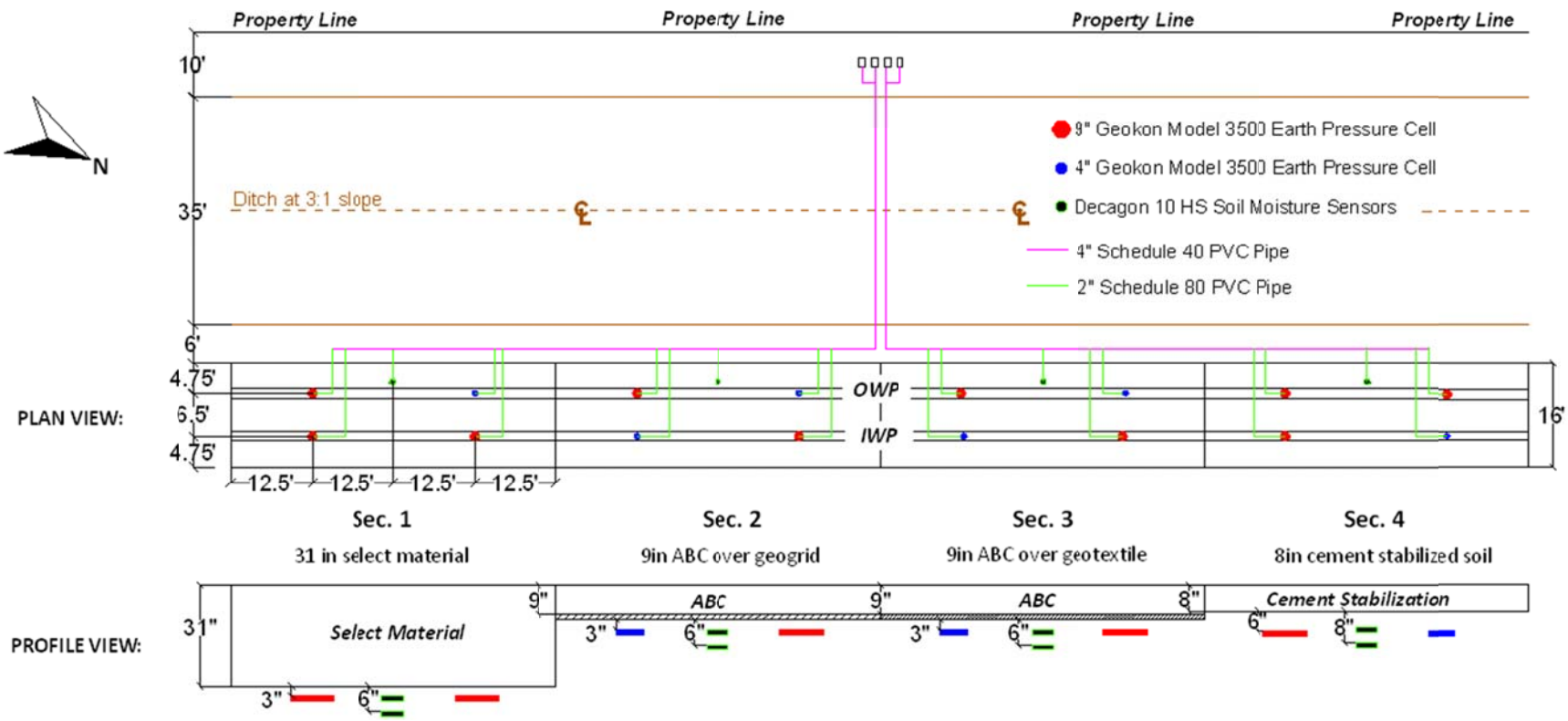

Figure 3-17: Sensor layout for the full-scale test pad

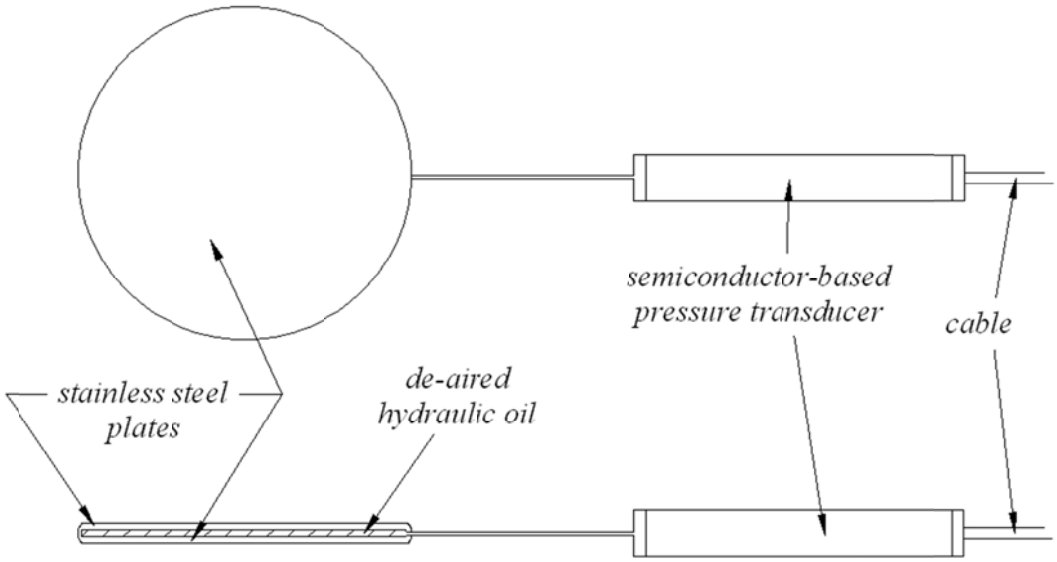

Figure 3-18: Geokon-Model 3500 Earth Pressure Cells

Soil Moisture Sensors

The volumetric water content (VWC) of the subgrade at each test section was measured using two Decagon 10HS Soil Moisture sensors (Figure 3-19). Each sensor was ten centimeters long with an 1100 cubic centimeter volume of influence. When the two probes are inserted into a mass of soil the sensor measures the dielectric permittivity of the soil using capacitance/frequency domain technology (Decagon Devices, Inc., 2010). Based on the dielectric permittivity the VWC can be determined using a manufacture provided calibration equation. However, the manufacturer notes that different soils have different soil properties (Cobos & Chambers, 2010). Thus, for the most precise results the manufacturer recommends calibrating the sensors in the lab using the soil specific to the project. Following their recommendation, the sensors were calibrated in the lab using the subgrade soil obtained from the field. A summary of the lab calibration procedure and the results is provided in Appendix E. A detailed discussion of the soil moisture sensor installation is provided later in this chapter.

Figure 3-19: Decagon 10HS Soil Moisture sensor (Decagon Devices, Inc., 2012)

Data Acquisition

Traffic-induced subgrade stresses measured from the EPCs were recorded using a control system from Vishay Micro-Measurements®. The control box housed a voltage calibration card, two analog input cards, a scanner card, a high level card, and a strain gauge card. This provided 16 useable channels for data acquisition, which were occupied by the 16 EPCs. Data were fed into a laptop computer with StrainSmart© software for recording. A sampling rate of 1000 readings per second was employed in conjunction with the filtering option previously mentioned to remove electrical noise coming from the overhead power lines.

The volumetric water content of the subgrade at each test pad was monitored using two EM 50 data loggers. Each data logger was a self-contained unit that provided five ports of which four were used (two ports per test section). During full-scale testing the soil moisture sensors were set to record the volumetric water content of the subgrade every five minutes. Prior to and after full-scale testing the number of measurements was scaled back to every two hours. After testing was complete the data were downloaded using a laptop computer with Decagon's ECH_2O Utility software. A picture of the data acquisition systems used at the field site is shown in Figure 3-20.

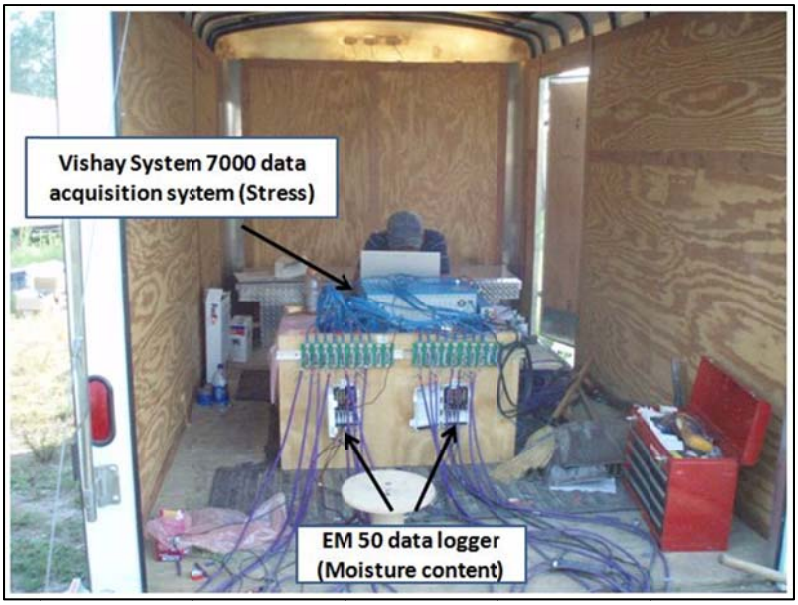

Figure 3-20: Data acquisition systems used to measure stress and moisture content

Test Pad Construction

The construction of the test pad was performed in coordination with both the NCDOT and the site contractor, Barnhill Contracting Company. A discussion of each phase in the construction process is provided below.

Undercutting

The construction of test pads began on May 23, 2011 with the undercutting of the three 50-foot long by 16-foot wide sections beginning at station 121+00 and ending at station 122+50. As mentioned previously, Test Section 1 was undercut 31 inches (790 mm) while Test Section 2 and 3 were each undercut 9 inches (230 mm). Shown in Figure 3-21 is an image of the three undercut sections as well as Test Section 4 (cement stabilized soil) which was constructed at a later date. All undercutting was performed in accordance with Section 225 of the NCDOT *Standard Specifications* (2012).

Figure 3-21: Test Sections 1, 2, and 3 undercut to their respective depths

Sensor Installation

After undercutting was complete, ground profile scanning was performed (discussed later) and the locations of the 16 EPCs were surveyed to ensure their installation was precisely within the wheel path of the test pad (white flags shown in Figure 3-21). At the location of each sensor a trench 18-inches wide by approximately 6-inches deep was dug so that the sensor cables ran perpendicular to the wheel path and out to the shoulder of the roadway (see Figure 3-17 for a sketch of the sensor layout). Trenches were also dug in Section 4 to a depth of approximately 16 inches in order to install the sensors prior to cement mixing. All digging was performed using a rubber-tired backhoe shown in Figure 3-22.

Figure 3-22: Digging trenches for sensor installation in Test Section 1

Once the trenches were completed a hole 15 inches in diameter by 6 inches deep was excavated at the location of each EPC. The center of the hole was aligned directly with the centerline of the wheel path. Inside the hole a three inch thick layer of compacted ASTM fine-graded silica sand was placed and compacted to avoid damaging the EPC from aggregate and roots in the immediate vicinity. Once the sand was in place, the EPCs were positioned parallel to the wheel path and leveled, as shown in Figure 3-23. After checking each EPC for functionality, an additional two inch layer of sand and three inch layer of subgrade material was hand compacted

on top of the EPC to prevent damage from above. After this was completed in Test Section 4, the hole was backfilled using a shovel with the same material that was dug out to install the EPCs. It is important to note that in Test Sections 1, 2, and 3 the EPCs were installed approximately 3 inches below the subgrade/base interface. However, in Section 4 the EPC's were installed approximately 6 inches below the subgrade/base interface to avoid damage from the rotating mixers when constructing the cement stabilized layer.

Figure 3-23: EPC installation in Test Section 1

Two Decagon 10HS Soil Moisture sensors were installed in the center of each test section near the outer wheel path. To prevent damaging the sensors during installation, a blade slightly thinner than the moisture sensor was pushed into the undisturbed subgrade to create a small opening. After removing the blade the sensor was carefully inserted making sure that the probes were in direct contact with the soil. In Test Sections 1, 2, and 3 the first sensor was installed

horizontally into the sidewall of the undisturbed subgrade at a depth of three inches below the undercut elevation. The second sensor was installed vertically into the undisturbed subgrade at a depth of six inches below the undercut elevation. Like the EPCs, the moisture sensors in Test Section 4 were installed six inches horizontally and eight inches vertically below the subgrade/base interface out of precaution from damage during the cement stabilized layer construction. Shown in Figure 3-24 is the installation of the soil moisture sensors for Test Sections 1 and 2.

Figure 3-24: Moisture sensors installed (left) in Test Section 1 and (right) in Test Section 2

To protect the sensor cables located in the roadway each cable was enclosed in a two inch schedule 80 PVC pipe. Once reaching the shoulder the cables were joined together within a four inch schedule 40 PVC pipe that ran parallel to the roadway and to the center of the test area (see Figure 3-25). At the center of the test area the PVC and enclosed sensor cables were routed across the ditch to allow for safe access away from the road. In addition, four vault boxes were installed on the opposite side of the ditch to provide storage for all sensor cables when not in use. The EM 50 data loggers were also installed in the vault boxes and connected to the soil moisture sensor cables to collect the volumetric water content data.

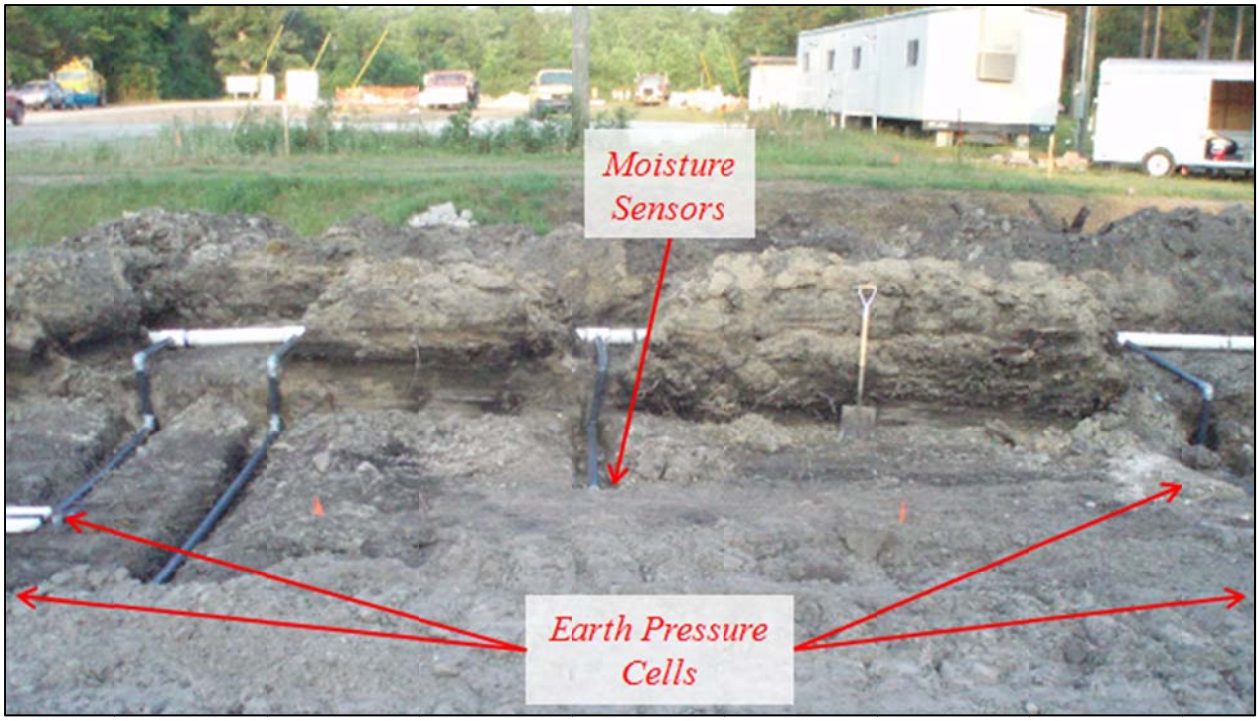

Figure 3-25: Sensor and PVC installation

Geosynthetic Installation

Prior to backfilling, the contractor installed Tensar's® BX 1500 biaxial geogrid in Test Section 2 and TenCate's™ HP 570 geotextile in Test Section 3 in accordance with Section 270 of the NCDOT *Standard Specifications* (2012). Each material was delivered in 16 foot wide rolls that were unrolled in the direction of travel with the machine direction parallel to the traffic pattern. The geosynthetics were cut and overlapped approximately two feet at the interface of the test sections and were pulled tight to minimize the amount of deformation required to mobilize the geosynthetic tensile strength. Several wire staples were used around the perimeter of the geosynthetics in order to hold it in place during backfilling. An image of the geosynthetics installed just prior to fill placement is shown in Figure 3-26.

Figure 3-26: The geogrid installed in Test Section 2 and the geotextile installed in Test Section 3

Backfilling and Compaction

Test Sections 1, 2, and 3 were each partially backfilled on May 26, 2011 under the supervision of NCDOT inspectors. Test Section 1 was backfilled first with the class II/type 2 select material that was placed in approximately two 12 inch lifts using an excavator as shown at the top of Figure 3-26. Once the select material had been placed it was compacted using a steel drum vibratory roller. After the contractor finished compacting the second 12 inch lift, ABC stone (Class IV) was dumped in Test Section 2 by driving the dump truck over Test Section 1 and unloading it directly onto the geogrid. The material was then spread and roughly leveled to a thickness of approximately six inches using an excavator positioned on the side of the test pad. As each truck load of ABC stone was dumped and leveled, the vibratory roller progressively moved forward over the test pad to compact the stone and provide a platform for the dump trucks to drive on (see Figure 3-27). Rather than dumping the backfill material from the side of the test pad, it was recommended by the TenCate^{TM} representative to slowly back the dump trucks over the areas with sufficient cover in order to unload the backfill material onto the exposed geosynthetics (Dull, 2011). This allows the geosynthetics to be pre-tensioned prior to trafficking in order to reduce the amount of initial rutting needed to mobilize their tensile strength. Due to a

lack of time at the end of the workweek, the test sections were only partially backfilled on May 26, 2011. The remaining backfill was placed on June 8, 2011 under the supervision of the NCDOT inspectors. After the last lift had been placed a series of quality control tests were performed on the each test section. A discussion of these tests is provided later in the chapter.

Figure 3-27: Compacting Test Sections 1 and 2 using a steel drum vibratory roller

Cement Stabilized Subgrade (CSS) Construction

On June 1, 2011 Site-Prep, Inc. of North Carolina constructed Test Section 4 in accordance with Section 542 of the NCDOT *Standard Specifications* (2012). Portland Type I/II cement (ASTM C150) provided by Lehigh Hanson was used to construct the test section. The area was first prepared by grading, leveling, and wetting the subgrade soil. Afterwards, the cement coverage area was marked off based on a 12% cement content or 77 pounds per square yard to a depth of 8 inches. As previously mentioned, this mix design was selected by the NCDOT using the UCS lab results on the cement-subgrade specimens. It is important to note that the dry cement was

spread using a tanker truck equipped with a deflector that drops the cement out of the back and onto the ground (see Figure 3-28). This method of spreading does not allow the operator to adjust the rate of flow. Consequently, the area of the cement coverage must be pre-determined and monitored in conjunction with emptying the truck in order to verify uniformity. Based on a total cement weight in the tanker of approximately 8100 lbs. it was determined that a coverage area of 946.8 square feet was required to provide a cement content of 12% within the top 8 inches of subgrade soil. Since the test section was 16 feet wide, the cement was spread over 59.2 linear feet of roadway starting at the interface of Test Section 3 and 4 (Station 122+50) and ending 9.2 feet pass the designated end of Test Section 4 (Station 123+9.2). In order to spread the cement evenly throughout the test section the operator made two consecutive passes with the first pass running alongside the shoulder of the roadway and the second pass running adjacent to the centerline of the road.

Figure 3-28: Spreading the cement in Test Section 4

After spreading was complete, the cement was mixed into the top eight inches of subgrade soil using a soil stabilizer shown in Figure 3-29. During this process any roots and debris observed in the soil-cement mixture were removed. Once the NCDOT inspector believed a homogenous and uniform mixture was produced, a sample was obtained to measure the moisture content and to verify it was within plus or minus two percent of optimum. After this was confirmed, the test section was compacted using a vibratory steel drum roller. The entire process took less than two hours from when the cement was spread to final compaction. Once the section was verified to have been compacted to greater than 97% of the maximum dry density using the rubber balloon method (discussed later), the contractor rewet the test pad and covered it with a plastic tarp to allow the soil-cement to cure for seven days. The plastic tarp was used as a replacement of the typical asphalt seal sprayed on top to keep the stabilized layer moist. Periodically during the curing process the contractor removed the tarp and rewetted the sections to prevent the surface from drying out (Simmons, 2011).

Figure 3-29: The soil stabilizer mixing the cement into the top 8 inches of subgrade soil

Quality Control Testing

After constructing each test section, quality control tests were performed by the NCDOT to ensure the constructed base layer met the density and moisture content requirements specified in the NCDOT *Standard Specifications* (2012). This section describes the two test methods that were conducted on the test pad.

Nuclear Moisture-Density Gauge

Soil moisture and density on the post-compacted ABC in Test Sections 2 and 3 were measured using a Troxler® Model 3440 nuclear moisture-density gauge (nuclear gauge). A total of five tests were performed within each test section using the direct transmission mode at a rod depth of six inches. An average dry density of at least 92% of the AASHTO T180 was required to pass quality control testing.

Rubber Balloon

Rubber Balloon density tests were performed in Test Sections 1 and 4 after compaction according to ASTM D2167. One test was performed after the last lift of select material in Test Section 1 while two tests were performed on the soil-cement base layer in Test Section 4. Water content was also measured during each test in Test Section 4. The select material in Test Section 1 required a dry density of 100% at a water content which is capable of producing the maximum dry density. A density of at least 97% was required by the NCDOT to pass compaction on the soil-cement base layer. In addition, the moisture content of the soil-cement mixture was required to be within plus or minus 2% of optimum. Figure 3-30 shows a NCDOT inspector performing a rubber balloon density test on Test Section 4.

Figure 3-30: Rubber Balloon testing in Test Section 4

In Situ Testing

At various stages throughout the project a number of in situ tests were performed on the test pad to obtain strength and modulus data of both the subgrade and base layer materials. A description of each test method is presented in this section.

Dynamic Cone Penetrometer (DCP)

Dynamic cone penetrometer (DCP) testing was performed during the following five stages of the project: (1) prior to undercutting, (2) after undercutting, (3) prior full-scale testing, (4) after repair of Test Section 1, (5) and after full-scale testing.

The DCP is used by lifting and releasing a hammer from a standard drop height onto an anvil which drives a cone tipped rod into the ground. Prior to beginning the test a wooden stake is positioned next to the DCP and a mark is made where the stake crosses the DCPs horizontal handle. After each drop of the hammer another mark is made on the wooden stake using the same horizontal handle as the point of reference. After the test is completed the distance between marks can be measured to determine the distance of penetration per blow (mm/blow) or DCP Index (DCPI). Testing was performed according to ASTM D6951 using a hammer weight of 8 kg (17.6 lbs.), a drop height of 576 mm (22.6 inches), a drive rod with a diameter of 16 mm (5/8 inch), and a cone tip angle of 60 degrees. A typical test is shown in Figure 3-31.

Figure 3-31: DCP testing prior to full-scale testing

Soil Stiffness Gauge (SSG)

A soil stiffness gauge (SSG) was used in accordance with ASTM D6758 to measure the small-strain stiffness of the base layer materials prior to and after construction traffic testing. The SSG, which is commercially known as the Humboldt GeoGauge™, is a hand-portable instrument that is cylindrical in shape and weighs approximately 22 lbs. At the base of the device a 3.5 inch diameter ring-shaped foot applies a small dynamic force at 25 steady state frequencies between 100 and 196 Hz and measures the resulting ground displacements. The soil stiffness is then determined at each frequency and averaged to obtain a single stiffness measurement. Stiffness is defined as the force required to produce a unit of elongation. Based on the measured stiffness, the soil elastic modulus can be determined using the following equation (Humboldt Mfg. Co., 2007):

$$\mathbf{E_{SSG}} = \mathbf{k_{SSG}} \frac{(1-\nu^2)}{1.77R} \qquad \textbf{Eq. 3-4}$$

Where:

E_{SSG} = SSG Soil Modulus (MPa)

K_{SSG} = SSG Soil Stiffness (MN/m)

ν = Poisson's Ratio (assumed .35)

R = Radius of the GeoGauge Foot (57.15 mm = 2.25 inches)

SSG testing was performed within each section at the center of both wheel paths. Prior to performing a test, the base layer surface was swept using a brush to remove any loose material. Next, a small sample of moist ASTM silica sand was placed and patted down to create a thin layer approximately $^1/_8$ to $^1/_4$ inch thick. The SSG was then placed on top of the sand and rotated $^1/_4$ of a revolution, as recommended by the manufacturer (Humboldt Mfg. Co., 2007). To verify precision, three tests were run per test location with the mean stiffness used as the reported value. Shown in Figure 3-32 is a typical SSG test being performed prior to full-scale testing.

Figure 3-32: SSG test being performed prior to full-scale testing

Falling Weight Deflectometer (FWD)

The load-displacement behavior of the constructed sections was measured by performing a series of Falling Weight Deflectometer (FWD) tests using a trailer-mounted Dynatest Model 8000 FWD. An FWD device consists of a subassembly that houses several weights stacked one on top of another. To begin a test the weights are hydraulically lifted to a specified height along guide bars mounted inside the subassembly. The weights are then dropped vertically by gravity onto a spring loaded plate that rests on the ground surface. The applied load is recorded using a calibrated load cell. In addition, several geophones are mounted along the trailer frame to measure the peak deflection due to the applied load (Dynatest Engineering, 1995). The FWD device used during field testing is shown in Figure 3-33. Three drops were performed at each test location at load levels' ranging between approximately 5 and 13 kips. Seven geophone sensors were spaced as follows: 0, 12, 18, 24, 36, 48, and 60 inches away from the center of the load plate. Prior to construction traffic testing an 18 inch load plate was used for FWD testing. However, due to issues with the software, FWD testing after construction traffic was performed using a 12 inch rather than 18 inch load plate. All FWD tests were performed according to ASTM D4694.

Figure 3-33: FWD testing performed after full-scale testing

Static Plate Load Testing (SPL)

As an additional measure of moduli, static plate load (SPL) tests were performed within each test section prior to truck loading. A truck mounted drilling rig was used to apply four load-unload cycles through a 12 inch diameter, $^{3}/_{4}$ inch thick steel plate onto the ground surface. The applied load was recorded using a calibrated load cell. Each test was conducted to a maximum load of approximately 40 psi to avoid preloading the test sections prior to full-scale testing. As the load was applied two dial gauges positioned on opposite sides of the plate measured the deflection. The dial gauges were mounted to a deflection beam with two supports located approximately 18 inches away from the center of the beam. At the time of testing no one on site recognized that the deflection beam supports were possibly located within the load-induced displacement area. According to ASTM D1195, the supports should be located at least eight feet from the circumference of the bearing plate. With this in mind, it was unknown if the measured deflections were accurate. To assess this problem a numerical analysis was performed that looked at the possible error involved with the SPL test data. The results from this analysis are provided in Appendix F. Based on the results, the possible error was too great to justify using the results as a measure of in situ modulus. Thus, the data from SPL testing is not presented is this report.

Full-Scale Testing

Full-scale testing was performed on the test pad to monitor the performance of each stabilization measure in terms of induced rutting and peak stress at the base/subgrade interface under repeated truck loading. This section describes the details of the full-scale procedure.

Truck Loading

A loaded tandem axle dump truck, shown in Figure 3-34, was used as the test vehicle for the application of field loading. The truck's layout consisted of one front axle, two drop axles, and two rear powered axles supporting dual wheels on each side. The drop axles were never used to bear any load and can be disregarded. The dump truck tire configuration and dimensions are provided in Appendix G. A total of ten load-bearing tires were on the dump truck with two on the front axle and four tires per rear axle. The tire pressure for all ten tires was set to 85 psi prior to testing and was rechecked periodically. Due to the changes in the ambient temperature as well as heat buildup from long periods of driving, the tire pressure fluctuated between approximately 75 and 95 psi. Prior to testing, the dump truck was loaded with ABC and weighted using a certified truck scale. Due to the close proximity of the rear axles, the combined rather than individual axle weight was measured. The front and combined back axles weighed 17,180 lbs. and 42,000 lbs., respectively. Assuming the load in the front and back axles was distributed evenly among all the tires, each front tire had an applied load of 8590 lbs. while each set of dual back tires had an applied load of 10500 lbs. (5250 lbs. per back tire).

On each side of the test pad the contractor provided a turn-around so that the test vehicle was always driven forward over the test sections. In addition, approximately 100 to 200 feet of constructed roadway was used on each side of the test pad to allow the truck to reach a constant rate of speed between 8 and 12 mph before entering the test sections. During testing the vehicle was first driven forward over the test pad in the North direction to make one pass. Once reaching the end of Test Section 4 the driver turned around and drove the truck back over the test pad in the South direction to complete two passes. A total of 1000 consecutive passes were conducted on the test pad within approximately the same wheel path over a period of four days. Orange construction spray paint was use to mark the location of the sensors to help the driver align the truck tires directly with the EPCs. Throughout testing the vehicle was driven by four

different operators with various levels of truck driving experience. The drivers will be referred to as Driver 1 for the first driver, Driver 2 for the second driver, and so on.

Figure 3-34: Dump truck used for construction traffic testing

Ground Profile Surveying (LiDAR)

To track the development of rutting in each test section a high definition ground profile survey was performed on the test pad after truck passes 1, 5, 10, 50, 100, 200, 300, 500, 700, 900, and 1000. After 200 truck passes, Test Section 1 showed excessive rutting that was repaired by leveling and rolling the select material and adding a two to three inch layer of ABC (discussed later). Thus, in addition to the intervals used for the other sections, a ground profile survey was also conducted on Test Section 1 after truck pass 210.

High definition ground profile surveying was performed using a Leica ScanStation C10 equipped with terrestrial light detection and ranging technology (LiDAR). LiDAR scanners such as the Leica ScanStation C10 emit an infrared light that is reflected off a distant object and detected by the scanner. A sensor can then determine the time from when the light was emitted to when it was reflected (time of flight). After the time of flight has been determined the distance from the scanner to the object can easily be computed using the following equation:

Eq. 3-5

Based on this distance and the angle at which the light was emitted, the scanner can determine the XYZ position of the reflected object. This process is performed at a maximum instantaneous rate of 50,000 data points per second with the scanner emitting light off of a vertically spinning mirror while the base of the unit slowly rotates 360 degrees horizontally. One scan takes approximately 20 minutes to perform. After the scan is complete, the XYZ coordinates of

millions of points are stored to create a point cloud. The degree of accuracy for measurements less than 50 meters away is provided in Table 3-11 (Flippin, 2012).

Table 3-11: The accuracy of one measurement made by the Leica ScanStation C10

	Units	Precision
Position	in (mm)	.24 (6)
Distance	in (mm)	.16 (4)
Angle (Hori./Vert.)	arc seconds (degrees)	12/12 (.003/.003)

In general, closer objects tend to give a higher reflection and more accuracy than an object farther away (FHWA, 2008). To combat this issue, two scans were performed with the first positioned at the interface of Test Sections 1 and 2 and the second at the interface of Test Sections 3 and 4. The data was then processed using Leica Cyclone 7.1.3 software and the two point clouds were meshed together to create a single, accurate point cloud of the test pad. As an example, refer to Figure 3-35 for the point cloud created from the LiDAR scans after Test Section 1, 2, and 3 had been undercut. The different colors represent different levels of elevation within the test pad.

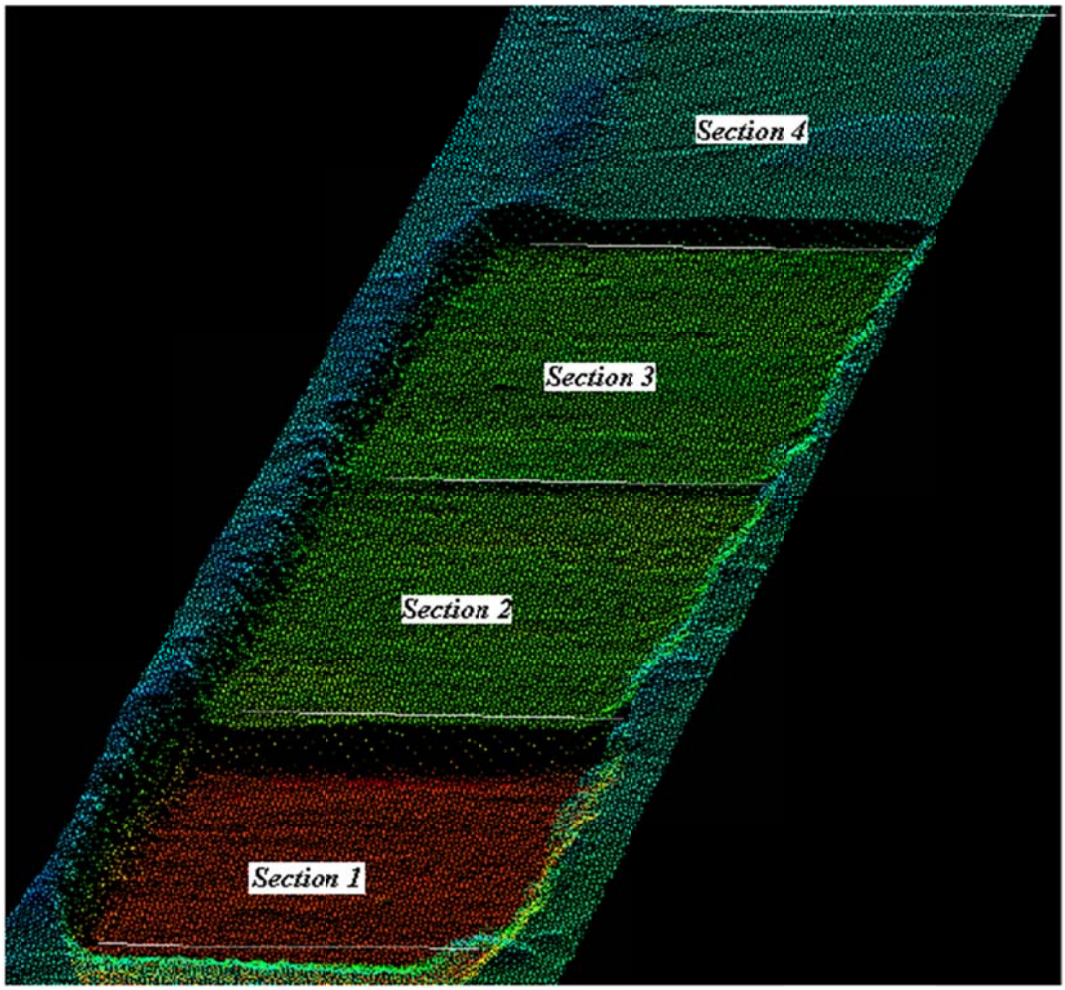

Figure 3-35: Point cloud of the test pad after undercutting Test Sections 1, 2 and 3

Proof Roll Loading

After full-scale testing was completed, each section was leveled and lightly re-compacted, under the guidance of the NCDOT, with approximately one to two passes using a vibratory steel drum roller (Simmons, 2011). A month later on August 4, 2011 proof rolling was performed on the repaired sections in accordance with Section 260 of the NCDOT *Standard Specifications* (2012). A bulldozer pulling a loaded single axle, four wheeled proof roll trailer conforming to the NCDOT specifications was used to perform two proof rolling tests at gross loaded weights of 35 and 50 tons, respectively (see Figure 3-36). For each gross loaded weight the proof roll trailer was towed twice, once in each direction, in the wheel paths at a speed of approximately 1 to 2.5 miles per hour. As the tires traveled over each section, two NCDOT inspectors visually monitored each wheel path for signs of recovered (pumping) and permanent (rutting)

deformation. A profile survey was performed prior to proof-rolling, after the 35 ton proof roll, and after the 50 ton proof-roll.

Figure 3-36: Proof rolling performed with 35 ton proof roller

CHAPTER 4: QUALITY CONTROL AND IN SITU TEST RESULTS

This chapter presents the results from quality control and in situ field tests performed at various stages of the project. All quality control tests were conducted in accordance with the NCDOT specifications by certified NCDOT inspectors. In situ tests were conducted by the NCSU research group along with the help of the NCDOT.

Quality Control Testing

After the test pad was constructed, the NCDOT performed quality control tests as required to assess the as-built density and water content of each test section. Shown in Table 4-12 are the final results from these tests. The relative density (D_R) is based on a maximum dry unit weight of 110.4 pcf for the select material, 132.0 pcf for the ABC, and 107.0 pcf for the soil-cement. The NCDOT relative density requirements for select material, ABC, and soil-cement are 100%, 92%, and 97%, respectively. The NCDOT did not test the water content of the select material. To verify density of the select material the inspector compared the bulk rather than dry density. The dry density shown in Table 4-12 for Test Section 1 is an estimate based on the relative bulk density and maximum dry density of the select material.

Table 4-12: Base course quality control testing results

Test Section	Test Method	γ_d (pcf)			w (%)			Number of Tests	Relative Density, D_R (%)	+ / - Optimum (%)
		Avg.	σ	C_V	Avg.	σ	C_V			
1	Balloon	≈113	n/a	n/a	-	n/a	n/a	1	102.2	-
2	Nuclear	127.8	1.2	0.01	8.1	1.2	0.15	5	96.8	0.0
3	Nuclear	126.5	0.9	0.01	8.62	0.6	0.07	5	95.8	+ .5
4	Balloon	106.9	1.4	0.01	18.5	1.1	0.06	2	99.9	+ 2.0

NOTE: - = Test not performed

Dynamic Cone Penetrometer (DCP)

DCP Data Analysis

When analyzing DCP data it must be interpreted to obtain a representative value of DCPI within each tested soil layer. In this study, a weighted average of DCPI was calculated using the following equation:

$$\mathbf{DCPI_{wt.\ avg.}} = \frac{\mathbf{1}}{\mathbf{H}}\sum_{\mathbf{i}}^{\mathbf{N}}(\mathbf{DCPI_i} \times \boldsymbol{z_i}) \qquad \textbf{Eq. 4-6}$$

Where:

z = Depth of penetration per blow (mm)

H = Total depth of the soil layer (mm)

A weighted average of DCPI was preferred over an arithmetic average based on the work performed by Allbright (2002) who reported that the weighted average DCPI produces a narrower standard deviation for the representative soil layer and also provides better correlations with other field tests.

When performing DCP tests on a layered profile there is typically a transition zone between adjacent layers making it difficult to establish the interface location. ASTM D6951 recommends plotting the cumulative blows as a function of depth and drawing lines that represent the average slope within each layer. The depth at which adjacent soil layer lines intersect is then defined as the interface. This approach was followed in this study to determine subgrade layer thicknesses and calculate the weighted average DCPI. As an example, Figure 4-37 demonstrates this process using field data performed on the subgrade at station 121+50 prior to undercutting. Based on the results, there is a layer interface located at approximately 450 mm (18 inches) below the ground surface.

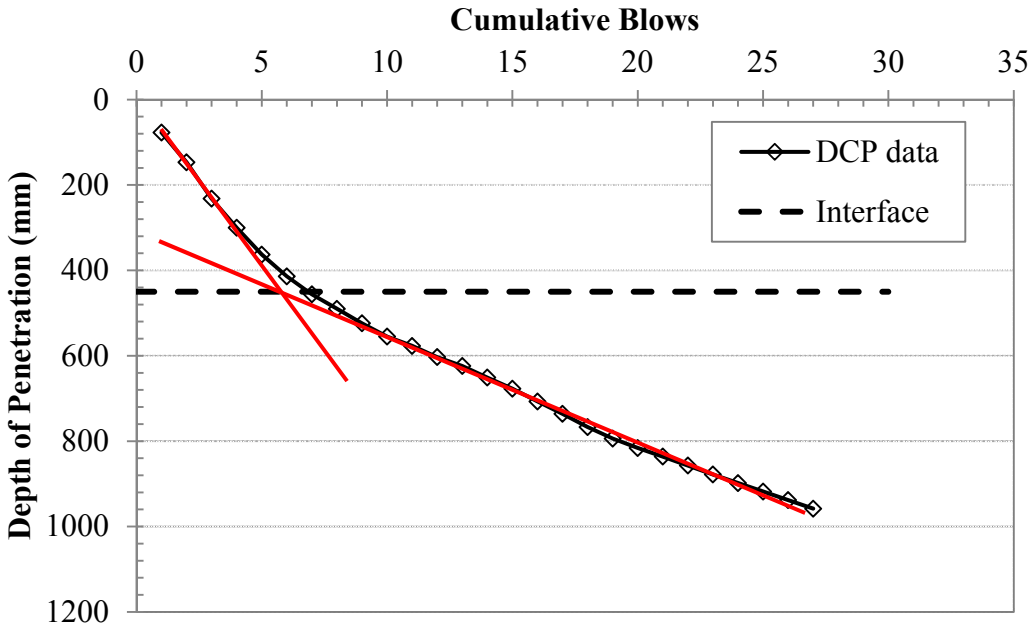

Figure 4-37: An illustration of how the interface of adjacent layers were defined

DCP Test Results

Prior to Undercutting

On February 23, 2011, a site visit was made to perform DCP measurements on the subgrade soils prior to undercutting. Shown in Figure 4-39 is a diagram of the test locations. The results are presented in Table 4-13 and plotted in Figure 4-38. Wainaina's (2006) undercut criterion, based on a DCPI of 38 mm/blow, is also shown in the figure with the region below the criteria shaded in pink. Estimated CBR and resilient modulus values are also provided in the table. CBR values are based on the following NCDOT recommended correlation equation (NCDOT, 1998):

$$\mathbf{CBR}\ (\%) = \mathbf{2.60 - 1.07 \times \log(DCPI)} \qquad \textbf{Eq. 4-7}$$

Resilient modulus values are based on the direct model developed by Herath *et al.* (2005):

$$\mathbf{M_r(MPa) = 16.28 + 928.24/DCPI} \qquad \textbf{Eq. 4-8}$$

In general, the weighted average DCPI of the top two feet of subgrade soil was found to be in excess of 38 mm/blow. Based on is observation, the NCDOT's current DCPI cut-off of 38 mm/blow was supported by field observations, and would yield a required CBR value of greater

than 5-8% or resilient modulus values greater than approximately 6 ksi (40 MPa). It should be noted, however, that the subgrade during testing appeared to be overly wet due to previous rainfall.

Table 4-13: DCP test results on subgrade soil prior to undercutting

Station	IWP/OWP	Depth From Grade (in)		Wt. Avg. DCPI	σ	C_V	N	Estimated CBR[1] (%)	Estimated M_r[2] (ksi)
		Min	Max	(mm/blow)					
121+50	OWP	0	39	46	11.2	0.24	23	6.6	5.3
	IWP	0	40	54	12.1	0.22	20	5.6	4.9
122+00	OWP	0	27	60	16.3	0.27	11	5.0	4.6
		27	36	14	2.1	0.15	16	23.4	11.9
	IWP	0	10	136	20.0	0.15	2	2.1	3.4
		10	23	47	10.3	0.22	10	6.4	5.2
		23	35	21	2.0	0.10	12	15.2	8.7
123+00	OWP	0	38	64	9.0	0.14	11	4.6	4.5
	IWP	0	18	68	13.7	0.20	7	4.4	4.3
		18	38	26	4.9	0.19	20	12.2	7.5

[1]CBR is based on NCDOT (1998)

[2]Resilient modulus is based on direct model developed by Herath *et al.* (2005)

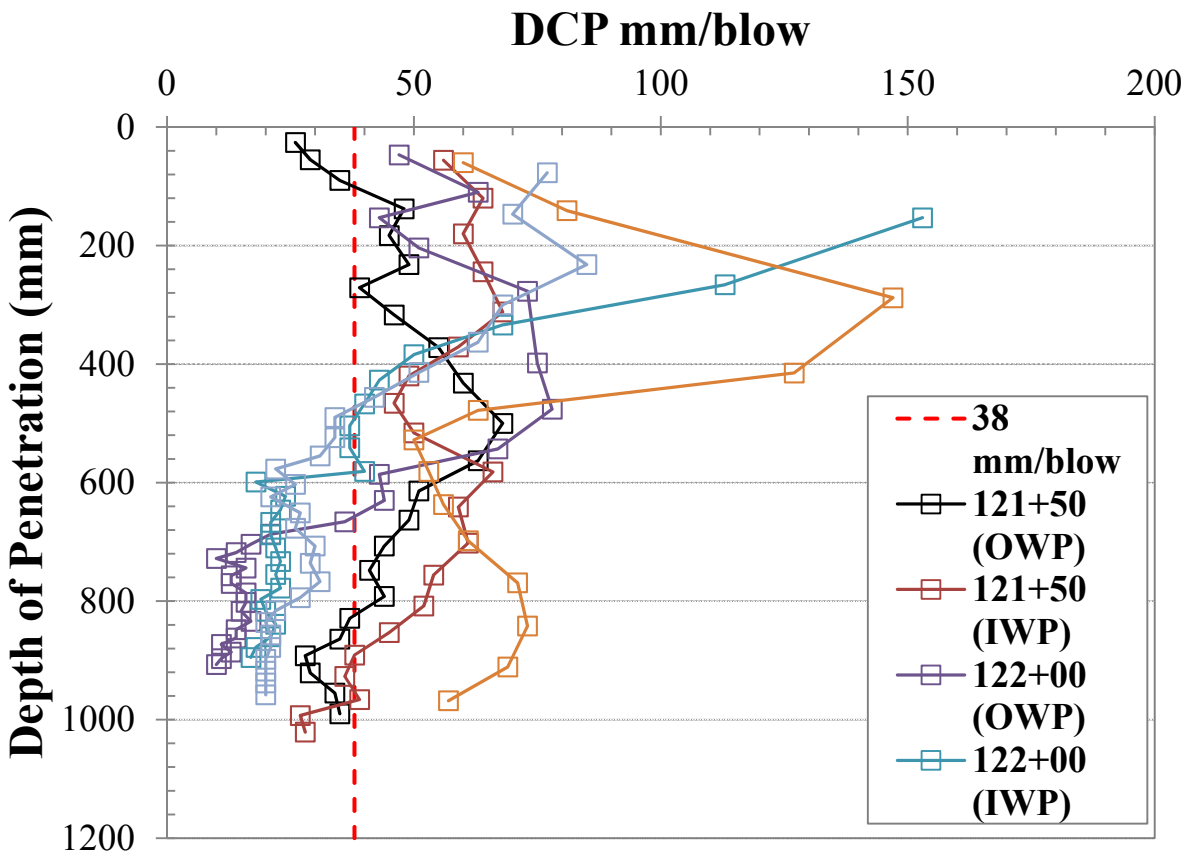

Figure 4-38: DCP plot for locations within the test pad prior to undercutting

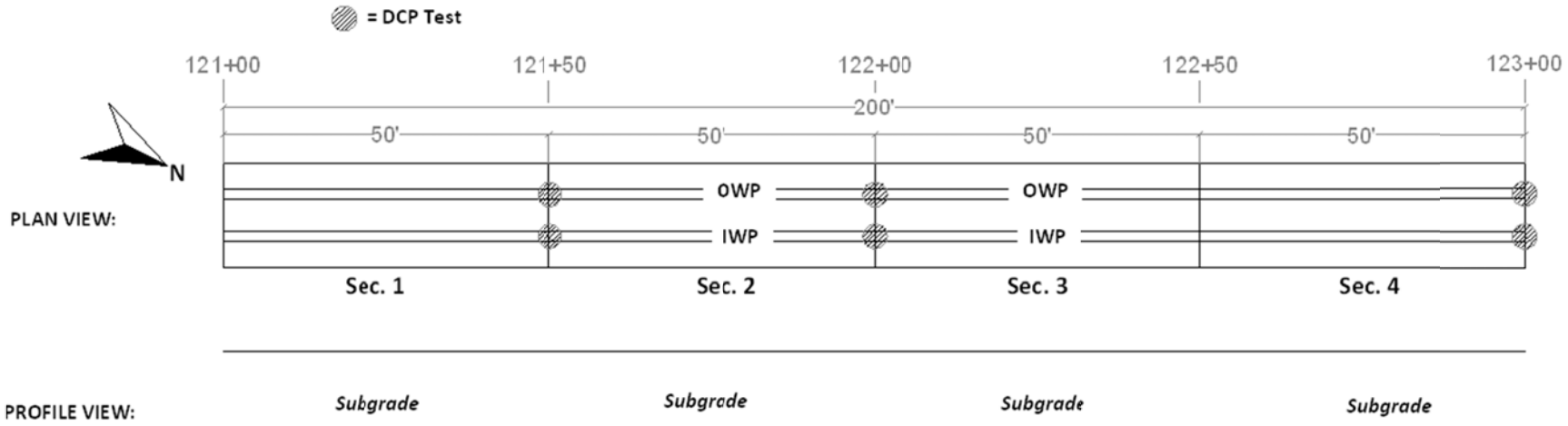

Figure 4-39: DCP test locations performed on the subgrade prior to undercutting

After Undercutting

Subsequently after Test Sections 1, 2, and 3 had been undercut on May 25, 2011, DCP testing was performed directly on the subgrade soils. Shown in Figure 4-40 is a diagram of the test locations. The results are provided in

Table **4-15** and plotted in Figure 4-41 through Figure 4-44. To help indicate the strength of the subgrade, the figures are color coded based on the DCPI-CBR ranges shown in Table 4-14 and correlated using the NCDOT (1998) equation.

Table 4-14: DCPI-CBR ranges based on NCDOT (1998) equation

DCPI (mm/blow)		CBR (%)	
Min	Max	Min	Max
< 4		> 100	
4	13	25	100
13	31	10	25
31	44	7	10
44	74	4	7
74	269	1	4
269+		< 1	

Looking at the results several points are worth mentioning. Despite undercutting, Test Sections 1, 2, and 3 still had an additional one to two feet of soft soil before reaching competent material with CBRs exceeding 10%. In Test Sections 2 and 3 there is a gradual increase in DCPI with depth. While this may be an indication of stiffer soils, it is important to keep in mind that some of this behavior is due to an increase in soil resistance along shaft of the DCP. Tests within Test Section 4 were conducted prior to soil-cement mixing. Looking beyond the top eight inches of soil that would eventually be stabilized, it is apparent that there was still a significant layer of soft soils with CBR's ranging between 5 and 8%.To validate the use of the Herath *et al.* (2005) model (Equation 4-8) in estimating the subgrade soils resilient modulus, the correlated modulus values were compared to the lab measured modulus values presented in Chapter 3. Shown in

Table 4-16 is the weighted average DCP value for the top two feet of subgrade material tested after undercutting. Also shown are the correlated modulus values based on the Herath *et al.* equation and a range of the lab measured resilient modulus values for the subgrade soil taken near the DCP tests locations. With the exception of Test Section 1, all correlated modulus values fall within the lab measured range for confining pressures between 2 and 6 psi. Based on this observation the use of the Herath *et al.* (2005) equation is justified for use with the subgrade soils encountered at the site.

Table 4-15: DCP tests on subgrade soil after undercutting

Test Section	Station	Depth From Grade (in)		Wt. Avg. DCPI	σ	C_V	N	Estimated CBR[1] (%)	Estimated M_r[2] (ksi)
		Min	Max	(mm/blow)					
1	121+12.5	31	39	96	6.5	0.07	2	3	3.8
		39	59	35	14.7	0.42	15	9	6.2
		59	69	16	3.3	0.21	17	21	10.9
	121+37.5	31	44	110	-	-	1	3	3.6
		44	62	14	5.2	0.38	42	24	12.2
2	121+62.5	9	14	65	2.5	0.04	2	5	4.4
		14	39	32	4.4	0.14	18	10	6.5
		39	46	12	2.5	0.22	14	29	13.9
	121+87.5	9	25	37	12.2	0.33	13	8	6.0
		25	32	44	3.3	0.08	3	7	5.5
		32	45	18	4.9	0.27	20	18	9.9
3	122+12.5	9	21	77	11.7	0.15	4	4	4.1
		21	39	38	11.1	0.29	13	8	5.9
		39	45	15	1.4	0.09	11	22	11.4
	122+37.5	9	29	36	5.5	0.15	14	8	6.1
		29	45	11	2.4	0.22	23	30	14.4
4	122+62.5	0	9	62	24.2	0.39	4	5	4.5
		9	16	17	1.6	0.09	10	19	10.1
		16	38	39	5.9	0.15	14	8	5.8
	122+87.5	0	17	24	7.2	0.30	20	13	7.9
		17	38	54	6.0	0.11	9	6	4.8

[1]CBR is based on NCDOT (1998)

[2]Resilient modulus is based on direct model developed by Herath *et al.* (2005)

Table 4-16: Correlated resilient modulus compared to the lab measured resilient modulus

Test Section	Soil Type	DCPI (blows/mm)	[1]Estimated M_r (ksi)	[2]Measured M_r (ksi)
1	Subgrade	61	4.6	1.4 - 2.9
2	Subgrade	39	5.8	4.7 - 8.2
3	Subgrade	45	5.4	5.3 - 8.9
4	Subgrade	39	5.8	3.7 - 11.6

[1]M_r is based on direct model developed by Herath *et al* (2005)

[2]Range in lab measured M_r at 2-6 psi confining pressure

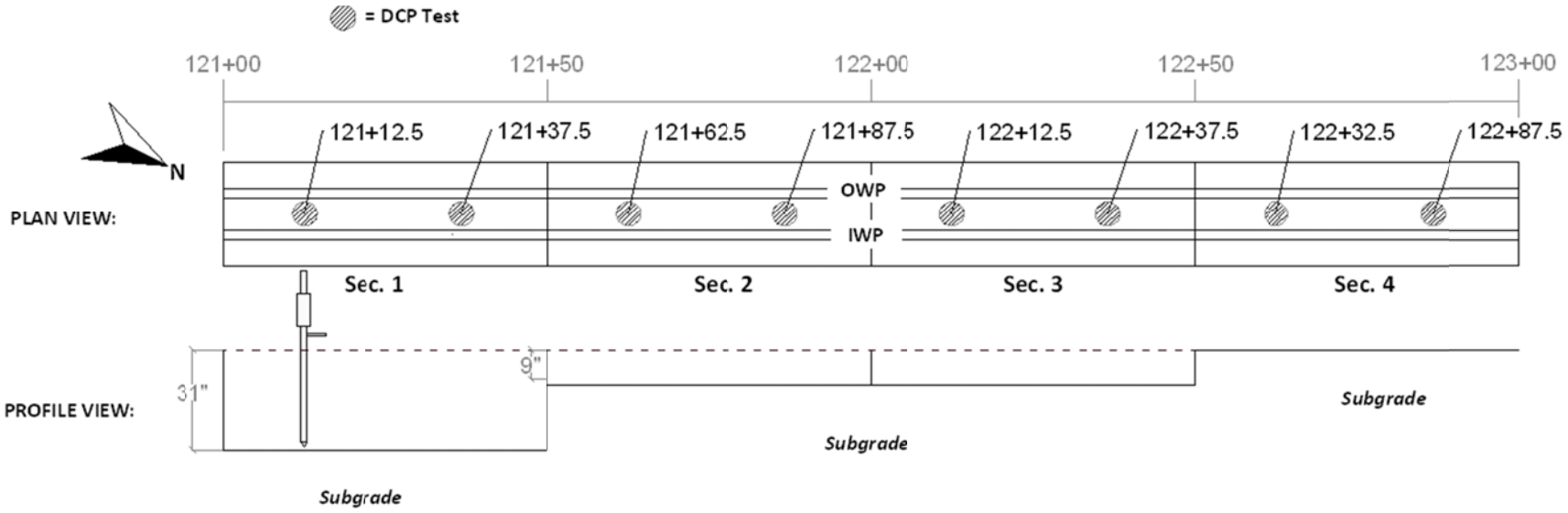

Figure 4-40: DCP test locations performed on the subgrade after undercutting

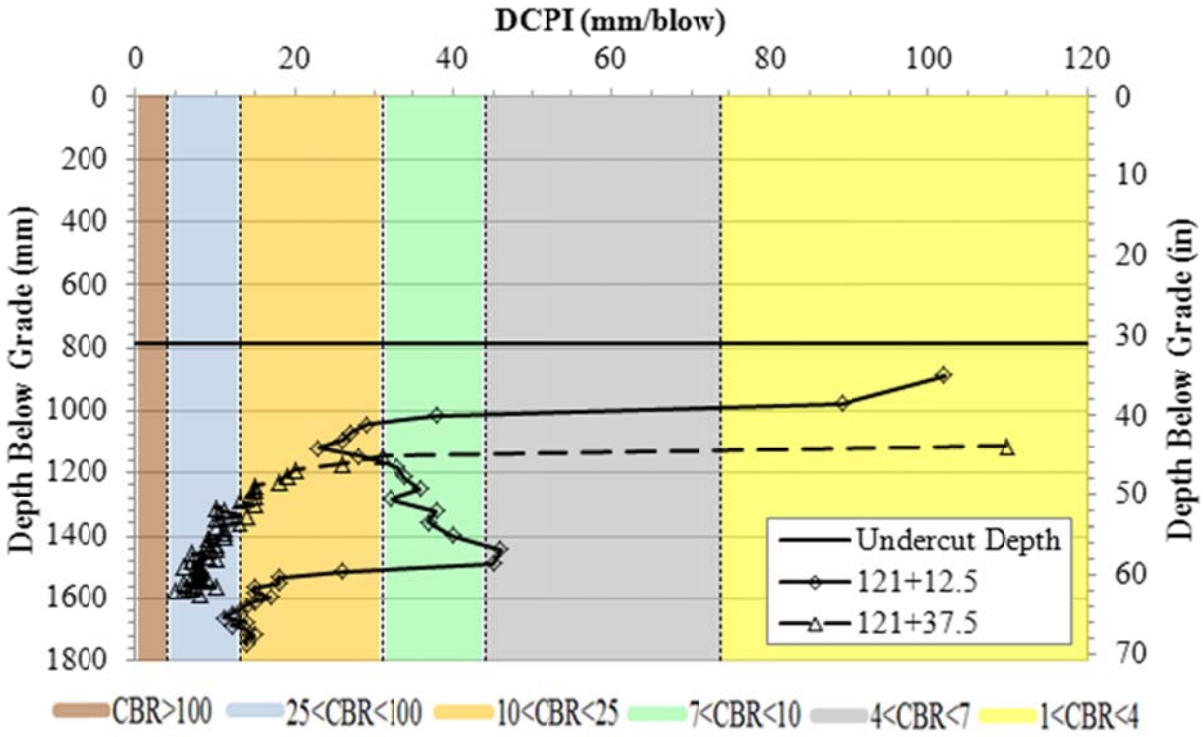

Figure 4-41: DCP results for tests performed on the subgrade in Section 1 after undercutting

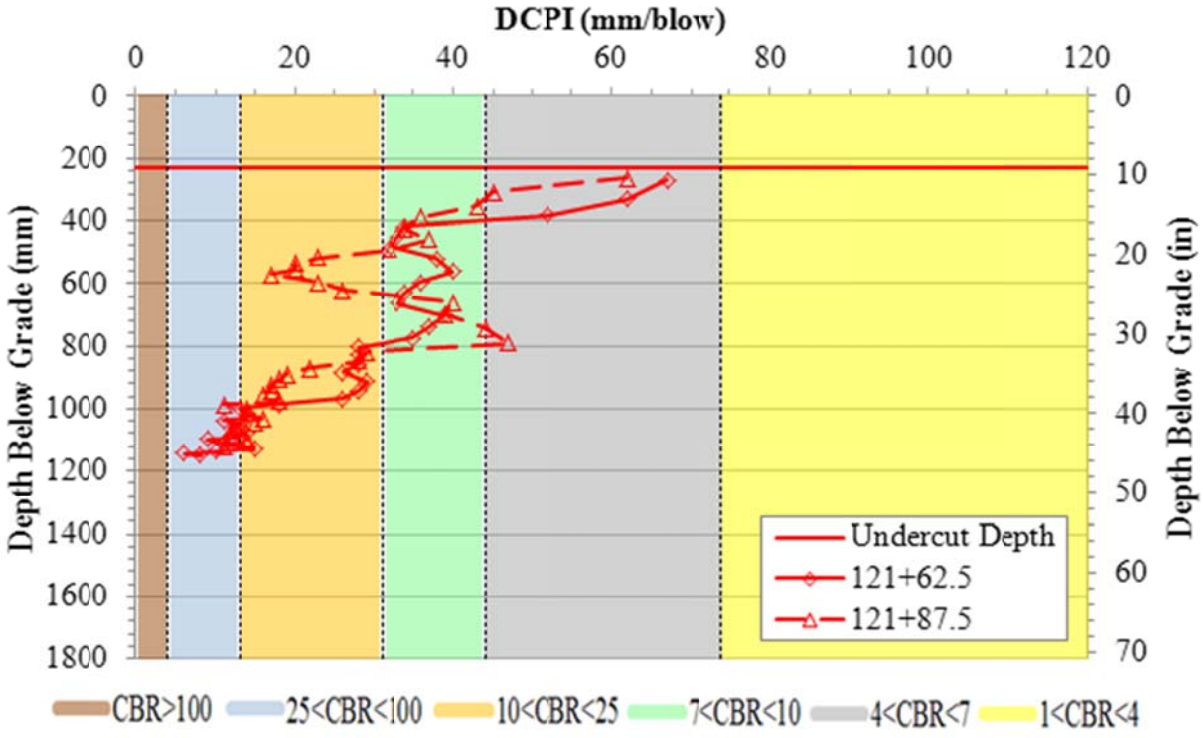

Figure 4-42: DCP results for tests performed on the subgrade in Section 2 after undercutting

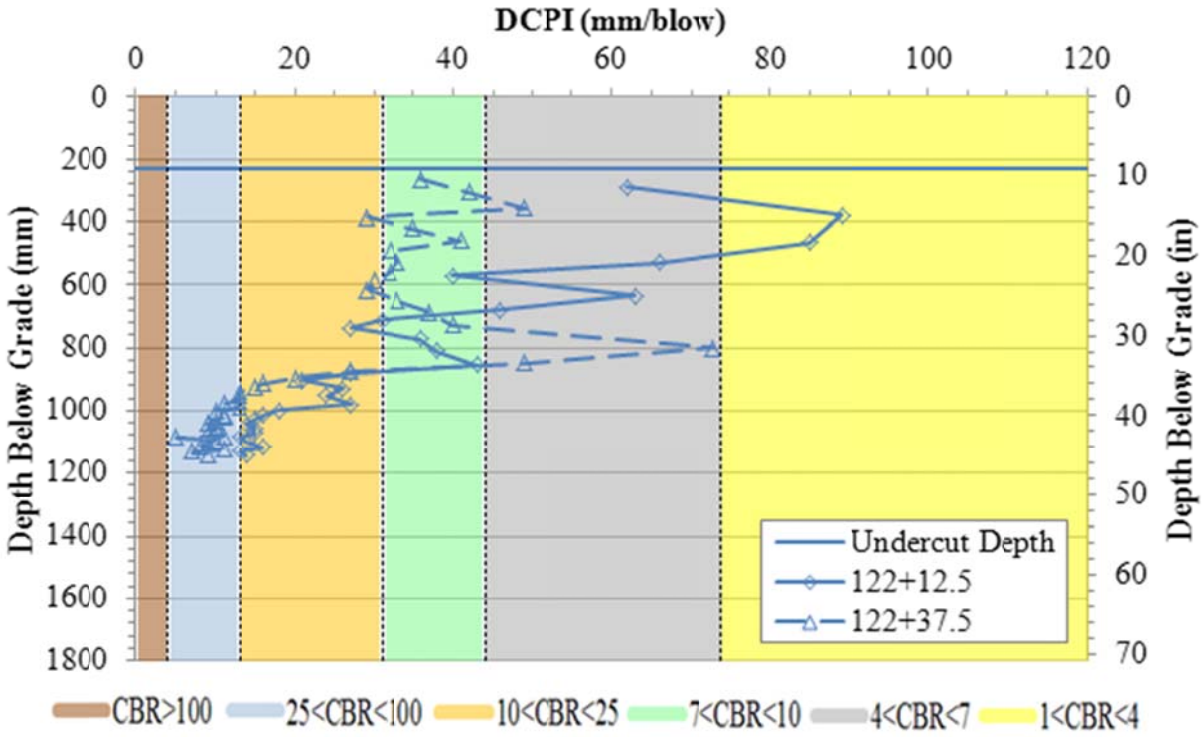

Figure 4-43: DCP results for tests performed on the subgrade in Section 3 after undercutting

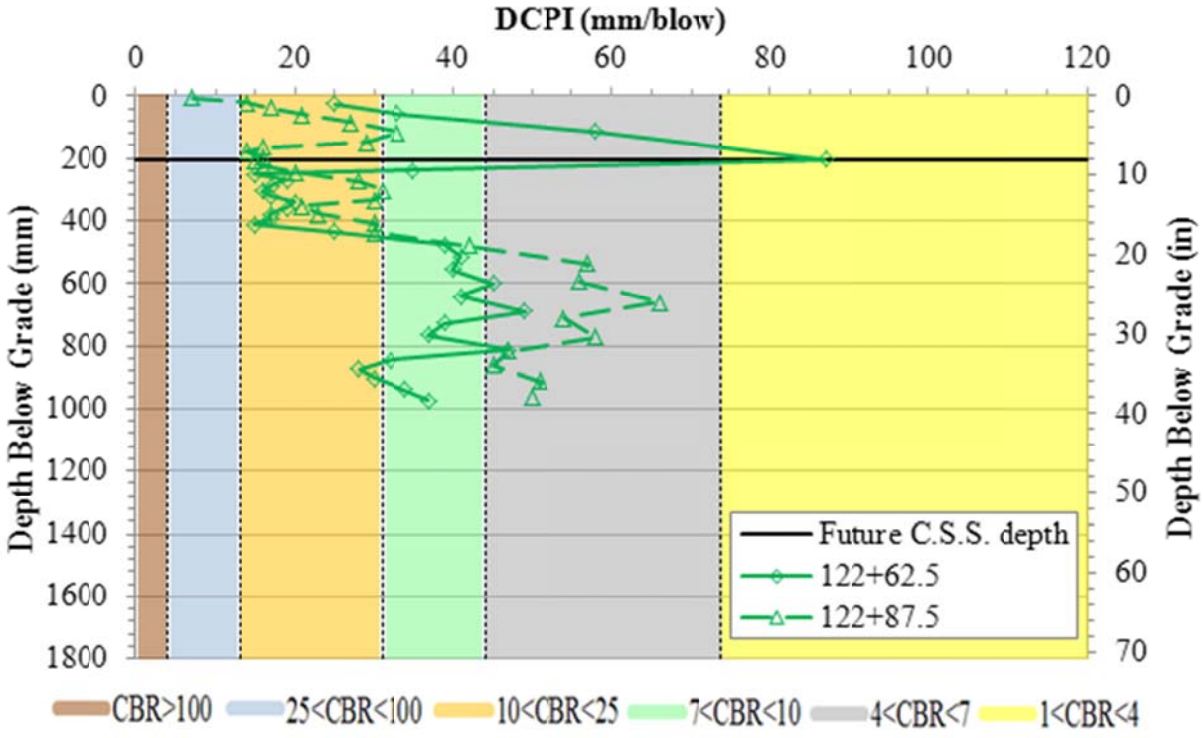

Figure 4-44: DCP results for tests performed on the subgrade in Section 4 prior to C.S.S

Prior to Full-Scale Testing

After the test sections were constructed a series of DCP tests were performed in each test section to assess the base layer material stiffness. Shown in Figure 4-45 is a diagram of the test locations. The results are provided in Table 4-17 and plotted in Figure 4-46 through Figure 4-49. Once again, the figures are color coded based on correlated CBRs using the NCDOT (1998) equation.

Tests on the select material in Test Section 1 measured higher DCPIs (i.e. weaker soils) within the top one foot of material. This is believed to be due to a lower confining stress and lower moisture content close to the ground surface relative to deeper depths in the base layer. Tests performed in Test Sections 2 and 3 displayed a relatively similar behavior with DCPIs ranging between four and eight, yielding a correlated resilient modulus between 20-35 ksi. Unfortunately, due to the absence of an unreinforced ABC section, it is cannot be determined whether the geosynthetics had any effect on the initial base layer stiffness. Tests in Test Section 4 measured DCPIs within the top five inches comparable to those measured in Test Sections 2 and 3. However, beyond the first five inches the DCPI values tend to increase indicating weaker soils. Based on this observation it is questionable whether the cement was thoroughly mixed into the complete eight inches of subgrade soil during the construction process. Another possibility is that the cement was in fact mixed the complete eight inches; however, during the compaction process the soil-cement structure may have densified resulting in a reduced base layer thickness.

To validate the use of the Herath *et al.* (2005) model (Equation 4-8) in estimating the base layer materials resilient modulus, the correlated modulus values were compared to the lab measured modulus values presented in Chapter 3. Shown in Table 4-18 is the weighted average DCP value for the base layer material tested prior to full-scale testing. Also shown are the correlated modulus values based on the Herath *et al.* equation and a range of the lab measured resilient modulus values on reconstituted samples of the base layer materials. Looking at the results, all correlated modulus values fall within the lab measured range for confining pressures between 3 and 5 psi. Based on this observation the use of the Herath *et al.* (2005) equation is justified for use with the base layer materials.

When analyzing a two-layer system (e.g. base and subgrade) it is common to use a modulus ratio as an indicator of performance. To estimate the modulus of the base layer soils, a weighted average DCPI was obtained from tests performed prior to trafficking. To estimate the modulus of the subgrade, a weighted average DCPI was obtained from the top two feet of subgrade soil measured after undercutting. Using these measurements, an empirically correlated resilient modulus value was estimated using Equation 4-8. The results are shown in Table 4-19 along with the modulus ratio of each test section. Note that the modulus ratio for Test Sections 2, 3, and 4 is estimated to be between four and five while Test Section 1 is slightly lower at two. These results will be used later when analyzing the full-scale testing results.

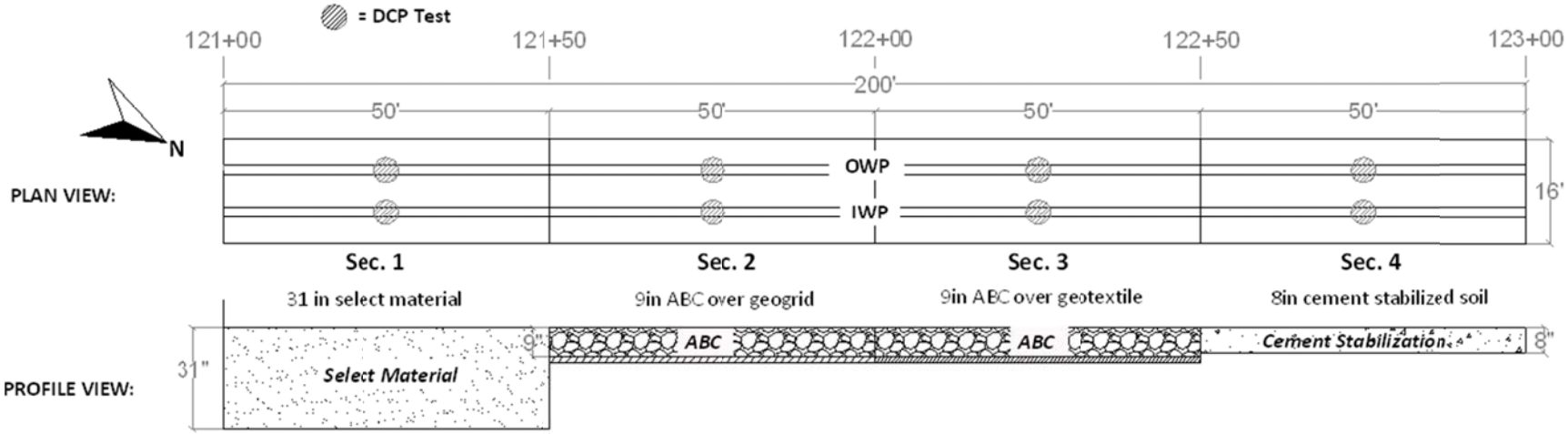

Figure 4-45: DCP test location performed on the base material prior to full-scale testing

Table 4-17: DCP tests on base material prior to full-scale testing

Test Section	OWP/IWP	Depth From Grade (in)		Wt. Avg. DCPI	σ	C_V	N	Correlated CBR[1] (%)	Correlated M_r[2] (ksi)
		Min	Max	(mm/blow)					
1	OWP	0	14	22	6.5	0.29	17	14.6	8.5
		14	27	10	1.7	0.18	38	35.4	16.4
		27	33	32	8.7	0.27	5	9.9	6.6
	IWP	0	12	26	7.2	0.28	10	12.3	7.6
		12	32	14	4.3	0.32	43	24.4	12.3
2	OWP	0	8	7	1.7	0.25	32	53.6	23.0
	IWP	0	9	6	2.0	0.34	42	59.4	25.1
3	OWP	0	11	5	1.4	0.28	60	72.6	29.8
	IWP	0	9	6	1.5	0.27	36	61.3	25.8
4	OWP	0	5	6	2.1	0.35	25	58.4	24.8
		5	13	11	2.3	0.22	20	31.9	15.1
	IWP	0	5	8	2.2	0.28	18	44.7	19.8
		5	13	14	1.8	0.13	14	23.6	12.0

[1]CBR is based on NCDOT (1998)

[2]Resilient modulus is based on direct model developed by Herath *et al.* (2005)

Table 4-18: Correlated resilient modulus compared to the lab measured resilient modulusTest Section	Soil Type	DCPI (blows/mm)	[1]Estimated M_r (ksi)	[2]Measured M_r (ksi)
1	Select Material	19	9.4	9.1-15.4
2	ABC	7	21.6	18.7 - 31.2
3	ABC	6	24.8	18.7 - 31.2

[1]M_r is based on direct model developed by Herath *et al* (2005)

[2]Range in lab measured M_r at 3-5 psi confining pressure

Table 4-19: Modulus ratio based on DCP tests prior to full-scale testing

Test Section	Avg. DCPI (mm/blow)		Correlated Resilient Modulus, Mr (ksi)		Modulus Ratio, Mr_1/Mr_2
	Base	Subgrade	Base	Subgrade	
1	19	61	9.6	4.6	2.1
2	7	39	23.1	5.8	4.0
3	6	45	26.8	5.4	5.0
4	7	39	21.6	5.8	3.7

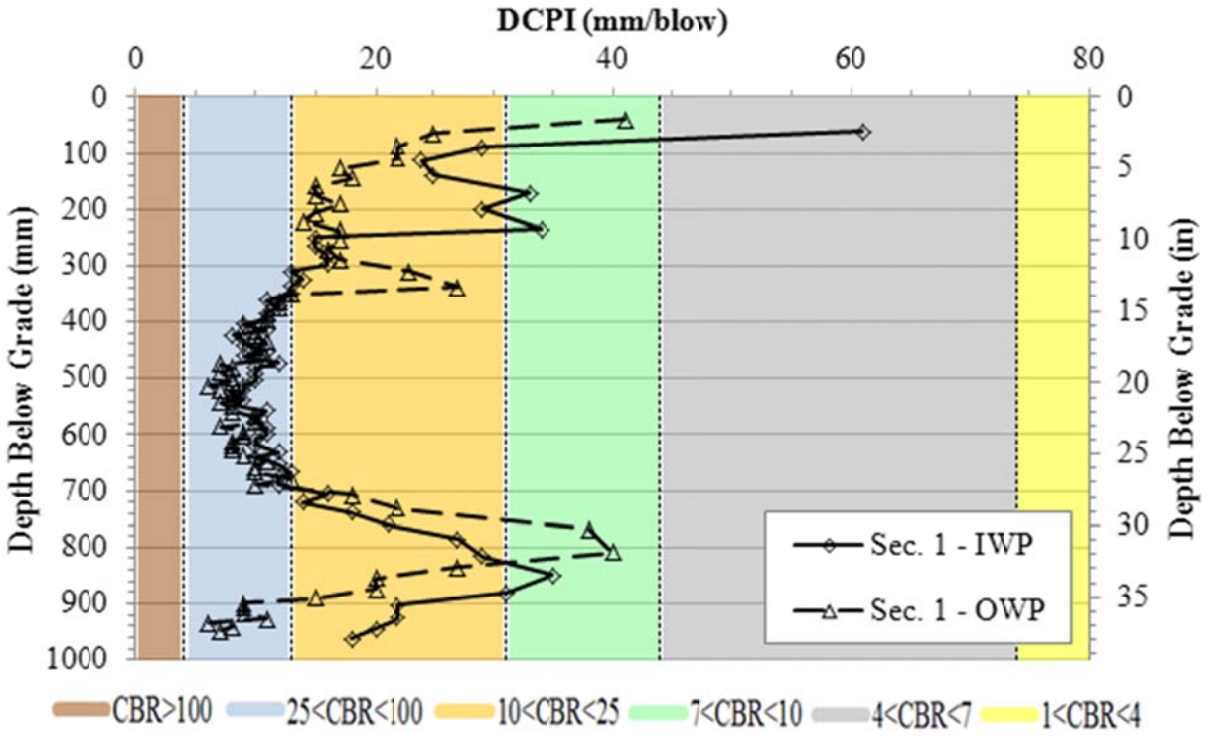

Figure 4-46: DCP results for tests performed in Section 1 prior to full-scale testing

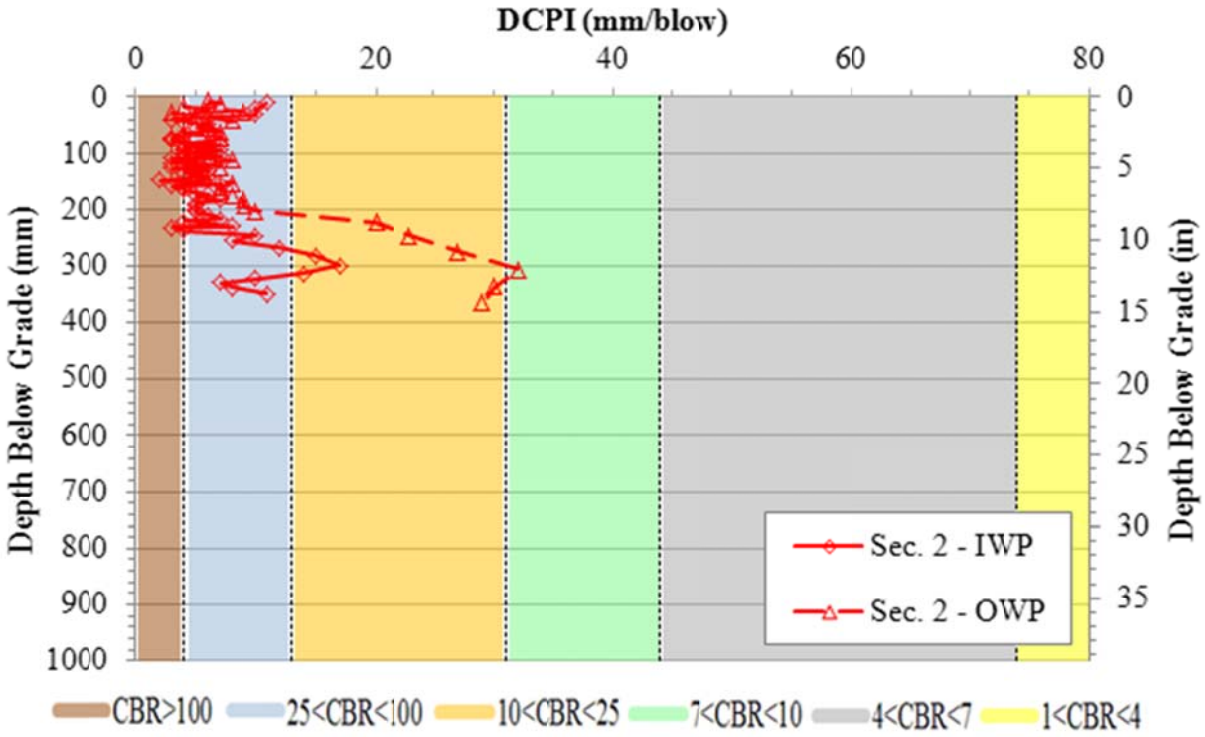

Figure 4-47: DCP results for tests performed in Section 2 prior to full-scale testing

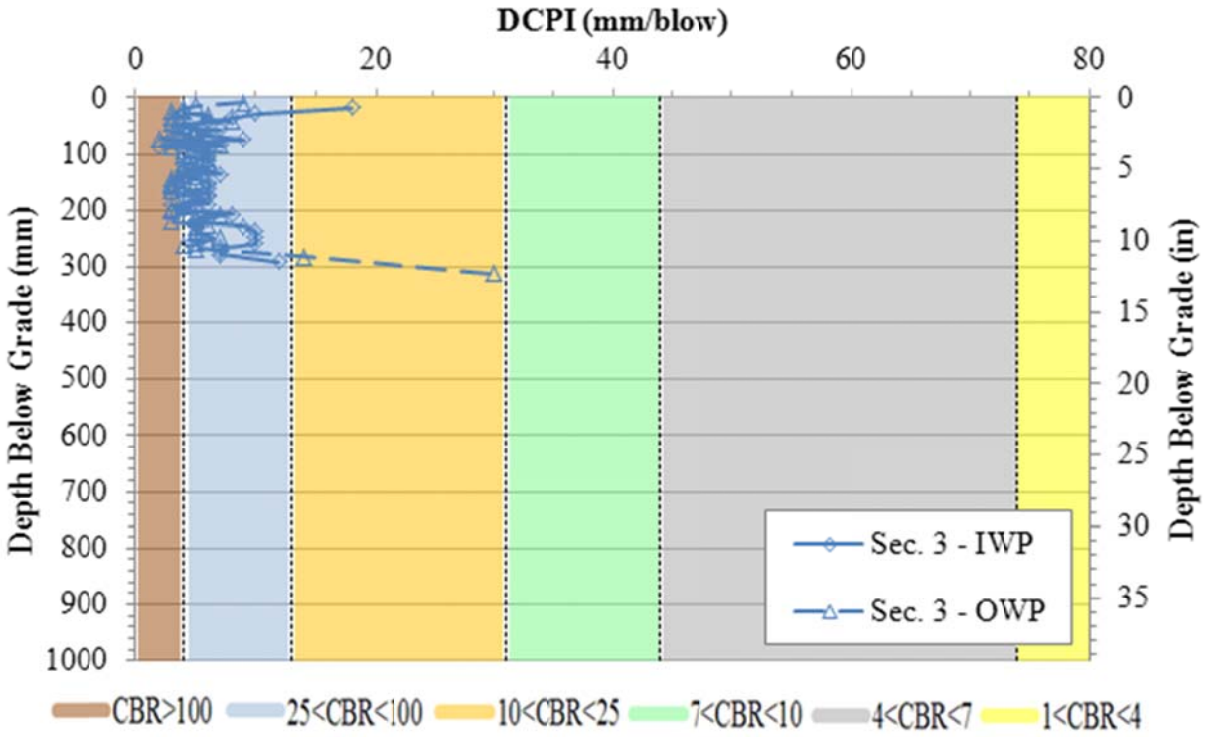

Figure 4-48: DCP results for tests performed in Section 3 prior to full-scale testing

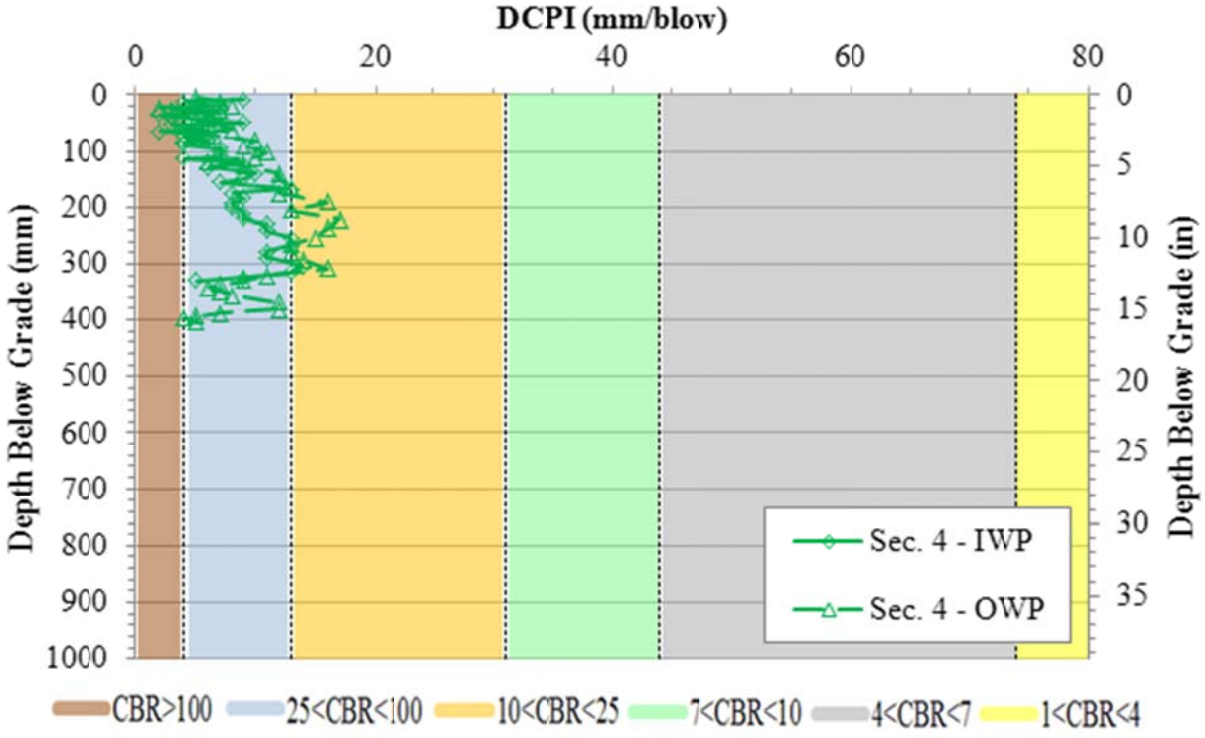

Figure 4-49: DCP results for tests performed in Section 4 prior to full-scale testing

After Repair of Test Section 1

During full-scale testing Test Section 1 failed in rutting after the first 200 truck passes and had to be repaired by leveling, wetting, and rolling the select fill and adding a two to three inch layer of compacted ABC stone. The details of the failure and repair process will be discussed later in the next chapter. After the repair of Test Section 1 was complete, two DCP tests were performed in the middle of the section (Station 121+25) at each wheel path to assess the new in situ stiffness. The results are provided in Table 4-20 and plotted in Figure 4-50. The measured DCPIs show that the top six to eight inches of ABC and select material failed to be adequately compacted using the steel drum roller. However, based on the rutting data the additional compaction due to repeated tire loading during full-scale testing provided enough densification of the top layer to control the cumulative rutting during the final 800 truck passes.

Table 4-20: DCP tests on base material after repairing Test Section 1

Test Section	OWP/IWP	Depth From Grade (in)		Wt. Avg. DCPI	σ	C_V	N	Correlated CBR[1] (%)	Correlated M_r[2] (ksi)
		Min	Max	(mm/blow)					
1	OWP	0	8	41	10.5	0.25	5	7	5.6
		8	32	11	2.4	0.21	57	30	14.2
1	IWP	0	10	33	8.4	0.25	8	9	6.4
		10	32	11	2.9	0.27	58	32	15.0

[1]CBR is based on NCDOT (1998)

[2]Resilient modulus is based on direct model developed by Herath *et al* (2005)

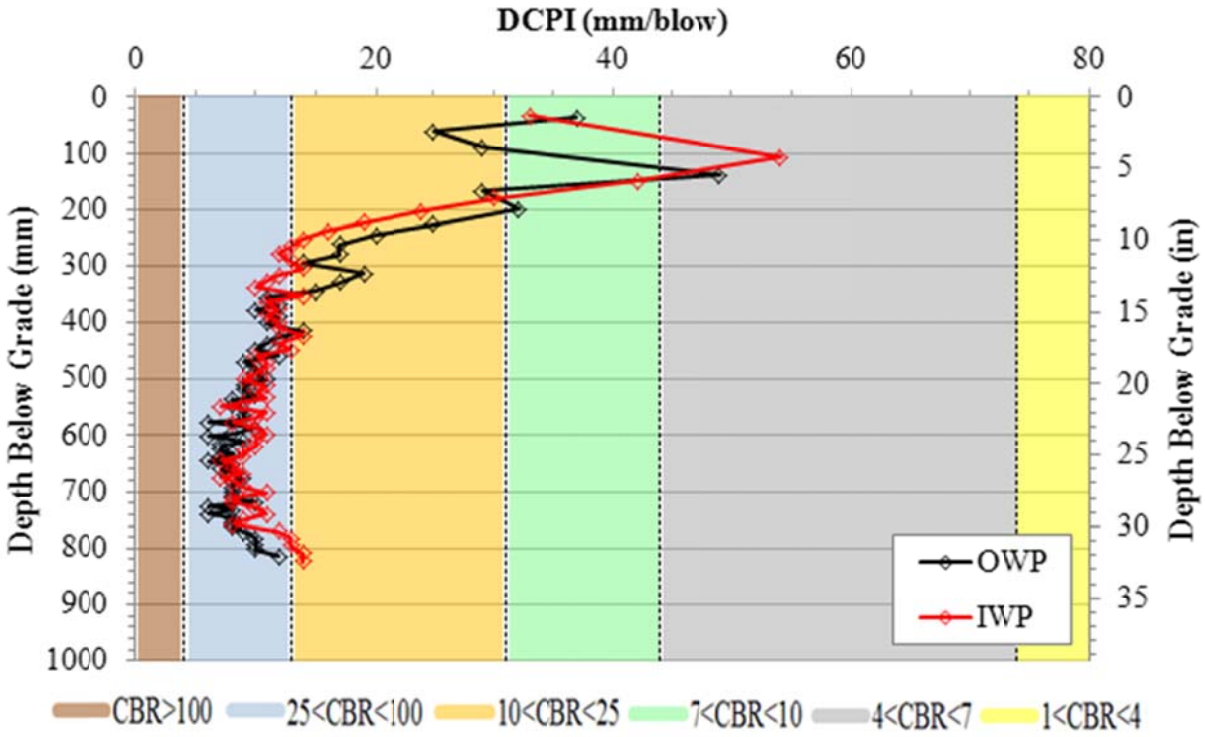

Figure 4-50: DCP results for tests performed in Section 1 after repair

After Full-Scale Testing

After full-scale testing was completed a number of DCP tests were performed throughout the test pad to evaluate the base layer stiffness of each test section after loading. Shown in Figure 4-51 is a diagram of the test locations. The results are provided in Table 4-21 and plotted in Figure 4-52 through Figure 4-55. Results in Test Section 1 generally show a softer layer within the top 6 to 12 inches ($13 < CBR < 28$) before reaching a stiffer layer with average DPCIs between 8 and 12 mm/blow ($CBR > 30$). In Test Sections 2 and 3 it is impossible to determine how much of an effect the geosynthetics had on the final base layer stiffness due to the absence of a control (unreinforced) ABC section. However, when comparing geosynthetics, no benefit can be discerned with using one product over the other in regards to influencing the final base layer stiffness after 1000 truck passes. DCP results in Test Section 4 varied depending on the test location. Areas in Test Section 4 that exhibited the least amount of rutting measured DCPIs comparable to Test Sections 2 and 3. However, other areas in Test Section 4 that had a significant amount of rutting develop (near DCP Test 9 and 14), exhibited higher DCPIs indicating a soil-cement structure that had deteriorated.

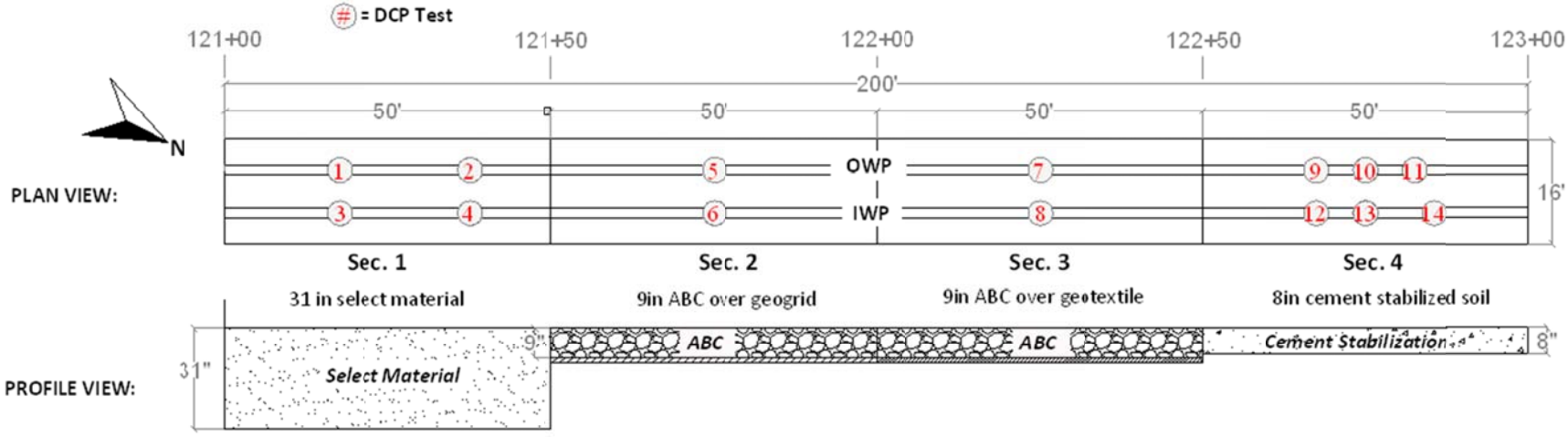

Figure 4-51: DCP test location performed on the base material after full-scale testing

Table 4-21: DCP tests on base material after full-scale testing

Test Number	Test Section OWP/IWP	Depth From Grade (in)		Wt. Avg. DCPI	σ	C_V	N	Correlated CBR[1] (%)	Correlated M_r[2] (ksi)
		Min	Max	(mm/blow)					
1	1 - OWP	0	9	12	4.7	0.39	22	28	13.5
		9	30	8	1.4	0.17	70	42	18.9
2	1 - OWP	0	9	20	4.9	0.24	12	16	9.1
		9	27	10	1.2	0.13	48	35	16.2
3	1 - IWP	0	6	17	4.7	0.28	10	20	10.4
		6	31	10	1.7	0.17	65	34	15.7
4	1 - IWP	0	11	24	7.1	0.30	13	13	8.0
		11	30	10	2.0	0.19	48	33	15.4
5	2 - OWP	0	7	5	2.0	0.42	51	76	31.1
6	2 - IWP	0	10	4	1.4	0.41	87	103	40.5
7	3 - OWP	0	9	3	1.3	0.38	88	110	42.9
8	3 - IWP	0	10	6	2.2	0.36	52	59	24.9
9	4 - OWP	0	6	9	1.6	0.19	19	40	18.2
10	4 - OWP	0	8	7	1.6	0.23	30	48	20.9
11	4 - OWP	0	10	5	1.2	0.23	51	65	27.2
12	4 - IWP	0	6	5	1.5	0.31	37	74	30.4
13	4 - IWP	0	10	6	2.1	0.34	46	57	24.1
14	4 - IWP	0	5	21	5.8	0.28	8	15	8.8

[1]CBR is based on NCDOT (1998)

[2]Resilient modulus is based on direct model developed by Herath *et al.* (2005)

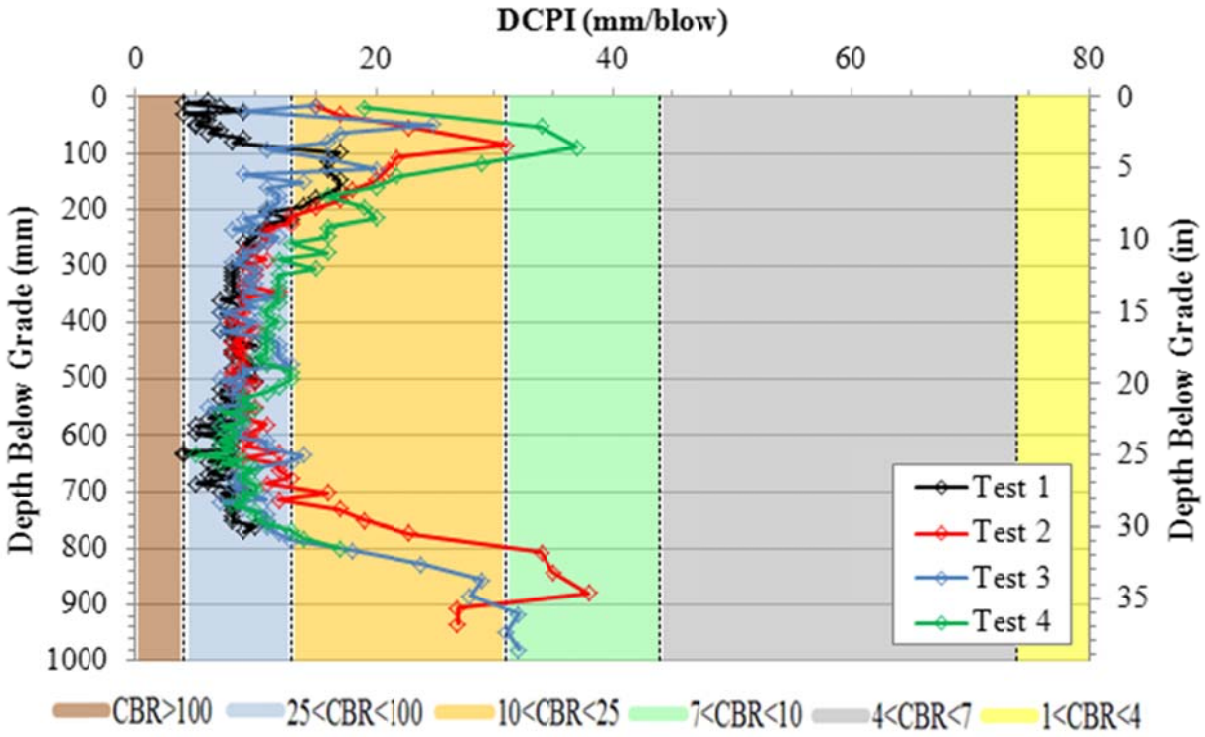

Figure 4-52: DCP results for tests performed in Section 1 after full-scale testing

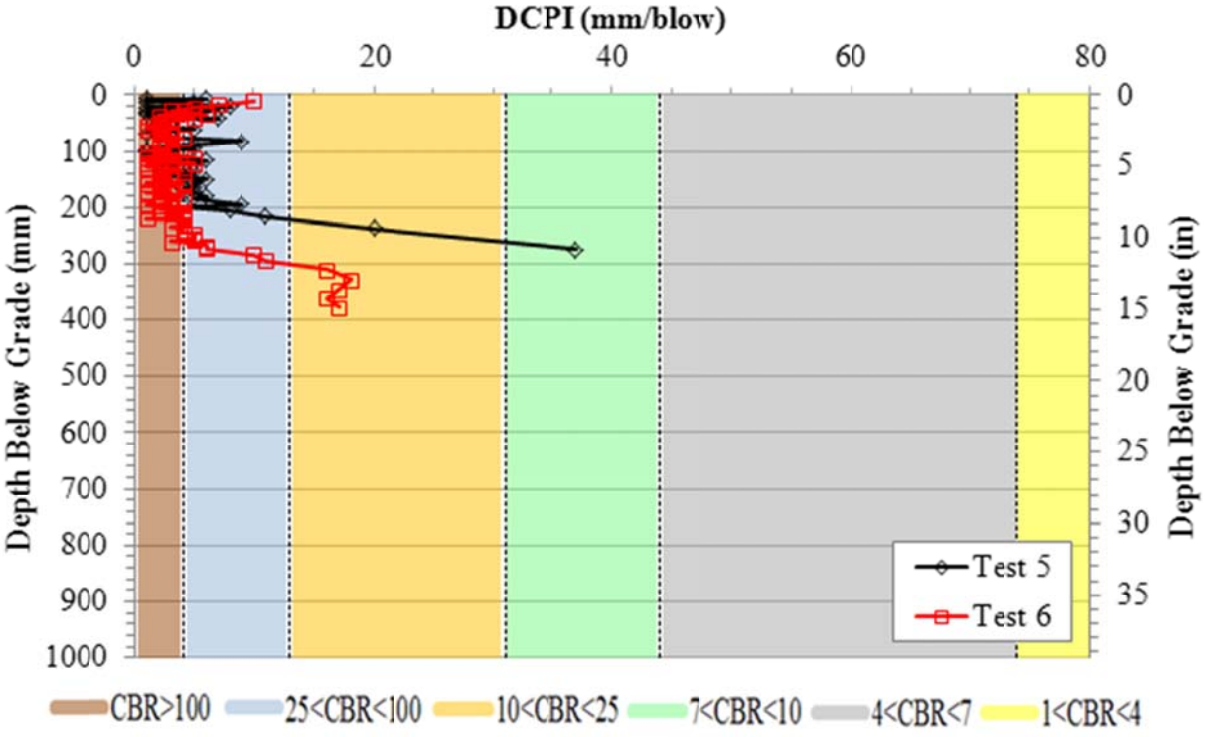

Figure 4-53: DCP results for tests performed in Section 2 after full-scale testing

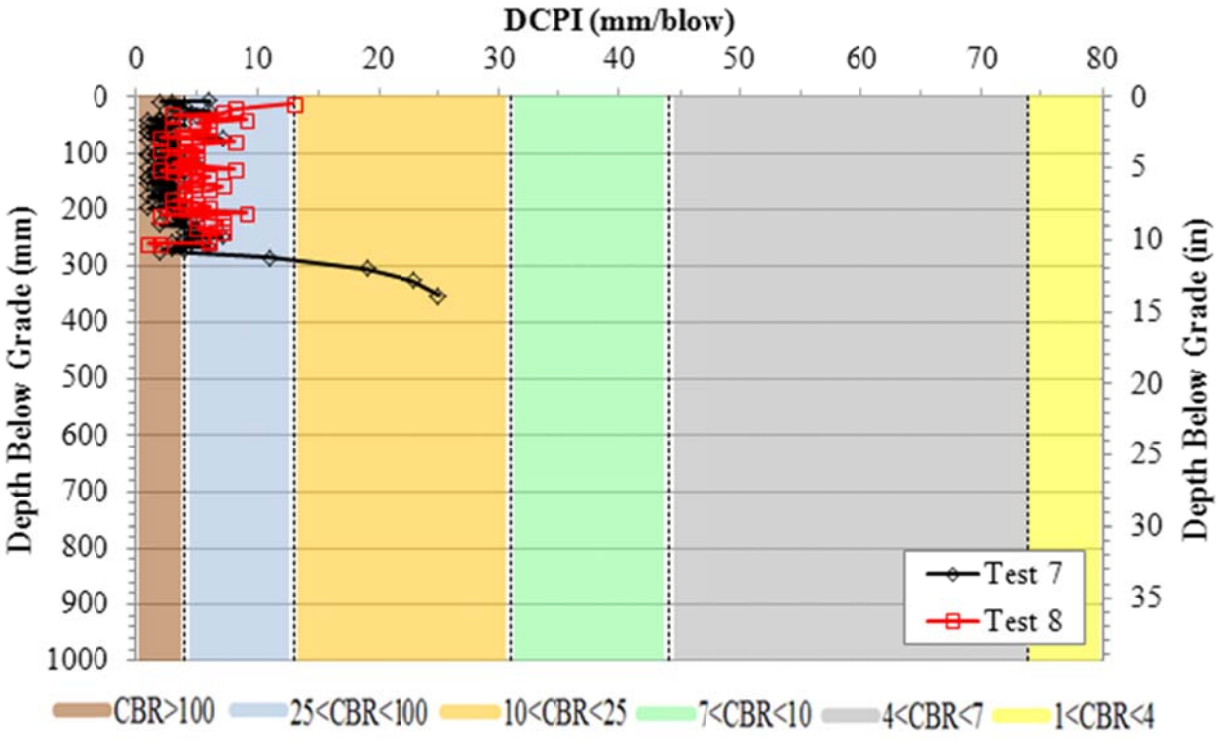

Figure 4-54: DCP results for tests performed in Section 3 after full-scale testing

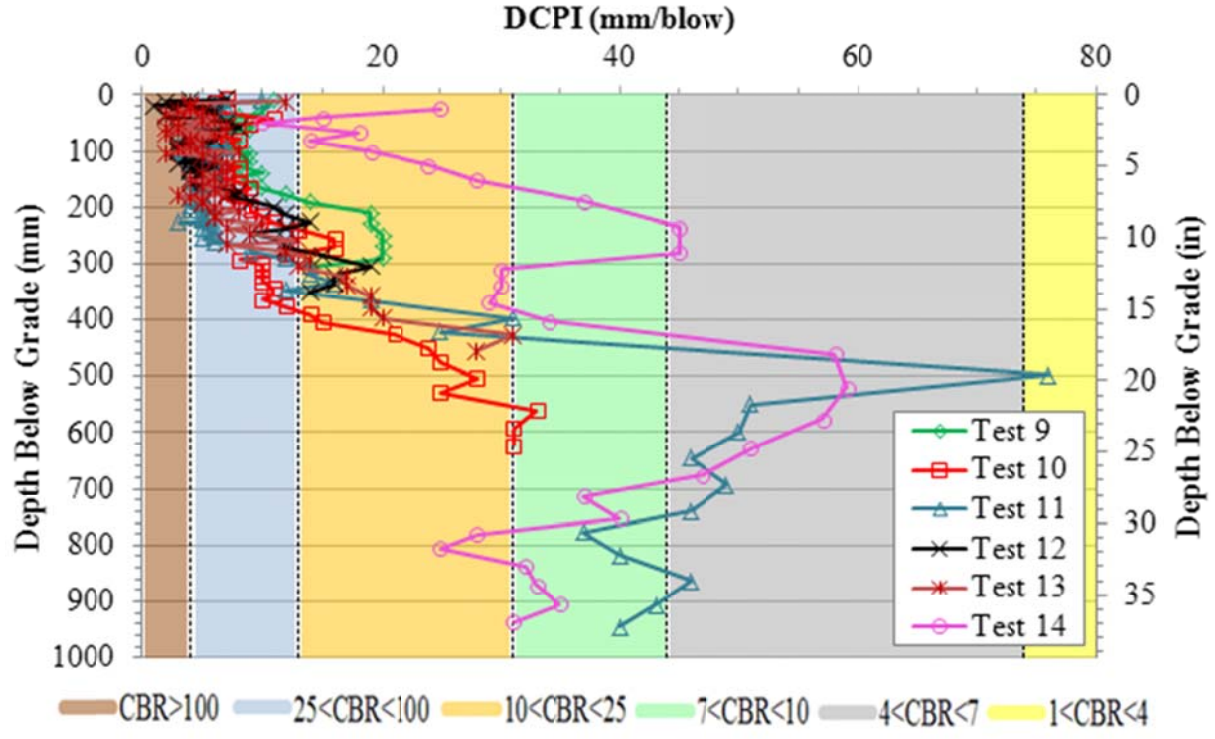

Figure 4-55: DCP results for tests performed in Section 4 after full-scale testing

Change in Base Layer Stiffness Due to Repeated Loading

To evaluate the change in the stiffness of each section due to repeated truck loading, weighted average DCPIs for tests performed in the center of the wheel paths for each test section are presented in Figure 4-56 through Figure 4-59. Generally, a decrease in DCPI (increase in stiffness) is observed in Test Sections 1, 2, and 3 presumably due to the densification of the base layer material during full-scale testing. In addition, the mobilization of the geosynthetic tensile strength within Test Sections 2 and 3 may have also contributed to the increase in stiffness; however, this cannot be validated due to the absence of an unreinforced ABC section. One exception is at the inner wheel path of Test Section 3. A possible explanation for the softening behavior may be due to geotextile damage possibly during installation or truck loading. A softer subgrade may also be the culprit; however, DCPI tests performed after undercutting did not indicate any major difference in strength in that area of the subgrade versus elsewhere in the test pad.

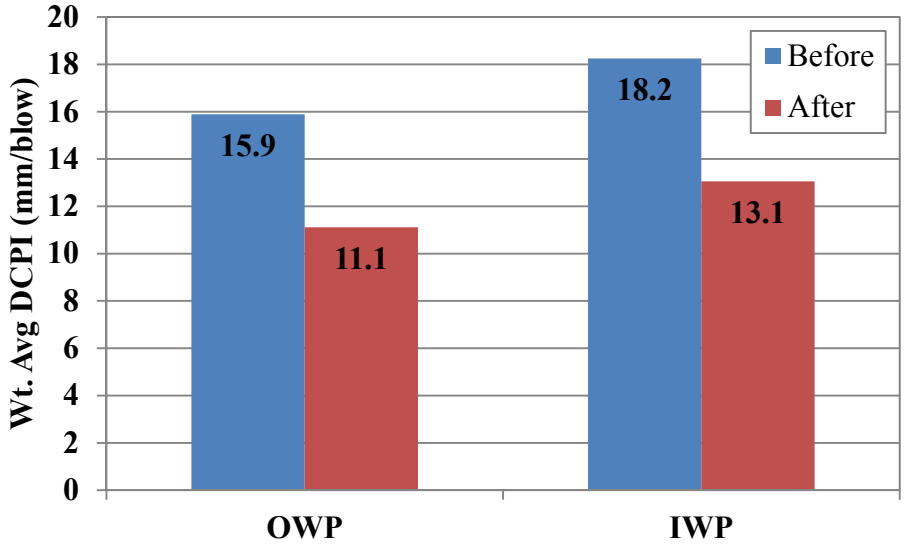

Figure 4-56: Weighted average DCPI in Section 1 before and after full-scale testing

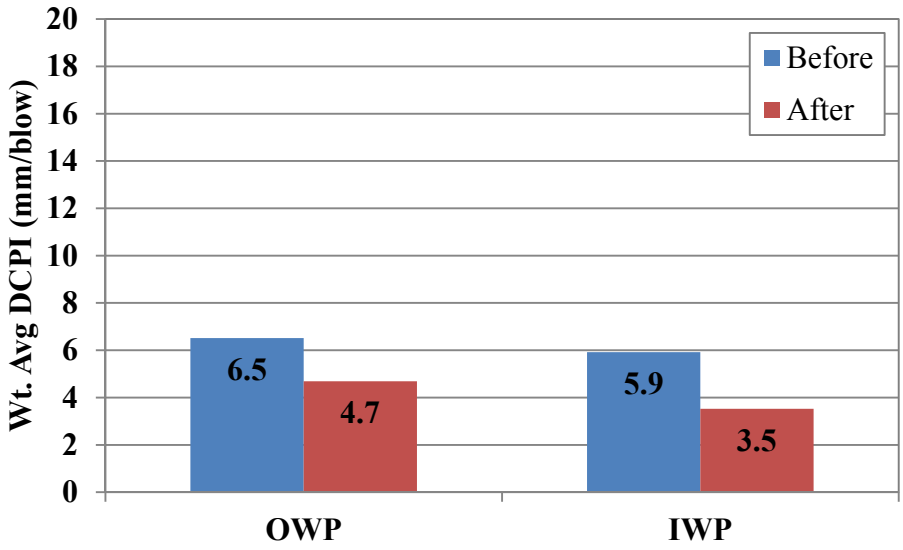

Figure 4-57: Weighted average DCPI in Section 2 before and after full-scale testing

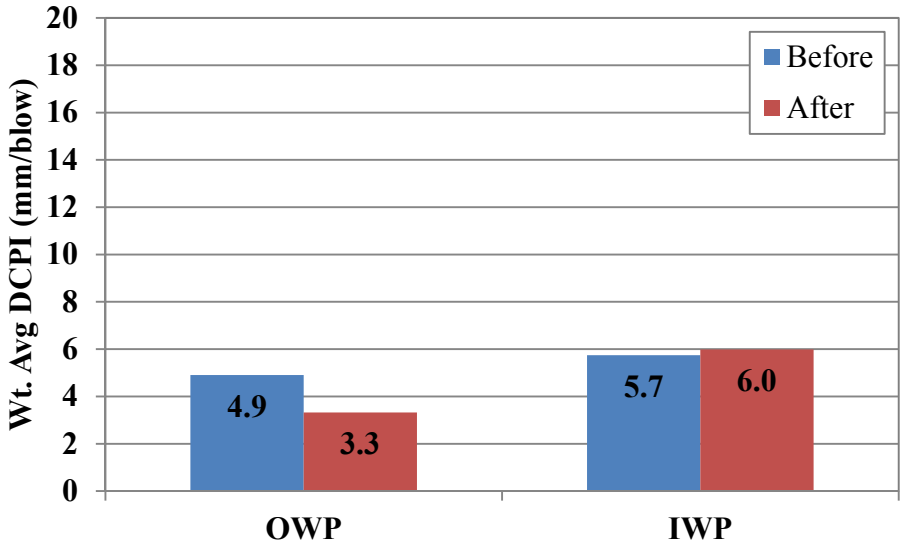

Figure 4-58: Weighted average DCPI in Section 3 before and after full-scale testing

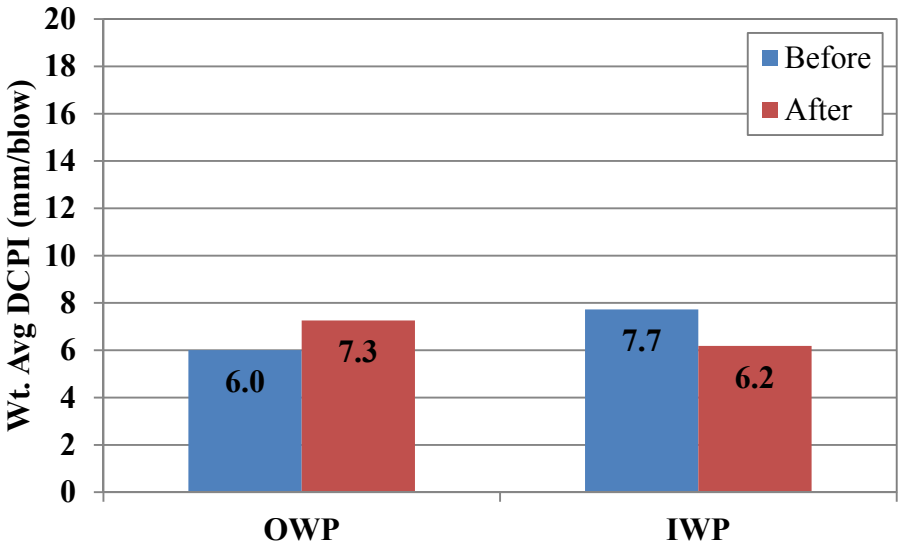

Figure 4-59: Weighted average DCPI in Section 4 before and after full-scale testing

DCP Summary

A series of DCP tests were performed throughout the test pad at various stages of the study. The first series of tests were conducted prior to undercutting to estimate the subgrade stiffness. In general, the weighted average DCPI of the top two feet of subgrade soil was found to be in excess of 38 mm/blow. This finding supports the NCDOT's current undercut criterion of 38 mm/blow as the DCPI cut-off, and would yield a required CBR value of greater than 5-8% or resilient modulus values greater than approximately 6 ksi (40 MPa). The second round of DCP tests were performed after the contractor undercut Test Sections 1, 2, and 3. DCP measurements generally indicated an additional one to two feet of soft soil before reaching competent subgrade material below the base/subgrade interface. The third, fourth, and fifth rounds of DCP testing were performed prior to, during, and after full-scale testing, respectively. Significant observations during these stages include the following:

- DCP results in Test Section 1 tend to indicate a softer layer of soil within the top one foot of select material. This is believed to be the result of lower confining stress and lower moisture content near the ground surface relative to deeper depths in the base layer.
- DCP results in Test Sections 2 and 3 show no benefit using one geosynthetic over the other in regards to influencing the base layer stiffness prior to or after repeated truck loading.
- DCP results in Test Section 4 indicate a soil-cement layer stiffness within the top five inches that is comparable to the stiffness measured in Test Sections 2 and 3. However, beyond the first five inches the DCPI values tend to increase indicating weaker soils. After full-scale testing, areas in Test Section 4 that performed acceptably measured DCPI's comparable to Test Section 2 and 3. However, other areas that developed excessive rutting measured higher DCPIs indicating a soil-cement layer that had deteriorated.
- With the exception of Test Section 4, DCP tests indicate a significant increase in base layer stiffness after full-scale testing presumably due to the densification of the base layer soils under repeated truck loading.
- DCP results indicate a correlated modulus ratio of two for Test Section 1 and four to five for Test Sections 2, 3, and 4.

Soil Stiffness Gauge (SSG)

The results from SSG testing performed before and after full-scale testing are provided in Table 4-22 and Table 4-23, respectively. The results from testing performed after repairing Test Section 1 are also presented in Table 4-22. As mentioned previously, SSG testing was performed within each test section at the center of both wheel paths. The reported SSG elastic modulus (E_{SSG}) is the average of three tests performed at the same location. The corresponding standard deviation and coefficient of variation for each set of tests is also shown in the tables. A Poisson's ratio of .35 was used for all test sections. It is important to note that the SSG has a depth of influence around 7.5 to 8 inches (190-200 mm). As a result, the modulus for Test Section 1 is a measure of only the top third of material that makes up the base layer. Furthermore, the top third of material within Test Section 1 was generally found to be the softest during DCP testing. Thus, it is reasonable to assume that the SSG modulus measured for Test Section 1 is not entirely representative of the total base layer stiffness.

Table 4-22: SSG test results performed prior to full-scale testing

Test Section	IWP/OWP	Avg. E_{SSG} (ksi)	σ	C_V
1	OWP	13.6	0.05	0.004
	IWP	14.5	0.04	0.003
2	OWP	42.4	0.04	0.001
	IWP	44.7	0.10	0.002
3	OWP	36.2	0.20	0.005
	IWP	32.3	0.25	0.008
4	OWP	51.1	0.57	0.011
	IWP	46.0	0.05	0.001

Table 4-23: SSG test results performed after full-scale testing

Test Section	IWP/OWP	Avg. E_{SSG} (ksi)	σ	C_V
1 REPAIR	OWP	10.8	0.30	0.028
	IWP	13.0	0.23	0.017
1	OWP	27.3	0.04	0.001
	IWP	17.0	0.18	0.011
2	OWP	24.5	0.10	0.004
	IWP	30.7	0.09	0.003
3	OWP	30.7	0.21	0.007
	IWP	26.1	0.34	0.013
4	OWP	25.6	0.27	0.010
	IWP	15.3	0.41	0.027

To compare the measured modulus for each test section, the results are plotted in Figure 4-60 and Figure 4-61. Prior to full-scale testing the SSG measured modulus values are significantly higher than the DCP correlated modulus values for each test section. At first, it was thought that this was due to the low strain levels being induced by the SSG device. However, the SSG modulus values measured after full-scale testing are comparable to the laboratory resilient modulus values at low confining stress which induce strain levels much higher than the SSG device. In addition, the range of SSG modulus values after full-scale testing are consistent with the resilient modulus correlations estimated from DCP tests. It is unclear why the SSG device did not remain consistent in estimating a higher modulus value than the DCP correlations. This would be expected since, as mentioned previously, the SSG induces a low level strain which should result in a high measure of modulus. A similar observation was noted by Sawangsuriya *et al.* (2003) who reported SSG modulus values corresponding to a strain amplitude approximately 20 times higher than the expected range. One explanation the writers postulate is that the SSG software may reduce the measured modulus by a factor to facilitate its use is pavement design. To the author's knowledge, however, this explanation was never validated with SSG manufacturer. Research has shown that the SSG device is highly sensitive to moisture content and cracking at or near the ground surface (Abu-Farsakh *et al.* 2003). It is suspected that a combination of these two factors may have influenced the SSG test results. Based on the

inconsistencies in moduli compared to lab and DCP measured moduli, a level of caution should be exercised when using the results measured from the SSG device.

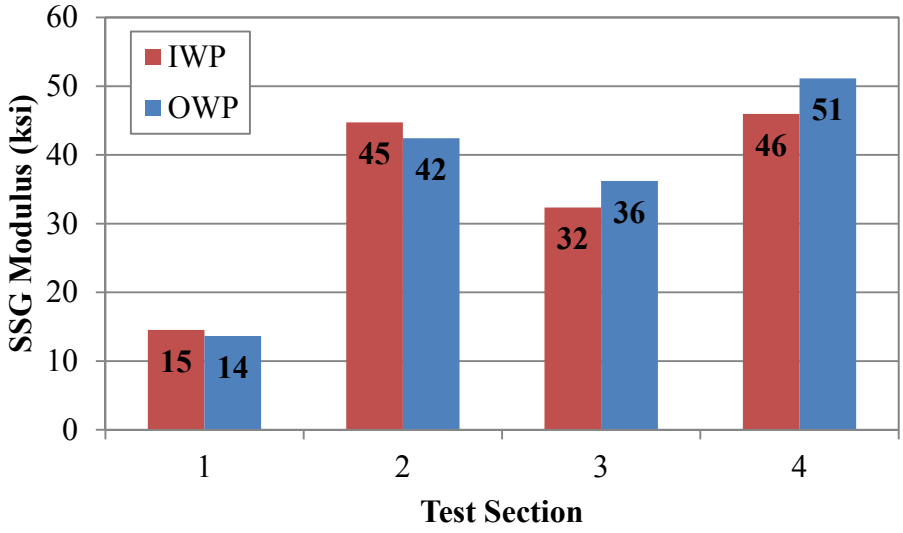

Figure 4-60: SSG modulus results prior to full-scale testing

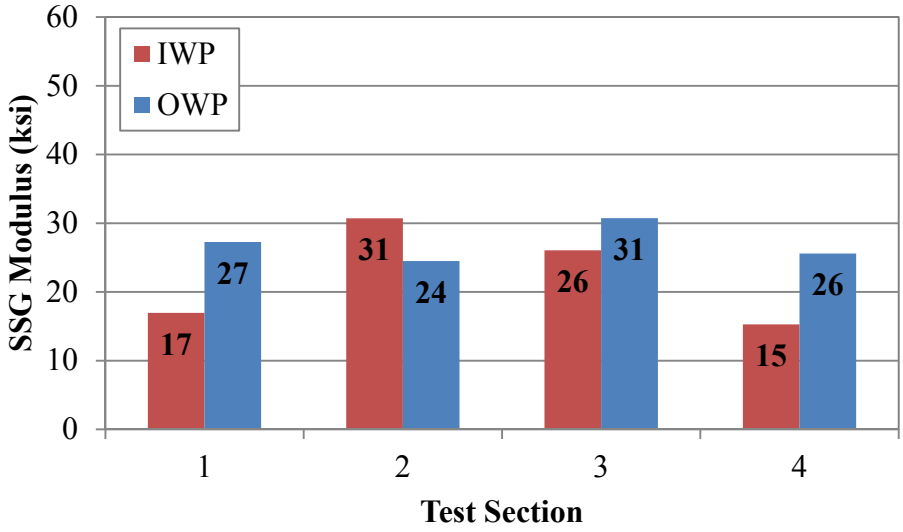

Figure 4-61: SSG modulus results after full-scale testing

Falling Weight Deflectometer (FWD)

FWD Data Analysis

The process of evaluating FWD results can vary significantly depending on the level complexity desired in the analysis. Backcalculation is one typical method used to analyze FWD results. Backcalculation is an iterative process where an initial estimate is made of the layer moduli in order to compute the surface deflection using the applied loads and known layer thicknesses. After the first computation the assumed moduli are adjusted, and the process is repeated until the predicted and measured deflection basins converge. Although this method of analysis has been shown to successfully provide a relatively accurate measure of layer moduli, a significant amount of experience is needed to confidently perform the procedure. In addition, difficulties are often associated with this process due to factors such as the presence of a stiff layer in the subgrade, a high groundwater table, and/or trying to use an elastic layer analysis to model base and subgrade soil properties that behave nonlinearly. Furthermore, the level of complexity multiples when FWD testing is performed directly on an uneven base layer material rather than a smooth pavement surface. This is due to the higher magnitudes of deflection, the difficulty in establishing good contact between the ground surface and geophones, and the overall lack of published literature on this topic. With these factors in mind, it was decided that a backcalculation analysis was beyond the scope of this study. Rather, a composite modulus was calculated for each FWD test using the following equation (Nassar *et al.* 2000):

$$\mathbf{E}_{FWD} = \frac{\pi(1-\nu^2)qa}{2d_o} \qquad \textbf{Eq. 4-9}$$

Where:

ν = Poisson's ratio (assumed .35)

q = Applied Pressure

a = Loading plate radius

d_o = Surface deflection at the center of the loading plate

When using the term "composite modulus" within in this study it is meant to indicate the computed modulus is based on the behavior of both the base and subgrade soils without considering layered effects. Although the composite modulus does not represent a true

engineering property, it provides a good indication of the stiffness of each test section, relative to the other test sections.

FWD Composite Modulus

Shown in Figure 4-62 and Figure 4-63 are the computed composite modulus values for each test section based on FWD measurements performed prior to and after full-scale testing, respectively. At the center of each wheel path in each test section a total of four tests were performed within two to three feet of proximity. As mentioned previously, for each test three consecutive drops were applied at load levels' ranging between approximately 5 and 13 kips. The average deflection basin was then computed for each load/drop level. Any test that produced abnormal deflections in relation to the other three tests was neglected from the analysis. Unfortunately, a consistent deflection basin could not be obtained for the cement stabilized material (Test Section 4) and thus the results are not included in the analysis.

Looking at the results, several trends are worth noting. Interestingly, the composite modulus values measured in Test Section 1 are generally equal to or greater than those measured in Test Sections 2 and 3. This deviates from measurements taken during DCP testing due to the fact that the DCP involves taking a single "point" measurement at a specific depth whereas the FWD encompasses the entire depth of influence. Based on the FWD results it is evident that the composite stiffness of Test Section 1 is comparable to that of the other sections due to the thicker base course layer that prevents higher stresses and corresponding deformations from reaching the soft subgrade.

When referring to Figure 4-63, note the substantially lower composite modulus calculated at the inner wheel path (IWP) of Test Section 3. FWD tests performed prior to full-scale testing did not indicate a substantial difference in composite modulus at this location versus elsewhere in the test pad. This observation suggests that this weak behavior is due to geotextile damage during full-scale testing rather than a softer subgrade.

When referring to Figure 4-64 and Figure 4-65, note that similar to DCP results, there is a significant increase in stiffness at each test section after trafficking. As mentioned before, this is apparently due to the densification of the base layer soils under repeated truck loading. However, it is also important to mention that the use of a smaller 12 inch plate versus the 18 inch

plate used before traffic testing may have also contributed to the increase in modulus. Understandably, when using a smaller plate the depth of influence decreases and causes the composite modulus to incorporate less of the soft subgrade and more of the stiff base.

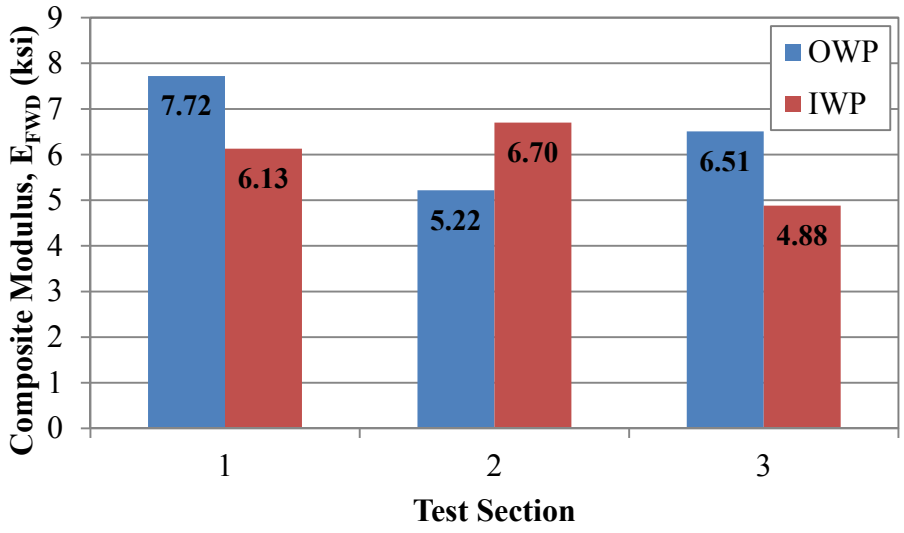

Figure 4-62: Composite modulus based on FWD tests performed prior to full-scale testing

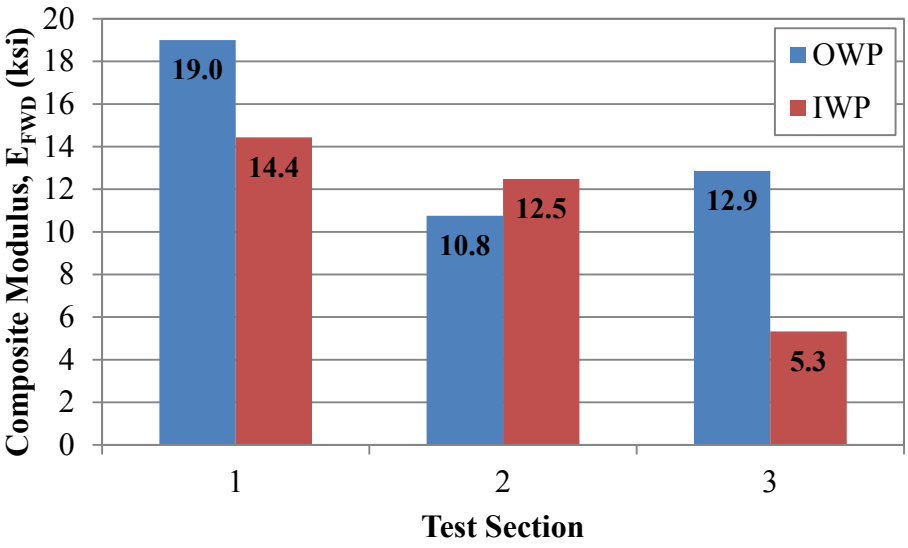

Figure 4-63: Composite modulus based on FWD tests performed after full-scale testing

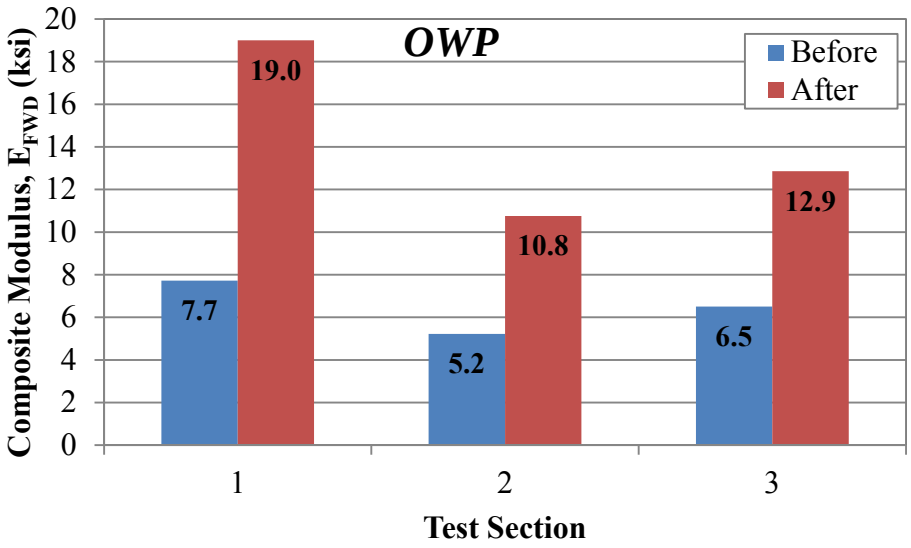

Figure 4-64: Composite modulus based on FWD tests performed along the OWP

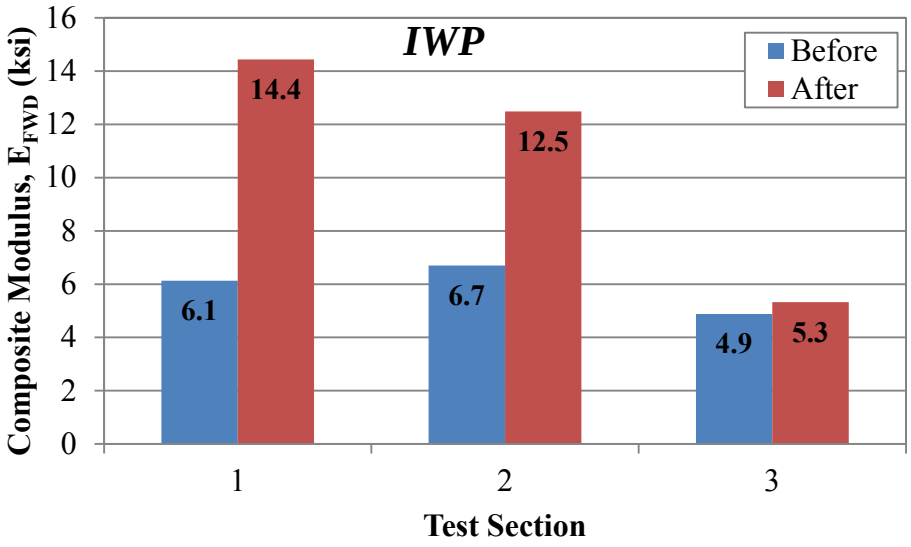

Figure 4-65: Composite modulus based on FWD tests performed along the IWP

FWD Deflection Basin Analysis

The deflection basins obtained from the third drop during FWD testing are shown in Figure 4-66 and Figure 4-67. To accurately compare the results, the deflections are normalized to a 13000 lb. and 9500 lb. load for tests performed prior to and after full-scale testing, respectively. This was needed since the magnitude of applied load varied slightly from test to test. Figure 4-66 and Figure 4-67 show that Test Section 1 produced the shallowest deflection basin during both phases of testing. Once again, the inner wheel path of Test Section 3 indicated a significantly weaker pavement section possibility due to geotextile damage. Unfortunately, due to the different sized plates during FWD testing, it is not possible to compare the deflection basins performed before and after traffic within each test section.

To evaluate the load distribution effectiveness of each tested area an analysis, proposed by Nassar *et al.* (2000), was implemented based on the deflection basin centroid coordinates (see Figure 4-68). This method of analysis was simplified by characterizing the deflection basin as a number of trapezoids and computing the coordinates (X_R, Y_R) of the area centroid with respect to the orthogonal axis passing through the center of the applied load. After finding the centroid, Nassar *et al.* recommend computing the ratio of the coordinates as follows:

$$\mathbf{N} = {}^{X_R}/_{Y_R} \qquad \textbf{Eq. 4-10}$$

When comparing the deflection basin centroid for various pavement sections a good load distribution ability is characterized by a relatively high X_R (flat basin), and a stiff profile is characterized by a low Y_R (shallow basin). As a result, an ideal deflection basin would have a relatively high N value (i.e. good load distribution ability and high stiffness). With that said, shown in Figure 4-69 through Figure 4-74 are the X_R and Y_R centroid coordinates as well as the N value for FWD tests performed before and after full-scale testing. Prior to full-scale testing all test sections appear to have a relatively equal load distribution ability and stiffness. However, the results from FWD after full-scale testing indicate Test Section 1 as having superior strength and stiffness over the two geosynthetically reinforced sections.

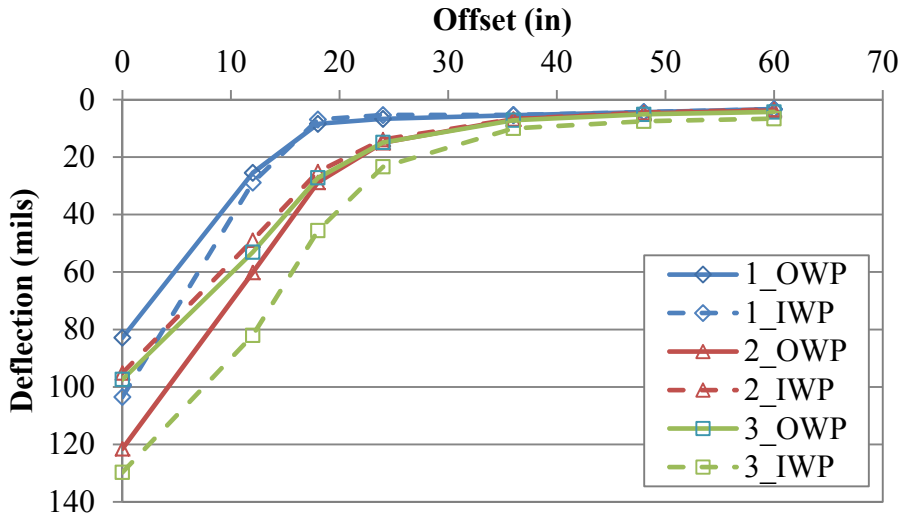

Figure 4-66: FWD deflection basins for tests performed prior to full-scale testing

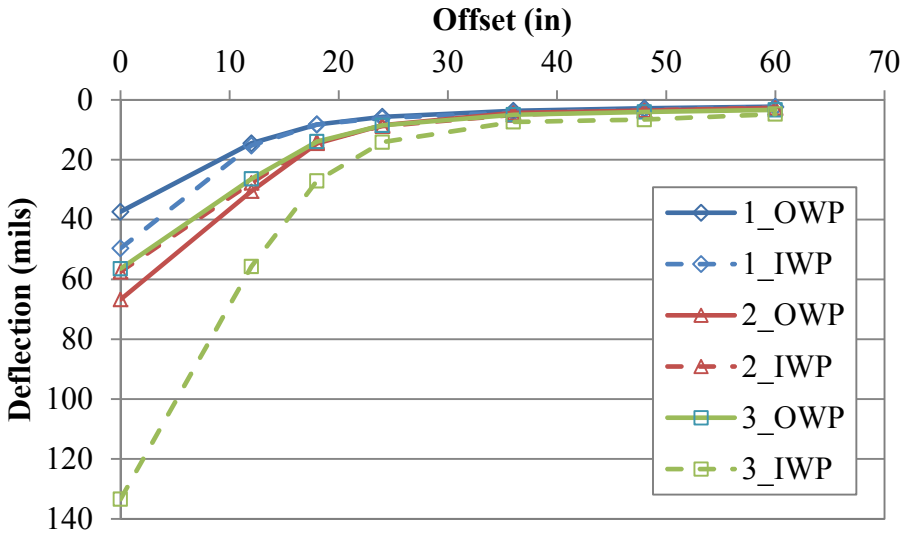

Figure 4-67: FWD deflection basins for tests performed after full-scale testing

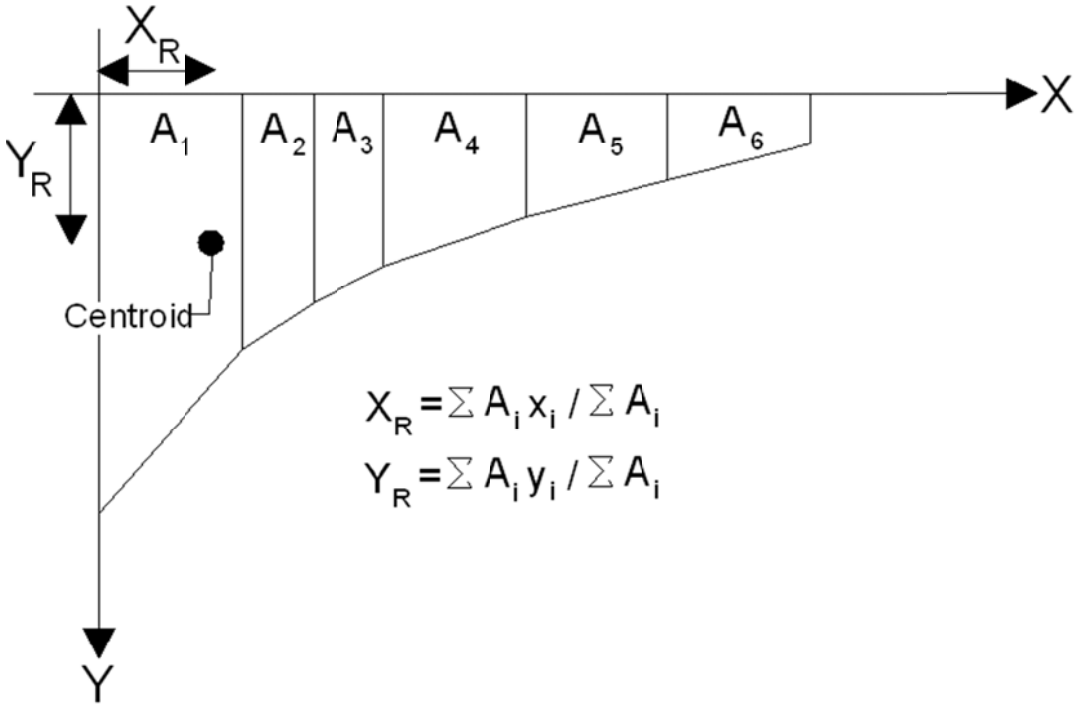

Figure 4-68: Calculation of R_X and R_Y from deflection basin area (Nassar et al. 2000)

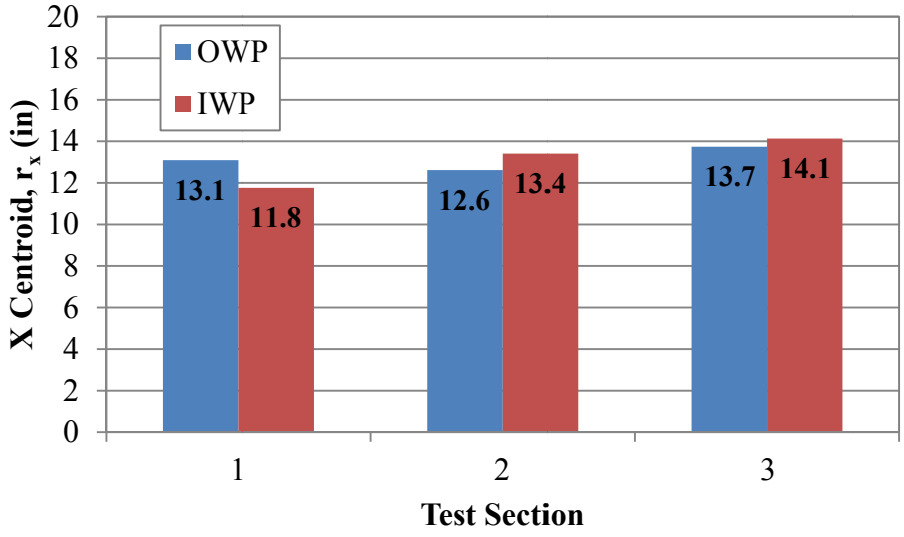

Figure 4-69: X_R coordinate for deflection basins from FWD tests performed prior to full-scale testing

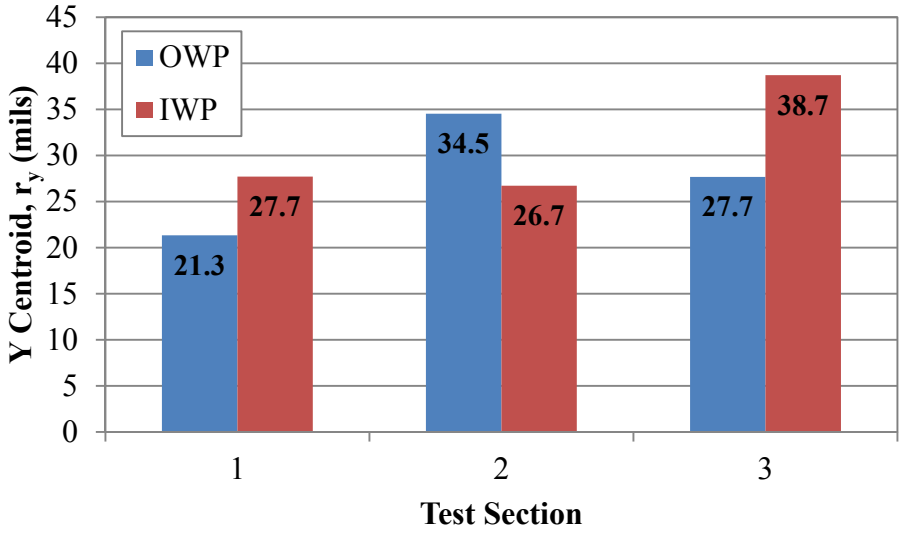

Figure 4-70: Y_R coordinate for deflection basins from FWD tests performed prior to full-scale testing

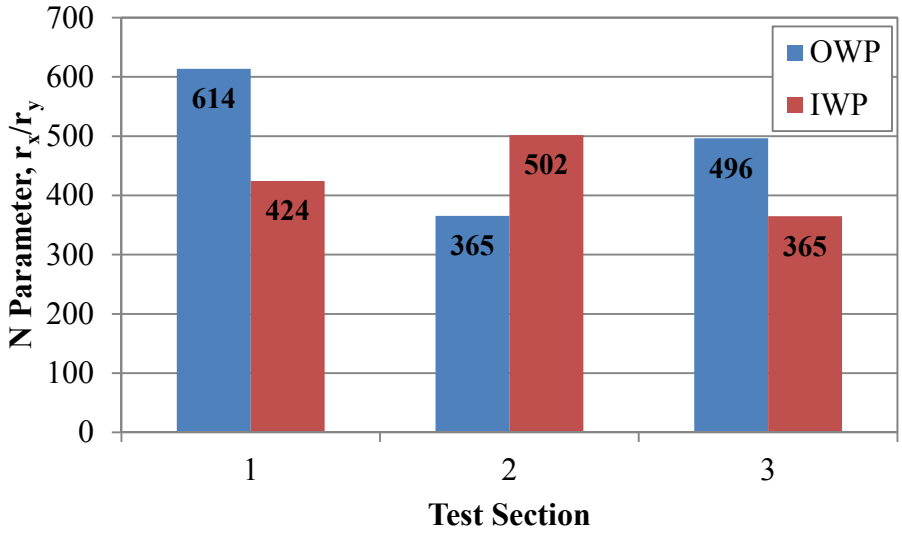

Figure 4-71: N parameter for deflection basins from FWD tests performed prior to full-scale testing

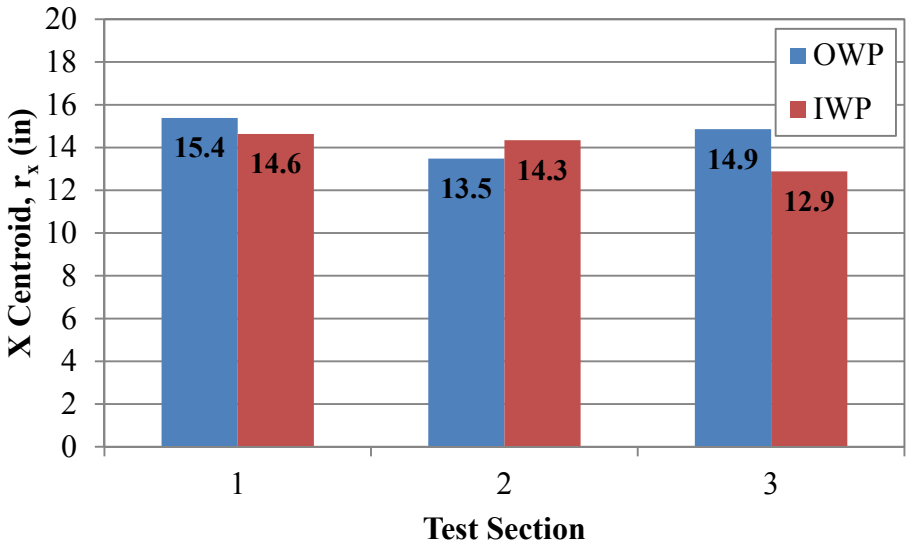

Figure 4-72: X_R coordinate for deflection basins from FWD tests performed after full-scale testing

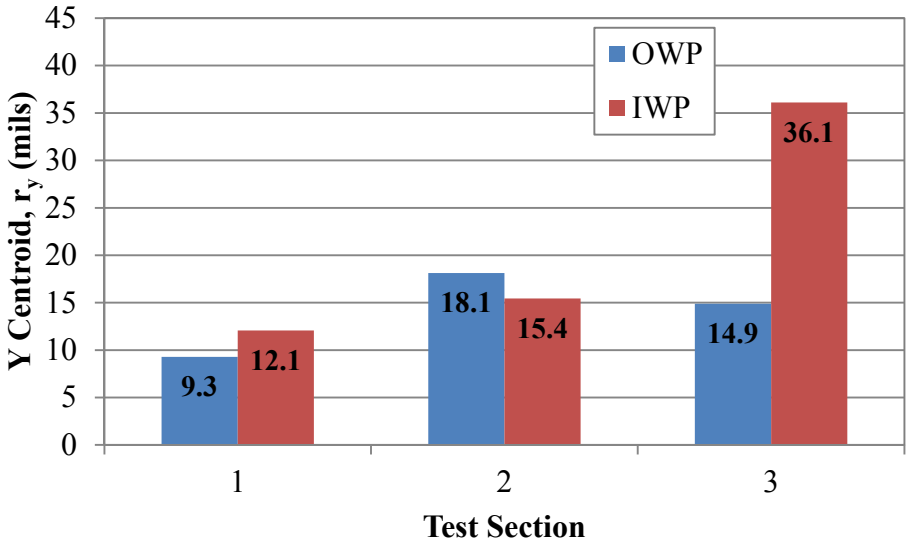

Figure 4-73: Y_R coordinate for deflection basins from FWD tests performed after full-scale testing

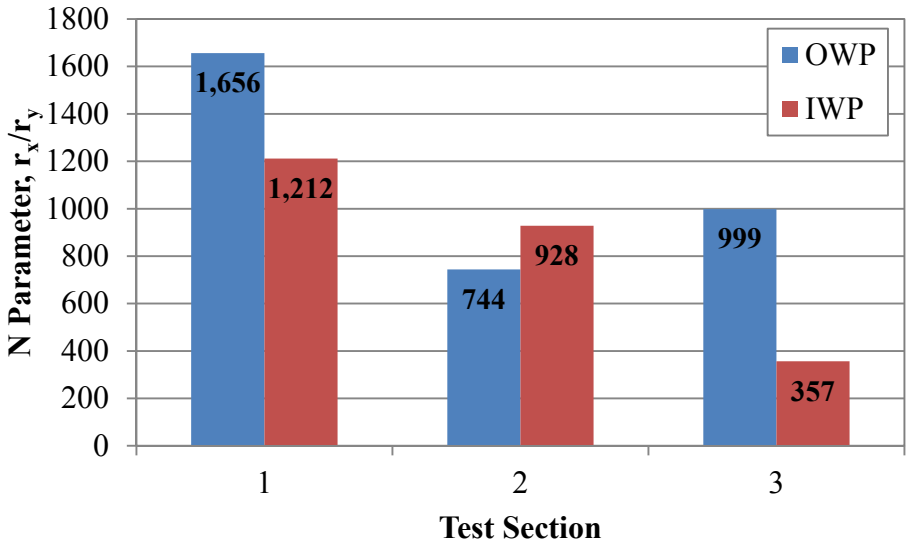

Figure 4-74: N parameter for deflection basins from FWD tests performed after full-scale testing

Chapter Summary

In summary, a number of quality control and in situ tests were conducted on the test pad to assess the soil properties in situ. Based on quality control tests, all stabilized sections were built as required to the specified relative density and water content requirements. DCP, SSG, and FWD tests were performed on the test pad at various stages throughout the project. Based on the results, the following observations were made:

- The NCDOT's current DCPI cut-off of 38 mm/blow was supported by field observations, and would yield a required CBR value of greater than 5-8% or resilient modulus values greater than approximately 6 ksi (40 MPa).
- The results from SSG testing should be used with caution due to the apparent sensitivities of the device.
- FWD results indicated that the composite stiffness and strength of Test Section 1 is comparable to that of the other sections due to the thicker base course layer that prevents higher stresses and corresponding deformations from reaching the soft subgrade.
- No benefit can be discerned with one geosynthetic over another in regards to influencing the base layer stiffness prior to or after repeated truck loading.
- In situ test results in Test Sections 2 and 3 indicate a lower base layer stiffness at the center of the inner wheel path in Test Section 3. This is possibly due to geotextile damage.
- DCP results in Test Section 4 indicated a base layer stiffness within the top five inches comparable to that measured in Test Sections 2 and 3. However, beyond the first five inches the DCPI values increased indicating weaker soils.
- With the exception of Test Section 4, there is a significant increase in base layer stiffness after full-scale testing presumably due to the densification of the base layer soils under repeated truck loading.

CHAPTER 5: FULL-SCALE TEST RESULTS

Field Observations

The full-scale test pad was trafficked the complete 1000 truck passes beginning on June 14, 2011 and ending four days later on June 17, 2011. During this time the test pad was monitored for visual signs of deterioration at the road surface. Observations were also made in regards to the ability of the truck driver to follow the same wheel path and drive directly over top of the earth pressure cells (EPCs). One hour breaks were taken periodically to allow the NCDOT to perform LiDAR surveying. In addition, short one to two minute breaks were taken every 20 truck passes to manage the file size of the stress data and to mitigate the risk associated with losing data in the case of a computer malfunction. This section documents the visual observations that were noted while conducting full-scale testing.

Test Section 1

In the early stages of trafficking Test Section 1 began to show visible signs of rutting after only a few truck passes. In fact, the rutting that had developed in Test Section 1 after a little over 50 truck passes was more than the cumulative rut depth after 1000 truck passes everywhere else in the test pad. As testing progressed the select material in Test Section 1 continued to displace laterally and accumulate on the outer and inner edges of each wheel path. Shown in Figure 5-75 is an image of Test Section 1 after 200 truck passes. It was at this point during testing that the under carriage of the test vehicle had begun scrubbing the mound of heaved soil that ran in-between the outer and inner wheel path. After consulting with the NCDOT it was decided that Test Section 1 had reached failure and was no longer a serviceable construction road. Thus, to allow for testing to precede and enable further evaluation of the stabilization measure, Test Section 1 was repaired by leveling, wetting, and rolling the select material and adding a two to three inch layer of compacted ABC stone (see Figure 5-76). This method of repair proved to be successful in reducing the rate of rutting and allowed for the test section to be trafficked the final 800 truck passes. Shown in Figure 5-77 is an image of Test Section 1 after 1000 truck passes.

Figure 5-75: Test Section 1 after 200 truck passes

Figure 5-76: Test Section 1 being repaired at 200 truck passes

Figure 5-77: Test Section 1 after 1000 truck passes

Test Sections 2 and 3

In terms of rutting, Test Sections 2 and 3 performed significantly better than the other two test sections. Shown in Figure 5-78 and Figure 5-79 is an image of Test Sections 2 and 3 after 1000 truck passes. With the exception of periodic wetting for dust control (which was also needed everywhere else at the field site) neither geosynthetically reinforced section required any maintenance or repair during the truck trafficking period. In terms of visible deterioration, alligator cracking, shown Figure 5-80, became prevalent throughout both sections after approximately 100 truck passes. A considerable amount of rutting did develop at the interface of adjacent test sections (Stations 121+50, 122+00, and 122+50); however, these areas were neglected from the analysis due to the overlapping stabilization measures.

Figure 5-78: Test Section 2 after 1000 truck passes

Figure 5-79: Test Section 3 after 1000 truck passes

Figure 5-80: Image of the OWP in Test Section 3 after 1000 passes. Note the alligator cracking which was prevalent in Test Sections 2 and 3.

Test Section 4

Shown in Figure 5-81 is an image of the cracking that began to develop in the Test Section 4 after only ten truck passes. These cracks propagated in both the longitudinal and transverse directions and were prevalent throughout most of the section after approximately 50 truck passes. In addition, rutting along the inner wheel path (IWP) became visibly apparent after approximately 50 truck passes. As truck trafficking progressed, a significant amount of rutting developed just outside of the second EPC along the IWP of Test Section 4. Due to the geometry of rut being deep in depth but short in length it acted as a pothole and caused the test vehicle to rock violently when passing over it. Out of concern that repeated passes may damage the test vehicle, the area was deemed to have failed after 500 truck passes. To allow for full-scale testing to proceed, the contractor filled the rut with ABC stone using a rubber tired back-hoe. Periodically, the ABC material had to be raked back into the rut due to lateral displacement that accumulated on the outer and inner edges of the wheel path. In addition, a significant amount of rutting also occurred at the first EPC along the outer wheel path (OWP) of Test Section 4. The rut depth for this area, however, did not reach the same magnitude as measured in the other area

of the test section and the complete 1000 passes were able to be conducted without any repair. An image of Test Section 4 after 1000 truck passes is shown in Figure 5-82.

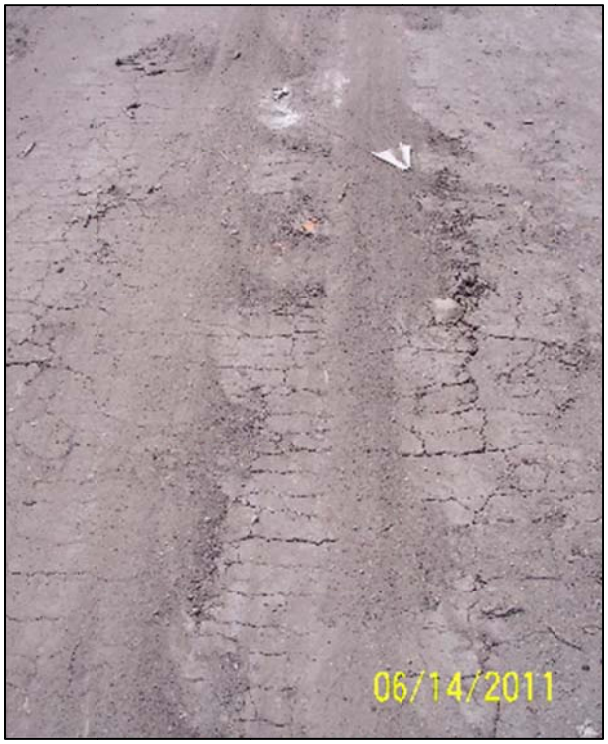

Figure 5-81: Cracks developing along the IWP in Test Section 4 after 10 truck passes

Figure 5-82: Test Section 4 after 1000 truck passes

Rut Development

LiDAR Data Analysis

After the point cloud from each LiDAR survey had been produced it was then transferred into MicroStation® for further processing. Within MicroStation® a coordinate geometry/design package known as GEOPACK® was used to create 13 longitudinal (direction of travel) alignments parallel to the centerline of each wheel path. These alignments, shown in red in Figure 5-83, spanned a total of 21 inches on each side of the centerline in order to capture the entire profile of the wheel path. Along each alignment the elevation was recorded at stations spaced every 3 inches apart from the center of the first EPC to the center of the second EPC. In other words, the elevation was recorded at every node where a longitudinal alignment (red line in Figure 5-83) crossed a transverse station (blue line in Figure 5-83). As mentioned previously, the portion of wheel path within each test section that ran outside the two EPCs was not included into the rutting analysis out of precaution that the overlapping test sections would not accurately represent their respective stabilization measure. One exception was along the IWP of Test Section 4 where the maximum amount of rutting occurred just outside of the second EPC. This exception was justified based on the fact that there was an additional 20 plus feet of roadway beyond the second EPC that was stabilized with cement.

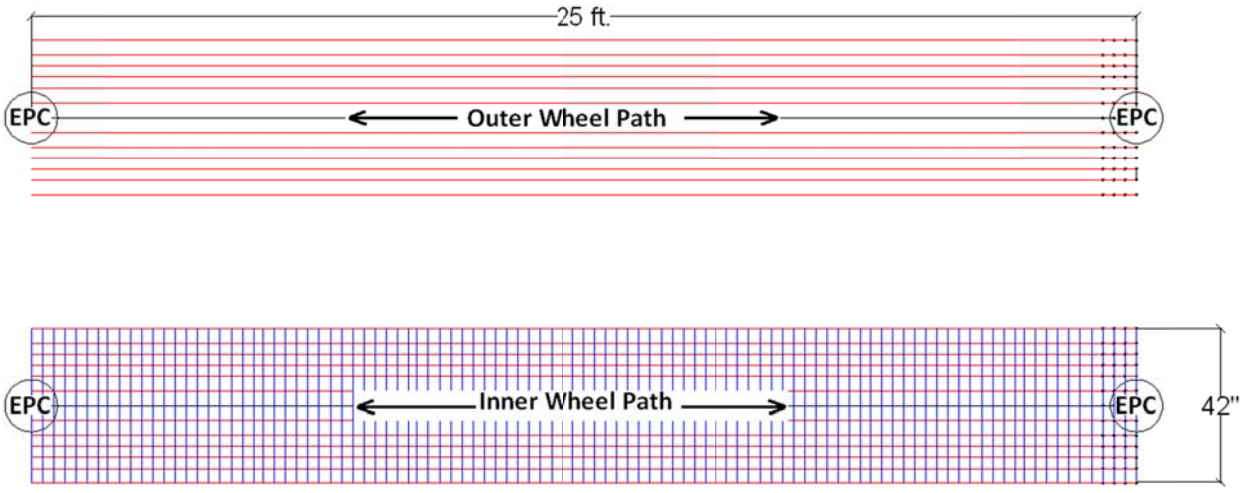

Figure 5-83: An illustration of the alignment (red lines) and stationing (blue lines) used to capture the elevation from the LIDAR data

It is important to note that within this report the depth of rutting at a specific station is defined as the maximum vertical settlement from the initial grade before traffic testing. For that reason, the elevation at each node was compared to the elevation at the same node prior to testing in order to obtain the change in elevation at that particular truck pass. The maximum amount of elevation change at each station was then designated as the rut depth. As an example, Figure 5-84 depicts the transverse profile of the IWP at station 121+20.50 of Test Section 1 after 200 truck passes. The measured profile before traffic testing is also shown as the initial grade which serves as the baseline reference to compute the cumulative rut depth. Based on the maximum difference in elevation, the rut depth for this station after 200 truck passes is 4.5 inches. This approach differs from what is known as "apparent rut" which uses the displaced soil on each side of the rut bowl as the baseline reference. Clearly the use of apparent rut versus actual rut would result in a significantly higher measurement of rut depth.

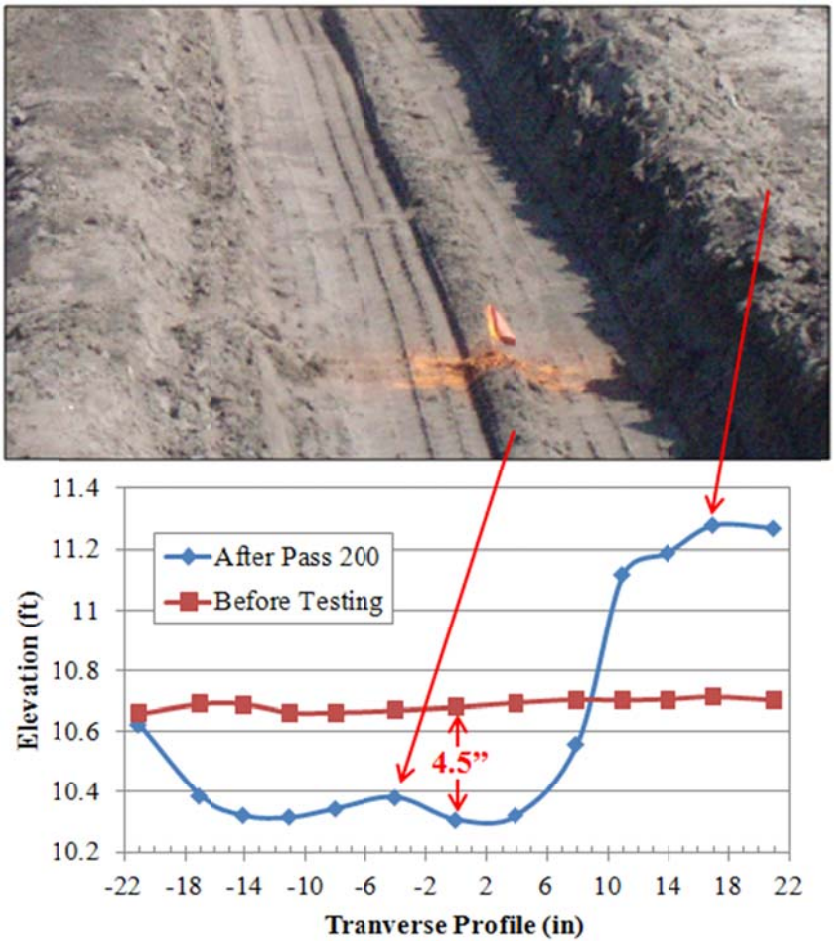

Figure 5-84: A transverse view of a station located in the inner wheel path of Test Section 1

Rut Depth Test Results

Shown in Figure 5-85 through Figure 5-88 are plots of rut depth at selected traffic intervals along the inner and outer wheel path for each test section. One of the first observations is the considerable fluctuation in rut depth within each test section. These differences are due in part to the natural variation in the strength and stiffness of the base and subgrade soils within each test section. In addition, large aggregate particles create an uneven ground surface as shown in Figure 5-89. A more in depth analysis of the variation in rut depth within each test section is provided below.

Test Section 1

Looking at Figure 5-85, the thin ABC layer placed after truck pass 200 worked well in providing vertical confinement over the select material to hamper incremental plastic strains during the remaining 800 truck passes. However, note the difference in the amount of rutting in each wheel path that develops between passes 200 and 300 after repair. Rutting along the IWP was in excess of 1.5 inches more than the rutting that developed along the OWP. Despite limited DCP tests which indicated otherwise, the IWP was clearly in a much looser state after repairing the test section. As a result, additional compaction of the ABC and select material occurred along the IWP during trafficking resulting in a higher magnitude of rut depth with repeated truck loading.

Test Section 2

When referring to Figure 5-86, both wheel paths produced with very little rutting. The OWP did produce a deeper rut than seen along the IWP presumably due to the lower base course stiffness measured during in situ testing.

Test Section 3

As mentioned earlier in Chapter 4, the geotextile at the center of the IWP in Test Section 3 is suspected of being damaged during full-scale testing. This observation is based on the in situ test results which indicated a substantially lower base and composite stiffness at this location versus elsewhere in the test section. The rutting results in Figure 5-87 support this notion based on the high cumulative rut depth with repeated truck pass.

Test Section 4

When referring to Figure 5-88, note the significant amount of rutting that developed at each end of the cement stabilized section. There are two possible factors for this behavior. These include:

(1) Localized area of weak subgrade
(2) Localized area of under-stabilized soil-cement base

In regards to the possible weak subgrade, recall that the holes dug to install the EPCs in Test Sections 1, 2, and 3 were approximately six inches deep from the base/subgrade interface. The sidewall of the holes was completely vertical and was backfilled using ASTM silica sand. However, in Test Section 4 the EPCs had to be installed prior to cement mixing. As a result, a hole 16 inches deep was dug at each sensor location. To prevent the holes from caving in, the sidewalls were sloped at angle thus disturbing a higher volume of subgrade soil. Once the EPCs were installed with three inches of sand above and below it, the subgrade soil was backfilled into the hole and compacted using a hand tamper. However, it is well known that a soils fabric structure has a significant influence on its strength, especially fine-grained soils. When disturbing the delicate fabric structure, the inter-particle forces are removed and the stress-deformation behavior is permanently altered (Mitchell & Soga, 2005). As a result, there is a possibility that the subgrade strength around the location of the EPCs was significantly lower relative to elsewhere in the test section and thus initiated the excessive rutting.

In regards to the possible under-stabilized soil-cement base, a single plate load test performed in the center of Test Section 4 using a four inch diameter plate indicated substantially lower base layer strength in the field compared to the lab. The four inch plate was used to limit the depth of influence to the eight inch stabilized layer (i.e. depth of influence = 2B). Shown in Figure 5-90 is a plot of the results. Recall that a 12% cement dosage rate was used when constructing the section in the field based on an average lab UCS of 137 psi. However, during plate load testing the base layer begins to reach an asymptotic value of approximately 70 psi, indicating that soil-cement has reached its performance capacity well below what should be expected based on lab results. Although this observation is limited to the area around the plate load test location, it does facilitate the inclination that other areas in Test Section 4 were more than likely much weaker than expected. It is important to note that while potential errors are involved in the plate load data (discussed in Chapter 3 and Appendix F), the errors would only indicate worse

behavior (i.e. lower strength of the soil-cement) and thus are justified for use in explaining the under-stabilized behavior in the test section.

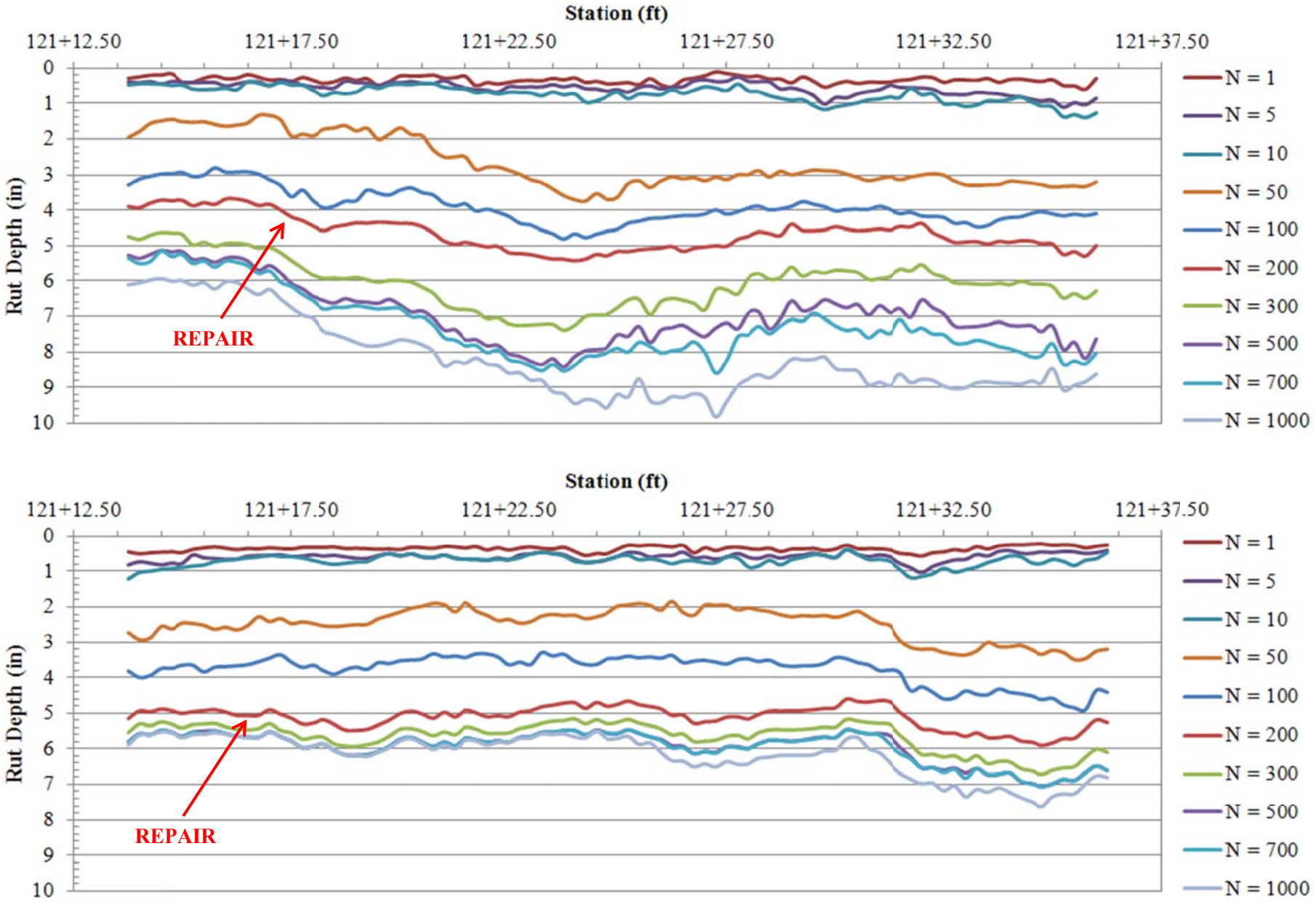

Figure 5-85: Permanent deformation along the IWP (top) and OWP (bottom) in Test Section 1

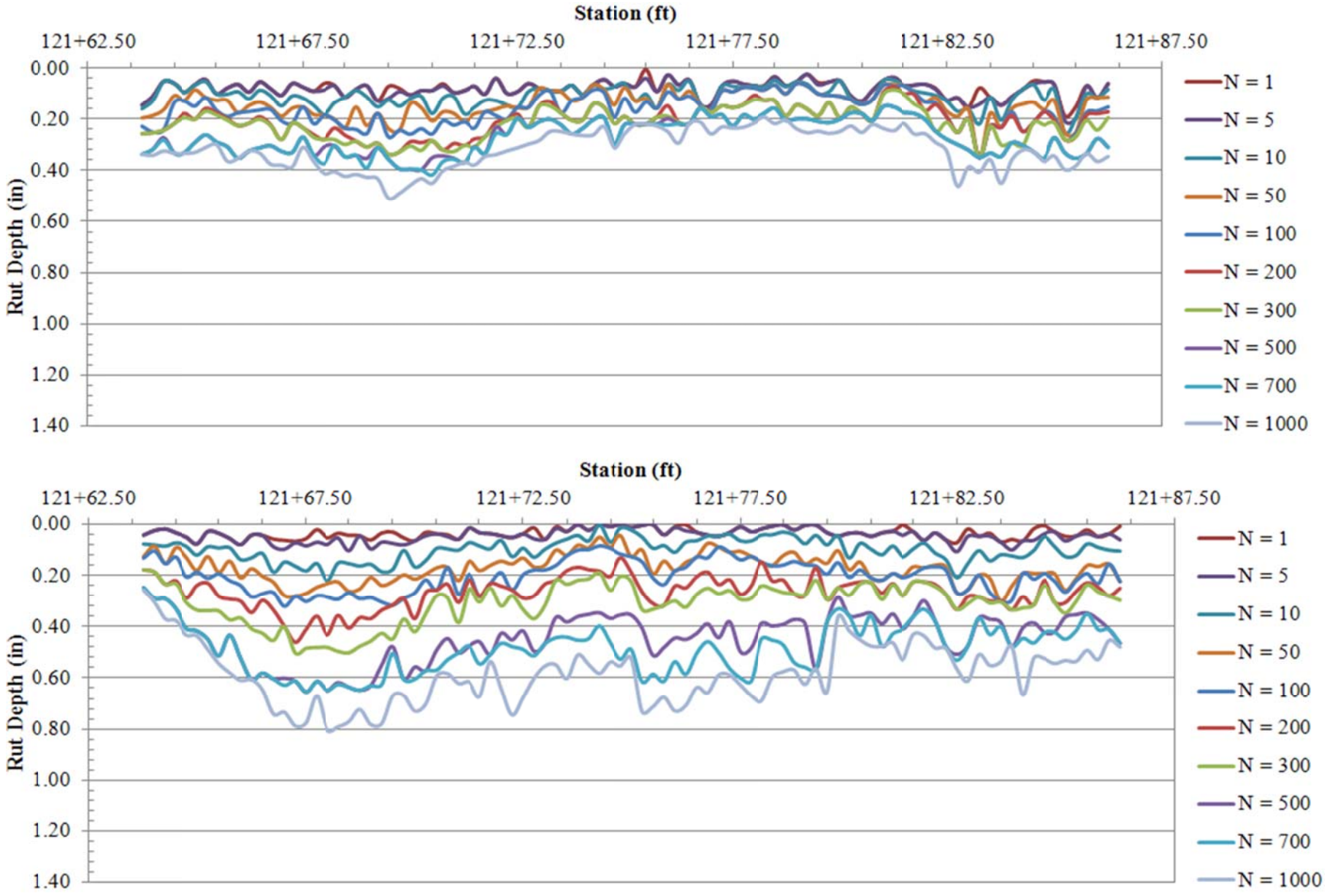

Figure 5-86: Permanent deformation along the IWP (top) and OWP (bottom) in Test Section 2

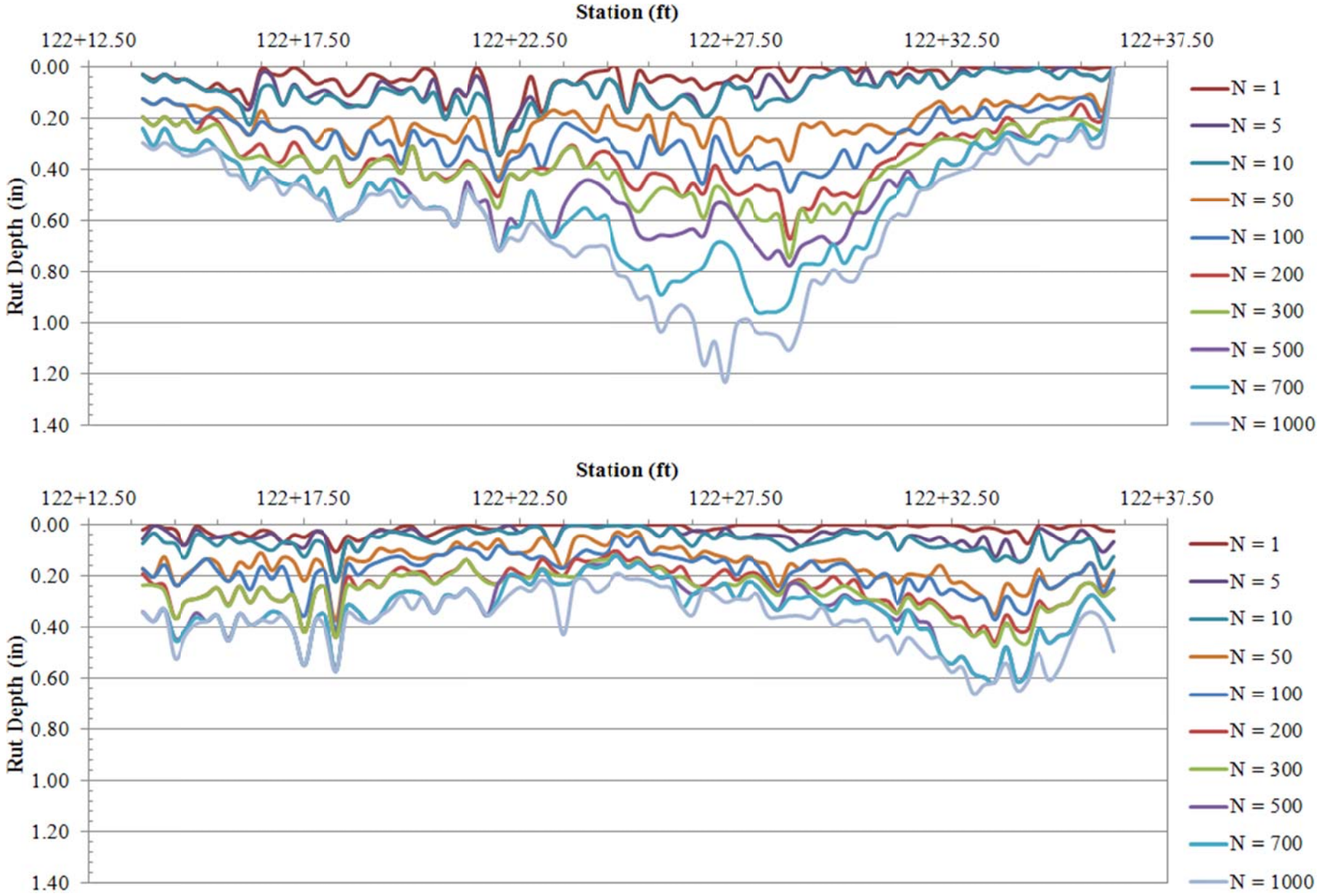

Figure 5-87: Permanent deformation along the IWP (top) and OWP (bottom) in Test Section 3

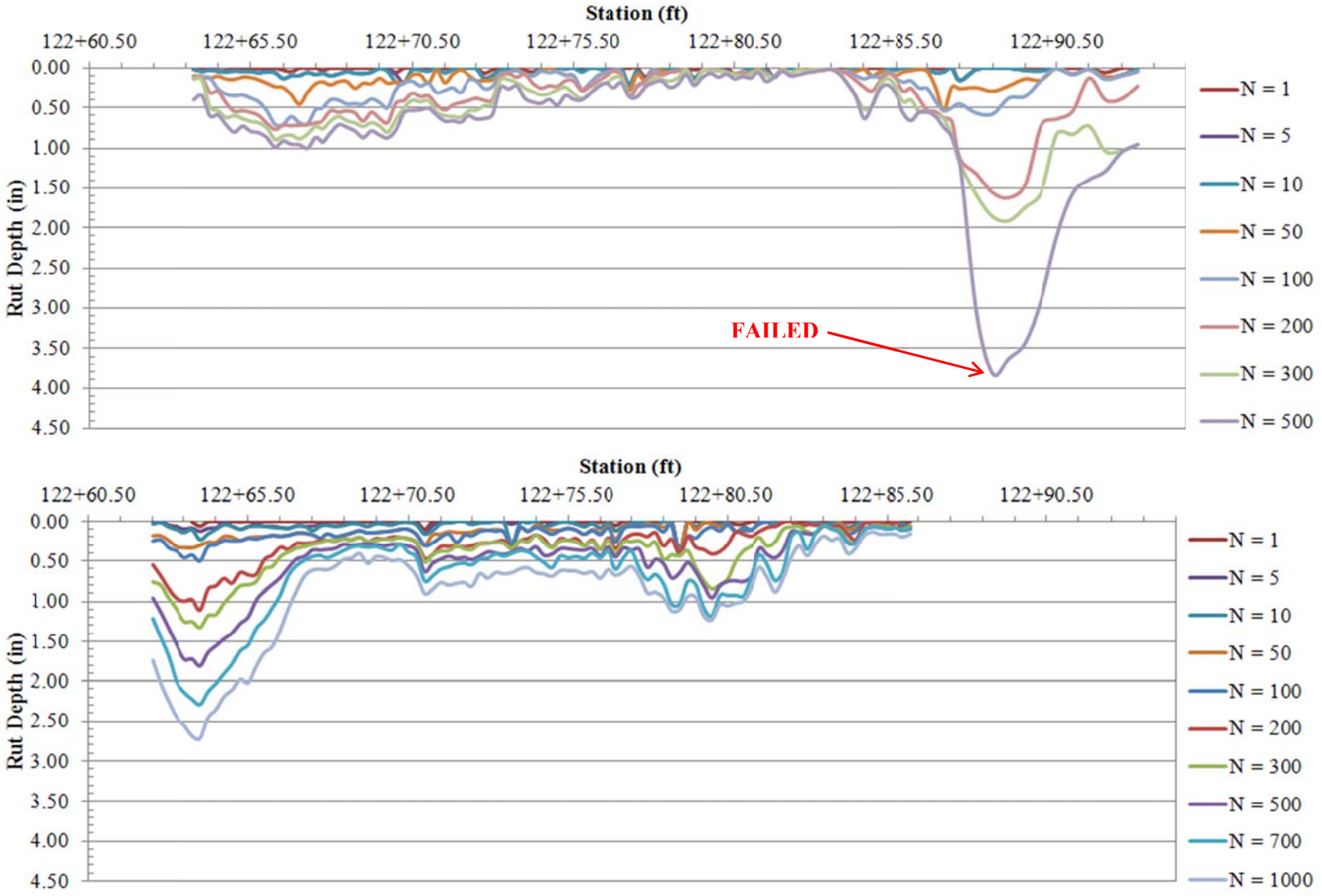

Figure 5-88: Permanent deformation along the IWP (top) and OWP (bottom) in Test Section 4

Figure 5-89: An image taken close to the ground surface of the OWP in Test Section 2

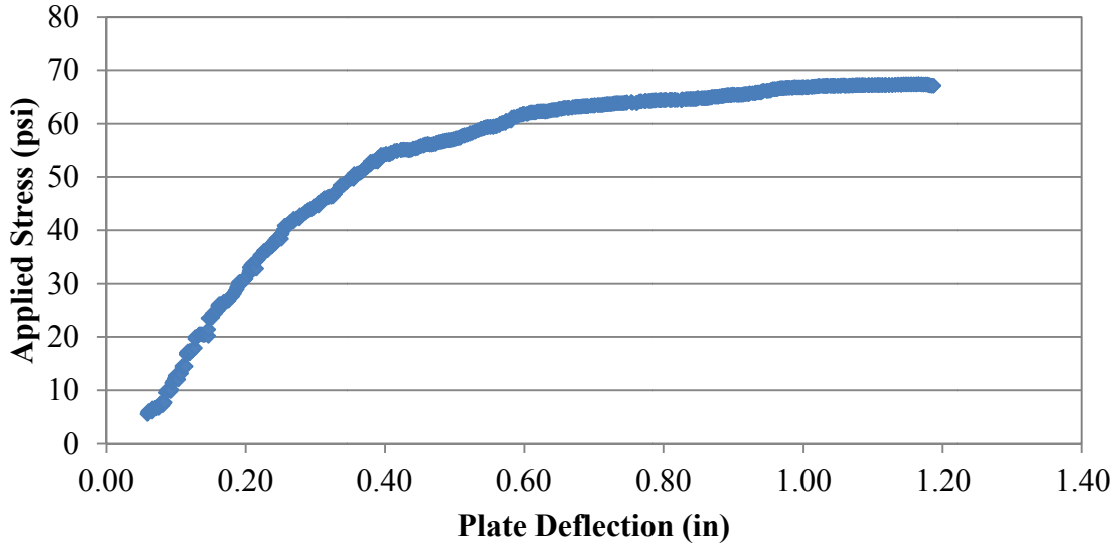

Figure 5-90: Plate load results performed using a 4 inch diameter plate in Test Section 4

The minimum, maximum, and average rut depth for both wheel paths in each test section is presented in Table 5-24 through Table 5-27. The equivalent single axle load (ESAL) is also provided in the tables. ESAL is used to convert the damage from various axle configurations and load magnitudes into a standard single axle 18 kip load for pavement design. The ESAL for all test sections is based on a terminal serviceability index of 2.5, a front axle load of 17.18 kips and a dual back axle load of 42 kips. In addition, the ESAL for Test Section 1 is based on an initial structural number of 3.15, while the ESAL for Test Sections 2, 3, and 4 is based on an initial structural number of 1.12. The ESAL for Test Section 1 was determined to be 3.31 per truck pass while the ESAL for Test Sections 2, 3, and 4 was determined to be 3.57 per truck pass. In other words, for every truck pass performed on Test Section 1, the damage induced is equivalent to 3.31 times the damage induced by one pass of an 18 kip single axle load.

Shown in Figure 5-91 is a plot of the average rut depth along both wheel paths for each test section as a function of truck pass. To present the results in terms of ESAL, Figure 5-92 and Figure 5-93 present the average rut depth for Test Section 1, and Test Sections 2, 3, and 4, respectively. Note that the scale for rut depth in Figure 5-93 has been reduced for easier readability.

Looking at the results, the geosynthetically reinforced sections produced the least amount of cumulative rutting. After the ABC densified during the initial stages of trafficking, the tensile strength of the geosynthetics was apparently mobilized, delaying further rut formation. Unfortunately, due to the absence of a controlled (unreinforced) ABC section, it is difficult to assess how much of the performance within Test Sections 2 and 3 is due to the geosynthetics and how much is due to the high quality fill (i.e. ABC). Regardless, for the soil and loading conditions presented, no increase in benefit was observed when using a high-strength geotextile versus a lower strength geogrid. Possible explanations for this behavior are twofold. Firstly, the deformation in both sections apparently induced a relatively low strain level in both geosynthetics. As a result, the mobilized tensile forces were below what was necessary to observe a dramatic difference in behavior between the two geosynthetics. This confirms the recommendation made by Hufenus *et al.* (2006) that specifying extremely stiff geosynthetics is impractical. Secondly, the stiffer subgrade (CBR between 2.5 and 4) apparently enabled aggregate interlock to develop between the geogrid apertures. As a result, base contamination

was less of an issue indicating reinforcement was the dominant geosynthetic function rather than separation. It is important to emphasize that the behavior of the geosynthetics observed in this study are limited to the soil and loading conditions presented.

Test Section 4 produced slightly higher average rut depths than the geosynthetically reinforced sections due to the localized areas of pronounced cumulative rutting. However, there were several areas of the soil-cement test section that performed as well and in some cases better than the geosynthetically reinforced sections. Regardless, any failure of the soil-cement layer requires extensive removal of the roadway in order for construction equipment to access and effectively repair the roadway section. This is one reason why the NCDOT limits the amount of traffic on newly constructed soil-cement roadways.

The deep undercut and select material backfill in Test Section 1 produced the highest cumulative rut depths among the four test sections. As mentioned before, throughout the early stages of trafficking rutting became progressively worse due to the constant lateral displacement of select material. After repair at truck pass 200 (ESAL=662), rutting did occur, however, at a much slower rate. In addition, the rutting appeared to be primarily due to the densification of the ABC and select material rather than heave. This is based on the observation that the cross sectional area of the rut bowl was higher than that of the heaved material on each side of the wheel path.

Table 5-24: Minimum, maximum, and average rut depth measured in Test Section 1 during full-scale testing

Truck Pass	ESAL	*Inner Wheel Path* - Rut Depth (in.)			*Outer Wheel Path* - Rut Depth (in.)		
		Minimum	Maximum	Average	Minimum	Maximum	Average
1	3.31	0.10	0.60	0.33	0.22	0.57	0.36
5	17	0.24	1.11	0.56	0.39	1.04	0.59
10	33	0.39	1.40	0.74	0.39	1.21	0.71
50	166	1.33	3.74	2.66	1.84	3.50	2.49
100	331	2.80	4.81	3.89	3.30	4.91	3.78
200	662	3.68	5.42	4.65	4.60	5.90	5.11
300	993	4.63	7.39	6.05	5.16	6.72	5.65
500	1655	5.13	8.44	6.92	5.46	7.06	5.94
700	2317	5.15	8.60	7.26	5.46	7.06	5.95
900	2979	5.94	9.82	8.15	5.50	7.62	6.14
1000	3310	5.94	9.82	8.20	5.50	7.62	6.17

Table 5-25: Minimum, maximum, and average rut depth measured in Test Section 2 during full-scale testing

Truck Pass	ESAL	*Inner Wheel Path* - Rut Depth (in.)			*Outer Wheel Path* - Rut Depth (in.)		
		Minimum	Maximum	Average	Minimum	Maximum	Average
1	3.57	0.00	0.19	0.08	0.00	0.08	0.03
5	18	0.02	0.21	0.08	0.00	0.11	0.04
10	36	0.05	0.25	0.11	0.00	0.22	0.10
50	179	0.06	0.35	0.14	0.04	0.30	0.17
100	357	0.06	0.35	0.17	0.08	0.32	0.20
200	714	0.07	0.35	0.21	0.13	0.46	0.27
300	1071	0.09	0.35	0.22	0.18	0.50	0.31
500	1785	0.15	0.40	0.27	0.25	0.66	0.44
700	2499	0.15	0.42	0.27	0.25	0.66	0.49
900	3213	0.15	0.51	0.30	0.26	0.80	0.53
1000	3570	0.19	0.51	0.32	0.26	0.80	0.58

Table 5-26: Minimum, maximum, and average rut depth measured in Test Section 3 during full-scale testing

Truck Pass	ESAL	*Inner Wheel Path* - Rut Depth (in.)			*Outer Wheel Path* - Rut Depth (in.)		
		Minimum	Maximum	Average	Minimum	Maximum	Average
1	3.57	0.00	0.34	0.05	0.00	0.11	0.02
5	18	0.00	0.34	0.08	0.00	0.22	0.05
10	36	0.00	0.34	0.09	0.00	0.22	0.06
50	179	0.11	0.43	0.22	0.03	0.37	0.15
100	357	0.12	0.49	0.28	0.04	0.41	0.18
200	714	0.14	0.67	0.36	0.10	0.46	0.25
300	1071	0.19	0.74	0.39	0.12	0.48	0.26
500	1785	0.22	0.77	0.48	0.12	0.61	0.33
700	2499	0.22	0.96	0.53	0.12	0.61	0.33
900	3213	0.22	1.05	0.55	0.15	0.61	0.35
1000	3570	0.24	1.23	0.61	0.19	0.66	0.38

Table 5-27: Minimum, maximum, and average rut depth measured in Test Section 4 during full-scale testing

Truck Pass	ESAL	*Inner Wheel Path* - Rut Depth (in.)			*Outer Wheel Path* - Rut Depth (in.)		
		Minimum	Maximum	Average	Minimum	Maximum	Average
1	3.57	0.00	0.11	0.01	0.00	0.36	0.01
5	18	0.00	0.21	0.03	0.00	0.41	0.04
10	36	0.00	0.22	0.04	0.00	0.41	0.05
50	179	0.00	0.54	0.11	0.00	0.41	0.12
100	357	0.00	0.71	0.21	0.00	0.50	0.14
200	714	0.00	1.62	0.34	0.00	1.11	0.31
300	1071	0.01	1.91	0.46	0.04	1.33	0.38
500	1785	0.01	3.82	0.63	0.05	1.81	0.53
700	2499	0.01	*Fail*	0.65	0.05	2.29	0.66
900	3213	0.02	*Fail*	0.69	0.06	2.61	0.78
1000	3570	0.02	*Fail*	0.75	0.13	2.72	0.86

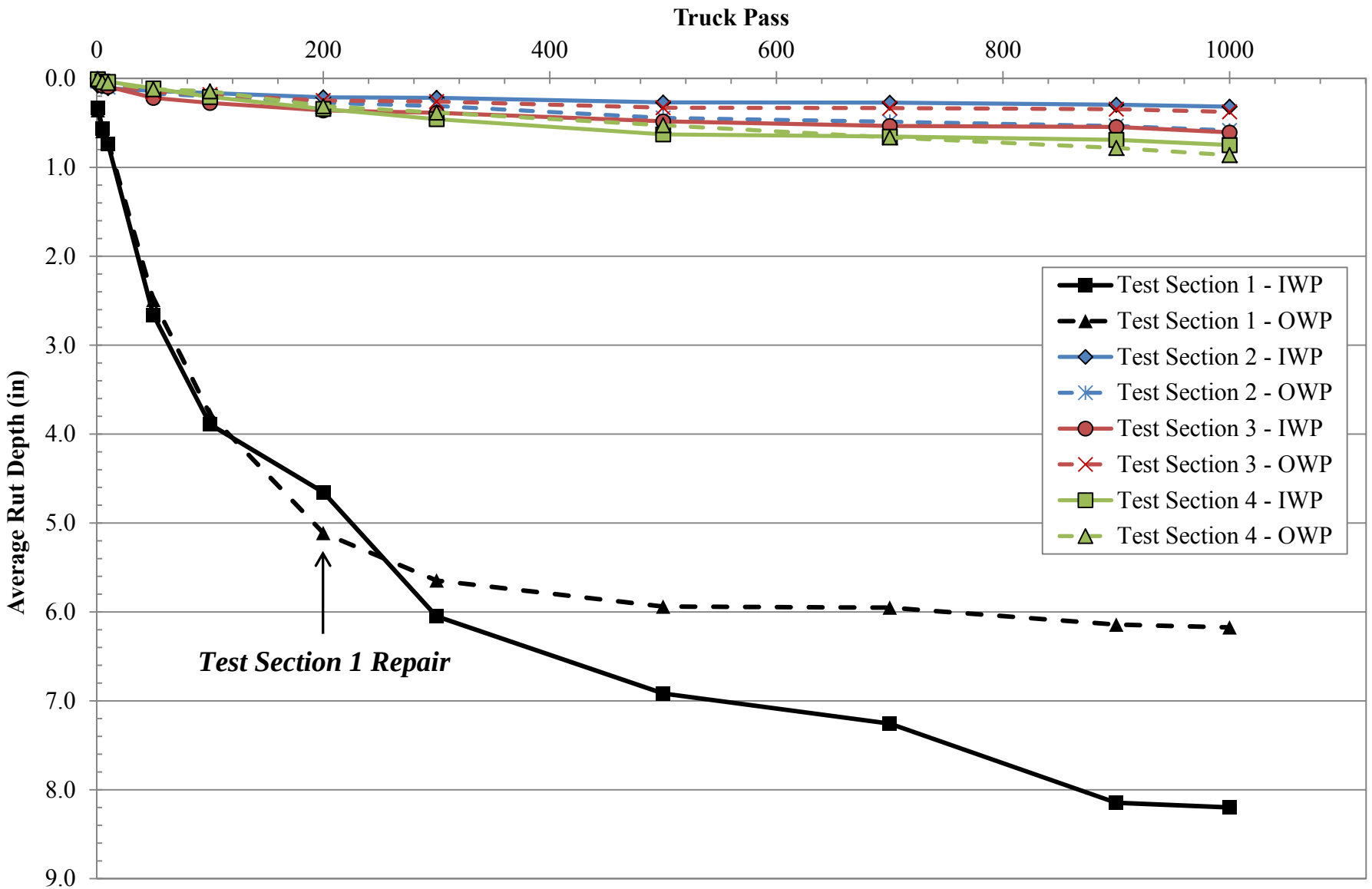

Figure 5-91: Average rut depth versus number of passes for all test sections

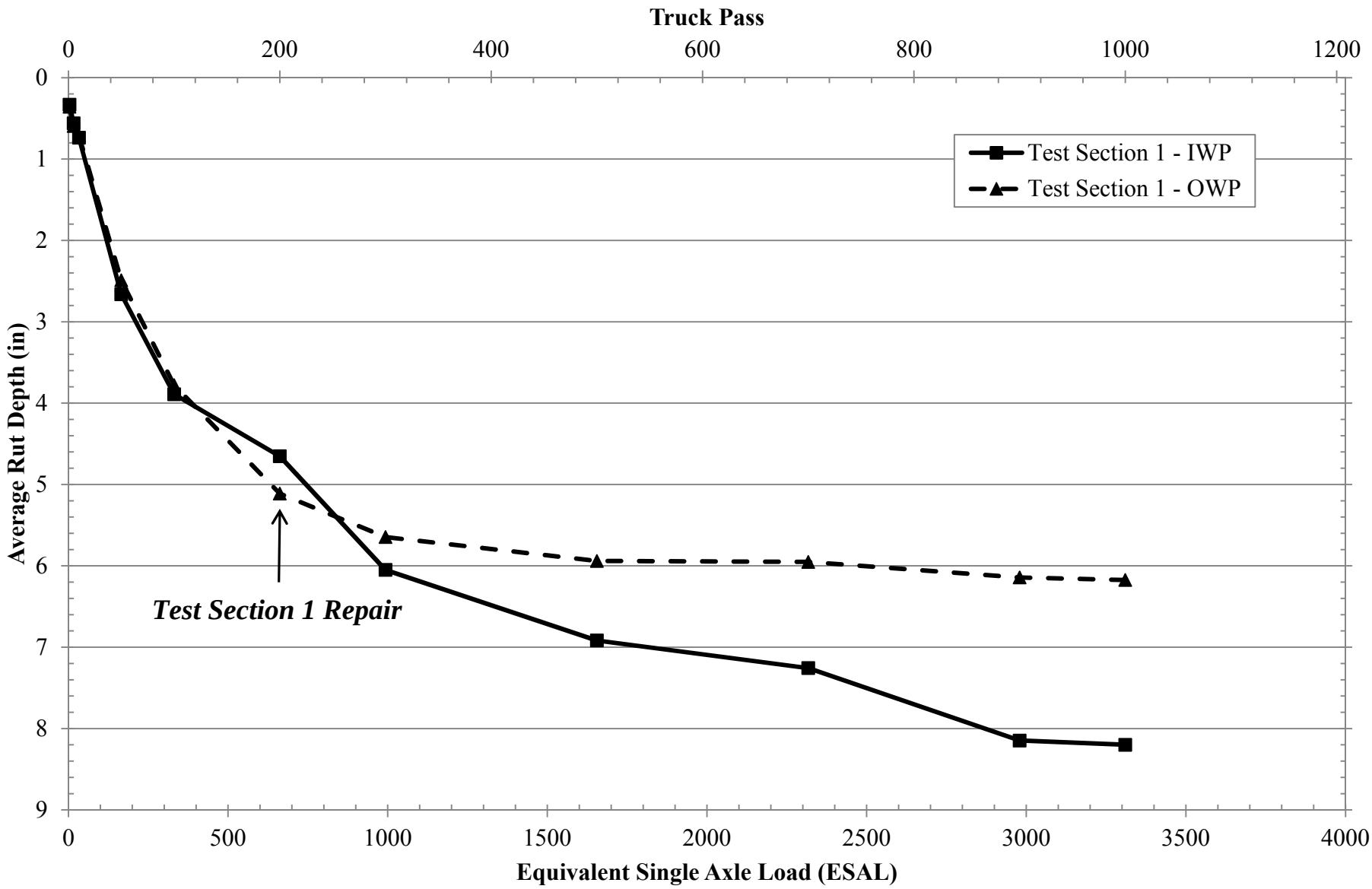

Figure 5-92: Average rut depth versus number of passes and ESAL for Test Section 1

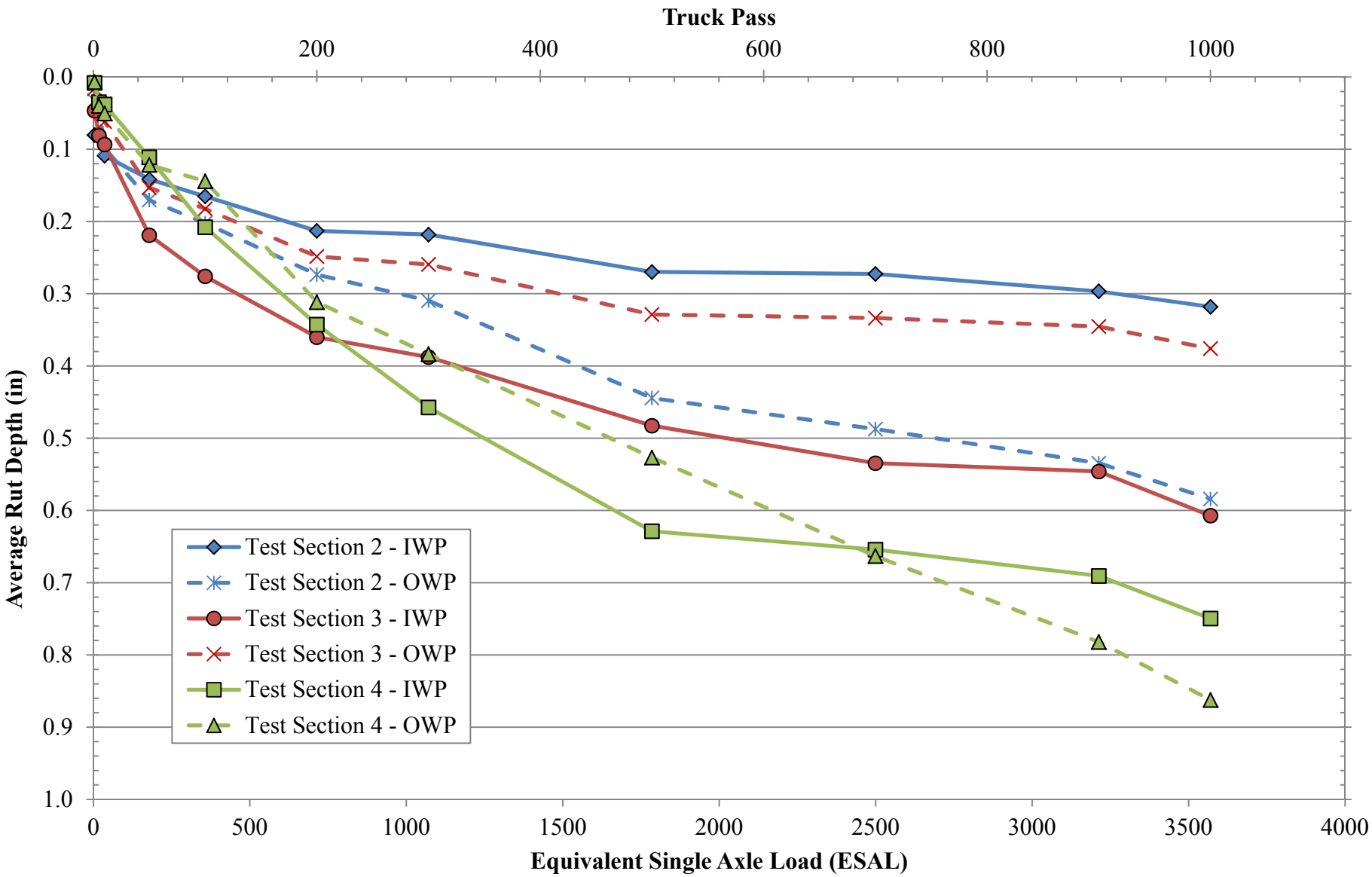

Figure 5-93: Average rut depth versus number of passes and ESAL for Test Sections 2, 3, and 4 (note the change in scale)

Stress Distribution

Earth Pressure Cell (EPC) Data Analysis

During each truck pass three dynamic loads were applied due to the trucks three axle configuration shown in Figure 5-94. After traffic testing was completed each wheel path had been subjected to a total of 3000 dynamic loads. During this time the traffic-induced subgrade stresses measured by the 15 working earth pressure cells (EPCs) were stored as text files after every 20 truck passes. To reduce the data, a MATLAB® program was written that processed the text files to determine the maximum magnitude of stress for each dynamic load. To do this the program searched for local maxima in the stress pulse produced by each axle; each peak value corresponded to the peak stress. In addition, the program also recorded the time at which the peak stress occurred and the corresponding axle that applied the load (i.e. front axle (FA), back axle 1 (BA1), and back axle 2 (BA2)). It is important to note that the EPCs were zeroed prior to testing and thus measured the increase in vertical stress without accounting for geostatic stresses.

Preliminary analyses revealed significant variability in the magnitude of stress increase on a short term (pass to pass) basis. Shown in Figure 5-95a is a graph of the maximum stress as a function of truck pass due to the applied load from BA1 and measured by EPC 8. Note that the degree of variability on a short term basis is approximately six psi. The primary reason for the short term variability was due to lateral wander. Lateral wander is a term used throughout the pavement industry to describe the lateral distribution of wheel loads which occurs naturally in the field due to driver habits, wind, etc. During full-scale testing the driver repeatedly following a different alignment depending on the direction of travel. As a result, the location of the applied load relative to each EPC consistently alternated from one location when traveling in the north direction to another location when travelling in the south direction. To better illustrate this point, Figure 5-95b shows the exact same data set as shown in Figure 5-95a, however, this time the truck passes are differentiated by color based on the direction of travel. It is apparent, based on the figure, that when the test vehicle traveled in north direction the back tire was closer to the EPC than when traveling in the south direction. Note that by distinguishing the truck passes by the direction of travel, the variability of the measured stress reduces from approximately six psi to three psi. The stress variability for passes conducted in the same direction is also due to lateral wander, however, this time on a smaller scale.

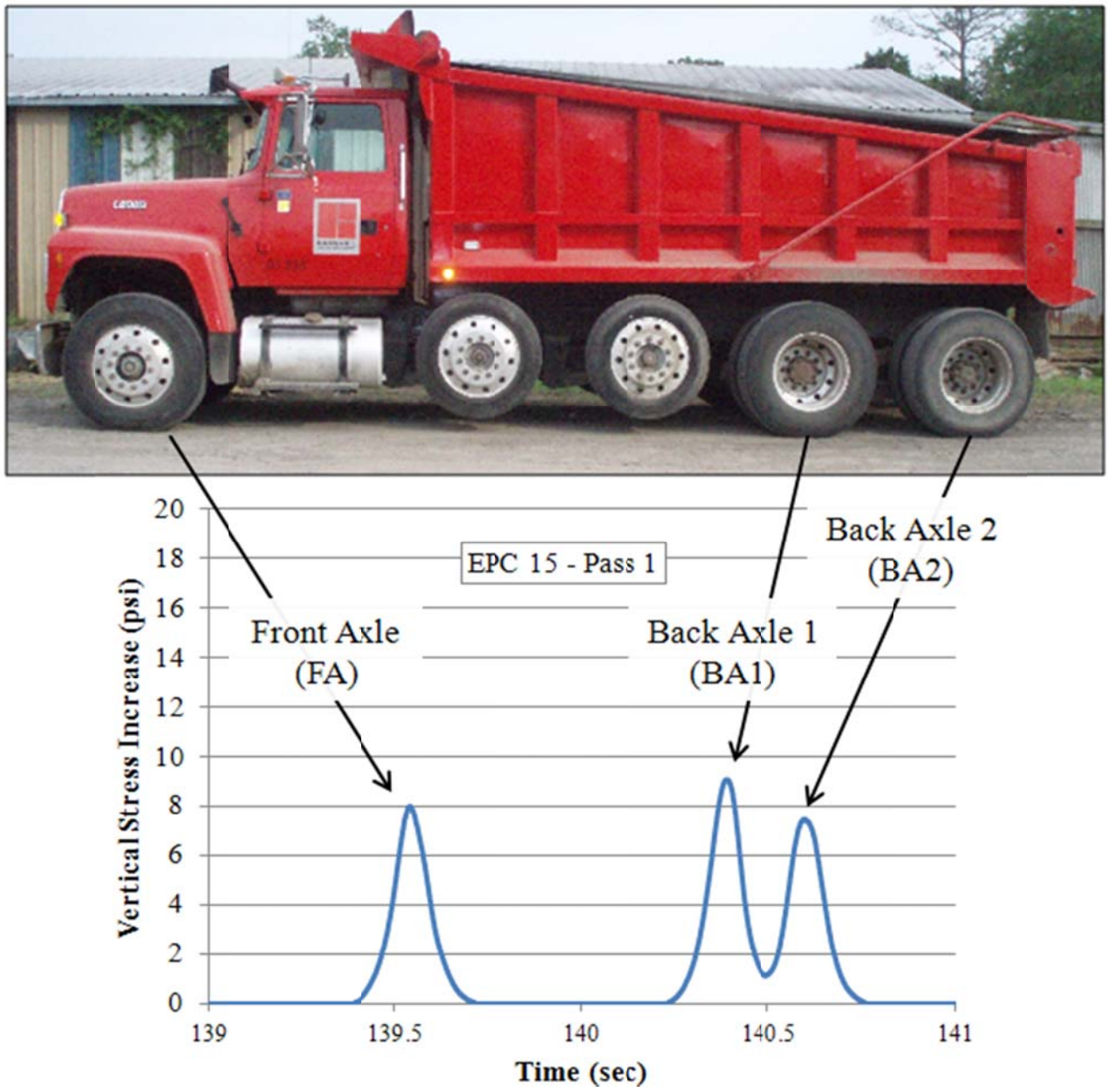

Figure 5-94: Truck used for loading and the EPC output during the first pass from EPC 15

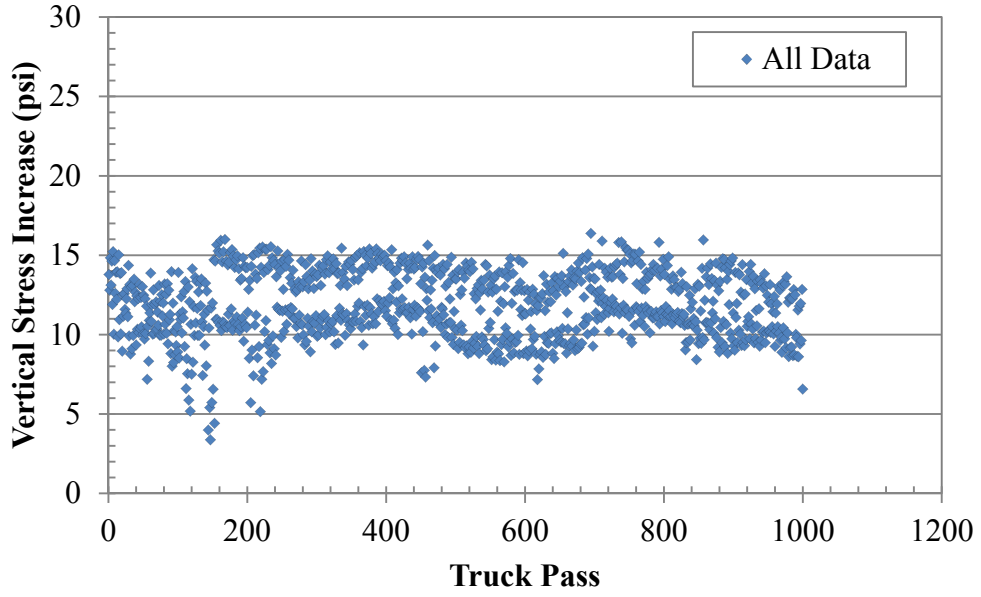

(a)

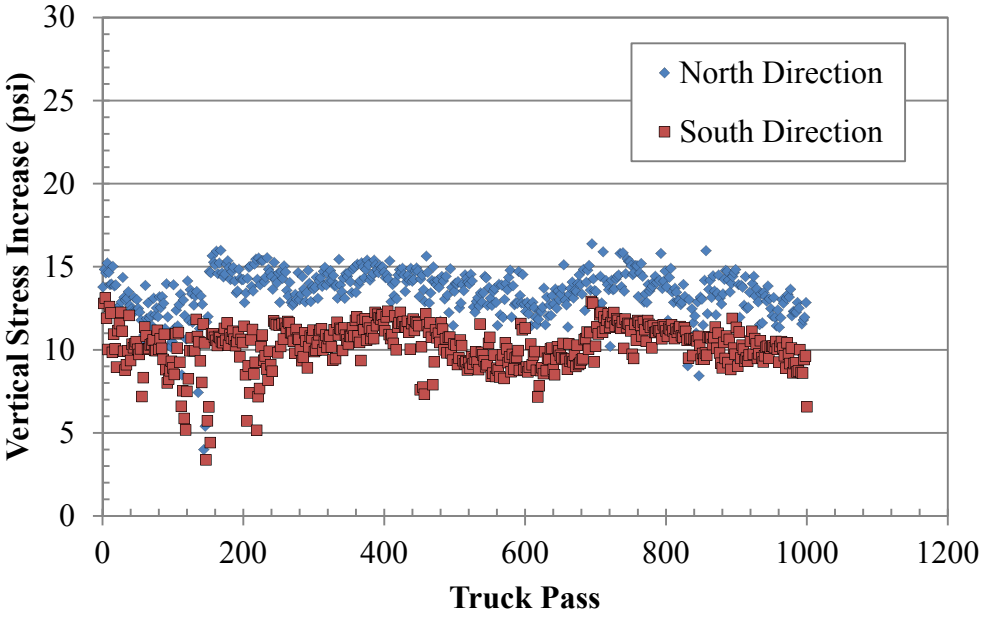

(b)

Figure 5-95: (a) Measured stress increase in both directions, (b) Measured stress increase in each travel direction

To support the premise of lateral wander, a static stress analysis was performed that looked at the range of stresses that would be expected at the if the dual tires traveled: (i) directly over the center of the EPC (max location), (ii) 6.5 inches from the center of the EPC (mid location), (iii) 14.5 inches from the center of the EPC (minimum location). These tire locations relative to the EPC are shown in Figure 5-96. The minimum location was based on field observations during construction traffic testing where researchers observed the outer edge of the exterior tire missing the EPC location by as much as half a tire width. To perform the analysis the tire contact area was replaced using a circular equivalent contact area with a radius "r" that was calculated using the following equation (Giroud & Han, 2004):

$$\mathbf{r} = \sqrt{\mathbf{P}/\boldsymbol{\pi p}} \qquad \textbf{Eq. 5-11}$$

Where:

r = radius of the equivalent contact area

P = wheel load (total load from dual tires)

p = tire contact pressure (assumed to be equal to the tire inflation pressure)

The static stress analysis was performed using tables developed by Ahlvin & Ulery (1962) that calculate the vertical stress increase for the laterally spaced locations relative to an applied circular load. It is important to note that although the actual field situation represents neither a static nor elastic condition, the results should provide a good indication of the degree of variability due to lateral wander. As an additional measure, the analysis also looked at what effect the tire pressure would have on the stress at the sensor depth. Tire pressures of 75, 85, and 95 psi were chosen to replicate the fluctuating tire pressures measured in the field.

The results of the static analysis are shown in Figure 5-97. Looking at the results it is apparent that vertical stress increase can deviate significantly when the point of load application moves laterally only a few inches. This is especially true for shallow depths similar to the depth at which the EPCs in Test Sections 2, 3, and 4 were installed. As the depth increases, the effect of lateral wander diminishes. This is consistent with the EPC data which showed a much smaller degree of stress variability in Test Section 1 when compared to the other three sections.

Another observation that can be made from Figure 5-97 is that changes in tire pressure within the range measured in the field (i.e. 75-95 psi) have a negligible effect on the measured stress increase at the subgrade when compared to the effects of lateral wander. This can be seen qualitatively when looking at Figure 5-96. Note that the three circles used to represent the equivalent tire contact area are to scale working from the outside in for tire pressures of 75 psi, 85 psi, and 95 psi, respectively. Based on the sketch it is rational that the small changes in tire contact area would not influence the measured vertical stress increase at the EPC as much as changing the location of the load.

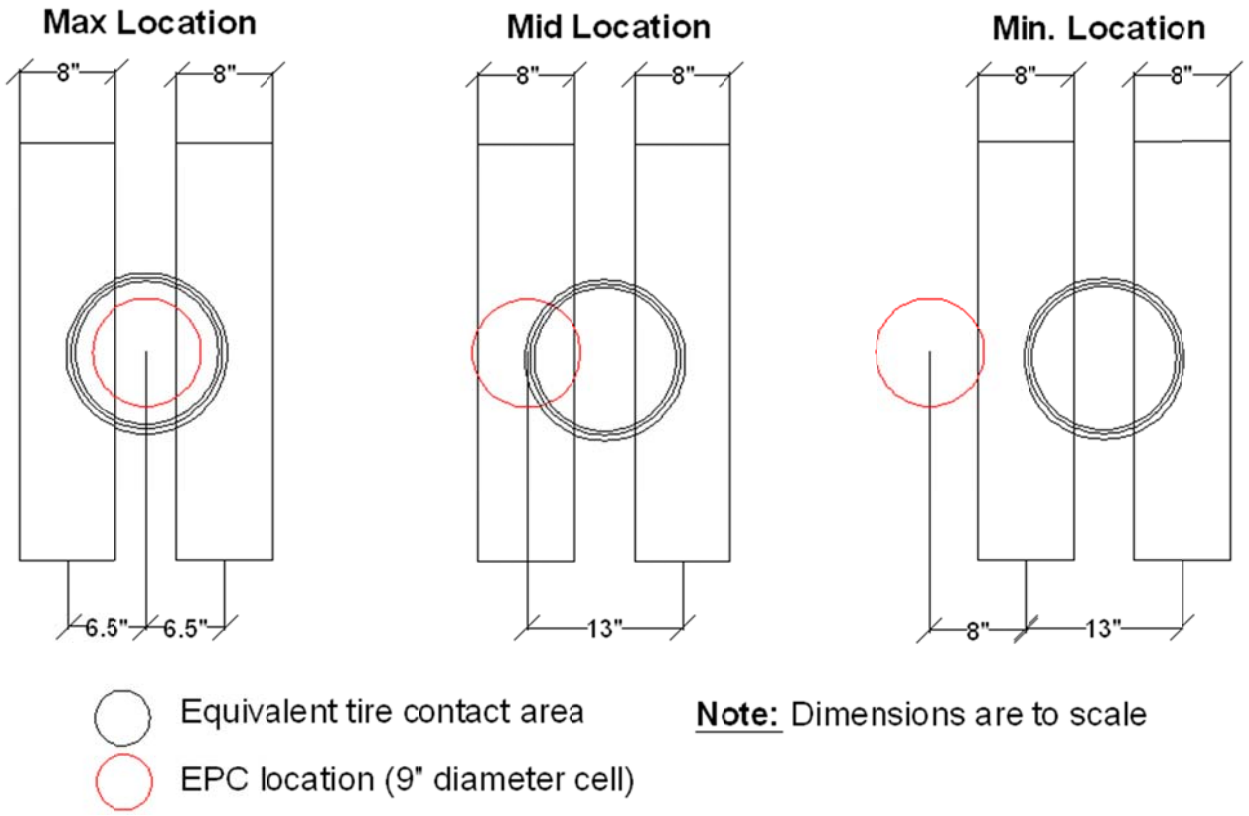

Figure 5-96: The dual tire locations relative to the EPC used to perform the stress analysis

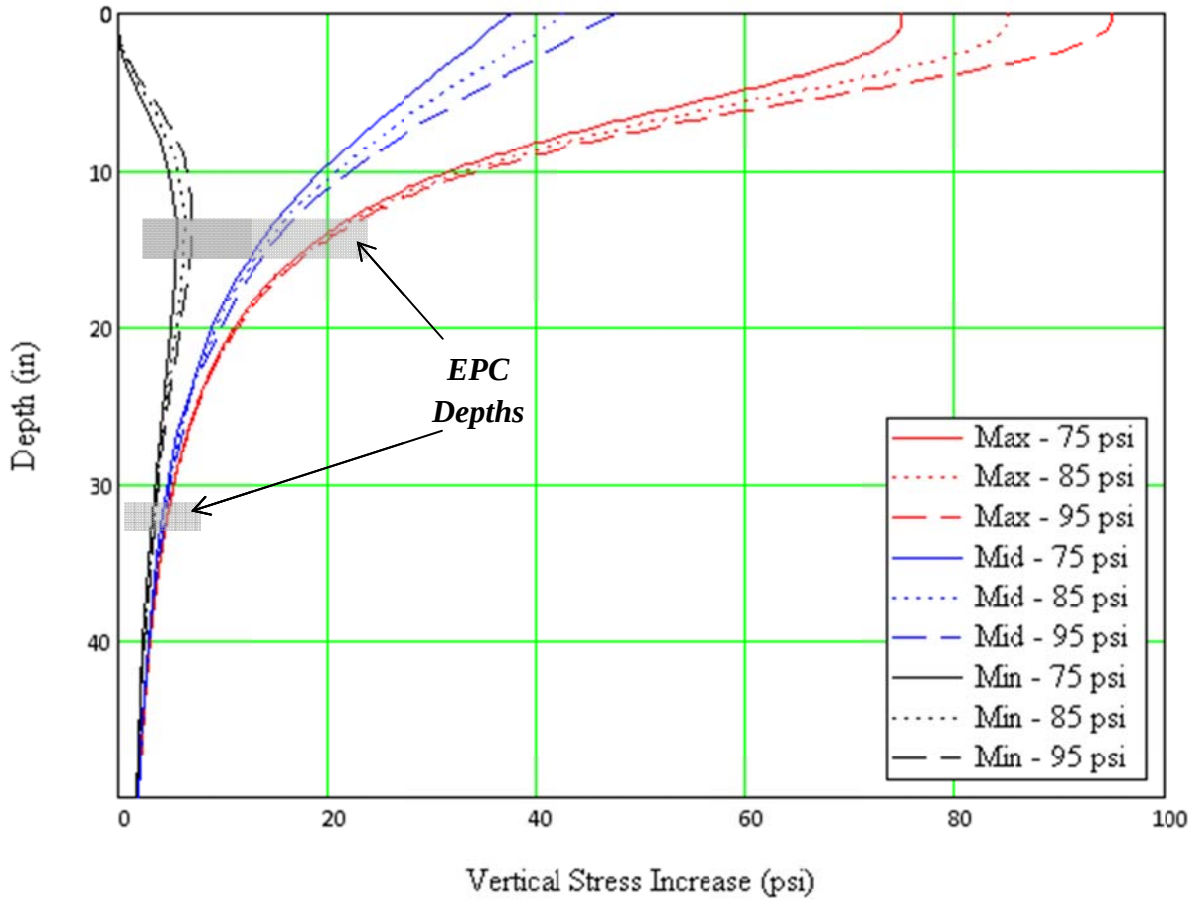

Figure 5-97: Estimate of the stress distribution at the EPC for different tire locations and changes in tire pressure

Besides lateral wander, periodic changes in truck driver and the travel velocity over the EPCs were two other sources that affected the measured stress. Shown in Figure 5-98 is a plot of the stress increase measured by EPC 8 and truck velocity when driven in the south direction. To identify where driver changes occurred, truck passes are color coded by driver. Truck velocity was calculated based on the time between load pulses between two EPCs and the known distance between the two EPCs (i.e. 25 feet). When looking at the figure it is apparent that when the test vehicle traveled at a high rate of speed, the magnitude of the stress increase began to fluctuate significantly. For example, during passes 101 through 160 the assigned driver (Driver 2) had never driven a dump truck before. Due to his inexperience, the driver had difficulty in maintaining a stable speed and consistently hitting the EPCs. After truck pass 160 a new driver was requested to avoid more inaccuracy in the stress data. Further analysis of Figure 5-98 shows that from pass 200 to pass 500 the driver (Driver 3) gradually increased his speed presumably as

he became more comfortable following a consistent alignment. At pass 500 testing ceased for approximately an hour and a half for lunch and to allow the NCDOT to take LiDAR measurements. After the break the same driver slowed down and evidently began to deviate from the previous wheel path causing the measured stress data to drop approximately 2 to 3 psi. At pass 800 we see an abrupt increase is stress which appears to be solely due to lateral wander as the driver presumably transitioned onto a new alignment that was closer to EPC 8.

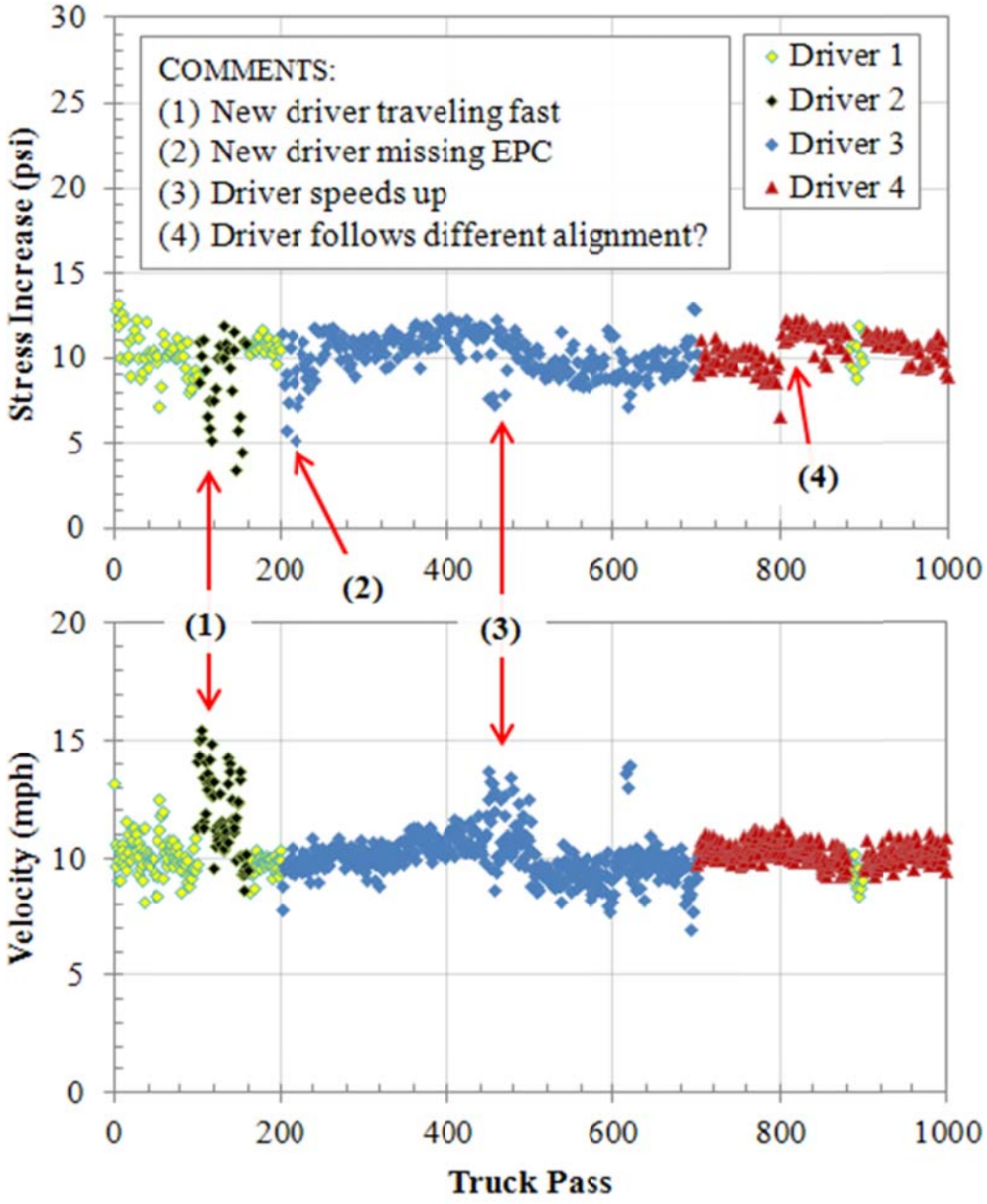

Figure 5-98: Measured stress increase and velocity at EPC 8 as a function of truck pass

Earth Pressure Cell Test Results

The vertical stress increase measured by the EPCs is plotted in Figure 5-99 through Figure 5-102 as a function of truck pass and ESAL. The base layer thickness of each EPC for Test Sections 1, 2, and 3 is also provided in the figures based on the LiDAR data. It is important to note that for each EPC the stress shown is only for one direction (i.e. north or south). The direction shown is the same direction that consistently measured the highest magnitude of stress. This reduction in data is justified based on the intent to present the peak stress at the subgrade level due to truck trafficking. Also note that Figure 5-99 through Figure 5-102 show only the stress increase due to back axle 1 (BA1). Refer to Appendix H for the vertical stress increase measured by the EPCs due to back axle 2 (BA2). The vertical stress measured due to the front axle is not presented due to the high variability, even in the same travel direction. This was the result of a smaller tire contact area (single tire versus dual tire) which magnified the effect of lateral wander.

One of the first observations is the difference in measured vertical stress among EPCs in the same test section. These differences are thought to be the result of a combination of the following factors:

- Natural variation in the strength and stiffness of the base and subgrade soils
- Lateral wander
- Variation in the base course thickness
- Slight differences in the installation depth of the EPC below the base/subgrade interface
- Deformation of the soils around the EPC causing it to tilt at an angle and measure stress from a direction not completely vertical.

Clearly, if the strength and stiffness of the base and subgrade soils vary within a test section, then the corresponding stress distribution will vary as well. Also, it was shown previously that lateral wander can be a major factor in causing the stress to vary at a point in the soil mass. Differences in base course thickness could also have a substantial effect on the measured vertical stress increase. When referring to Figure 5-100, note that EPC 8 measures the lowest stress among EPCs in that particular section. This is believed to be due, in part, to the two to three inches of additional base course thickness. This may have also been a factor in Test Section 4 at EPC 16; however, this cannot be validated due to the absence of tests to determine the exact stabilization

depth over top of each sensor. An additional discussion of the influence base course thickness has on the subgrade stress is provided later in this chapter.

In regards to the installation depth, every attempt was made to install each sensor in the exact same manner at the same depth. In reality, however, human error may have caused the installation of some sensors to be more than or less than the prescribed depth. Recall that in Test Sections 1, 2, and 3 each EPC was installed three inches below the base/subgrade interface with silica sand placed below and on top. Measurements were made to ensure each EPC was three inches below what was perceived to be grade; however, sometimes it can be difficult to establish grade when spoil piles are located around the perimeter of the hole. Also, during compaction the EPCs may have displaced downward causing the depth to EPC to be less than the assumed three inches. Deformation of the surrounding soils either during compaction or full-scale testing could also have caused the EPC to shift from its horizontal position and become tilted at an angle. Consequently, this would cause the EPC to measure the applied stress at an angle other than the normal.

Looking at Figure 5-99, the measured stress increase in Test Section 1 is on the order of three to five psi. At such low stresses, it can be concluded that the deep rutting failure was due to shallow, incremental bearing capacity failures rather than large deformations in the subgrade. With the exception of EPC 8, both geosynthetically reinforced sections measured early stresses around 15-20 psi that gradually increased to as much as approximately 25 psi. This gradual increase is presumably due to the deterioration of the unpaved roadway after continuous loading. The lowest stress measured in Test Section 4 was by EPC 16, which coincidently, was also the EPC located near the failure area. One or more of the factors mentioned above are possible explanations for this discrepancy. More than likely, the vertical stresses near the failure area were as high if not higher than the stress measured by the other three EPCs. Also, note that the stresses in Test Section 4 cannot be directly compared to the stresses in Test Sections 2 and 3. Recall that the EPCs in Test Sections 2 and 3 were installed three inches below the base/subgrade interface whereas the EPCs in Test Section 4 were buried six inches below the base/subgrade interface. As a result, the stresses measured in Test Section 4 are generally lower than the stresses measured Test Sections 2 and 3.

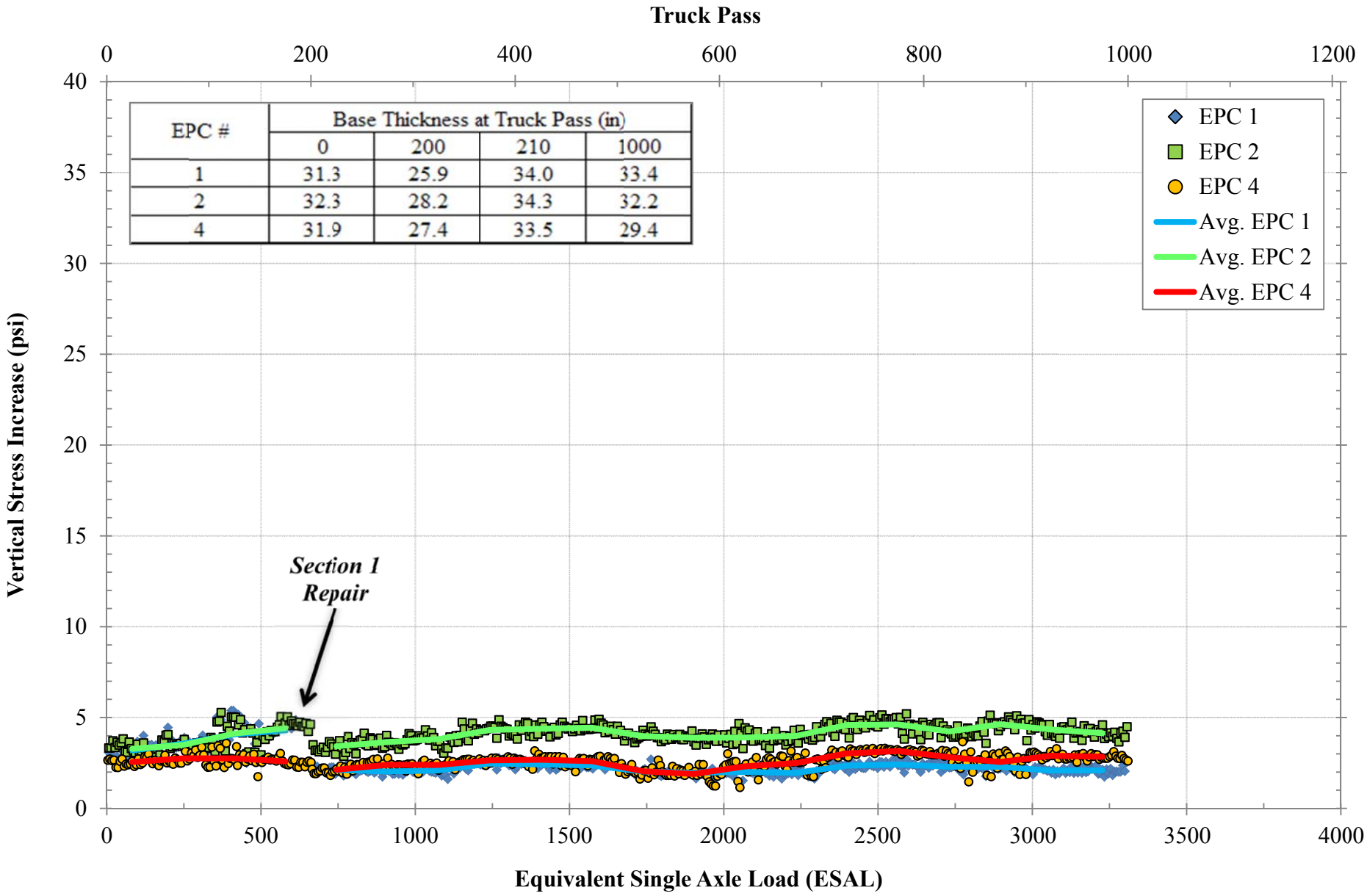

EPC #	Base Thickness at Truck Pass (in)			
	0	200	210	1000
1	31.3	25.9	34.0	33.4
2	32.3	28.2	34.3	32.2
4	31.9	27.4	33.5	29.4

Figure 5-99: Vertical stress increase three inches below the base/subgrade interface for Test Section 1

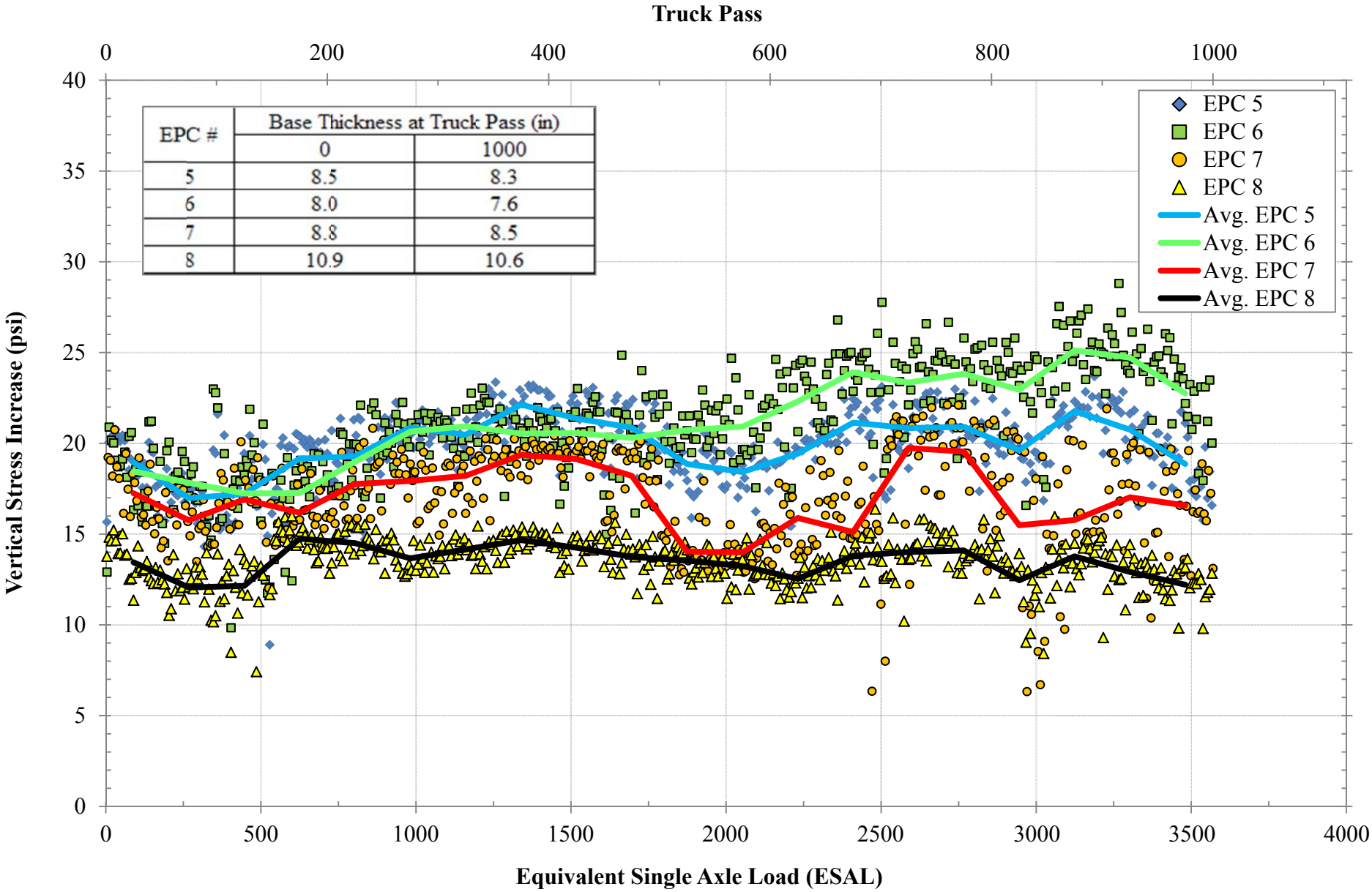

EPC #	Base Thickness at Truck Pass (in)	
	0	1000
5	8.5	8.3
6	8.0	7.6
7	8.8	8.5
8	10.9	10.6

Figure 5-100: Vertical stress increase three inches below the base/subgrade interface for Test Section 2

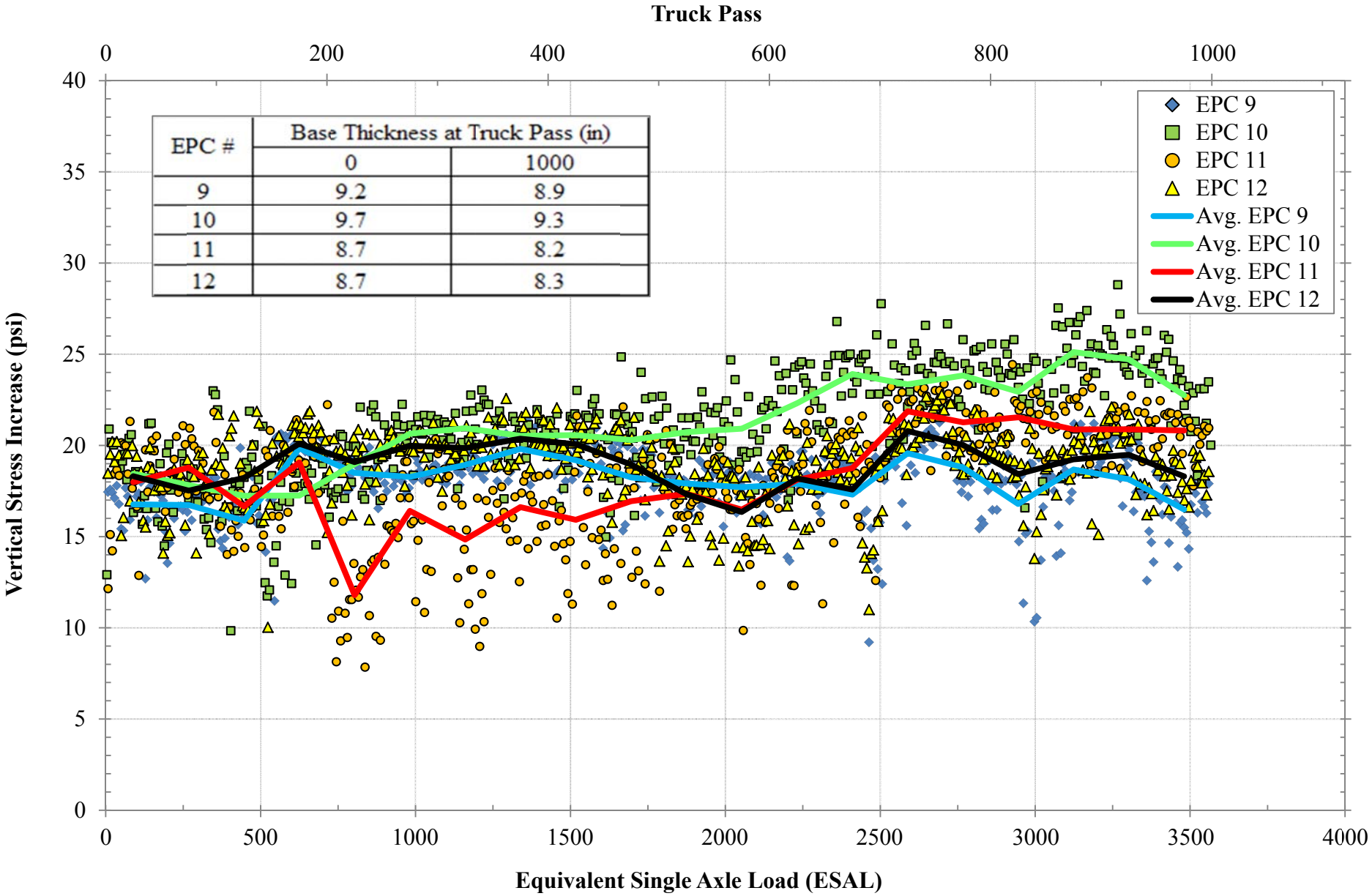

EPC #	Base Thickness at Truck Pass (in)	
	0	1000
9	9.2	8.9
10	9.7	9.3
11	8.7	8.2
12	8.7	8.3

Figure 5-101: Vertical stress increase three inches below the base/subgrade interface for Test Section 3

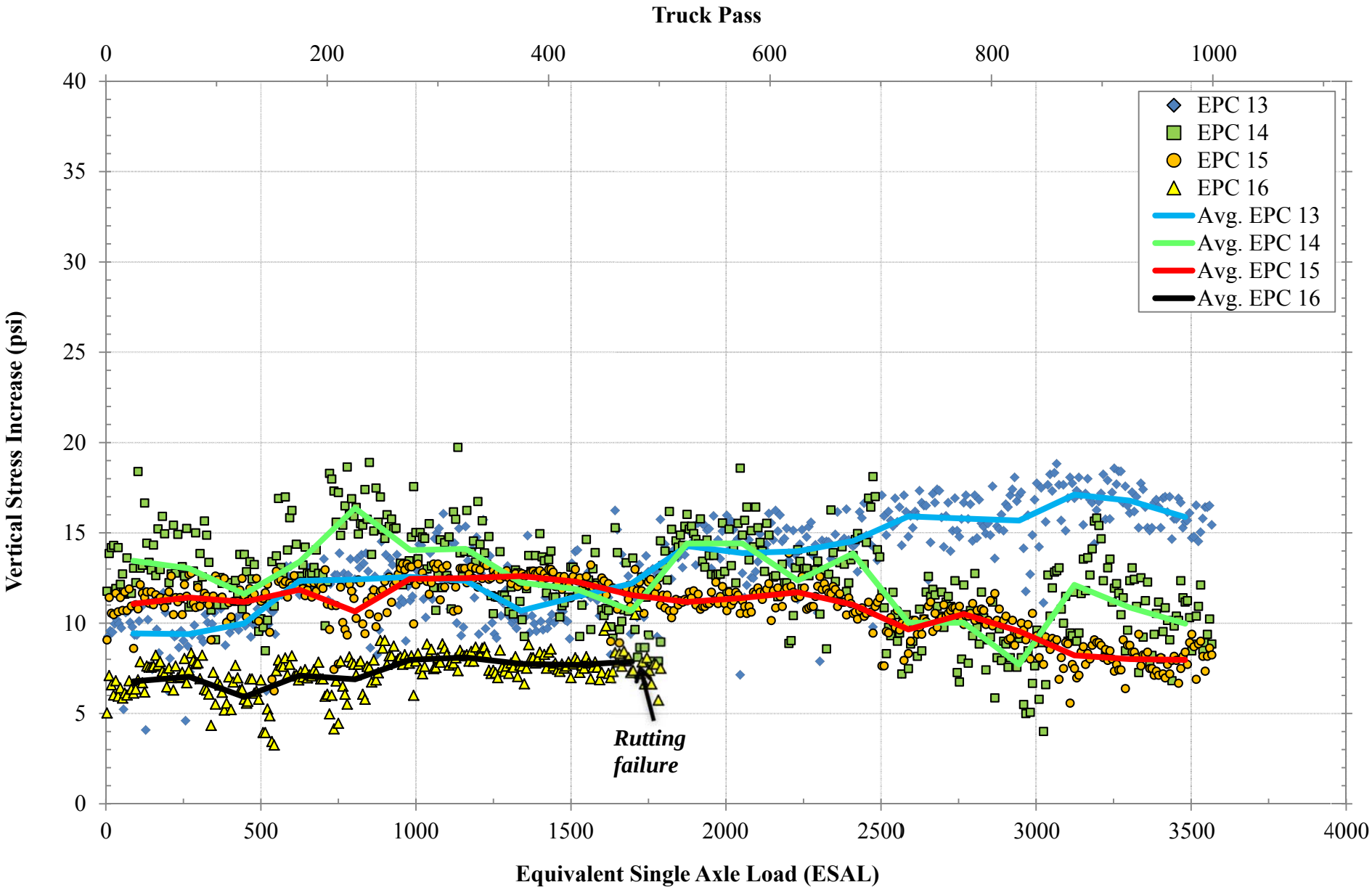

Figure 5-102: Vertical stress increase six inches below the base/subgrade interface for Test Section 4

Comparison to Existing Solutions

Before comparing the EPC results to existing stress distribution solutions, it is important to first understand the effects of a layered system. Shown in Figure 5-103 is a sketch taken from Coduto (2001) that illustrates how the distribution of stresses will vary when accounting for layered strata. Whenever a stiffer layer is overlain by a softer layer (i.e. $E_1>E_2$), such as the case in this study, load spreading in the upper layer is markedly improved causing lower calculated stresses throughout the soil profile. As a result, solutions that assume a homogenous medium (e.g. Boussinesq) will tend to over predict the induced stresses.

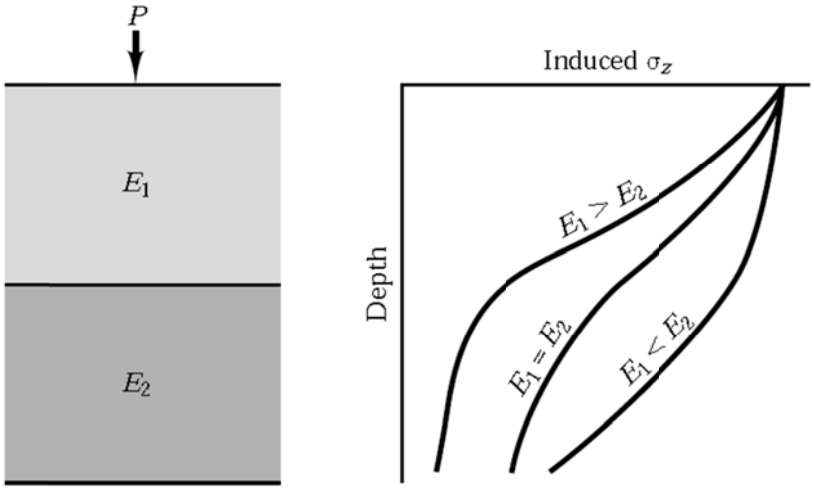

Figure 5-103: Distribution of stresses in layered strata (Coduto, 2001)

Over the years several stress distribution solutions have been proposed to account for a layered profile. One of the simplest solutions uses the Method of Equivalent Thickness by Odemark (1949) to convert a multi-layer system into a single layer system of equivalent thickness using the following equation:

Eq. 5-12

Where:

h_e = the equivalent thickness of layer one

f = an adjustment factor; .9 for two-layer system; 1.0 for a multi-layer system

E_1 and E_2 = modulus of layer one and two, respectively

After calculating an equivalent thickness, a single layer solution such as Boussinesq can be used to calculate the stress at any depth in the soil profile.

The Giroud and Han (2004) method was developed to determine the stress at the subgrade for unreinforced and geosynthetically reinforced unpaved roads. The solution is based on the conventional pyramidal stress distribution approach; however, it allows the user to account for traffic and its influence on the base course layer's load spreading ability. Depending on the assumed modulus ratio, an initial stress distribution is first calculated using a reference stress distribution angle of 38.5 degrees. After "N" axle passes, the initial stress distribution angle is reduced at a rate dependent on the base course thickness (Figure 5-104). Also, the authors calibrated the model to account for the inclusion of two specific geogrids[1] based on their aperture stability modulus. When accounting for geogrid inclusion, the model reduces the rate of change in the stress distribution angle based on the premise that geogrids provide additional lateral confinement from aggregate interlock. However, in a recently published article the authors note that the calibrated model is specific to the geogrids used in their study and should be recalibrated when used with other geogrid types (Giroud & Han, 2012).

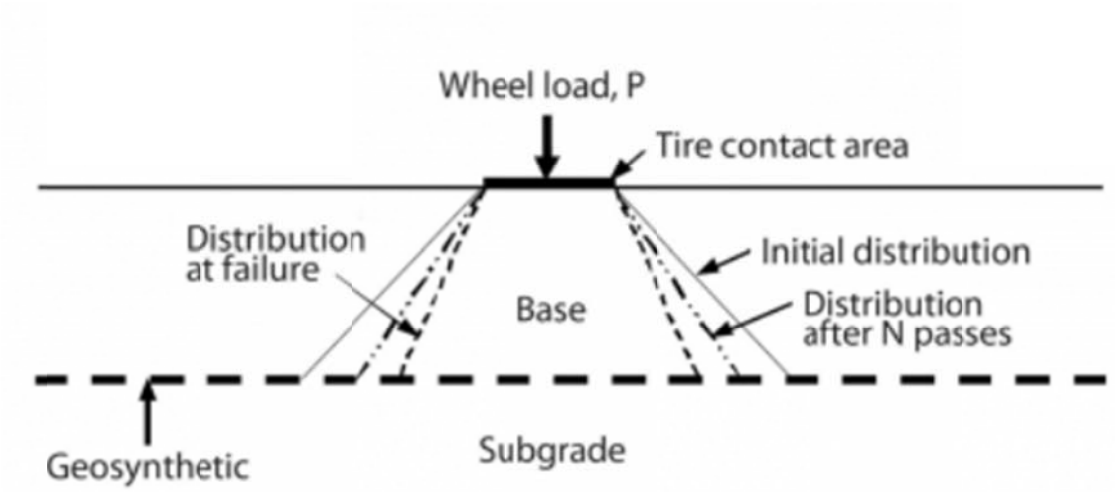

Figure 5-104: Giroud and Han (2004) stress distribution solution for unreinforced and reinforced unpaved roads (image obtained from Giroud and Han (2012))

[1] Tensar®, BX 1100 and BX 1200

To demonstrate the stress reduction effect for a two-layer system, the load and tire configuration applied by the back axles was input into the solutions mentioned above to estimate the stress three inches below the base/subgrade interface (i.e. the installation depth of the EPCs in Test Sections 1, 2, and 3). To evaluate the influence of the base course layer, its thickness was varied between 6 and 36 inches. Once again, the tire contact area was replaced using a circular equivalent tire contact area with a radius "r" that was calculated using Equation 5-1. Modulus ratios of two, four, and six were used with the Odemark solution. The modulus ratio was set to four when using the Giroud and Han approach with the number of truck pass intervals varying between 5, 50, and 1000. Also, no reinforcement was considered when using the Giroud and Han method. The results are presented in Figure 5-105 as a function of base course thickness normalized by the equivalent tire contact diameter. For comparison, the average EPC stresses measured during truck pass 1-50 and 950-1000 are shown for Test Sections 1, 2, and 3. Note that the passes are identified as axle passes "N" in the legend, thus, 1, 50, and 1000 truck passes is equal 3, 150, and 3000 axle passes, respectively, for the three axle test vehicle.

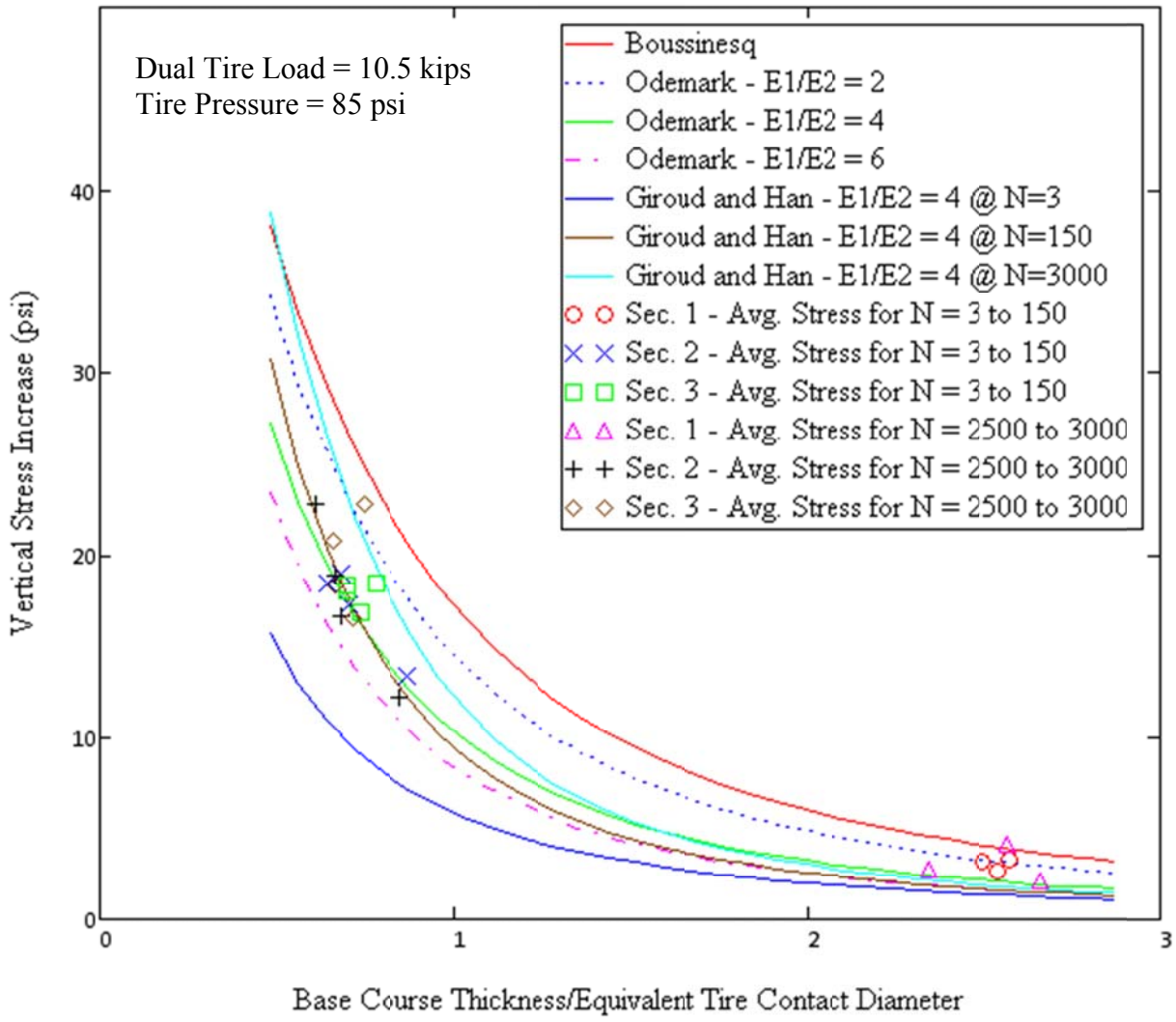

Figure 5-105: Vertical stress increase three inches below the base/subgrade interface

When comparing the various solutions it is evident that there is a significant stress reduction when a two-layer system is considered. Depending on the modulus ratio, Odemark's method predicts substantially lower stresses than Boussinesq's single layer, homogeneous solution. For the set conditions, the Giroud and Han method also predicts lower stresses than the Boussinesq. Further analysis of Figure 5-105 also indicates that small differences in base course thickness can cause significantly different measured stresses for base course to loaded diameter ratio's less than one. Besides lateral wander, this helps explain why such a high variability in EPC stress was measured in the thinner base course sections.

Generally, the EPC data for the geosynthetically reinforced sections exhibit a similar decreasing trend in vertical stress with increased base course thickness. Based on Odemark's method the

modulus ratio for the three sections is between two and six which is consistent with the DCP correlated modulus values presented in Table 4-7. When comparing the EPC data for Test Sections 2 and 3 to the Giroud and Han method, the majority of the data agrees well with axle pass 150. For Test Section 1, the Giroud and Han under predicts the actual stresses by approximately 0.5 to 2 psi.

To analyze the Giroud and Han method when accounting for geogrid reinforcement, Figure 5-106 presents a plot of the EPC data from Test Section 2 along with the Giroud and Han method for no geogrid, for the BX 1100 geogrid, for the BX 1200 geogrid, and for the BX 1500 geogrid. As mentioned previously, the Giroud and Han method was originally calibrated for use only with the BX 1100 and BX 1200 geogrids. However, the BX 1500 is made by the same manufacturer using the same manufacturing process as the BX 1100 and BX 1200. When analyzing the relevant geosynthetic properties provided by the manufacturer, the following comments can be made when comparing the BX 1500 geogrid to the BX 1200 geogrid:

- Both have approximately the same aperture dimensions
- Both have approximately the same minimum rib thickness
- The BX 1500 has approximately 30% higher tensile strength in the machine direction and approximately the same tensile strength in the cross-machine direction.
- The BX 1500 has a higher flexural stiffness (2,000,000 to 750,000 mg-cm)
- The BX 1500 has a slightly higher aperture stability modulus (.75 to .65 m·N/degree)

Given that the model is calibrated for a less stiff, lower strength product it would be expected that the Giroud and Han method would either accurately predict the measured subgrade stress in Test Section 2 or predict higher stresses. However, looking at the results in Figure 5-106 it is clear that this is not the case. When using the aperture stability modulus of the BX 1500 geogrid in the field (J = .75 m·N/degree), the Giroud and Han method predicts stresses 40 to 50% lower than measured by the EPCs. Rather, the best prediction is found when neglecting geogrid inclusion all together. Based on these results, it can be concluded that the Giroud and Han method over predicts the amount of benefit geogrid reinforcement can provide in reducing the stress at the subgrade.

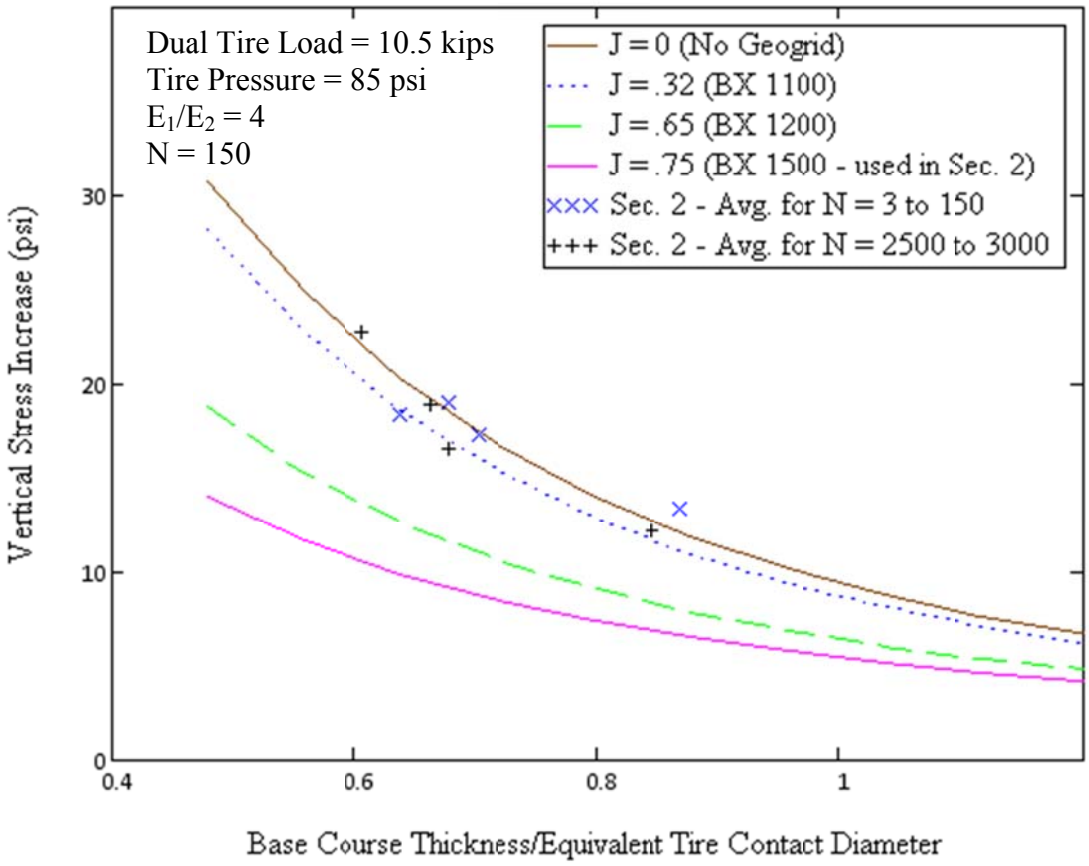

Figure 5-106: Vertical stress increase three inches below the base/subgrade interface for various geogrid aperture stability modulus values

Soil Moisture

Engineers typically refer to soils gravimetric rather than volumetric water content. As a result, the volumetric water content measured in the field was converted to gravimetric water content using the following equation:

$$\mathbf{w} = \left(\boldsymbol{\theta\gamma_w}/\boldsymbol{\gamma}\right) \times \mathbf{100} \qquad \textbf{Eq. 5-13}$$

Where:

w = gravimetric water content (%)

θ = volumetric water content (m^3/m^3)

γ_w = unit weight of water

γ = bulk unit weight

From this point forward, gravimetric water content will simply be referred to as water content. The measured water content by each sensor during full-scale testing is presented in Figure 5-107. Due to the extremely dry conditions in eastern North Carolina during the 2011 summer, the measured data shows little to no change in moisture content throughout the truck trafficking period. The average water content measured by each sensor is provided in Table 5-28 along with the lab measured water content from Shelby tube samples taken in the same sections. Generally, there is good agreement between the lab and field measured water contents.

Table 5-28: Average water content measured by each sensor during full-scale testing

Test Section	Measured Water Content (%)		[3]Lab Measured Water Content (%)
	[1]H. Sensor	[2]V. Sensor	
1	20.2	20.6	31.6
2	19.2	19.7	15.9 / 19.7
3	16.2	17.3	18.1 / 21.8
4	19.7	17.7	14.7 / 26.7

NOTE: [1]H = horizontally installed; [2]V = vertically installed;
[3]Measured from Shelby tube samples in the same test section

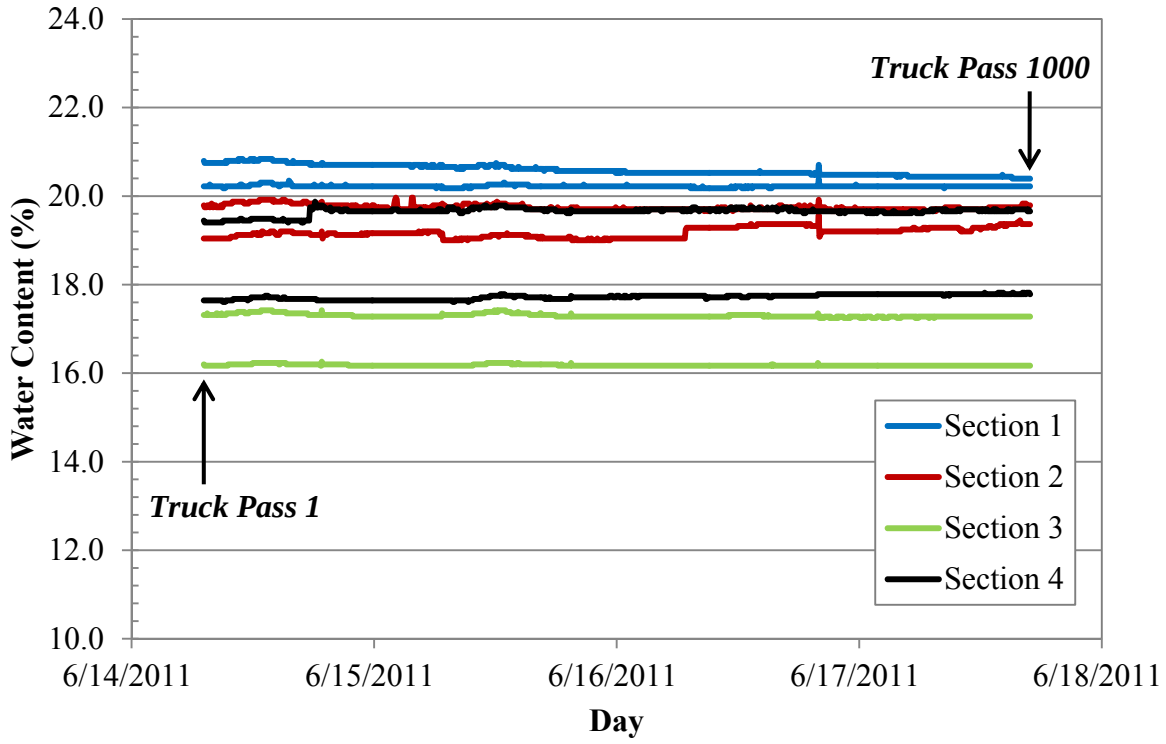

Figure 5-107: Measured water content at the base/subgrade interface during field testing

Shown in Figure 5-108 are four graphs of the recorded water content in each section throughout the duration of field project (about 2 months). Also included in the top left graph is the amount of rain in inches during heavy rainfall events measured by a NOAA weather station located near the site. The results show that sensors were working properly due to the sudden spikes in water content that preceded a heavy rainfall event. Note that in the case of Test Section 4 there is little to no response after rainfall. This is potentially due to the cementitious bonds that reduce the void ratio of the soil-cement structure and create a base layer with low permeability.

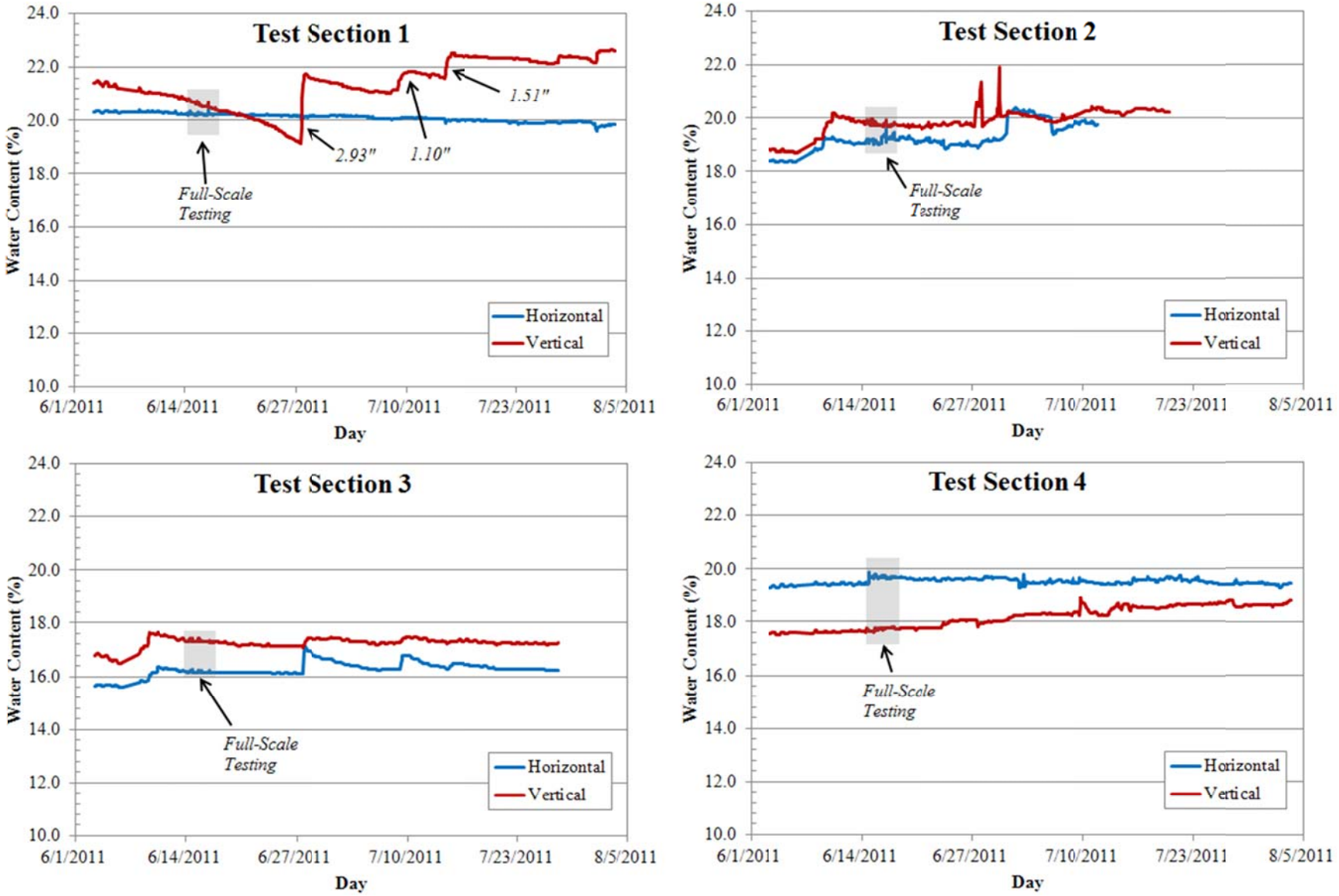

Figure 5-108: Measured water content at the base/subgrade interface throughout the duration of the project (about 2 months)

Proof Roll Testing

After proof roll testing was complete, NCDOT inspectors agreed that Test Sections 1, 2, and 3 showed no visible signs of pumping and an acceptable amount of rutting that was primarily the result of indentations from the bulldozer tracks and trailer tires. In Test Section 4 the magnitude of rutting was also considered to be acceptable. However, both inspectors agreed that a significant amount of pumping occurred in certain areas of the cement stabilized section. These areas were primarily located near the locations where excessive rutting was measured during full-scale testing. Out of concern that the cement stabilized subgrade would not provide long-term stability, Test Section 4 was deemed to have failed proof roll testing and had to be replaced. A few weeks later the contractor removed the soil-cement base layer, undercut an additional three feet, and replaced the soft subgrade with select material.

The minimum, maximum, and average rut depth measured after the 35 and 50 ton proof roll tests is shown in Table 5-29. Also, a plot of the cumulative rut depth is provided in Figure 5-109. Note that the results are a measure of permanent deformation only and do not consider any recovered deformation (pumping). Based on the results it is apparent that the majority of rutting occurred during the first phase of testing using the 35 ton proof roll trailer.

Table 5-29: Minimum, maximum, and average rut depth measured after proof roll testing

Test Section	IWP/OWP	Rut Depth After 35 Ton Trailer (in.)			Rut Depth After 50 Ton Trailer (in.)		
		Minimum	Maximum	Average	Minimum	Maximum	Average
1	IWP	0.11	0.20	0.15	0.13	0.24	0.18
	OWP	0.15	0.57	0.34	0.23	0.64	0.40
2	IWP	0.10	0.17	0.13	0.13	0.24	0.18
	OWP	0.10	0.23	0.16	0.12	0.29	0.19
3	IWP	0.01	0.10	0.05	0.04	0.20	0.10
	OWP	0.02	0.15	0.07	0.04	0.33	0.16
4	IWP	0.07	0.47	0.23	0.14	0.54	0.30
	OWP	0.23	0.74	0.37	0.26	0.84	0.43

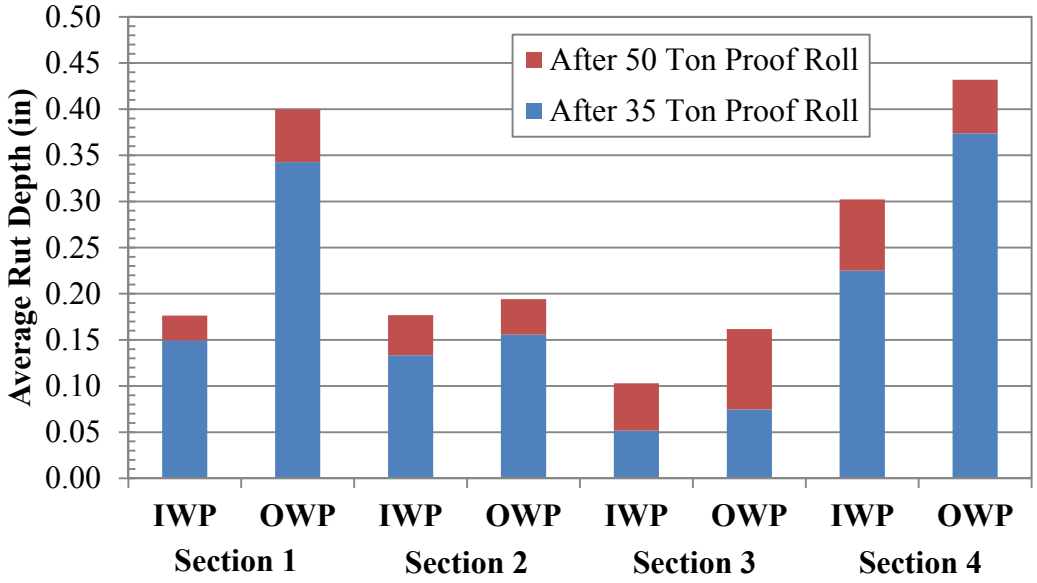

Figure 5-109: Average rut depth measured after proof roll testing

CHAPTER 6: ASSESSMENT OF UNDERCUT CRITERIA

To this point, the discussion has primarily focused on documenting the details and results of field testing. This chapter summarizes the development of undercut criteria and uses the in situ and full-scale test results to validate its use as an effective tool in determining when to undercut.

Development of Undercut Criteria: Summary

The development of undercut criteria was covered during research project 2008-07 and is discussed in detail in Chapter 10 of the NCDOT final report titled "Establishment of Subgrade Undercut Criteria and Performance of Alternatives Stabilization Measures" by Borden *et al.* (2010). This section is intended to serve as a short summary of the main points in developing the undercut criteria.

The development of undercut criteria was based on extensive numerical modeling via the finite difference platform. Using an elastic-perfectly plastic soil model, static and proof roller loading modes were applied to the soil medium in the plane strain and axisymmetric modes. The plane strain mode was used to simulate the proof roll trailer configured with multiple wheels per axle. The axisymmetric mode was used to simulate the effects of construction traffic (or a single wheel), rather than a series of axle loads that are closely spaced. The assumption was made that pumping in the field is associated with a plain strain type of loading that affects the deep layers and is a function of the stiffness parameters. Alternatively, rutting was associated with plastic deformation within the shallow layers and was considered to be a function of the shear strength parameters.

After each loading sequence, the settlement under the uniformly loaded area and the maximum shear strain at the boundary of the uniformly loaded area were calculated. This analysis was performed for a wide range of material strength and stiffness properties for the subgrade soil. These material properties included the elastic modulus, Poisson's ratio, cohesive strength, and friction angle. In order to focus on varying strength and stiffness values, the density and Poisson's ratio of the soil medium were assumed to be constant. The range of properties used in modeling is presented in Table 6-30.

Table 6-30: Material properties used in developing the undercut criteria

Items	Total Density (slugs/ft^{3*})	Total Unit Weight (lbs/ft^3)	Elastic Moduli, E (psi)	Poisson's Ratio, ν	Cohesion, c (psi)	Friction Angle, Ø (degree)
Values	3.997	128.5	500 - 30,000	0.4	1.0 - 50	0, 10, 20, and 30

* slugs/ft^3 = density unit in English unit system, 1 slug = 1 lbf-s^2/ft

Shown in Figure 6-110 and Figure 6-111 are the undercut criteria charts based on axisymmetric and plain strain loading for friction angles of 0, 10, 20, and 30 degrees, respectively. Note that the term "ξ" is defined as the performance capacity ratio. Performance capacity is defined as the pressure corresponding to the asymptotic value of the pressure deformation relationship (see Figure 6-112). The performance capacity ratio, ξ, is defined as follows:

$$\xi = \frac{Performance\ Capacity}{70\ psi} \qquad \textbf{Eq. 6-14}$$

The 70 psi in the denominator is assumed to be the maximum applied pressure from both static and proof roller loading. During the numerical analysis it was determined that the performance capacity correlates linearly with cohesion, however, is mainly independent of stiffness. As a result, the performance capacity ratio in the design charts increases with an increase in cohesion and generally does not change with an increase in stiffness.

The deformation curves shown in the undercut charts are dependent on the elastic modulus of the subgrade soil. For each curve it represents a specific modulus value which is normalized by atmospheric pressure and shown in the right hand side of the charts. In order to plot specific field data into the axisymmetric design charts, the following power function can be used to estimate the normalized settlement at the center of the loaded area:

$$\left(\frac{\delta}{B}\right) = \left\{-2.13\times10^{-6} + 3.61\left(\frac{E}{p_a}\right)^{-1}\right\} + \left(.085 + 1.32\times e^{-.25\emptyset}\right)\left(\frac{E}{p_a}\right)^{-1}\left(\frac{c}{p_a}\right)^{.22-7.75\,e^{-.046\emptyset}} \qquad \textbf{Eq. 6-15}$$

Likewise, to plot field data into the plain strain design charts, the following function can be used:

$$\left(\frac{\delta}{B}\right) = \left\{-1.89\times10^{-4} + 5.27\left(\frac{E}{p_a}\right)^{-1}\right\} + \left(.56 + 5.06\times e^{-.3\emptyset}\right)\left(\frac{E}{p_a}\right)^{-1}\left(\frac{c}{p_a}\right)^{1.13-7.52\,e^{-0.04\emptyset}} \qquad \textbf{Eq. 6-16}$$

An acceptable rut is defined as less than 25 mm (≈ 1 inch), and the acceptable performance capacity ratio is set to 1.5. These values can be changed according to NCDOT practice or the desired level of conservatism. Subgrade soils that plot outside of the shaded area are considered unacceptable and need to be undercut. It is important to note that in some cases, soil strength and stiffness properties that are found to be acceptable in the axisymmetric loading case yield displacements that are unacceptable in the plain strain loading case. This finding highlights the difference between the axisymmetric and place strain conditions and suggests why the use of proof rolling performance as a criterion has been providing acceptable results in the field.

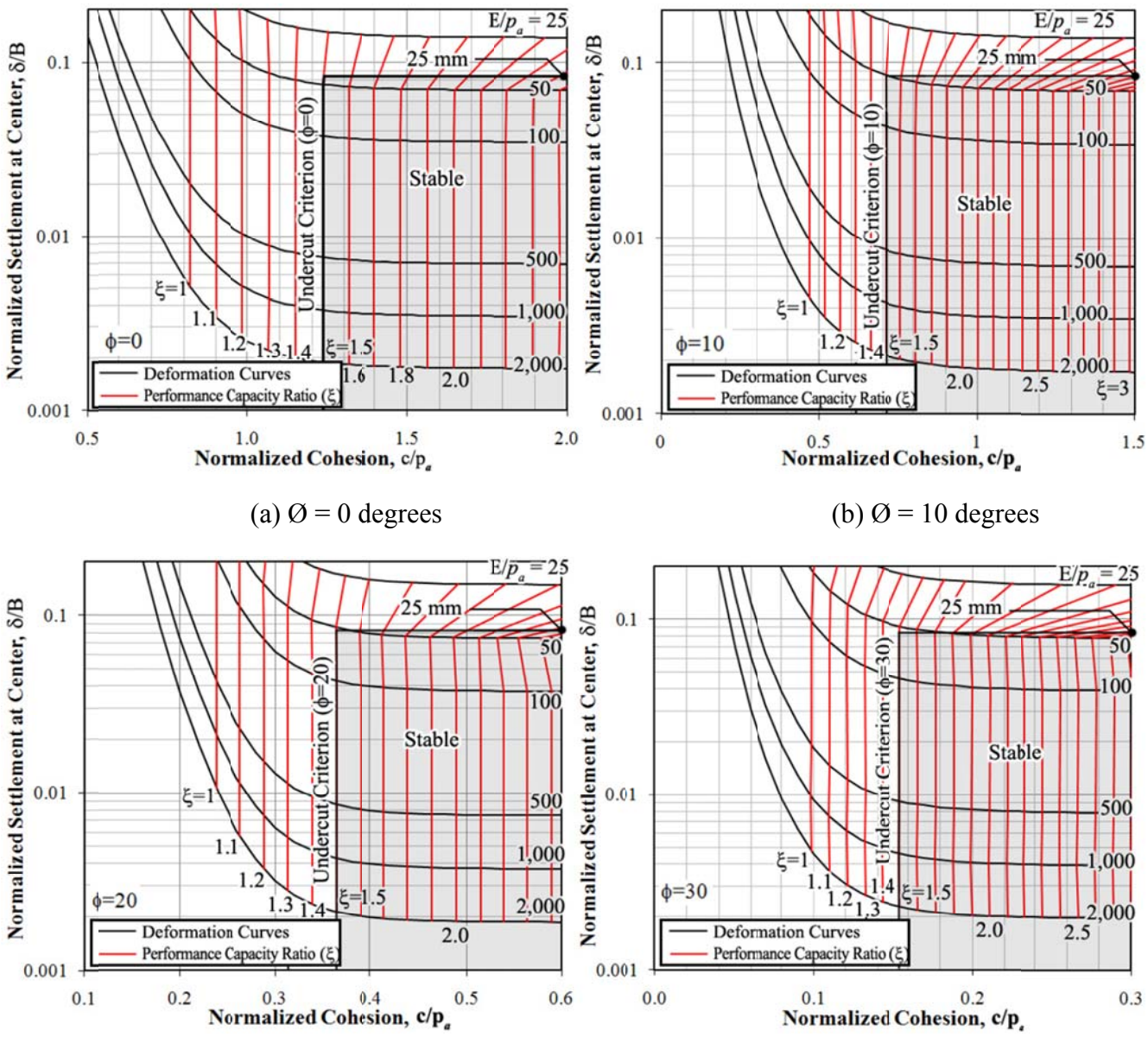

(a) Ø = 0 degrees

(b) Ø = 10 degrees

(c) Ø = 20 degrees

(d) Ø = 30 degrees

Figure 6-110: Undercut design criteria charts for axisymmetric loading condition

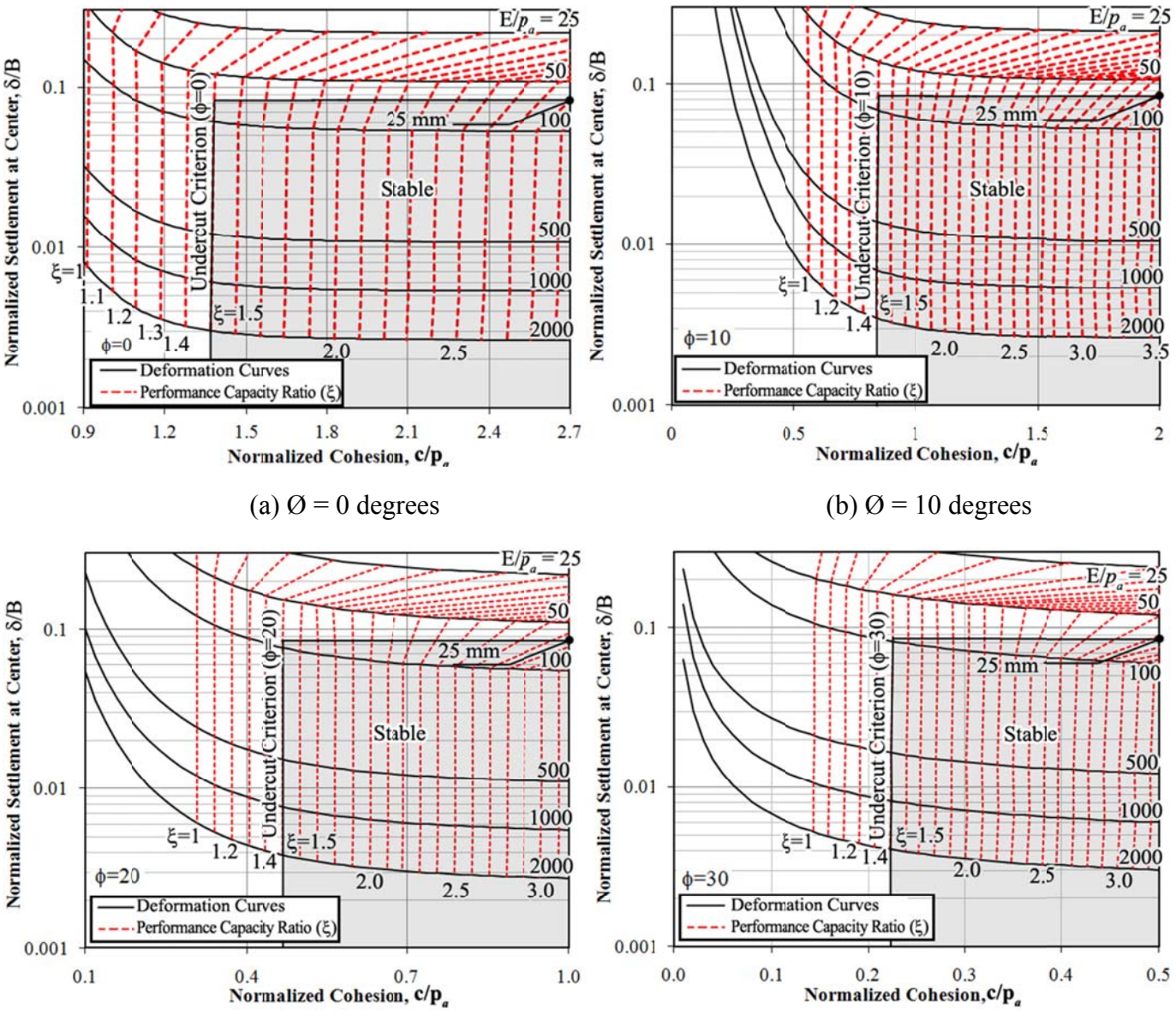

(a) Ø = 0 degrees

(b) Ø = 10 degrees

(c) Ø = 20 degrees

(d) Ø = 30 degrees

Figure 6-111: Undercut design criteria charts for plain strain loading condition

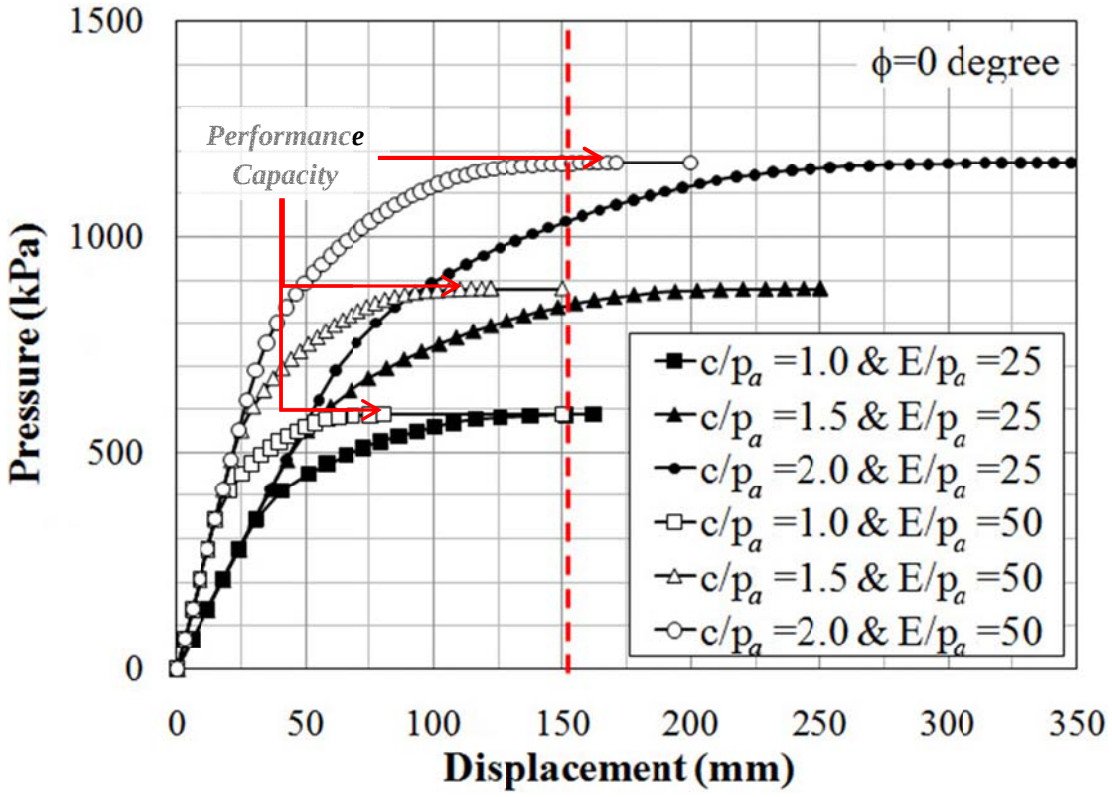

Figure 6-112: Pressure and displacement plots dependent on strength and stiffness

Evaluation of Undercut Criteria

When utilizing the undercut criteria the first step is to determine the subgrade soil strength and stiffness properties. During the initial site investigation this can typically be obtained through laboratory tests (i.e. triaxial and resilient modulus). Once construction begins, however, the need for quick estimation of the soil properties can be obtained through DCP testing. To analyze the use of both methods for selection of soil properties, two independent evaluations of the undercut criteria will be performed. The first evaluation will use the triaxial and resilient modulus data from the subgrade soil presented in Chapter 3. The second evaluation will use the DCP test data measured on the soft subgrade soils and presented in Chapter 4 to obtain correlated strength and stiffness properties.

Laboratory Determined Subgrade Soil Properties

Before proceeding it is important to note that with the exception of Test Section 4, the Shelby tube samples obtained in the field are from the subgrade after undercutting. As a result, triaxial and resilient modulus tests performed in the lab measured the soil properties of the subgrade below the stabilized base layer. However, DCP data presented in Chapter 4 showed that the top 24 to 36 inches of strata generally measured a consistent DCPI. Based on this finding, it is assumed that soil properties measured from the Shelby tube samples taken from Test Sections 2, 3, and 4 are representative of the undercut subgrade soils.

As mentioned earlier, a single resilient modulus test provides 15 measures of resilient modulus at 15 loading sequences. To select the appropriate value of resilient modulus, an estimate has to be made regarding the stress state of the subgrade during trafficking. In the case of this study, the subgrade soils were located at shallow depths with little to no overburden. As a result, it is assumed that the level of confining stress in the subgrade soil was equal to- or less than two psi. In addition, when analyzing the resilient modulus test results in Chapter 3 it was found that at a low confining stress (i.e. two psi) the deviator stress had little influence on resilient modulus. Thus, it was determined that the best estimate of in situ resilient modulus would come from an average lab measured resilient modulus at two psi confining stress. Table 6-31 presents the average resilient modulus from the Shelby tube samples obtained from Test Sections 2, 3, and 4.

To reduce the data to a single measure of resilient modulus for evaluation the undercut criteria, an average was taken among the four Shelby tube soil samples.

Table 6-31: Average resilient modulus at 2 psi confining stress

Soil Sample	Resilient Modulus, Mr	
	psi	MPa
ST-2	4740	32.7
ST-4	5340	36.8
ST-6	6788	46.8
ST-7	3704	25.5
Average	5143	35.5

The undrained shear strength results at low confining stress (two to three psi) from consolidated undrained (CU) triaxial tests on the subgrade soil are shown in Table 6-32. Also shown is the average resilient modulus taken from Table 6-31. These results were then used to estimate the displacement at the center of the loaded area using Equations 6-15 and 6-16. A plot of the results in the undercut chart will be presented later in this chapter.

Table 6-32: Subgrade properties based on triaxial and resilient modulus tests

Soil Sample	Confining Stress (psi)	Resilient Modulus, Mr			Undrained Shear Strength, S_U		
		psi	MPa	M_r/p_a	psi	kPa	S_U/p_a
ST-3	3.0	5143	32.5	321	15.7	108.4	1.07
ST-5	2.2				7.5	51.5	0.51

DCP Determined Subgrade Soil Properties

Shown in Table 6-33 is a list of the weighted average DCPI's measured within the top two feet of subgrade soil for the six DCP tests performed on the test pad prior to undercutting. Based on each tests respective DCPI, the correlated resilient modulus was calculated using the direct model developed by Herath *et al.* (2005). To estimate the subgrades undrained shear strength from DCPI, the following equation published by Park *et al.* (2012) was used:

$$S_U = -.282 \times (10^{2.6} \times DCPI^{-1.07})^2 + 14.97 \times (10^{2.6} \times DCPI^{-1.07}) \qquad \textbf{Eq. 6-17}$$

This equation was derived from and undrained shear strength-CBR relationship suggested by Danistan and Vipulanandan (2009) for use on clays, and the CBR-DCPI relationship recommended by the NCDOT (1998). It is important to note that this equation is limited to soft soils with high DCPI's.

Table 6-33: Subgrade properties based on DCP tests performed prior to undercutting

ID	Station	IWP/ OWP	Avg. DCPI (mm/blow)	Resilient Modulus, Mr			Undrained Shear Strength, S_U		
				psi	MPa	M_r/p_a	psi	kPa	S_U/p_a
1	121+50	OWP	45.9	5292	36.5	360	12.6	86.8	0.86
2		IWP	53.9	4859	33.5	331	10.9	74.8	0.74
3	122+00	OWP	59.9	4610	31.8	314	9.8	67.7	0.67
4		IWP	87.9	3892	26.8	265	6.7	46.5	0.46
5	123+00	OWP	38.1	5894	40.6	401	14.9	102.7	1.01
6		IWP	57.4	4705	32.4	320	10.2	70.5	0.70

Undercut Criteria Results - Subgrade

The soil properties presented in Table 6-32 and Table 6-33 were plotted in the axisymmetric and plain strain undercut charts shown in Figure 6-113. Based on the acceptance line in the charts (i.e. 25 mm of rutting and ξ=1.5), the subgrade soil did not satisfy the criteria in either the axisymmetric or plain strain loading condition. This is consistent with the NCDOT's recommendation to undercut subgrade soils that produce DCPIs in excess of 38 mm/blow. Furthermore, this finding is consistent with the construction practices at the field site where the majority of the roadway subgrade was required to be undercut two to three feet.

As expected, the soil properties determined from laboratory testing and DCP testing showed general agreement. This finding validates the use of the DCPI and the respective correlation equations as a quick and effective means for the estimation of strength and stiffness parameters in situ. However, it is important to emphasize the effect of the current moisture conditions when performing DCP tests. As mentioned previously, during the DCP tests performed prior to undercutting, the soils appeared to be overly wet due to previous rainfall. Clearly, higher estimates of strength and stiffness would be expected had the soil been in a drier state. When such a scenario arises, the potential for deteriorating subgrade conditions should be considered prior to using the undercut charts.

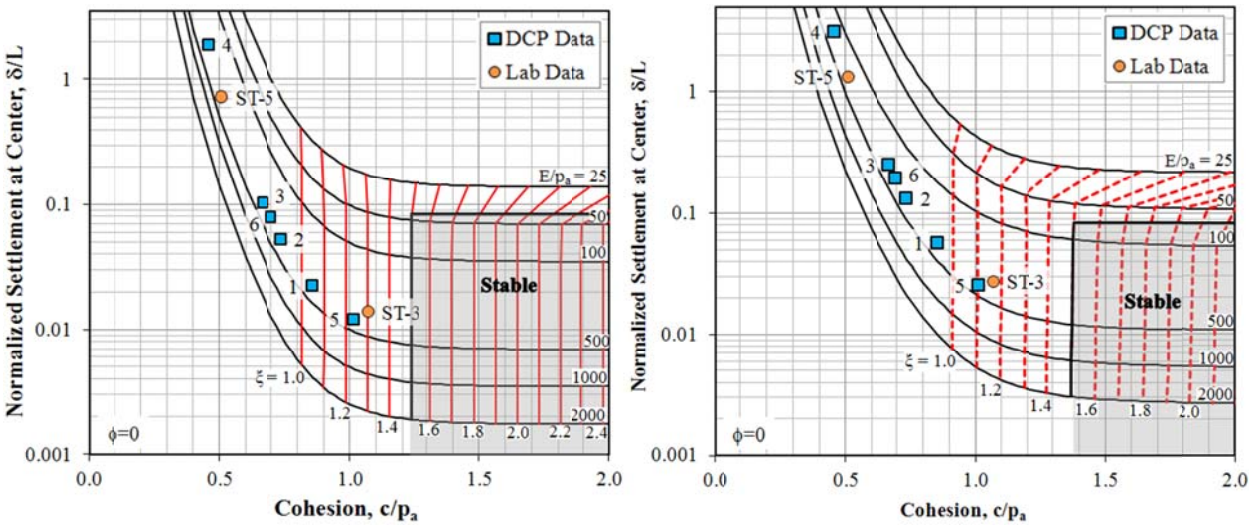

(a) axisymmetric condition (b) plain strain condition

Figure 6-113: Application of undercut criteria for the subgrade

DCP Determined Stabilized Material Properties

The DCP test results obtained before and after full-scale testing were used to estimate the soil properties of the stabilized base layer materials for further evaluation of the undercut charts. Once again, the direct model developed by Herath *et al.* (2005) was used to estimate the soils resilient modulus. Since the DCP test is performed relatively quickly (less than 2 to 3 minutes per test) and because the base materials contained more than five percent fines, it was assumed that all of the stabilized materials were tested in an undrained condition. As a result, the friction angle for all stabilized materials was assumed to be zero. The undrained shear strength for the select material and ABC was estimated using the following equation proposed by Ayers (1989):

$$S_U = \frac{1}{2} \times (37.0 - 9.0 \times PR + 7.8 \times MAS) \qquad \textbf{Eq. 6-18}$$

Where:

PR = Penetration rate (inch/blow)

MAS = Maximum aggregate size (inch)

Note that the above equation was designed to correlate the penetration rate (PR) to the shear strength of granular soils at a confining stress of five psi. A maximum aggregate size (MAS) of .08 inches (2 mm) and 1.5 inches (38.1 mm) was used for the select material and ABC, respectively. The unconfined compressive strength (UCS) for the cement stabilized soil was estimated using the following equation proposed by Holderby and Cerato (2011):

$$UCS = 5.527 \times DCPI + 13.567 \times t + 3.955 \times SC + 373.138 \qquad \textbf{Eq. 6-19}$$

Where:

UCS = Unconfined compressive strength (kPa)

DCPI = DCP Index (mm/blow)

t = Curing time in days (used 7 days)

SC = Stabilizer content in percent (used 12%)

The soil properties estimated from DCP tests performed on the stabilized test sections prior to and after full-scale testing are shown in Figure 6-114 and Figure 6-115, respectively.

Table 6-34: Base layer properties based on DCP tests performed prior to full-scale testing

Test Section	IWP/ OWP	Soil Type	Avg. DCPI (mm/blow)	Resilient Modulus, Mr			Undrained Shear Strength, S_U		
				psi	MPa	M_r/p_a	psi	kPa	S_U/p_a
1	OWP	S.M	19.4	9311	64.2	634	15.4	106.0	1.0
	IWP	S.M	18.2	9739	67.1	663	15.6	107.4	1.1
2	OWP	ABC	8.5	18200	125.5	1238	22.8	157.5	1.6
	IWP	ABC	9.3	16790	115.8	1142	22.7	156.5	1.5
3	OWP	ABC	10.6	15121	104.3	1029	22.5	155.0	1.5
	IWP	ABC	8.7	17905	123.4	1218	22.8	157.3	1.6
4	OWP	S.C.	8.8	17671	121.8	1202	*81.8	*564.2	5.6
	IWP	S.C.	11.5	14043	96.8	956	*84.0	*579.3	5.7

NOTE: S.M = select material; S.C. = soil-cement; *unconfined compressive strength (UCS)

Table 6-35: Base layer properties based on DCP tests performed after full-scale testing

Test Section	IWP/ OWP	Soil Type	Avg. DCPI (mm/blow)	Resilient Modulus, Mr			Undrained Shear Strength, S_U		
				psi	MPa	M_r/p_a	psi	kPa	S_U/p_a
1	OWP	S.M+ABC	9.3	16909	116.6	1151	17.2	118.4	1.2
	OWP	S.M+ABC	13.1	12616	87.0	858	16.5	113.6	1.1
	IWP	S.M+ABC	11.3	14235	98.1	969	16.8	115.8	1.1
	IWP	S.M+ABC	15.5	11072	76.3	753	16.1	110.8	1.1
2	OWP	ABC	7.3	20846	143.7	1418	23.1	159.0	1.6
	IWP	ABC	9.6	16434	113.3	1118	22.7	156.2	1.5
3	OWP	ABC	9.5	16550	114.1	1126	22.7	156.3	1.5
	IWP	ABC	10.3	15413	106.3	1049	22.5	155.3	1.5
4	OWP	S.C.	8.5	18152	125.2	1235	*81.6	*562.7	5.6
	OWP	S.C.	7.3	20900	144.1	1422	*80.6	*555.7	5.5
	IWP	S.C.	20.9	8816	60.8	600	*91.5	*630.8	6.2

NOTE: S.M = select material; S.C. = soil-cement; *unconfined compressive strength (UCS)

Undercut Criteria Results – Stabilized Material

Using the soil properties presented in Table 6-34 and Table 6-35, the deformation of the soil was estimated using Equations 6-15 and 6-16. The results prior to full-scale testing are plotted in Figure 6-114 and the results after full-scale testing are plotted in Figure 6-115. In Figure 6-114, the select material in Test Section 1 plots outside of the acceptable range of subgrade strength and stiffness for both the axisymmetric and plain strain loading condition. This is consistent with observations made during full-scale testing where the select material displaced laterally with continued traffic causing rutting failure at truck pass 200. In Figure 6-115, the 3 inch layer of ABC plus 31 inch layer of select material also plots outside of the acceptable area. This is also consistent with rutting measurements in excess of one inch after 1000 truck passes. In the case of the geosynthetically reinforced sections, both Test Section 2 and Test Section 3 plot within the acceptable area of the undercut charts prior to full-scale testing and after full-scale testing. Based on average rut measurements less than one inch in both geosynthetically reinforced test sections, it can be concluded that the charts accurately gauge the effectiveness of the stabilization measure when subjected to less than 1000 truck passes. Compared to typical soil cohesion values, the UCS of soil-cement is quite high ($UCS/p_a > 5$). As a result, for UCS values greater than 30 psi ($UCS/p_a > 1.5$), which is typically the case with soil-cement, the stabilization measure will always plot well inside the stable area of the undercut charts. With that said, it is not recommended to use the design charts as a measure of quality control on cement stabilized soil material.

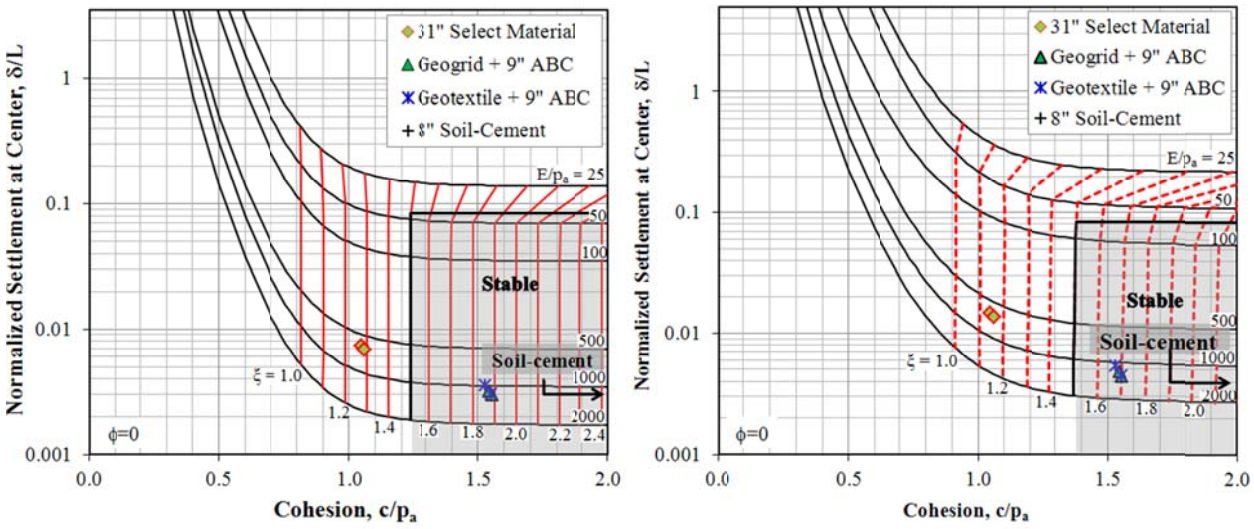

(a) axisymmetric condition (b) plain strain condition

Figure 6-114: Application of undercut criteria for the stabilized test sections prior to full-scale testing

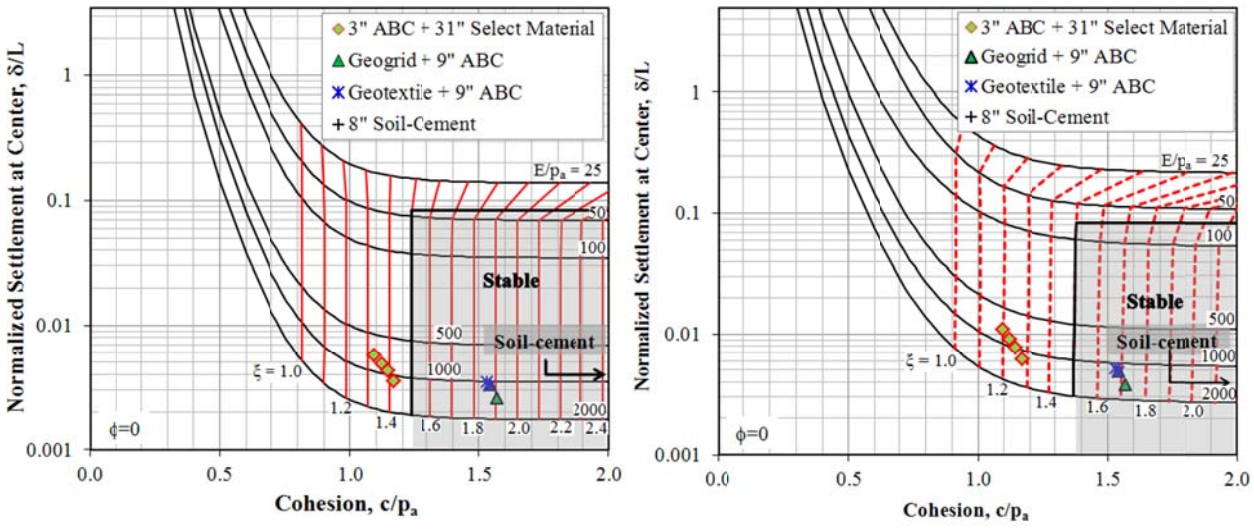

(a) axisymmetric condition (b) plain strain condition

Figure 6-115: Application of undercut criteria for the stabilized test sections after full-scale testing

Chapter Summary

The undercut criteria charts were originally developed under the scope of NCDOT research project 2008-07. Using numerical analysis for static and proof roller loading, two modes of modeling were considered, plain stain and axisymmetric conditions. The plane strain mode was used to simulate proof roller loading and indicate the potential for excessive pumping and rutting. The axisymmetric mode provides similar information, however, this time under the effects of construction traffic (or a single wheel), rather than a series of axle loads that are closely spaced. The results of the numerical analysis were used to create undercut criteria charts for both the axisymmetric and plain strain modes. Depending on the soils strength and stiffness properties, the criteria charts provide an estimate of the potential for excessive pumping and rutting. The charts presented in the report defined an acceptable rut depth as less than 25 mm or 1 inch, and an acceptable performance capacity ratio of 1.5 or greater. These values can be changed at the discretion of the NCDOT.

To evaluate the proposed criteria, two analyses were conducted using the subgrade soil from the field project. The first evaluation analyzed the undercut criteria when estimating the soil properties from laboratory tests (i.e. triaxial and resilient modulus). This would typically be the case during the preliminary stages of construction. The second evaluation analyzed the undercut charts when estimating the soil properties from DCP tests performed on the subgrade prior to undercutting. This would typically be the case during the later stages of construction when a quick answer is needed out in the field. Based on the results, the subgrade soil did not satisfy the criteria in either the axisymmetric or plain strain loading condition. This was consistent with the NCDOT's recommendation to undercut subgrade soils that produce DCPIs in excess of 38 mm/blow. Furthermore, this was also consistent with the construction practices at the field site where the majority of the roadway subgrade was required to be undercut two to three feet. Also, the soil properties determined from laboratory testing and DCP testing showed general agreement validating the use of the DCP and the respective correlation equations as a quick and effective means for the estimation of strength and stiffness parameters in situ.

The undercut criteria charts were also evaluated using DCP correlated soil properties of the stabilized material. Based on the results it was found that the charts accurately predict the performance of the mechanically stabilized test sections (i.e. Test Sections 1, 2, and 3), however,

should not be used on chemically stabilized material. This is based on the fact at almost any magnitude of UCS; chemically stabilized materials will almost always plot within the acceptable area of the undercut charts.

The results of the multiple evaluations validate the proposed criteria as a reasonable tool for discerning when to undercut roadway subgrade soils. Furthermore, the proposed criteria can also be used to predict the performance in terms of pumping and rutting of mechanical stabilization measures, however, should not be used in conjunction with chemical stabilization.

CHAPTER 7: PERFORMANCE COST ANALYSIS

The full-scale test results were analyzed to determine the relative cost in terms of rutting for each stabilization measure. This chapter provides the details and results from the performance cost analysis so that an informed decision on cost-effective stabilization can be made.

Unit Costs

Several sources were consulted to determine the unit costs associated with the relevant tasks and materials for each stabilization measure. Shown in Table 7-36 are the unit costs and corresponding items numbers obtained from the NCDOT bid averages of 2011 statewide projects (NCDOT, 2011). Also shown are the unit costs for items that were billed to the NCDOT project where full-scale testing was performed (Edens, 2012). Note that the select material used for the project was actually billed as "borrow material", however, classified as Class II/Type 2 select material. For future reference, the unit costs for both granular fill items were applied to the performance of Test Section 1.

The "Soil Cement Base" item is the cost of constructing the soil-cement layer, while "Portland Cement" is the cost of the raw cement material. When consulting with the soil-cement contractor, it was mentioned that the majority of the soil-cement projects performed during the 2011 year were for new roadways. Due to a number of factors, the contractor noted that new roadways will typically bid at a lower cost than roadway widening or rehabilitation projects. To account for this, the contractor recommended a slightly higher unit cost that to his knowledge was more representative of all soil cement projects (Carroll, 2012). Also, included in the items is the bid average for asphalt curing seal. As mentioned previously, on normal state projects an asphalt curing seal is applied within 24 hours of soil-cement mixing to help retain moisture and allow the cement to hydrate and gain strength. In the case of the field project, a plastic tarp was used instead; however, the cost of the plastic tarp was neglected from the analysis. Instead the statewide average for asphalt seal was also applied to the unit cost of State Project R-3403.

Table 7-36: Unit costs from NCDOT 2011 statewide bid average and from Project R-3403

Item Description	NCDOT Item #	Statewide Bid Avg. Cost ($)	NC Project R-3403 Cost ($)	Units
Undercut Excavation	0036000000-E	$6.72	$4.55	/yd^3
Borrow Material	0106000000-E	$7.43	$8.00	/yd^3
Select Granular Material	0194000000-E	$10.17	-	/yd^3
Aggregate Base Course	0314000000-E	$30.00	$24.00	/ton
Soil Cement Base	1176000000-E	$1.83	[1]$2.10	/yd^2
Portland Cement	1187000000-E	$114.75	[2]$114.75	/ton
Asphalt Curing Seal	1209000000-E	$3.75	-	/gal/yd^2

NOTE:[1]Well-rounded cost provided by the soil-cement contractor; [2]Contractor confirmed statewide average

The "Aggregate Base Course" and "Portland Cement" items had to be converted from per ton units into per cubic yard units. For the ABC, this was done using the average unit weight from quality control testing. With an average dry unit weight of 127 pcf (1.715 ton/cy), the ABC converted to $51.44 and $41.15 per cubic yard for statewide average and project unit cost, respectively. For cement, the price equated to $20.08 assuming an application rate of 12% by unit weight of subgrade soil. The dry unit weight of the subgrade soil was assumed to be 108 pcf based on untreated standard proctor compaction tests presented in Chapter 3.

The unit cost for the "asphalt curing seal" item had to be converted from per gallon units into per square yard units based on an application rate of .15 gallons per square yard. This rate was selected based on the NCDOT specified rate of .1 to .2 gallons per square yard (NCDOT, 2012). This equated to a unit cost of $0.56 per square yard of asphalt curing seal.

All costs per cubic yards were then multiplied by the stabilization layer depth to obtain the unit cost of each item on a per square yard basis. Geosynthetic manufacturers were contacted for the average unit costs of their products. These values are summarized in Table 7-37 (Dull, 2012; Isenhour, 2012). For later calculations, the large volume unit costs were used to represent the typical large-volume state projects. All reported costs through personal communication are listed for reference.

Table 7-37: Geosynthetic unit costs provided by the manufacturers

Geosynthetic	Avg. Cost ($/yd^2)	
	Large Volume	Small Volume
HP 570 Geotextile	$2.50	$3.25
BX 1500 Geogrid	$6.60	$7.25

Initial Construction Cost:

Using the unit costs of each item, the cost per square yard to construct the various stabilization measures was calculated with the results presented in Table 7-38 and plotted in Figure 7-116. Generally, the stabilization costs for State Project R-3403 were less than the statewide average. The most expensive measure to construct was determined to be the nine inch undercut section with ABC and the inclusion of the BX 1500 geogrid. This was due to the high unit cost of the ABC and BX 1500 geogrid. The cheapest measure to construct was determined to be the soil-cement stabilization since in-place mixing occurs without undercut and replacement.

Table 7-38: Stabilization method cost per square yard

Test Section	Stabilization Description	Unit Cost ($/yd^2)	
		Statewide Bid Avg.	State Project R-3403
1	31" Borrow Material	$12.18	$10.81
	31" Select Material	$14.54	-
	31" Borrow Material + 3" ABC	$16.47	$14.24
	31" Select Material + 3" ABC	$18.83	-
2	9" ABC + BX 1500	$21.14	$18.02
3	9" ABC + HP 570	$17.04	$13.92
4	8" Soil-Cement	$6.85	$7.12

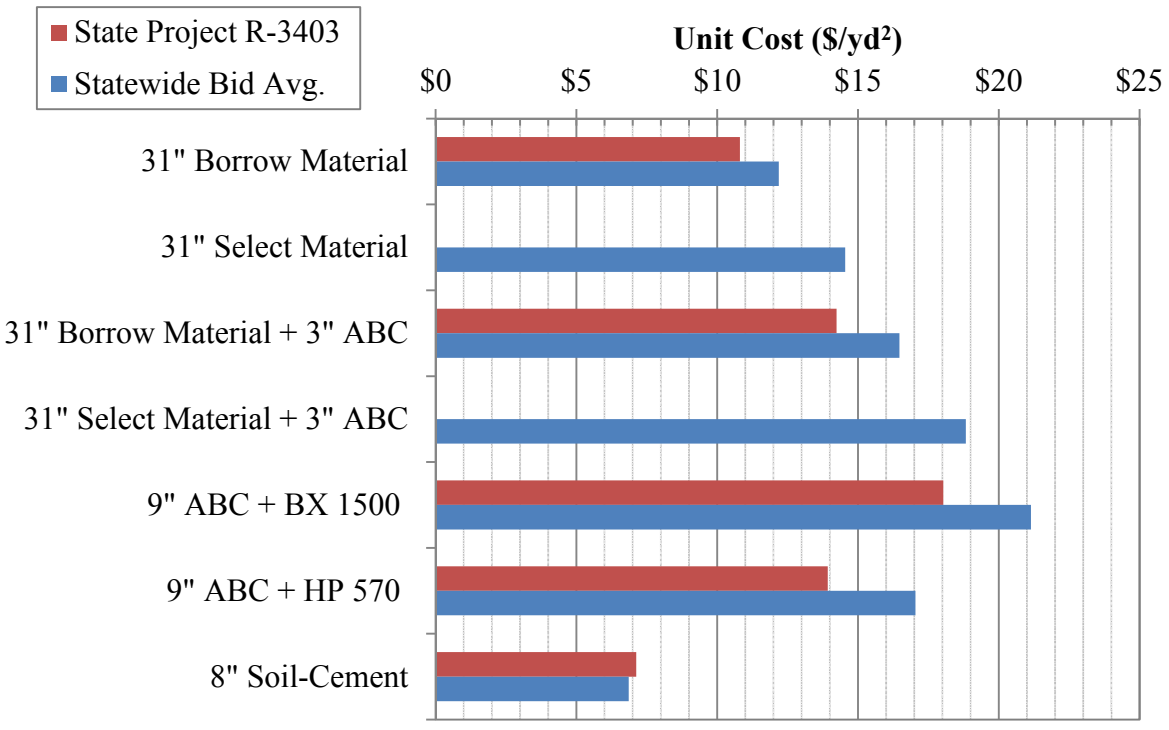

Figure 7-116: Unit cost for stabilization type

Performance Cost Calculation:

After determining the costs to implement each stabilization measure, the unit costs were then multiplied by the maximum, minimum, and average cumulative rutting measured in the corresponding test section. This was done at all traffic intervals where LiDAR scanning was performed. The results are presented in Table 7-39 through Table 7-45. In Test Section 1, the analysis was broken down into two stabilization measures. The rutting that occurred during the first 200 truck passes was assigned to the 31 inches of borrow or select material. After repairing Test Section 1, the cumulative rutting was zeroed and the rutting thereafter was used to calculate the performance cost of 31 inches of borrow or select material plus 3 inches of ABC.

Shown in Figure 7-117 is the average performance cost of the stabilization measures based on the 2011 statewide bid average unit costs. Looking at the results, soil-cement stabilization was found to be the most cost effective stabilization measure followed by the two geosynthetically reinforced sections. As expected, the performance cost for the 31 inch undercut stabilization

measure with select or borrow material was the highest. This was due to the excessive rutting that occurred in Test Section 1 during the first 200 truck passes. The vertical confinement provided by the placing an additional three inch layer of ABC, reduced the average performance cost by more than 50%. Shown in Figure 7-118 is the average performance cost of each stabilization measure based on the unit costs from State Project R-3403. In general, the results indicate the same findings; however, note that with the reduced cost of ABC from $30.00 to $24.00 per ton, the average performance cost of the geosynthetically reinforced measures becomes more comparable to the soil-cement stabilization measure.

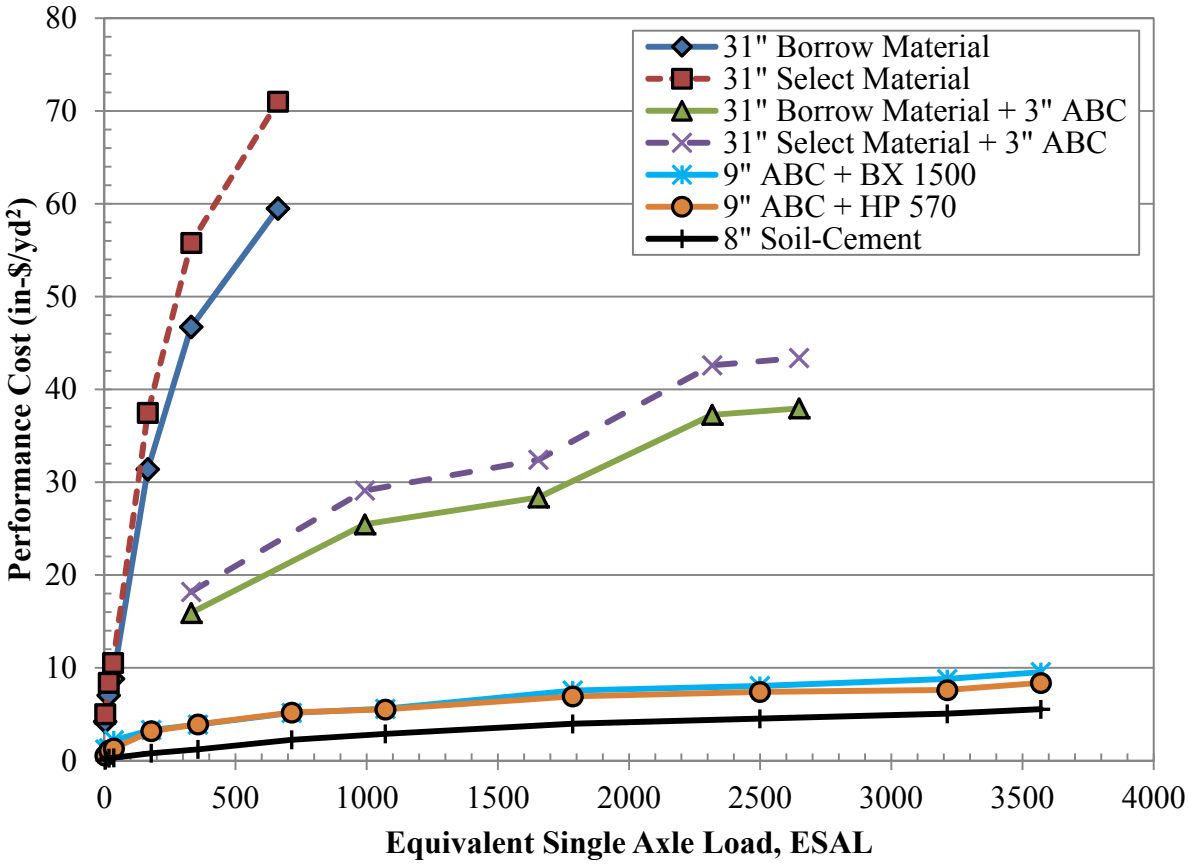

Figure 7-117: Average performance cost of stabilization measures based on unit costs from the 2011 statewide bid average

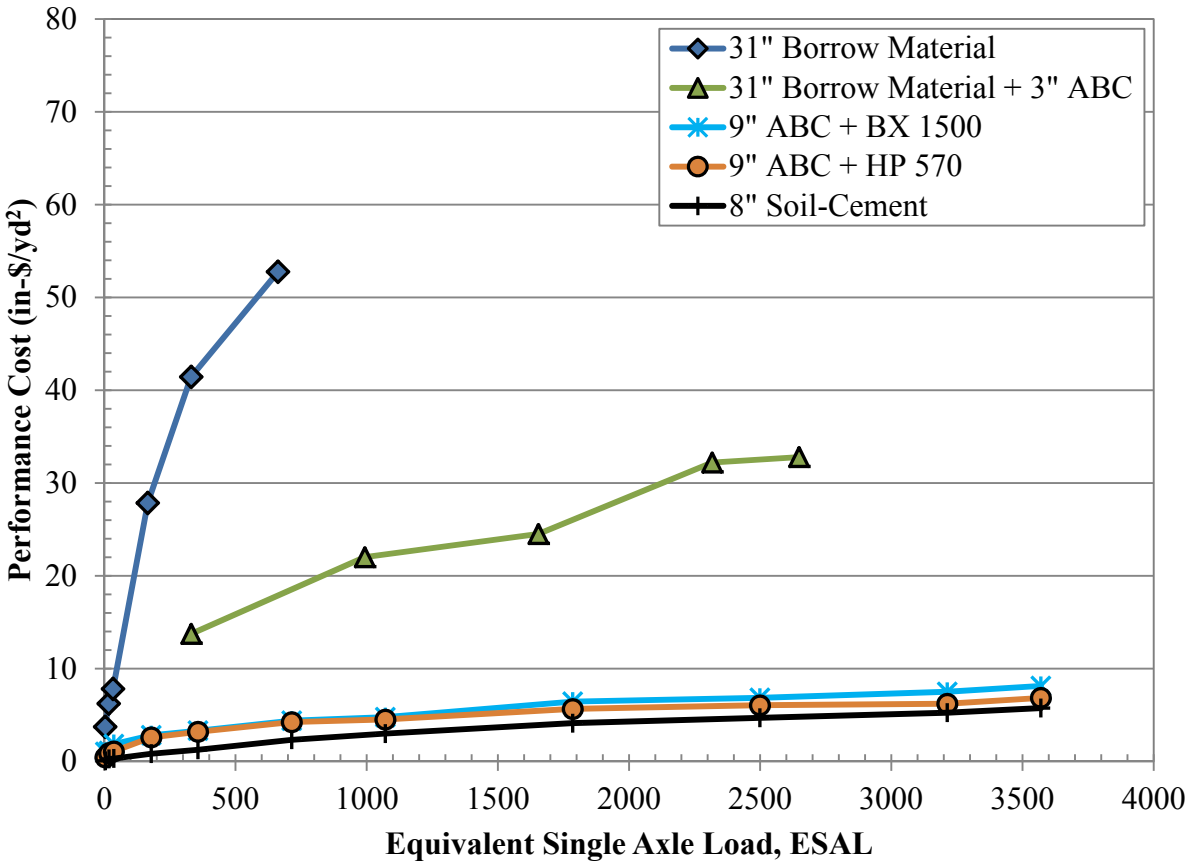

Figure 7-118: Average performance cost of stabilization measures based on unit costs from State Project R-3403

Table 7-39: Performance cost for 31" borrow material stabilization measure

Stabilization Description	Truck Pass	ESAL	Performance Cost (in-$/yd^2)					
			Statewide Bid Average			NC 17 Project		
			Min	Max	Avg.	Min	Max	Avg.
31" Borrow Material	1	3.31	1.24	7.27	4.20	1.10	6.45	3.72
	5	17	2.95	13.48	7.03	2.62	11.96	6.23
	10	33	4.69	17.03	8.82	4.16	15.11	7.82
	50	166	16.24	45.60	31.39	14.41	40.45	27.84
	100	331	34.11	59.77	46.73	30.26	53.01	41.44
	200	662	44.87	71.85	59.49	39.80	63.73	52.77

Table 7-40: Performance cost for 31" select material stabilization measure

Stabilization Description	Truck Pass	ESAL	Performance Cost (in-$/yd^2)					
			Statewide Bid Average			NC 17 Project		
			Min	Max	Avg.	Min	Max	Avg.
31" Select Material	1	3.31	1.48	8.67	5.01	-	-	-
	5	17	3.53	16.09	8.39	-	-	-
	10	33	5.60	20.33	10.53	-	-	-
	50	166	19.39	54.44	37.47	-	-	-
	100	331	40.72	71.35	55.78	-	-	-
	200	662	53.56	85.76	71.01	-	-	-

Table 7-41: Performance cost for 31" borrow material plus 3" ABC stabilization measure

Stabilization Description	Truck Pass	ESAL	Performance Cost (in-$/yd^2)					
			Statewide Bid Average			NC 17 Project		
			Min	Max	Avg.	Min	Max	Avg.
31" Borrow Material + 3" ABC	100	331	15.54	24.53	15.90	13.43	21.20	13.75
	300	993	23.90	41.82	25.46	20.65	36.15	22.01
	500	1655	24.17	44.57	28.36	20.89	38.52	24.51
	700	2317	29.87	64.63	37.26	25.81	55.86	32.21
	800	2648	29.94	64.63	37.95	25.88	55.86	32.80

Table 7-42: Performance cost for 31” select material plus 3” ABC stabilization measure

Stabilization Description	Truck Pass	ESAL	Performance Cost (in-$/yd^2)					
			Statewide Bid Average			NC 17 Project		
			Min	Max	Avg.	Min	Max	Avg.
31" Select Material + 3" ABC	100	331	17.76	28.04	18.18	-	-	-
	300	993	27.32	47.81	29.11	-	-	-
	500	1655	27.64	50.96	32.42	-	-	-
	700	2317	34.14	73.89	42.60	-	-	-
	800	2648	34.23	73.89	43.38	-	-	-

Table 7-43: Performance cost for 9” ABC plus BX 1500 stabilization measure

Stabilization Description	Truck Pass	ESAL	Performance Cost (in-$/yd^2)					
			Statewide Bid Average			NC 17 Project		
			Min	Max	Avg.	Min	Max	Avg.
9" ABC + BX 1500	1	3.57	0.00	3.96	1.20	0.00	3.37	1.02
	5	17.85	0.00	4.36	1.33	0.00	3.72	1.13
	10	35.7	0.03	5.35	2.19	0.02	4.56	1.87
	50	178.5	0.89	7.38	3.30	0.76	6.29	2.81
	100	357	1.27	7.38	3.88	1.08	6.29	3.31
	200	714	1.55	9.74	5.14	1.32	8.31	4.39
	300	1071	1.80	10.63	5.58	1.54	9.06	4.76
	500	1785	3.17	13.85	7.55	2.70	11.81	6.44
	700	2499	3.17	13.85	8.03	2.70	11.81	6.85
	900	3213	3.17	17.00	8.79	2.70	14.49	7.49
	1000	3570	4.06	17.00	9.54	3.46	14.49	8.13

Table 7-44: Performance cost for 9” ABC plus HP 570 stabilization measure

Stabilization Description	Truck Pass	ESAL	Performance Cost (in-$/yd^2)					
			Statewide Bid Average			NC 17 Project		
			Min	Max	Avg.	Min	Max	Avg.
9" ABC + HP 570	1	3.57	0.00	5.77	0.53	0.00	4.71	0.44
	5	17.85	0.00	5.77	1.08	0.00	4.71	0.88
	10	35.7	0.00	5.77	1.32	0.00	4.71	1.08
	50	178.5	0.49	7.34	3.17	0.40	6.00	2.59
	100	357	0.76	8.30	3.91	0.62	6.78	3.19
	200	714	1.74	11.39	5.19	1.42	9.31	4.24
	300	1071	2.02	12.66	5.51	1.65	10.34	4.51
	500	1785	2.04	13.19	6.91	1.67	10.78	5.65
	700	2499	2.04	16.28	7.40	1.67	13.30	6.04
	900	3213	2.51	17.83	7.59	2.06	14.57	6.21
	1000	3570	3.23	20.98	8.38	2.64	17.14	6.85

Table 7-45: Performance cost for 8” soil-cement stabilization measure

Stabilization Description	Truck Pass	ESAL	Performance Cost (in-$/yd^2)					
			Statewide Bid Average			NC 17 Project		
			Min	Max	Avg.	Min	Max	Avg.
8" Soil-Cement	1	3.57	0.00	2.48	0.05	0.00	2.58	0.05
	5	17.85	0.00	2.78	0.26	0.00	2.89	0.27
	10	35.7	0.00	2.78	0.30	0.00	2.89	0.32
	50	178.5	0.00	3.68	0.80	0.00	3.83	0.83
	100	357	0.00	4.87	1.21	0.00	5.06	1.25
	200	714	0.00	11.12	2.24	0.00	11.56	2.33
	300	1071	0.07	13.09	2.88	0.07	13.61	3.00
	500	1785	0.09	26.20	3.96	0.09	27.23	4.12
	700	2499	0.09	Fail	4.51	0.09	Fail	4.69
	900	3213	0.15	Fail	5.05	0.15	Fail	5.25
	1000	3570	0.15	Fail	5.52	0.15	Fail	5.74

Factors Not Considered in the Analysis:

The performance costs presented in this analysis are believed to accurately represent each stabilization measure. However, it is important to emphasize the fact that with each stabilization measure there are additional factors that are difficult (or impossible) to quantify and as a result were not considered in this analysis. In some cases, these factors can have a significant influence on the final decision to implement one stabilization measure over another. These factors include but are not limited to the following:

- The expedience of construction time. As the saying goes, "time is money" and this is especially true in the construction industry. Depending on the desired turnaround time between stabilizing the subgrade and placing the successive layer of material (i.e. base course or binder material), time may be an overriding factor. In the case of a short turnaround, soil-cement stabilization would be discouraged since a period of approximately seven days is required to allow the soil-cement to cure.
- Transportation costs for the various materials. Depending on the site location, the contractor may be within close proximity to a select or borrow material source but far away from an ABC source or vice versa.
- The time and costs associated with repairing the various stabilization measures. If a project site has multiple access points (such as a widening project), the frequency of traffic on the stabilized roadway may be minimal. In this case, short-term loading is less of an issue and repair will probably not be needed. As a result, decisions can be focused on long-term performance and the initial construction costs presented in Table 7-38.
- In the case of soil-cement, the additional fuel and time costs associated with construction equipment traversing the site using an alternate, presumably longer route since driving on the soil-cement layer is not permitted. This would not be a factor on a multiple access site similar to the one mentioned in the previous bullet point.
- Additional laboratory and quality control costs associated with soil-cement stabilization versus mechanical stabilization methods. This includes proctor-compaction and UCS tests in the lab, and more involved density, moisture, and sampling tests required in the field.

- Time of the year during construction. As mentioned earlier, based on NCDOT specifications soil-cement construction cannot occur when the air temperature is below 40 degrees Fahrenheit (NCDOT, 2012). Depending on time of the year, this factor may rule out the use of soil-cement stabilization for a particular project.
- High moisture and high groundwater table. Chemical stabilization may not work for soils with a high moisture content or under conditions dominated by high ground water for long periods of time.

Large Scale Test Comparison:

During research project 2008-07 a similar performance cost analysis was conducted based on unit costs obtained from the NCDOT 2008 statewide bid averages and the settlement magnitudes measured during 22 large scale laboratory tests. Similar to the current study, chemical stabilization, lime in the case of that project, was found to be the most economical alternative because of the low construction cost as well as the low surface deformation. Thick (16-20 inches) unreinforced ABC stabilization was also found to be an economical measure. This could not be validated, however, due to the absence of an unreinforced ABC test section.

In regards to geosynthetic reinforcement, the previous project found that the high displacements that occurred during the initial load cycles hurt their performance cost. This was presumably due to the need for some displacement in order to mobilize the geosynthetic tensile forces. In the case of the field project, high initial displacement was not a factor. This is believed to be due to attempts to pre-tension the geosynthetics during construction by allowing traffic on the roadway prior to final compaction. As a result, the tensile forces in the geosythetic were mobilized prior to full-scale testing so that high initial displacements were not necessary. In addition, large steel drum rollers were used in the field to apply a much higher compactive energy to the base and subgrade soils than capable in the test pit. This also helped in mobilizing the geosynthetic tensile forces as well as densifying the base and subgrade soils to reduce the initial displacement.

Similar to the field project, the select material by itself (no thin ABC layer) performed poorly due to punching shear failure at low cycles. However, after placing an additional three inch layer of ABC on top of the select material, the rate of displacement was reduced making the unreinforced deep undercut stabilization measure a more economical option.

Chapter Summary:

In summary, the performance cost analysis provides a quantitative comparison in inches of displacement to the cost per square yard to implement the various stabilization measures so that an informed decision on cost-effective stabilization can be made. This analysis, however, does not consider several other factors such as construction time, site location, and possible repair costs that may be overriding factors in the decision making process. The following conclusions can be made about the performance cost after 1000 truck passes during full-scale testing:

- Soil-cement stabilization was the most economical alternative because of the low initial construction cost as well as low cumulative rutting.
- Geosynthetic reinforcement tends to have the highest initial construction cost due to the high price of ABC. However, at $24.00 per ton of ABC, the performance of the geosynthetically reinforced sections outweighs its high initial costs leading to a performance cost that is comparable to soil-cement stabilization.
- Deep undercut (31 inches) and backfill with select material have moderate initial construction costs and perform poorly due incremental bearing capacity failures that lead to excessive rutting at low truck passes. However, by placing an additional three inch layer of ABC on top of the select material, the vertical confinement curtails the rate of rutting leading to a reduction in performance cost by more than 50%.

CHAPTER 8: SUMMARY AND CONCLUSIONS

The work in this report has focused on presenting the results of field testing on instrumented roadway sections to validate undercut criteria as developed from the laboratory testing and numerical modeling study covered under NCDOT research project 2008-07. To that end, this research project has sought to:

vi. *Identify a test site for implementation of alternative or supplemental approaches to undercut, including the use of geosynthetics and/or chemical stabilization.* The selected test site was part of an NCDOT widening project (State Project R-3403) located in Craven County, North Carolina on soft subgrade soils that were identified during the design phase as needing to be undercut.

vii. *Instrument four test sections at the identified site and monitor the performance in terms of induced rutting and stress distribution under repeated truck loading.* Four 16 feet wide by 50 feet long stabilized test sections were built on poor subgrade soils encountered in the Coastal Plain region of North Carolina. One test section encompassed undercutting and replacement with select material (Class II), the second and third test sections included reinforcement using a geogrid and geotextile, respectively, in conjunction with undercutting and replacement with ABC (Class IV), and a fourth test section included cement treatment of the soft subgrade soil. Full-scale field testing was conducted on the test sections by applying 1000 consecutive truck passes using a fully loaded tandem-axle dump truck. During this time, data was collected in regards to the peak vertical stress and moisture conditions measured by the installed instrumentation at the subgrade. In addition, profile surveying was performed at periodic intervals to provide permanent deformation (rutting) data with increasing number of truck passes.

viii. *Perform field testing using a Dynamic Cone Penetrometer (DCP), Soil Stiffness Gauge (SSG), and Falling Weight Deflectometer (FWD) to collect information on soil properties using in situ techniques.* DCP, SSG, and FWD tests were performed throughout the test pad at various stages in the study to obtain strength and modulus data in situ of both the

subgrade and base layer materials. This data was then used to explain full-scale testing results and investigate the validity of the proposed undercut criteria for defining the depth of undercut and predicting the performance of the replacement layer.

ix. *Use the field data to validate the proposed undercut evaluation criteria as developed from the laboratory and modeling study.* The proposed undercut criteria were evaluated based on a series of analyses that looked at estimating the subgrade soil properties using laboratory and in situ testing techniques. In addition, an evaluation was also performed based on the soil properties of the stabilized test sections to see if the undercut criteria charts could effectively gauge the performance of each test section subjected to repeat trafficking.

x. *Use the field data to calibrate the comparative cost analysis based on results from the laboratory study, and illustrate the relative cost of each measure such that an informed decision on cost-effective subgrade stabilization can be made.* The full-scale test data was analyzed to determine the relative cost in terms of rutting for each stabilization measure. Qualitative factors were also identified that could not be accounted for in the analysis but have an influence on the decision to implement particular stabilization measures. Lastly, comparisons were made relative to the performance cost analysis developed from the results of the laboratory study during research project 2008-07.

Based on the work conducted in this study, the following conclusions and observation are advanced:

In Situ Testing:

- In general, the weighted average DCPI of the top two feet of subgrade soil was found to be in excess of 38 mm/blow. This finding supports the NCDOT's current undercut criterion of 38 mm/blow as the DCPI cut-off, and would yield a required CBR value of greater than 5-8% or resilient modulus values greater than approximately 6 ksi (40 MPa).
- The moduli results obtained from the SSG were inconsistent with the stain level being induced by the SSG device. In addition, research has shown that the SSG device is highly sensitive to water content and cracks that develop at the ground surface (Abu-

Farsakh *et al.* 2003). Based on these observations, it was asserted that a level of caution should be exercised when using the results measured from the SSG.

- DCP and FWD test results on the mechanically stabilized test sections (Test Sections 1, 2, and 3) indicated an increase in base layer stiffness along the wheel paths after full-scale testing. This is presumably the result of soil densification that occurs from the repeated loading of the truck tires.

Full-Scale Testing Results:

- The deep undercut (31 inch) and select material backfill produced the highest cumulative rut depths due to lateral displacement of the select material initiated by incremental plastic strains induced during each axle pass.
- Thin ABC surface layers (2 to 3 inch) over select material providing sufficient vertical confinement to reduce the rate of rutting and allow for more than four times the number of traffic passes permissible with select material alone.
- Tensar's BX 1500 biaxial geogrid and TenCate's HP 570 geotextile resulted in a relatively equal performance in all aspects of the study including: influencing the base layer stiffness, reducing the rate of rutting, and influencing the vertical stress measured at the base/subgrade interface.
- The geosynthetically reinforced sections produced the least amount of cumulative rutting after 1000 truck passes despite measuring the highest magnitude of vertical stress at the base/subgrade interface. After the ABC densified during the initial stages of trafficking, the tensile strength of the geosynthetics was apparently mobilized, delaying further rut formation. Unfortunately, due to the absence of a controlled (unreinforced) ABC section, it is difficult to assess how much of the performance within the geosynthetic sections is due to the geosynthetics and how much is due to the high quality fill (i.e. ABC).
- The cement stabilized section produced slightly higher average rut depths than the geosynthetically reinforced sections due to the localized areas of pronounced cumulative rutting. However, there were several areas of the soil-cement test section that performed as well and in some cases better than the geosynthetically reinforced sections.
- Lateral wander of the truck tires has a more significant effect on the measured stress increase at the subgrade than changes in tire pressure that are on the order of +/- 10psi.

Lateral wander is further complicated when multiple driver changes occur due to natural tendencies to follow different alignments and travel at different rates of speed.

- Small differences in base course thickness can cause dramatic differences in the estimated stress at the subgrade for base course thicknesses that are equal to or less than the diameter of the equivalent tire loaded area.
- Based on EPC measurements collected in the geogrid reinforced test section, the Giroud and Han (2004) method over predicts the amount of benefit geogrid reinforcement can provide in reducing the stress at the subgrade.
- Subgrade moisture had very little influence on the full-scale testing results due to the extremely dry conditions in eastern North Carolina during the summer of testing.

Undercut Criteria Evaluation:

- The use of the undercut criteria on Coastal Plain subgrade soils was validated using soil properties estimated from laboratory testing (i.e. triaxial and resilient modulus) and/or DCP testing.
- The soil properties determined from laboratory testing and DCP testing showed general agreement validating the use of the DCP and the respective correlation equations as a quick and effective means for the estimation of strength and stiffness parameters in situ.
- The undercut criteria can be used to predict the performance in terms of pumping and rutting of mechanical stabilization measures after 1000 truck passes, however, should not be used in conjunction with chemical stabilization. This is based on the fact at almost any magnitude of unconfined compressive strength; chemically stabilized materials will almost always plot within the acceptable area of the undercut charts.

Performance-Cost Analysis:

- Soil-cement stabilization was the most economical alternative because of the low initial construction cost as well as low cumulative rutting. However, certain factors such as time, ambient air temperature, expected construction traffic, and the costs associated with repair should be considered prior to implementing soil-cement mixing as a stabilization measure.

- Geosynthetic reinforcement tends to have the highest initial construction cost due to the high price of ABC. However, at $24.00 per ton of ABC, the performance of the geosynthetically reinforced sections outweighs its high initial costs leading to a performance cost that is comparable to soil-cement stabilization.
- Deep undercut (31 inches) and backfill with select material has a moderate initial construction cost and performs poorly due to excessive rutting at low truck passes. However, by placing an additional three inch layer of ABC on top of the select material, the vertical confinement curtails the rate of rutting leading to a reduction in performance cost by more than 50%.

REFERENCES

AASHTO. (1993). *Guide for Design of Pavement Structures.* American Association of State Highway and Transportation Officials.

AASHTO. (1999). *AASHTO T 307: Standard Method of Test for Determining the Resilient Modulus of Soils and Aggregate Materials.*

AASHTO. (2005). *AASHTO T 134: Standard Method of Test for Moisture-Density Relations of Soil-Cement Mixtures.*

Abu-Farsakh, M. Y., Alshibli, K., Nazzal, M., & Seyman, E. (2003). *Assessment of In-Situ Test Technology for Construction Control of Base Courses and Embankments.* Baton Rouge: Louisiana Transportation Research Center.

Ahlvin, R. G., & Ulery, H. H. (1962). Tabulated values for determining the complete pattern of stresses, strains, and deflections beneath a uniform load on a homogeneous half space. *Highway Research Board, Bulletin 342*, 1-13.

Allbright, R. L. (2002). *Evaluation of the Dynamic Cone Penetrometer and its Correlations with Other Field Instruments.* M.S. Thesis, Department of Civil and Environmental Engineering, University of Wisconsin-Madison, WI.

ASTM. (2004). *ASTM D 4767-04: Standard Test Method for Consolidated Undrained Triaxial Compression Test for Cohesive Soils.* West Conshohocken: American Society for Testing and Materials.

ASTM. (2006). *ASTM D 2166 -06: Standard Test Method for Unconfined Compressive Strength of Cohesive Soil.* West Conshohocken: American Society for Testing and Materials.

ASTM. (2007). *ASTM D 4959 - 07: Standard Test Method for Determination of Water (Moisture) Content of Soil By Direct Heating.* West Conshohocken, PA: American Society for Testing and Materials.

ASTM. (2008). *ASTM D 6758-08: Standard Test Method forMeasuring Stiffness and Apparent Modulus of Soil and Soil-Aggregate In-Place by Electro-Mechanical Method.* West Conshohocken: American Society for Testing and Materials.

ASTM. (2009). *ASTM D 1557-09: Standard Test Methods for Laboratory Compaction Characteristics of Soil Using Modified Effort.* West Conshohocken: American Society for Testing and Materials.

ASTM. (2009). *ASTM D 6951-09: Standard Test Method for Use of the Dynamic Cone Penetrometer in Shallow Pavement Applications.* West Conshohocken: American Society of Testing and Materials.

ASTM. (2010). *ASTM D 4318-10: Standard Test Methods for Liquid Limit, Plastic Limit, and Plasticity Index of Soils.* West Conshohocken: American Society for Testing and Materials.

ASTM. (2010). *ASTM D6938-10: Standard Test Method for In-Place Density and Water Content of Soil and Soil-Aggregate by Nuclear Methods (Shallow Depth).* West Conshohocken: ASTM International.

ASTM. (2011). *ASTM D 558-11: Moisture-Density (Unit Weight) Relations of Soil-Cement Mixtures.* West Conshohocken: American Society for Testing and Materials.

Austin, D. N., & Coleman, D. M. (1993). A Field Evaluation of Geosynthetic Reinforced Haul Roads Over Soft Foundation Soils. *Conference Proceedings, Geosynthetics '93.* Vancouver, Canada.

Ayers, M. E. (1989). Rapid shear strength evaluation of in situ granular materials. *Transportation research record*, 134-146.

Borden, R. H., Cote, B. M., Gabr, M. A., Park, Y., Pyo, S., & Robinson, B. R. (2010). *Establishment of Subgrade Undercut Criteria and Performance of Alternative Stabilization Measures.* Raleigh: NCDOT.

Boswell, W. F. (2000). Soil Stabilization/Soil Cement Mark-Lang, Inc.'s Approach. *Geo-Denver* (pp. 26-35). Denver: ASCE.

Carroll, M. L. (2012, March). Personal Communication. Site-Prep, Inc. of NC.

Catton, M. D. (1939). Laboratory and field investigation of soil-cement mixtures. *Engineering Society of Wisconsin, Report, v 14, n 3*, 72-89.

Chaddock, B. C. (1988). Deformation of Road Foundations with Geogrid Reinforcement. *Research Report 140. Transportation and Road Research Laboratory*, Berkshire, U.K.

Chen, H., & Wang, Q. (2006). The behaiviour of organic matter in the process of soft soil stabilization using cement. *Bulletin of Engineering Geology and the Environment*, 445-448.

Cobos, D. R., & Chambers, C. (2010, November 17). *Calibrating ECH2O Soil Moisture Sensors.* Retrieved January 27, 2012, from Decagon Devices: http://www.decagon.com/assets/Uploads/13393-04-CalibratingECH2OSoilMoistureProbes.pdf

Coduto, D. P. (2001). *Foundation Design: Principles and Practices - 2nd Edition.* Upper Saddle River, NJ: Prentice-Hall.

Cote, B. M. (2009). *Performance Comparison of Mechanical and Chemical Stabilization of Undercut Subgrades.* Raleigh, NC: North Carolina State University: Masters Thesis.

Daniels, J. L., Janardhanam,, R., Anderson,, J. B., Lei, S., Baucom,, I. K., DeBlasis,, N. J., & Bowers, B. F. (2010). *Subgrade Stabilization Alternatives to Lime and Cement.* Charlotte, NC: The University of North Carolina at Charlotte.

Danistan, J., & Vipulanandan, C. (2009). "Relationship between CBR values (un-soaked) and undrained shear strength of artificial CH soils. *Proceedings of CIGMAT-2009 Conference & Exhibition.* Houston, TX: University of Houston.

De Gardiel, R., & Javor, E. (1986). Mechanical Reinforcement of Low-Volume Roads by Geotextiles. *Proceedings, Third International Conference on Geotextiles*, (pp. 1021-1026). Vienna, Austria.

DeBlasis, N. J. (2008). *The Influence of Curing Temperature on Cement Stabilization of North Carolina Soils.* Skokie, IL: Portland Cement Association.

Decagon Devices, Inc. (2010). *10HS Soil Moisture Sensor Operator's Manual: Version 3.* Pullman: Decagon Devices, Inc.

Decagon Devices, Inc. (2012, February 14). *10HS Soil Moisture, large area of influence*. Retrieved from Decagon Devices: http://www.decagon.com/products/sensors/soil-moisture-sensors/10hs-soil-moisture-large-area-of-influence/

Dull, S. (2011, May 26). Personal Communication. TenCateTM. (T. Cowell, Interviewer)

Dynatest Engineering. (1995). *Dynatest 8000 FWD Test System Owner's Manual.*

Edens, J. (2012, March). Personal Communication. North Carolina Department of Transportation.

Fannin, R. J., & Sigurdsson, O. (1996). Field Observations on Stabilization of Unpaved Roads with Geosynthetics. *Journal of Geotechnical Engineering*, 544-553.

FHWA. (1996). *LTTP P46: Resilient Modulus of Unbound Granular Base/Subbase Materials and Subgrade Soils.* McLean: U.S. Department of Transportation.

FHWA. (2008). *Ground-Based LiDAR: Rock Slope Mapping and Assessment.* Lakewood: FHWA: Central Federal Lands Highway Division.

Flippin, B. N. (2012). Personal Communication. NCDOT.

Fonseca, A. V., Cruz, R. C., & Consoli, N. C. (2009). Strength Properties of Sandy Soil–Cement Admixtures. *Geotechnical and Geological Engineering, v 27, n 6*, 681-686.

Geokon, I. (2007). *Instruction Manual: Model 3500, 3510, 3515, 3600.* Lebanon.

Giroud, J. P., & Han, J. (2004). Design Method for Geogrid-Reinforced Unpaved Roads: I. Development of Design Method. *Journal of Geotechnical and Geoenvironmental Engineering, ASCE*, 775-786.

Giroud, J. P., & Han, J. (2012). The Giroud-Han design method for geosynthetic-reinforced unpaved roads. *Geosynthetics*.

Giroud, J. P., & Noiray, L. (1981). Geotextile-Reinforced Unpaved Road Design. *Journal of Geotechnical Engineering, ASCE, 107(9)*, 1233-1254.

Guthrie, W. S., & Rogers, M. A. (2010). Variability in Construction of Cement-Treated Base Layers: Material Properties and Contractor Performance. *Journal of the Transportation Research Board*, 78–89.

Herath, A., Mohammad, L. N., Gaspard, K., Gudishala, R., & Abu-Farsakh, M. Y. (2005). The use of Dynamic Cone Penetrometer to Predict Resilient Modulus of Subgrade Soils. *Geotechnical Special Publication No. 130: Advances in Pavement Engineering, Geo-Frontiers*, (pp. 17-32).

Holderby, E., & Cerato, A. B. (2011). Field Verification of Stabilized Soil Strength. *ASCE Geo-Frontiers* (pp. 2454-2463). Dallas, TX: American Society of Civil Engineers.

Hufenus, R., Rueegger, R., Banjac, R., Mayor, P., Springman, S. M., & Bronnimann, R. (2006). Full-scale field test on geosynthetic reinforced unpaved roads on soft subgrades. *Geotextiles and Geomembranes, 24*, 21-37.

Humboldt Mfg. Co. (2007). *GeoGauge User Guide.* Norridge: Humboldt Mfg. Co.

Keller, K. (2008). *Electrical Safety Code Manual.* Oxford: Elsevier.

Kennedy, T. W., Smith, R., Holmgreen Jr., R. J., & Tahmoressi, M. (1987). An Evaluation of Lime Cement Stabilization. *Transportation Research Record, 1110*, 11-25.

Leica Geosystems. (2012). *Leica ScanStation C5.* Retrieved January 26, 2012, from Leica Geosystems: http://www.leica-geosystems.us/en/Leica-ScanStation-C5_94573.htm

Mitchell, J. K., & Soga, K. (2005). *Fundamentals of Soil Behaivor: 3rd Edition.* Hoboken: John Wiley and Sons, Inc.

Nassar, W., Al-Qadi, I. L., Flintsch, G. W., & Appea, A. (2000). Evaluation of Pavement Layer Response at the Virginia Smart Road. *Pavement Subgrade, Unbound Materials, and*

Nondestructive Testing: Proceedings of Sessions of Geo-Denver 2000 (pp. 104-118). Denver: ASCE.

NCDOT. (1998). *Pavement Condition Survey Manual.* Raleigh, NC: North Carolina Department of Transportation.

NCDOT. (2007). *Geotechnical Inventory Report, NCDOT, State Project: 34538.1.1 (R-3403 A).*

NCDOT. (2011). *North Carolina Department of Transportation: Project Letting.* Retrieved from http://www.ncdot.org/doh/preconstruct/ps/contracts/bidaverages/avgdefault.html

NCDOT. (2012). *Standard Specifications for Roads and Structures.* Raleigh: North Carolina Department of Transportation.

NCHRP. (2008). *NCHRP Synthesis 382: Estimating Stiffness of Subgrade and Unbound Materials for Pavement Design.* Washington: Transportation Research Board.

North Carolina Department of Transportation (NCDOT). (2012). *Standard Specifications for Roads and Structures.* Raleigh.

Odemark. (1949). *Investigations as to the Elastic Properties of Soils and Design of Pavements according to the Theory of Elasticity.* Stockholm: Statens Väginstitut, Mitteilung No. 77.

Park, Y. J., Gabr, M. A., Robinson, B. R., & Borden, R. H. (2012). Subgrade Undercut Criteria Based on Modeling of Rutting and Pumping. *Journal of Geotechnical and Geoenvironmental Engineering*.

Petry, T., & Wohlgemuth, S. K. (1988). The Effects of Pulverization on the Strength and Durabiility of Highly Active Clay Soil Stabilized with Lime and Portland Cement. *Transportation Research Record, 1190*, 38-45.

Pyo, S. C. (2011). Personal Communication. North Carolina State University.

Rahim, A. M., & George, K. P. (2005). Models to estimate subgrade resilient modulus for pavement design. *The International Journal of Pavement Engineering*, 89–96.

Roberts, J. D. (1986). Performance of Cement-Modified Soils: A Follow-Up Report. *Transportation Research Record, 1089*, 81-86.

Sariosseiri, F., & Muhunthan, B. (2009). Effect of cement treatment on geotechnical properties of someWashington State soils. *Engineering Geology, 104*, 119–125.

Sariosseiri, F., & Muhunthan, B. (2009). Effect of cement treatment on geotechnical properties of someWashington State soils. *Engineering Geology*, 119–125.

Sawangsuriya, A., Edil, T. B., & Bosscher, P. J. (2003). Relationship Between Soil Stiffness Gauge Modulus and Other Test Moduli for Granular Soils. *Transportation Research Record*, 3-10.

Scullion, T., Sebesta, S., Harris, J. P., & Syed, I. (2005). *Evaluating the Performance of Soil-Cement and Cement-Modified Soil for Pavements: A Laboratory Investigation.* Skokie, Illinois: Portland Cement Association.

Simmons, L. (2011). Personal Communication. Barnhill Contracting Company.

Tastan, E. O., Edil, T. B., Benson, C. H., & Aydilek, A. H. (2011). Stabilization of Organic Soils with Fly Ash. *Journal of Geotechnical and Geoenvironmental Engineering*, 819-833.

Tergazi, K. (1943). *Theoretical Soil Mechanics.* New York: Wiley.

Tingle, J. S., & Jersey, S. R. (2009). Full-Scale Evaluation of Geosynthetic-Reinforced Aggregate Roads. *Transportation Research Record: Journal of Transportation Research Board, No. 2116*, 96-107.

Tingle, J. S., & Webster, S. L. (2003). Corps of Engineers Design of Geosynthetic-Reinforced Unpaved Roads. *Transportation Research Record: Journal of Transportation Reseach Board, No. 1849*, 193-201.

US Army. (1994). *Soil Stabilization for Pavements: TM 5-822-14/AFMAN 32-8010.* WASHINGTON, DC: Department of the Army, the Navy, and the Air Force.

Wachman, G. S., & Labuz, J. F. (2011). Soil-Structure Interaction of an Earth Pressure Cell. *ASCE Journal of Geotechnical and Geoenvironmental Engineering*, 843-845.

Wainaina, N. (2006). *Geotechnical Problems and Practical Solutions.* Retrieved from Presentation, NCDOT Construction Engineers Conference: http://www.ncdot.org/doh/Operations/dp_chief_eng/constructionunit/CEC2006/pdfs/H1.pdf

Webster, S. L., & Alford, S. J. (1978). *Investigation of Construction Concepts for Pavements Across Soft Ground.* Vicksburg, Miss.: Technical Report S-78-6. U.S. Army Corps of Engineers Waterways Experiment Station.

Webster, S. L., & Watkins, J. E. (1977). *Investigation of Construction Techniques for Tactical Bridge Approach Roads Across Soft Ground.* Vicksburg, Miss.: Technical Report S-77-1. US Army Corps of Engineers Waterways Experiment Station.

APPENDIX

APPENDIX A: RESULTS OF CU TRIAXIAL TESTING FOR SUBGRADE SOIL

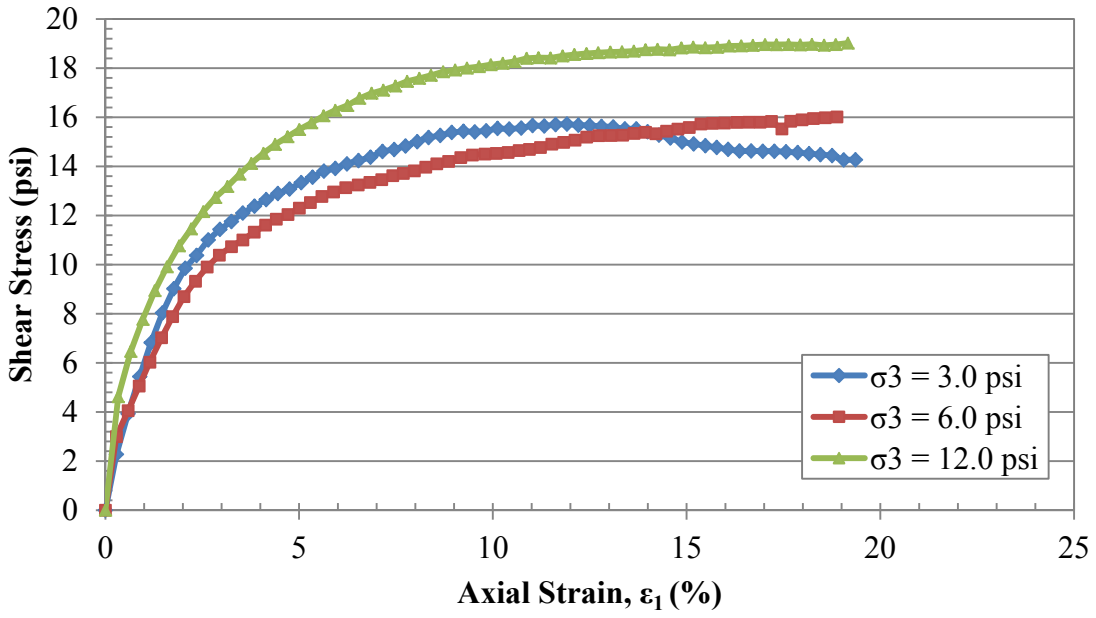

Figure A119: Shear stress versus axial strain during shearing stage (Shelby tube 3)

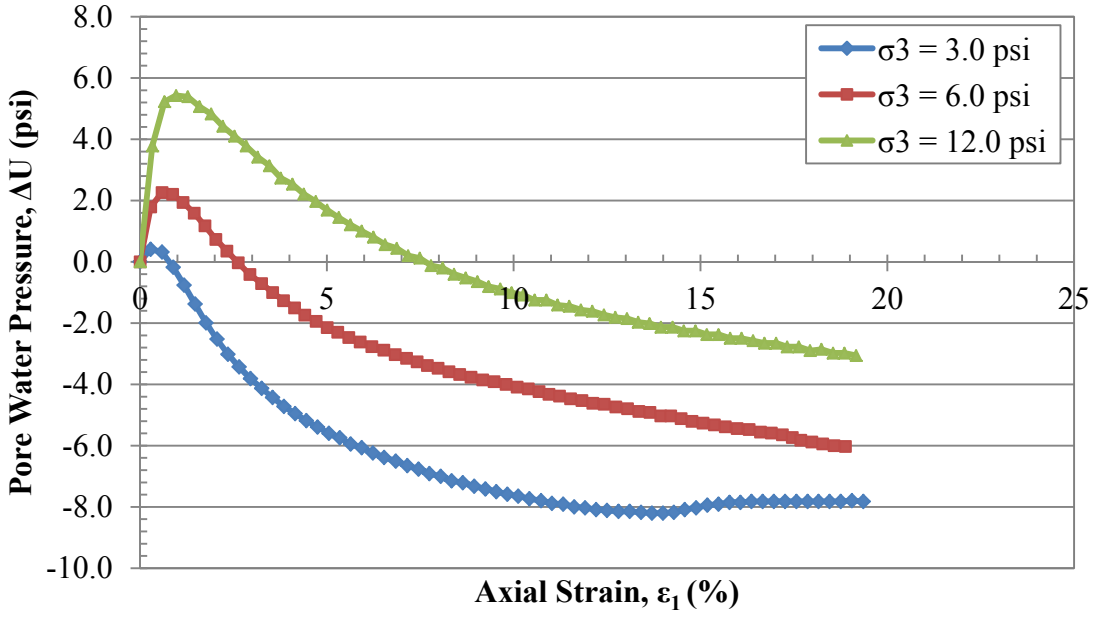

Figure A120: Pore water pressure versus axial strain during shearing stage (Shelby tube 3)

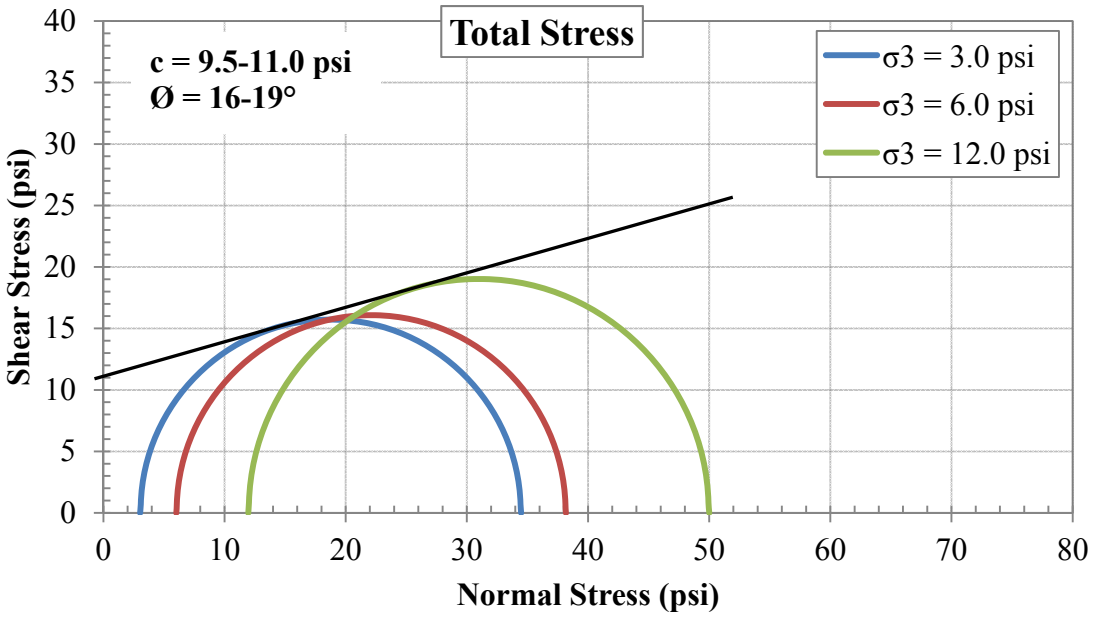

Figure A121: Mohr circles in terms of total stress (Shelby tube 3)

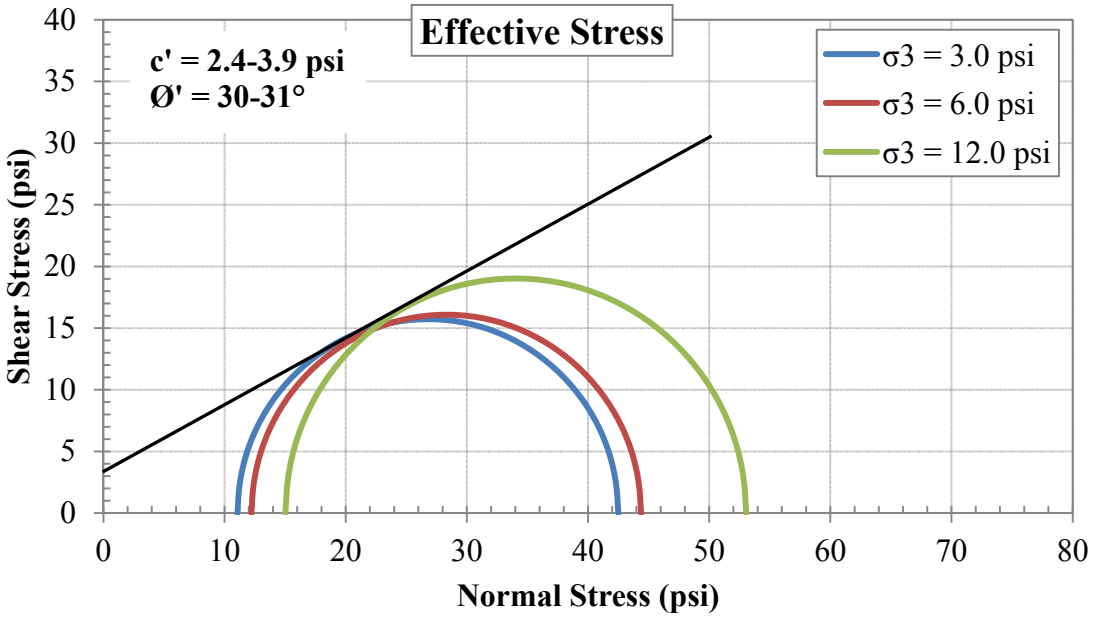

Figure A122: Mohr circles in terms of effective stress (Shelby tube 3)

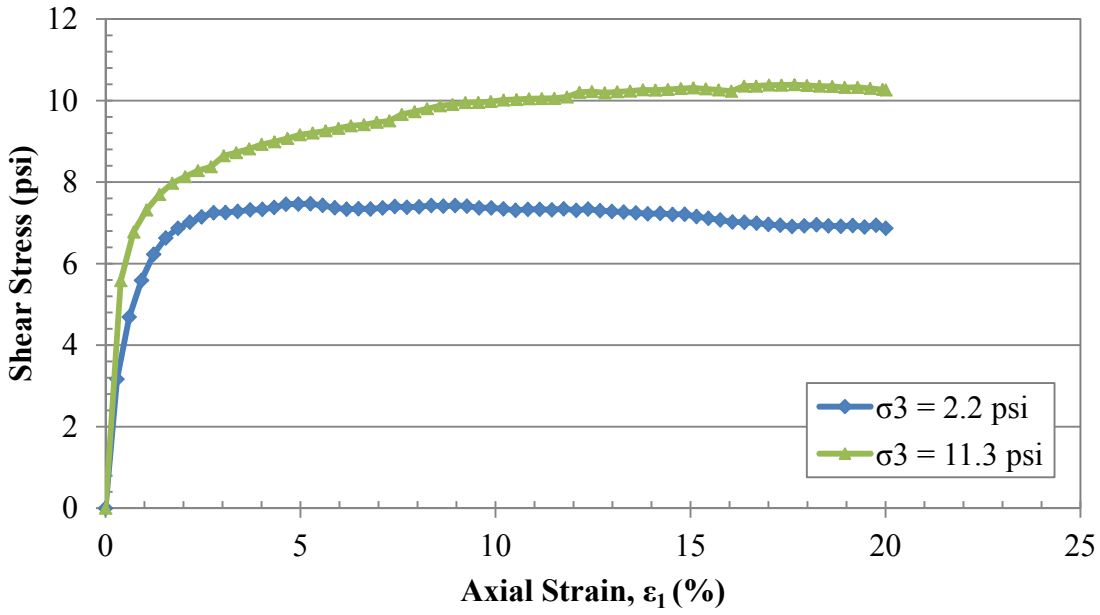

Figure A123: Shear stress versus axial strain during shearing stage (Shelby tube 5)

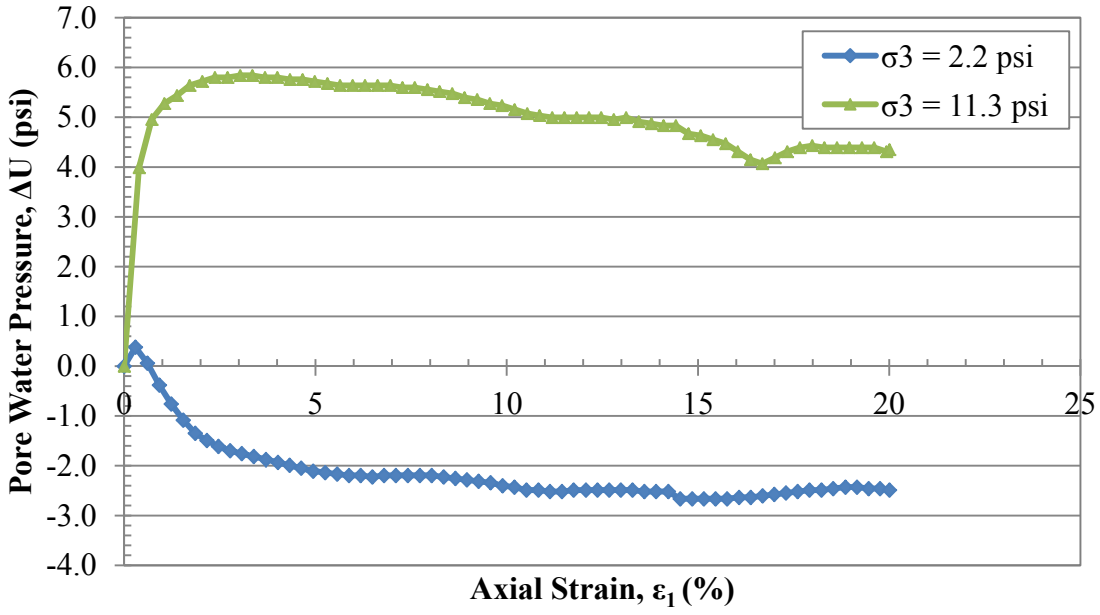

Figure A124: Pore water pressure versus axial strain during shearing stage (Shelby tube 5)

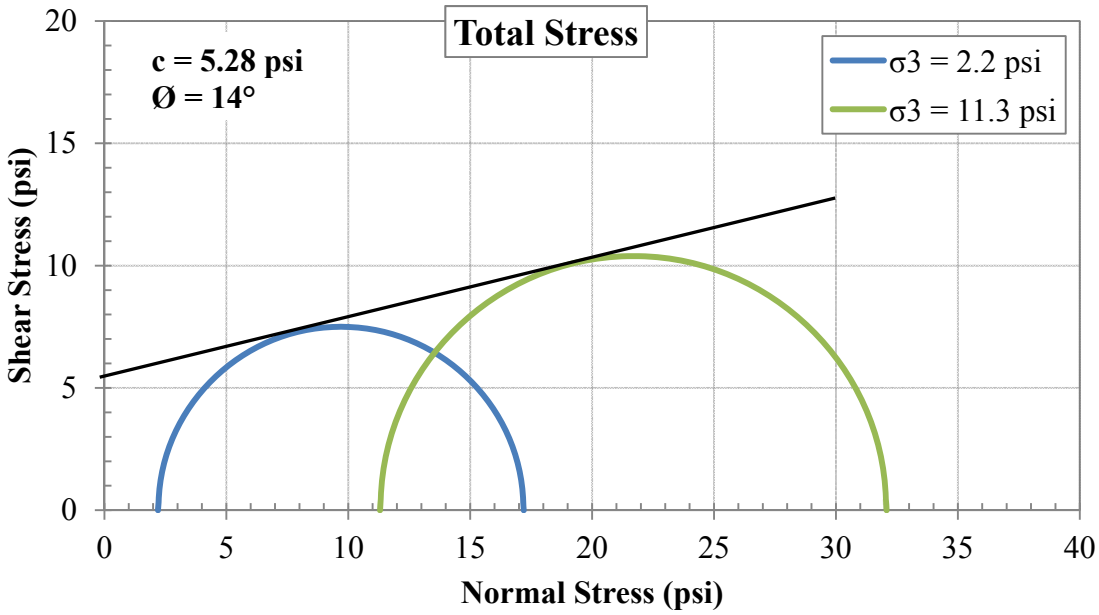

Figure A125: Mohr circles in terms of total stress (Shelby tube 5)

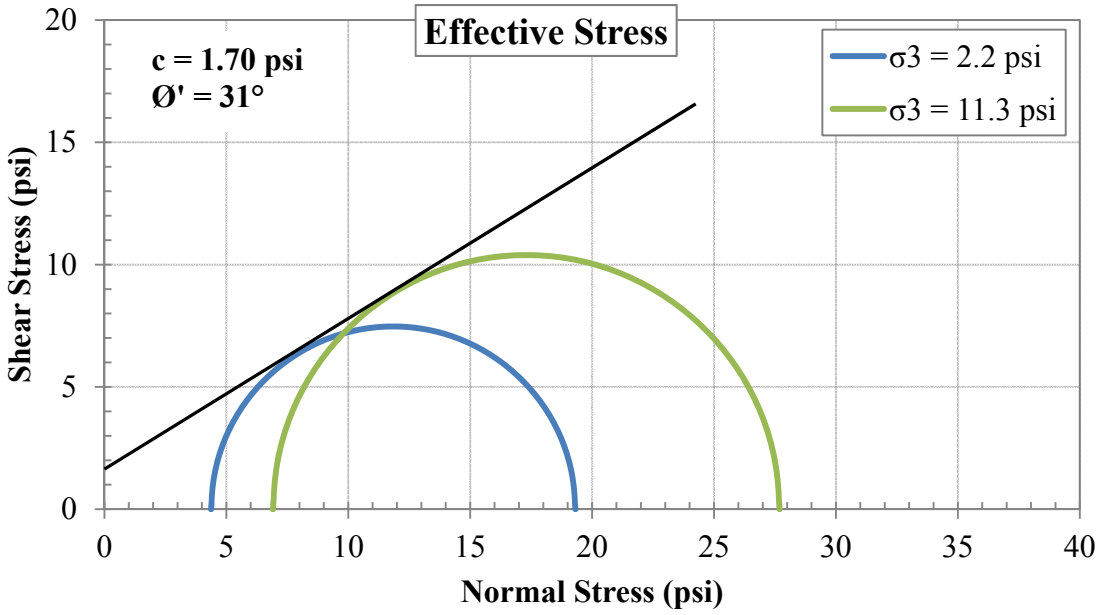

Figure A126: Mohr circles in terms of effective stress (Shelby tube 5)

APPENDIX B: GEOSYNTHETIC PROPERTIES

Table B46: Geosynthetic Index Properties

			HP 570 (geotextile)		BX 1500 (geogrid)	
Property	Specifications	Units	MD	CD	MD	CD
Ultimate Tensile Strength	ASTM D 4595	kN/m (lb/ft)	70.0 (4800)	70.0 (4800)	27.0 (1850)	30.0 (2050)
Tensile Strength (2% Strain)	ASTM D 4595	kN/m (lb/ft)	14.0 (960)	19.3 (1320)	8.5 (580)	10.0 (690)
Tensile Strength (5% Strain)	ASTM D 4595	kN/m (lb/ft)	35.0 (2400)	39.4 (2700)	17.5 (1200)	20.0 (1370)
UV Resistance (500 hours)	ASTM D 4355	% Retained Strength	80		100	

NOTE: MD = machine direction, CD = cross-machine direction

Table B47: Geotextile Fabric Properties

Property	Specifications	Units	HP 570 (geotextile)
Factory Seam Strength	ASTM D 4884	lb/ft (kN/m)	3000 (43.8)
Permeability	ASTM D 4491	cm/sec	0.05
Permittivity	ASTM D 4491	sec^{-1}	0.40
Apparent Opening Size (AOS)	ASTM D 4751	U.S. Sieve (mm)	#30 (.60)

Table B48: Geogrid Structural Properties

Property	Specifications	Units	BX 1500 (geogrid)
Junction Efficiency	GRI-GG2-05	%	93
Flexural Stiffness	ASTM D 5732	mg-cm	2,000,000
Aperture Stability	USACE Method	m-N/deg	0.75

References:

Mirafi, TenCate. "Mirafi HP570." 2011. *TenCate.* 2012. <http://www.tencate.com/TenCate/Geosynthetics/documents/HP%20Series/TDS_HP570A.pdf>.

Tensar Internation Corporation. "Product Specification Tensar Biaxial Geogrid." 2012. *Tensar.* 2012. <http://www.tensarcorp.com/uploadedFiles/SPECTRA_MPDS_BX_1.09.PDF>.

APPENDIX C: EARTH PRESSURE CELL LOCATION AND DIMENSIONS

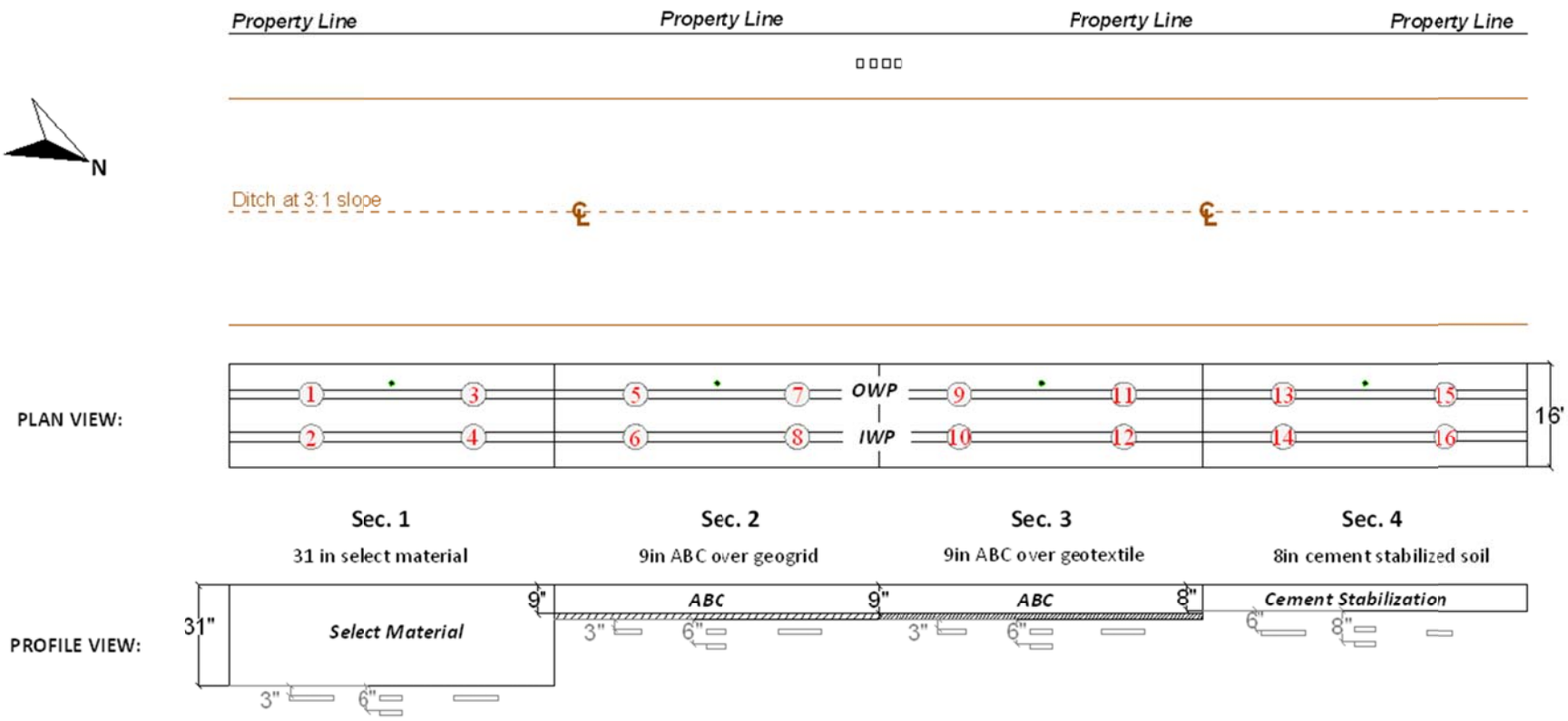

Figure C127: EPC location and identification number

Table C49: EPC dimensions and capacity

Pressure Cell #	Diameter (in)	Capacity	
		psi	kPa
1	9	87	600
2	9	87	600
*3	4	58	400
4	9	87	600
5	9	87	600
6	4	58	400
7	4	58	400
8	9	87	600
9	9	87	600
10	4	145	1000
11	4	36	250
12	9	87	600
13	9	36	250
14	9	87	600
15	9	87	600
16	4	36	250

*EPC # 3 quit working prior to full-scale testing

APPENDIX D: EARTH PRESSURE CELL CALIBRATION

As mentioned previously, earth pressure cells (EPCs) has a manufacturer provided calibration factor that is determined by applying a known uniform fluid pressure and measuring the corresponding output. This procedure, however, does not take into account that when the EPC is installed into a soil mass the stress applied to the surface of the EPC is non-uniform due to inclusion and/or soil arching effects (Labuz & Theroux, 2005). To account for these factors, a number of laboratory tests were performed in a concrete test pit at the Constructed Facilities Laboratory at North Carolina State University. The test pit was constructed to mimic field testing conditions. A diagram of the test setup is shown in **Figure D128**.

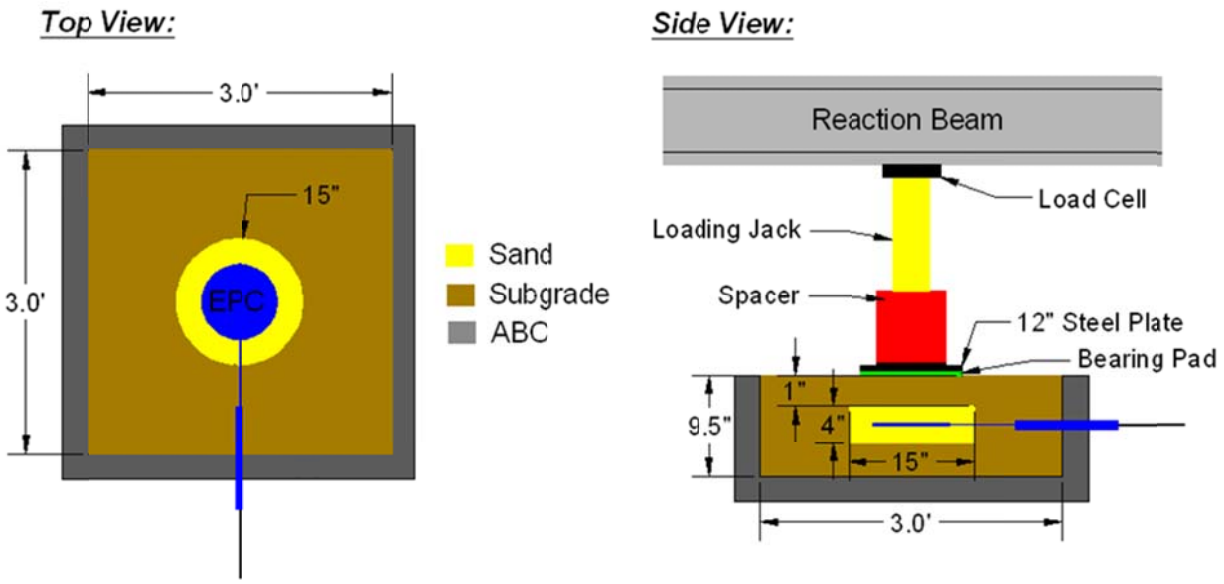

Figure D128: Diagram of the EPC laboratory calibration test setup

Subgrade material taken from Test Sections 1, 2, and 3 was placed approximately at its average in-situ moisture content and density as determined from Shelby tube samples. To verify soil moisture and dry unit weight, quality control testing was conducted using a Troxler Model 3440 nuclear moisture-density gauge. The results of the nuclear gauge testing are provided in Table D50. To replicate EPC installation in the field, a 15 in. diameter by 5 in. deep hole was dug out of the compacted subgrade and replaced with a 3-inch thick layer of compacted ASTM fine-graded silica sand. Once the sand was in place, the earth pressure cell was positioned on top and leveled. An additional, 2-inch layer of sand and 1 inch layer of subgrade material was hand compacted above the EPC to complete the soil profile. The test section was loaded using an Enerpac® 10 ton capacity hydraulic jack with a 10 inch stroke. The jack loaded the section

through a 12 inch diameter, one inch thick steel load plate. A ½ inch thick neoprene bearing pad was placed beneath the steel plate to help level the configuration and provide uniform stress at the ground surface. A picture of the completed test setup is shown in Figure D129.

Table D50: Avg. subgrade unit weight and water content in the lab during EPC calibration

Lab Test Number	Dry Density (pcf)	Wet Density (pcf)	Water Content (%)
1	100.1	119.0	18.9
2	99.6	118.6	19.1
3	99.5	118.5	19.0
Lab Average	99.7	118.7	19.0
Average Field	96.4	116.5	21.2
% Field Density	103.5	101.9	-
+/- Field Moisture	-	-	-2.2

Figure D129: EPC laboratory calibration test setup

During testing the EPC was loaded in 5 psi increments up to approximately 40 psi; the maximum stress measured in the field. A calibrated load cell was placed between the reaction beam and jack to measure the applied load from the jack. The EPC and load cell readings were recorded throughout the test using a Vishay 7000 data acquisition system. Each test consisted of 5 load/unload cycles with the results from the fifth load cycle being used for calibration. A total of 9 tests were performed in the lab; three tests using a 9 inch - 250 kPa capacity EPC, two tests using a 9 inch - 600 kPa capacity EPC, and four tests using a 4 inch - 250 kPa capacity EPC.

Prior to lab testing the assumption was made that the manufacturer provided calibration factor was inaccurate exclusively due the non-uniform stress distribution and the soil arching effect. Furthermore, it was assumed that every EPC of equal diameter is constructed to relatively the same dimensions and stiffness. As a result, the data obtained in the lab is solely a function of the EPC's diameter and soil conditions. After replicating the field soil conditions in lab, the results could be applied directly to all of earth pressure cells used in the field.

To account for the stress dissipation within the three inch layer of overburden soil, an elastic analysis was performed using tables developed by Ahlvin & Ulery to calculate the vertical stress at points along the earth pressure cell's radius (1962). Shown in Figure D130 is the calculated vertical stress along the face of the nine inch diameter cell as a function of the applied circular load. A weighted average of the vertical stress was then calculated based on the surface area of the EPC. Shown in Figure D131 is the average vertical stress at the face of the EPC as a function of the applied load. Note that the average stress at the 4 inch EPC is higher than the average stress at the 9 inch EPC. This is due to the 4 inch EPC's smaller surface area that is primarily concentrated at the center of the load application where the highest magnitude of stress is distributed.

To obtain the calibration equation for the 4 inch and 9 inch diameter EPCs, the average vertical stress was compared to the fluid calibrated stress reading. The results are shown in Figure D132 along with the best fit line, R-squared value, and the calibration equation that was used to adjust all measured stresses from the field EPCs. Note that both the 4 inch and 9 inch EPCs over register the magnitude of applied stress. This is the result of a phenomenon known as passive arching where the surrounding soft soil displaces downwards while the stiff EPC remains in its original position. Consequently, downward shear stresses develop around the perimeter of the

EPC causing it to measure a higher magnitude of stress (Tien, 1996). An illustration of passive arching is shown in Figure D133.

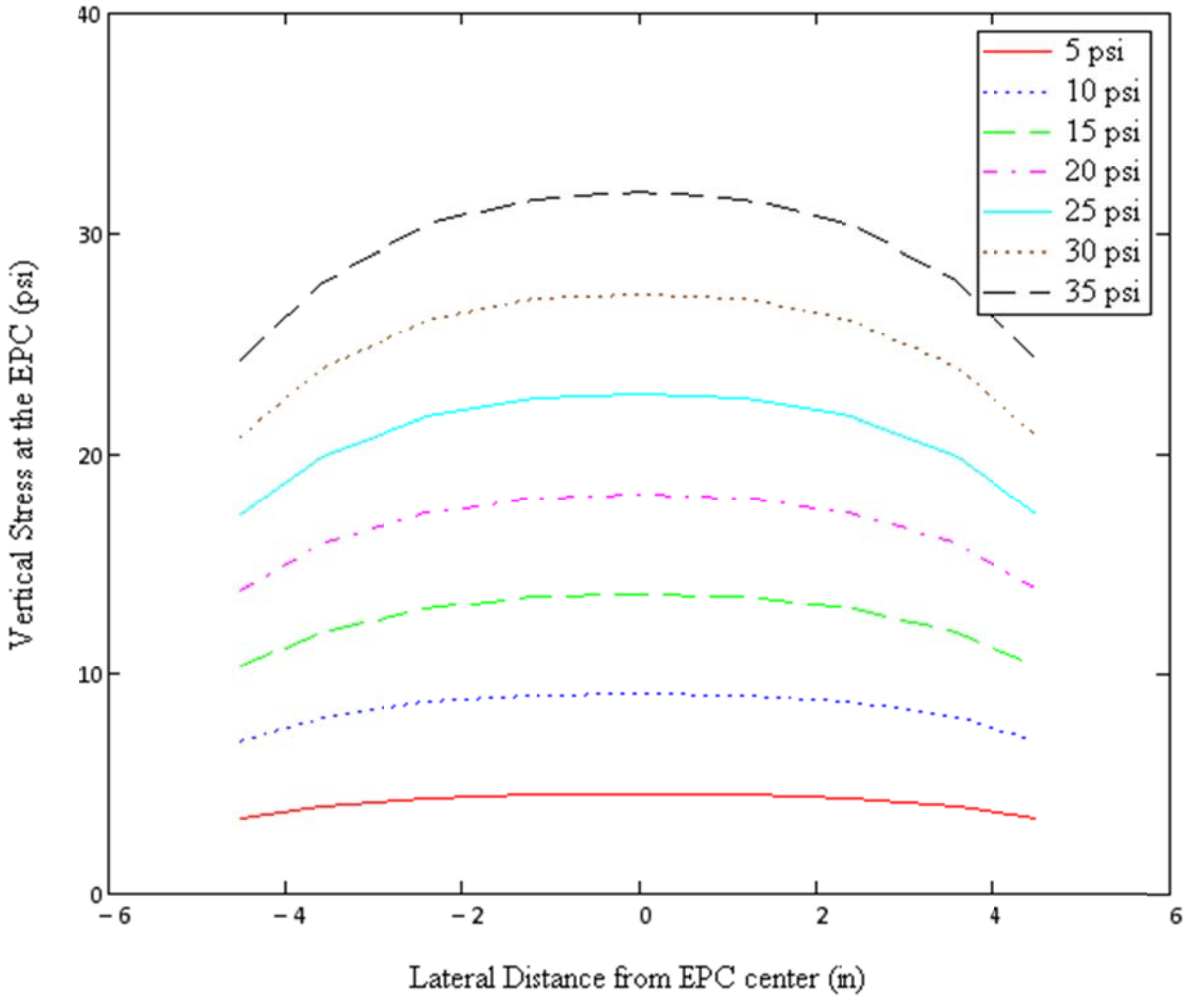

Figure D130: The vertical stress over the face of a 9 inch diameter EPC installed 3 inches below the ground surface (Ahlvin & Ulery, 1962)

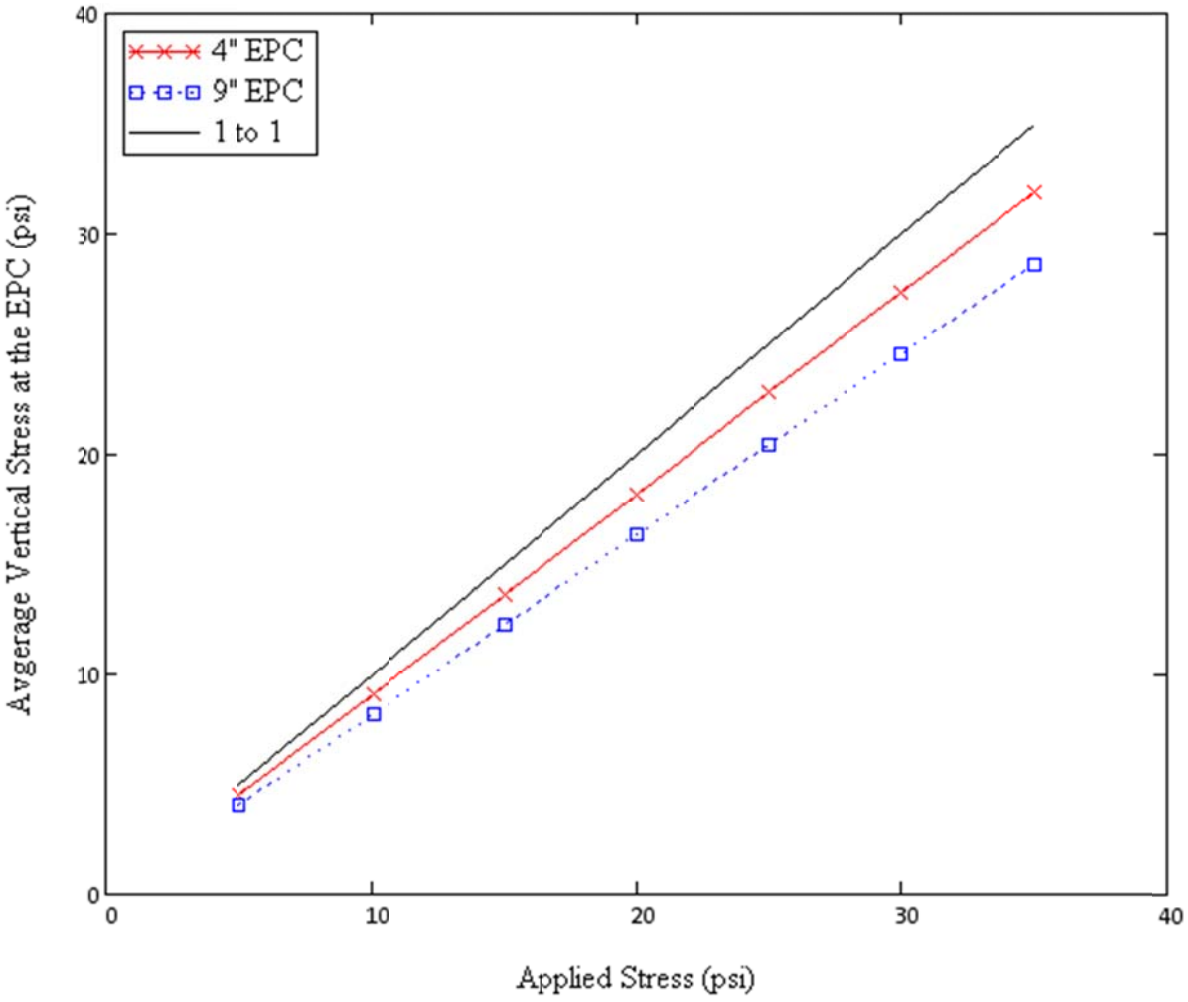

Figure D131: The average vertical stress at the face of the 4 inch and 9 inch EPC as a function of applied stress (Ahlvin & Ulery, 1962)

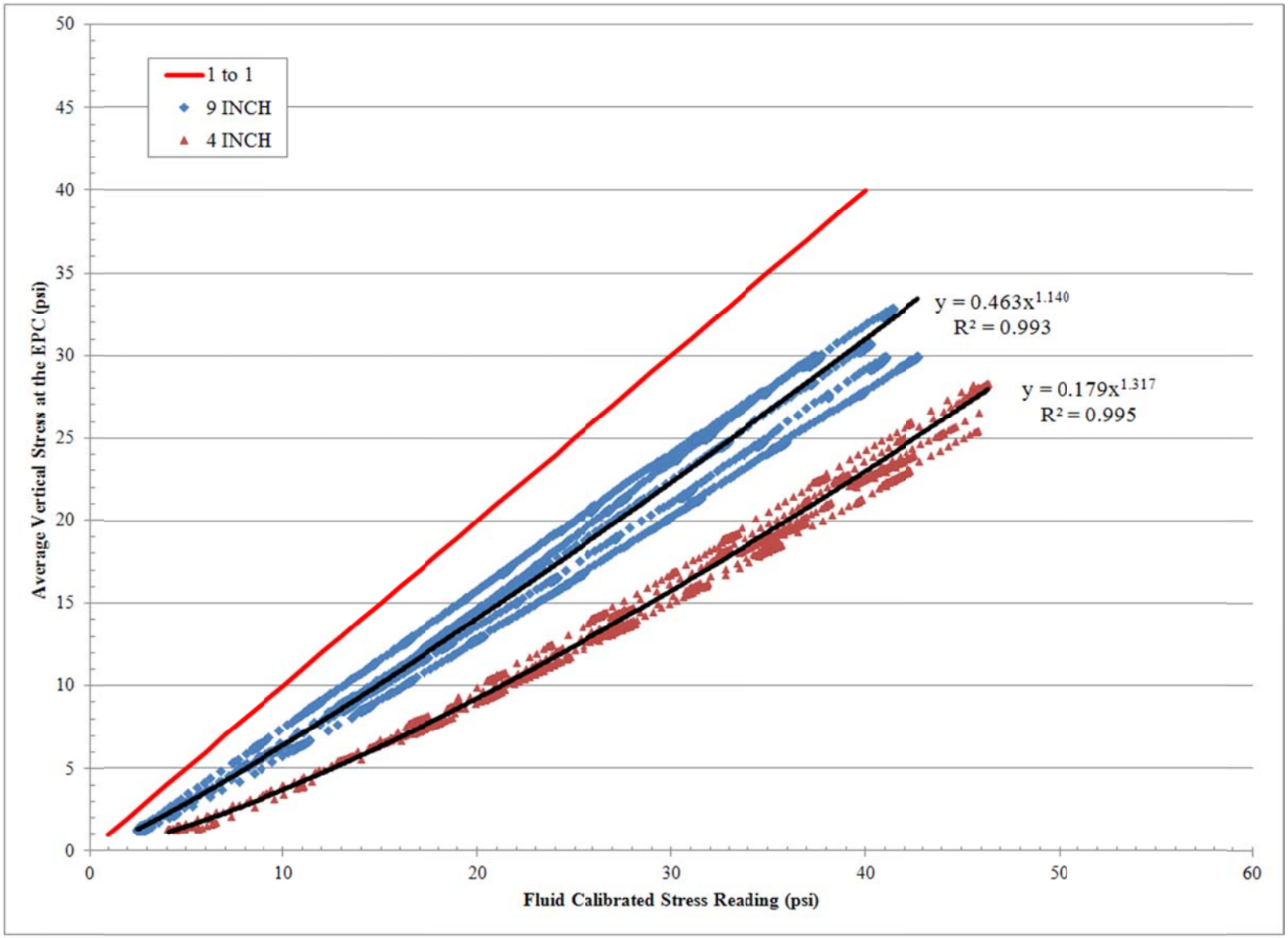

Figure D132: EPC calibration results from lab testing

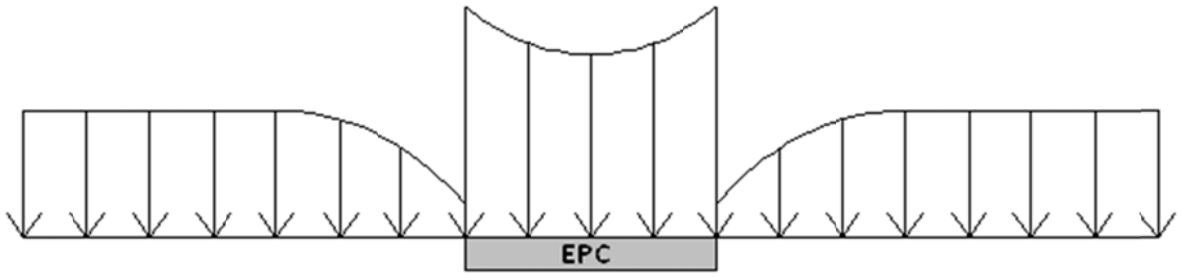

Figure D133: An illustration of passive arching with an earth pressure cell

References:

Ahlvin, R. G., & Ulery, H. H. (1962). Tabulated values for determining the complete pattern of stresses, strains, and deflections beneath a uniform load on a homogeneous half space. *Highway Research Board, Bulletin 342*, 1-13.

Labuz, J. F., & Theroux, B. (2005). Laboratory Calibration of Earth Pressure Cells. *Geotechnical Testing Journal*, 1-9.

Tien, H.-J. (1996). *A Literature Study of the Arching Effect.* Cambridge: Massachusetts Institute of Technology.

APPENDIX E: SOIL MOISTURE SENSOR CALIBRATION

As mentioned previously, the Decagon 10HS Soil Moisture sensors used in the field project measure the dielectric permittivity of the soil using capacitance/frequency domain technology (Decagon Devices, Inc., 2010). Based on the dielectric permittivity the VWC can be determined using a manufacture provided calibration equation. However, different soils have different soil properties (Cobos & Chambers, 2010). Thus, for the most precise results the manufacturer recommends calibrating the sensors in the lab using the soil specific to the project. Following their recommendation, the sensors were calibrated in the lab using the subgrade soil obtained from the field.

To calibrate the sensors a series of standard compactions tests were performed in accordance with Method C of ASTM D698-07. Using the six inch diameter mold, samples at various water contents were placed and compacted in three separate lifts. After the specimens were trimmed and weighted the same blade used in the field (discussed in Chapter 3) was pushed into the center of the sample to create an opening slightly thinner than sensor probes. The probes were then gently inserted into the opening and the subgrade material on top was packed around the black plastic portion of the sensor. Shown in Figure E134 is an image taken of calibration setup.

Figure E134: Soil moisture sensor calibration setup

After the sensor was inserted into the soil, raw data readings were collected for approximately ten minutes. Soil samples were also obtained to determine the volumetric water content (VWC). Shown in Figure E135 are the results from the lab calibration. A trendline was fitted to the lab measured data using a third degree polynomial. Looking at the results, the manufacturer's calibration was actually quite close to the measured water content. Nevertheless, the lab calibration equation was used to convert all raw field data to volumetric water content.

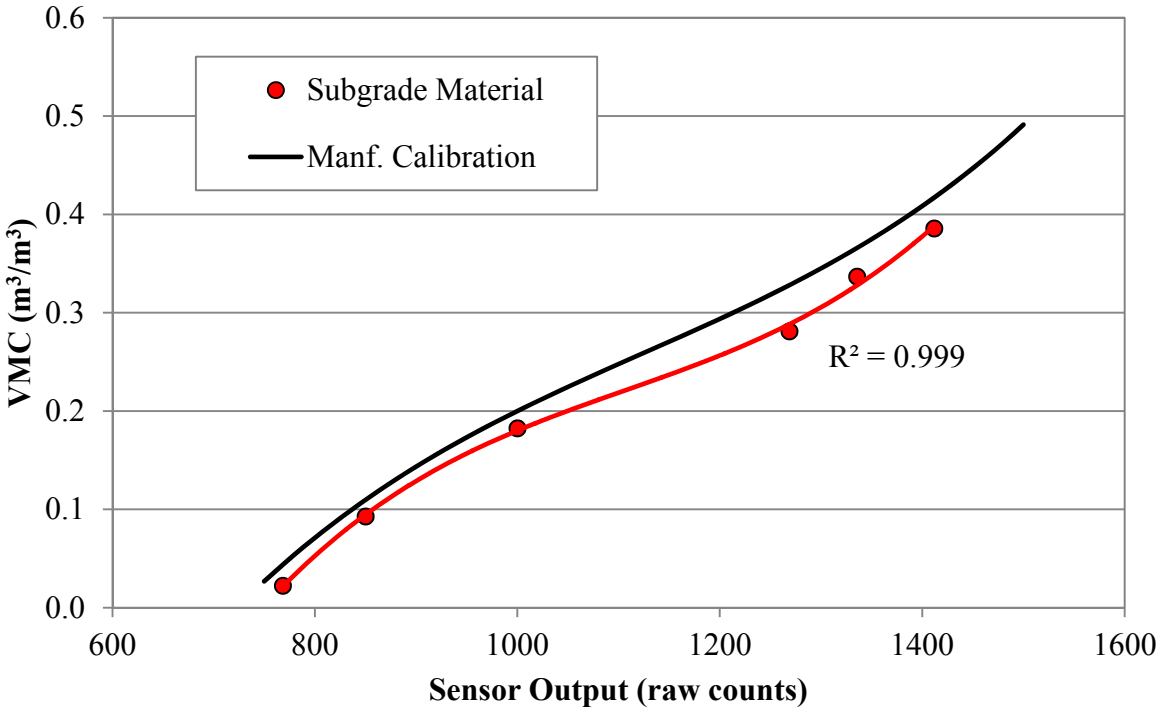

Figure E135: The results from the lab calibration of the soil moisture sensors

References:

ASTM. (2007). *D698-07 Standard Test Methods for Laboratory Compaction Characteristics of Soil Using Standard Effort.* American Society for Testing and Materials.

Cobos, D. R., & Chambers, C. (2010, November 17). *Calibrating ECH2O Soil Moisture Sensors.* Retrieved January 27, 2012, from Decagon Devices: http://www.decagon.com/assets/Uploads/13393-04-CalibratingECH2OSoilMoistureProbes.pdf

Decagon Devices, Inc. (2010). *10HS Soil Moisture Sensor Operator's Manual: Version 3.* Pullman: Decagon Devices, Inc.

APPENDIX F: STATIC PLATE LOAD TESTING SETUP - ERROR ANALYSIS

As mentioned in Chapter 3, the dial gauges used to measure the plate deflection during static plate load (SPL) testing were mounted to a beam with two supports located approximately 18 inches away from the center of the beam. At the time of testing no one on site recognized that the deflection beam supports were possibly located within the load-induced displacement area (see Figure F136). According to ASTM D1195, the supports should be located at least eight feet from the circumference of the bearing plate. With this in mind, it was unknown if the measured deflections are accurate. As a result, a numerical analysis was performed to determine what effect the proximity of the supports to the loaded plate would have on the SPL base layer modulus (E_{SPL}).

To encompass the range of base layer material properties measured in the field; three separate analyses were conducted using a base layer modulus "E_1" of 10, 20, and 30 ksi. Also, to obtain a conservative estimate of the potential deflection at the reference supports, a base/subgrade modulus ratio "E_1/E_2" of 5 was held constant throughout the three analyses. This was based on DCP data that estimated a modulus ratio between two and five throughout the test pad (see Chapter 4). Finally, to remain conservative an eight inch base layer thickness was assigned in all three analyses to estimate the maximum potential deflection that should be expected at the reference supports. Static loading was applied in the form of a 12 inch diameter loaded area at stresses of 20, 40, 60, and 80 psi to incorporate the range of stresses applied in the field.

The surface deflections measured from the numerical analysis are presented in Figure F137 as a function of radial distance from the center of loaded area. Also denoted in the figure is the approximate location of the reference beam supports which were estimated to be 18 inches away from the center of the loaded plate. As expected, the amount of surface deflection decreases as the base course (and subgrade modulus) increases.

After running the numerical analysis the surface deflection at the beam supports were then plotted as a function of applied load in Figure F138. Note that for the set conditions there is a linear correlation between applied stress and surface deflection at the supports. As a result, a linear trendline was fit to the data in order to estimate the deflection at the beam supports for any magnitude of load within the range of applied stresses. Using the equations obtained from the trend lines, the calculated surface deflection at the beam support "$\delta_{support}$" was added to the measured deflection "$\delta_{measured}$" to estimate the actual deflection of the plate "δ_{actual}".

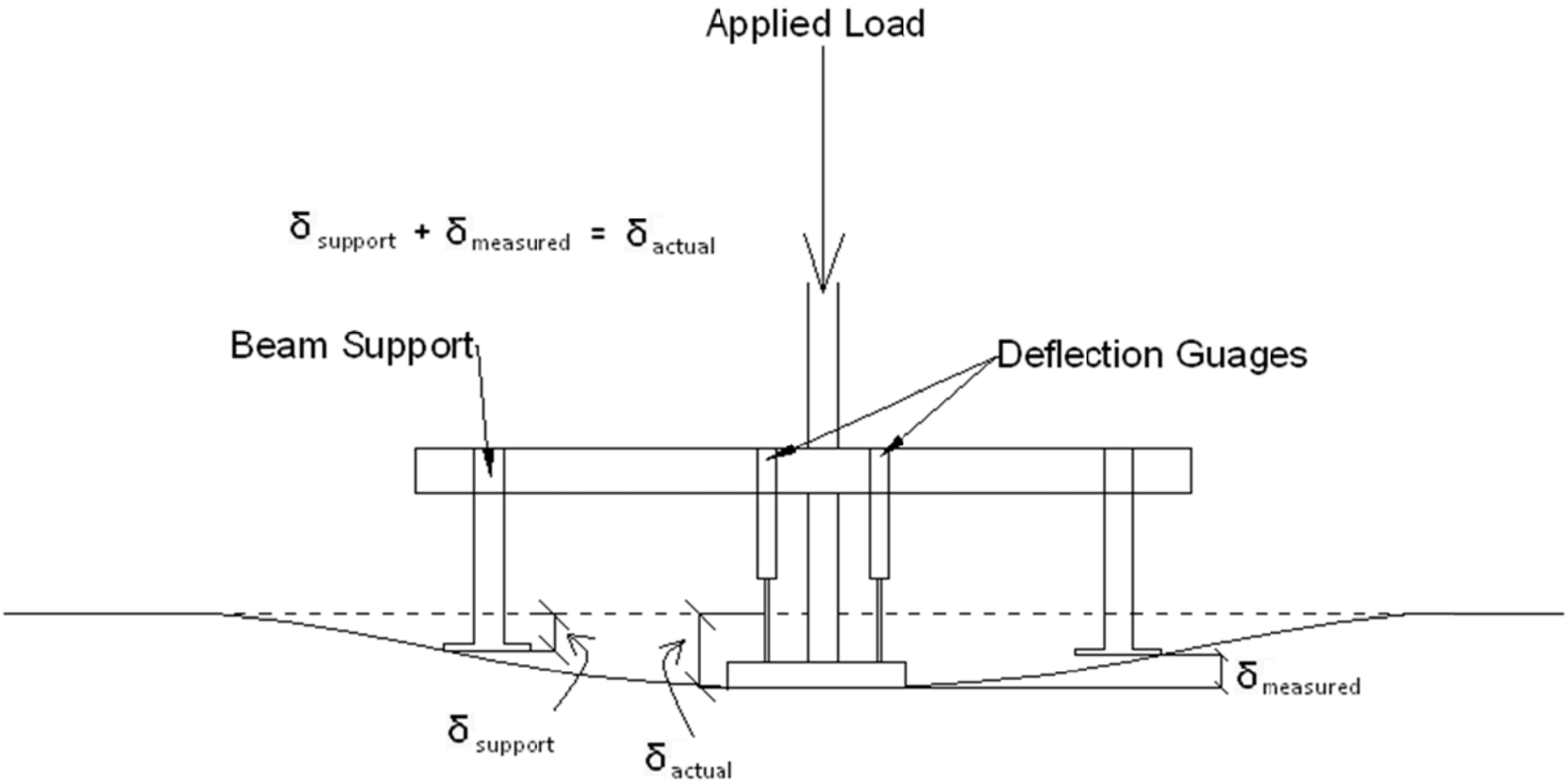

Figure F136: Sketch of the possible surface deflection scenario during SPL testing

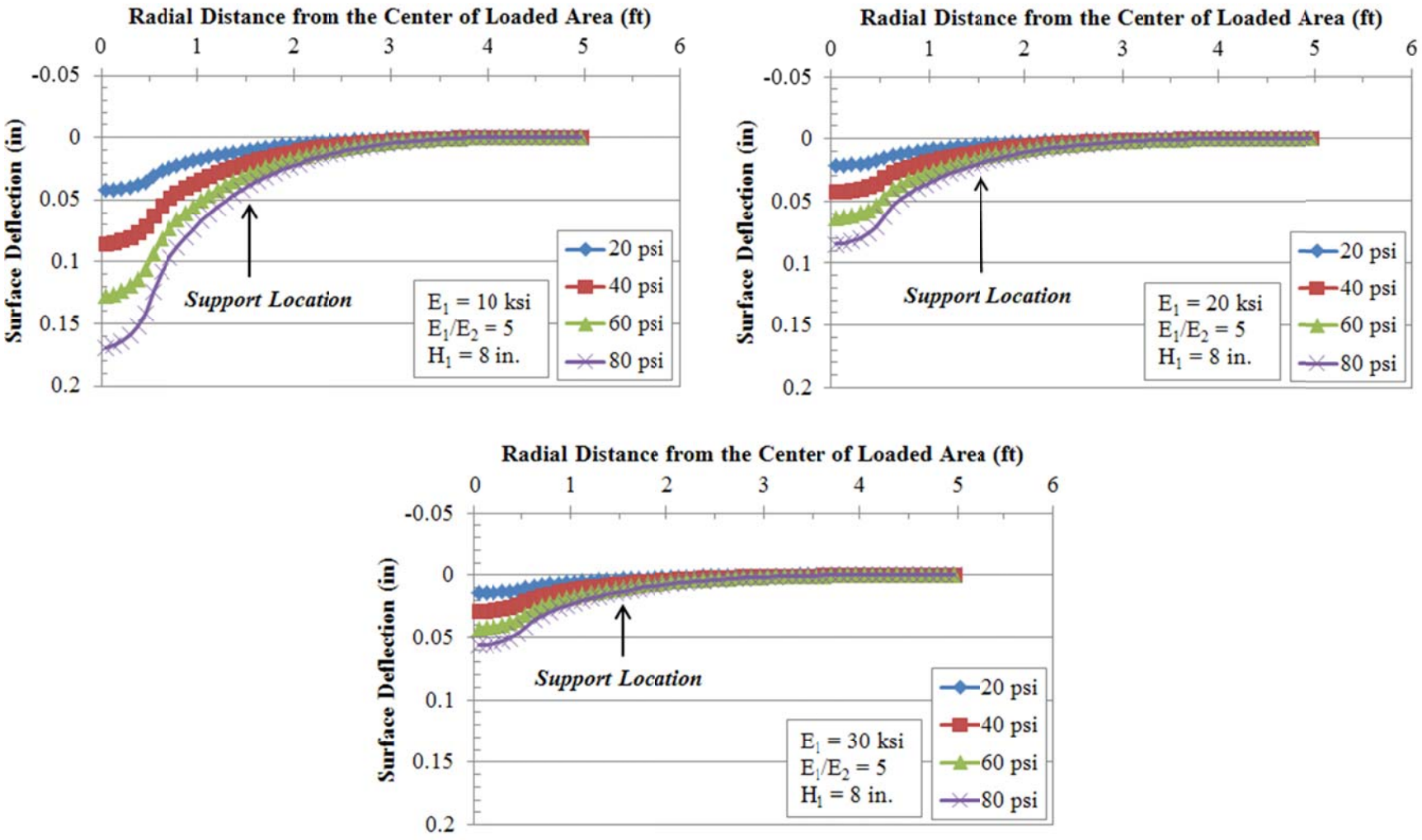

Figure F137: Surface deflection versus lateral distance away from the center of the loaded area

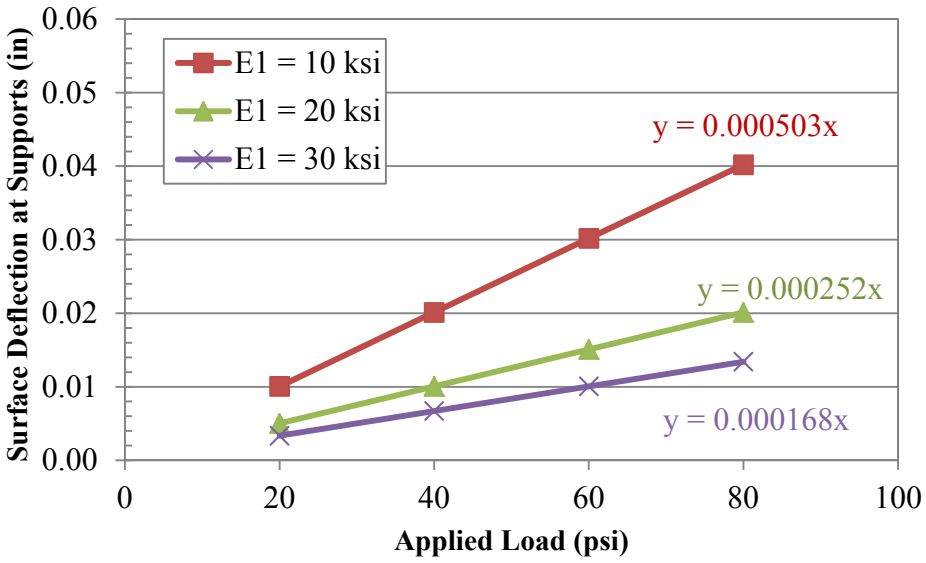

Figure F138: Surface deflection at the beam supports as a function of applied load

Once the "actual" deflections had been estimated an analysis was then performed to calculate the modulus of the base layer material using: 1) the measured deflection; 2) the "actual" deflection assuming E_1 = 30 ksi; 3) the "actual" deflection assuming E_1 = 20 ksi; and 4) the "actual" deflection assuming E_1 = 10 ksi. To determine the base layer modulus two separate methods had to be employed. In Test Section 1 the depth of influence was less than the base layer thickness. As a result, it could be treated as a single layer using the following elastic equation recommended by the NCDOT:

$$E_{SPL} = \frac{2aq(1-\nu^2)}{\delta} \qquad \textbf{Eq. F20}$$

Where:

E_{SPL} = Base layer modulus

a = radius of the plate

q = Applied stress

ν = Poisson's Ratio (assumed .35 for both layers)

δ = Plate deflection

In Tests Sections 2, 3, and 4 the depth of influence extended into the subgrade requiring a multi-layered analysis. This was performed using Burmister's two-layer elastic solution shown below:

$$E_{SPL} = \frac{2aq(1-\nu^2)I_p}{\delta} \times \left(\frac{E_1}{E_2}\right) \quad \textbf{Eq. F21}$$

Where:

I_P = Deflection factor obtained from design chart of Thenn de Barros (1966)

E_1/E_2 = base/subgrade modulus ratio

The calculated base layer modulus results are shown in Figure F139. Looking at the results it is evident that by incorporating the deflection at the beam supports there is a considerable decrease in the estimated base layer modulus. To quantify the decrease relative to the base modulus when neglecting the deflection of the supports, the percent error is presented in Figure F140. When assuming E_1 = 30 ksi there is a percent error of approximately 20 to 40 %. For E_1=20 ksi the percent error is between 30 to 50 % and when assuming E_1=10 ksi there is a percent error on the order of 50 to 65%. Based on these results, the possible error was considered too great to justify using the results as a measure of in situ modulus. Thus, the data from SPL testing is not presented is this report.

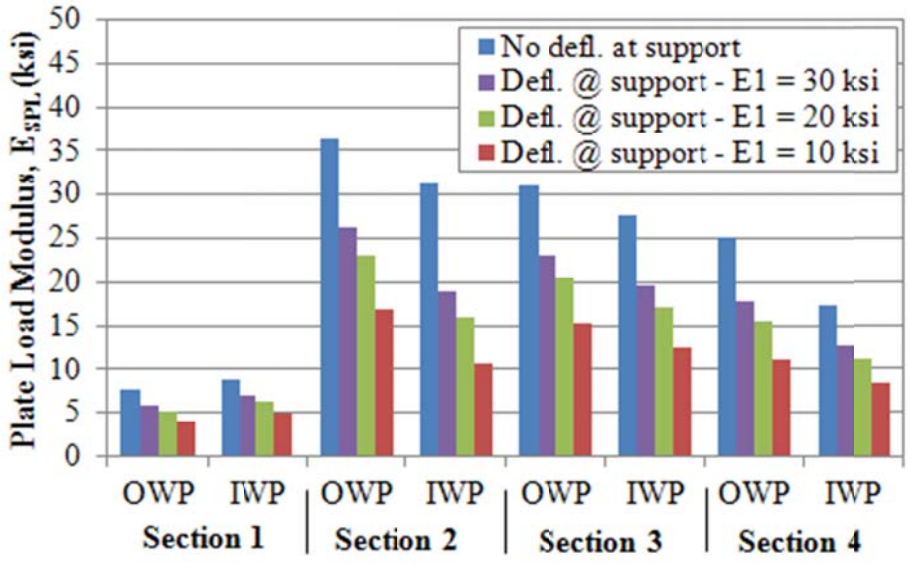

Figure F139: Base layer modulus when not accounting for and when accounting for the deflection at the beam supports

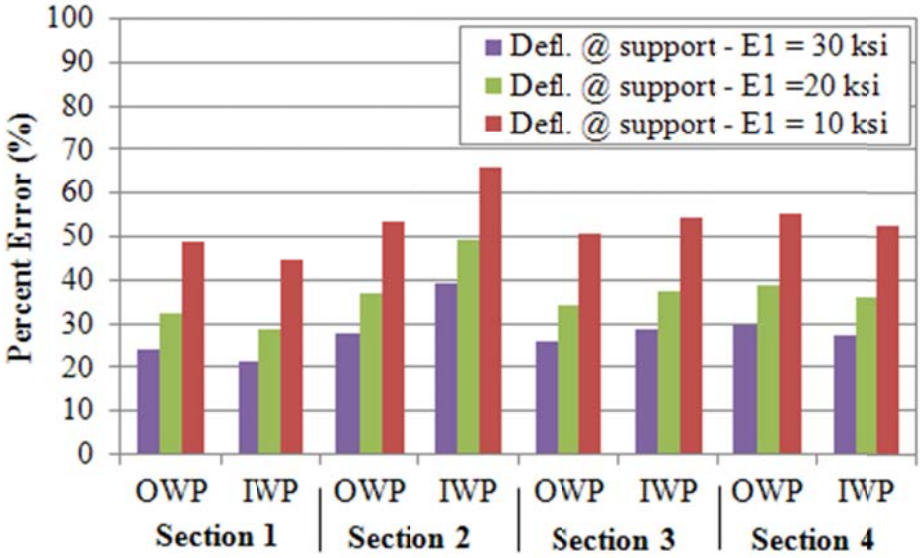

Figure F140: Percent error in the calculated base layer modulus

APPENDIX G: DUMP TRUCK CONFIGURATION AND DIMENSIONS

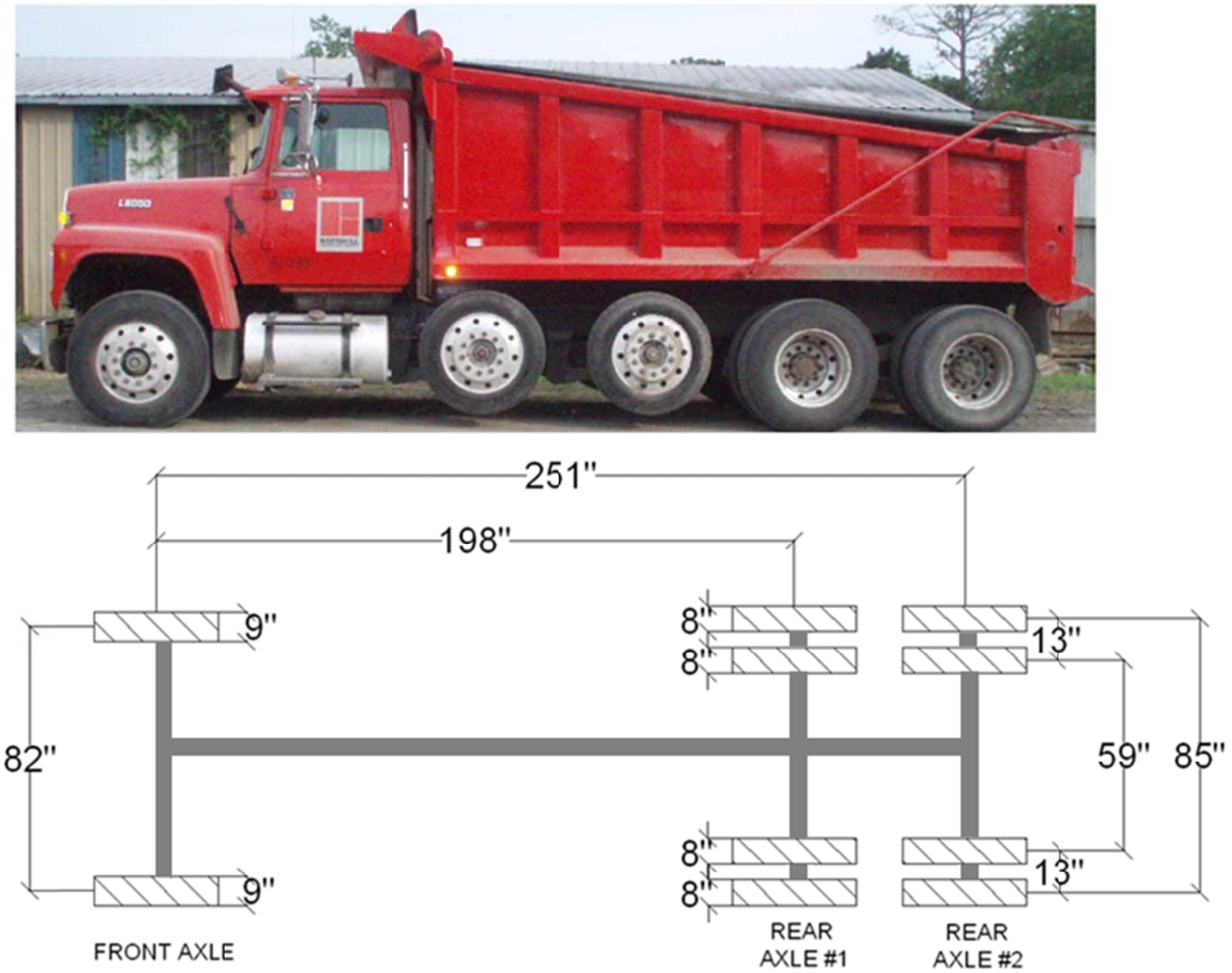

Figure G141: Dump truck configuration and dimensions

APPENDIX H: EPC TEST RESULTS FOR BACK AXLE TWO

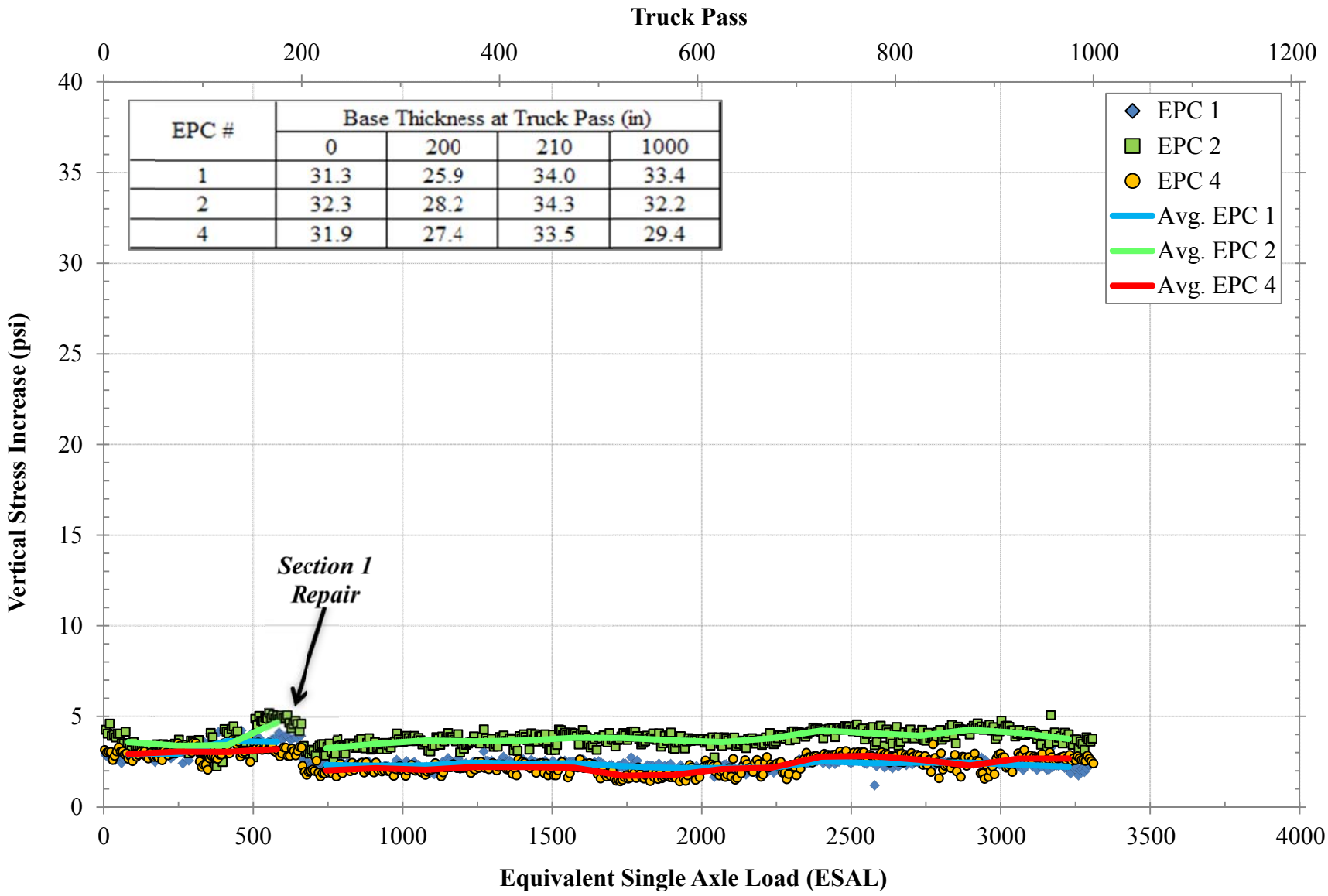

EPC #	Base Thickness at Truck Pass (in)			
	0	200	210	1000
1	31.3	25.9	34.0	33.4
2	32.3	28.2	34.3	32.2
4	31.9	27.4	33.5	29.4

Figure H142: Vertical stress increase three inches below the base/subgrade interface for Test Section

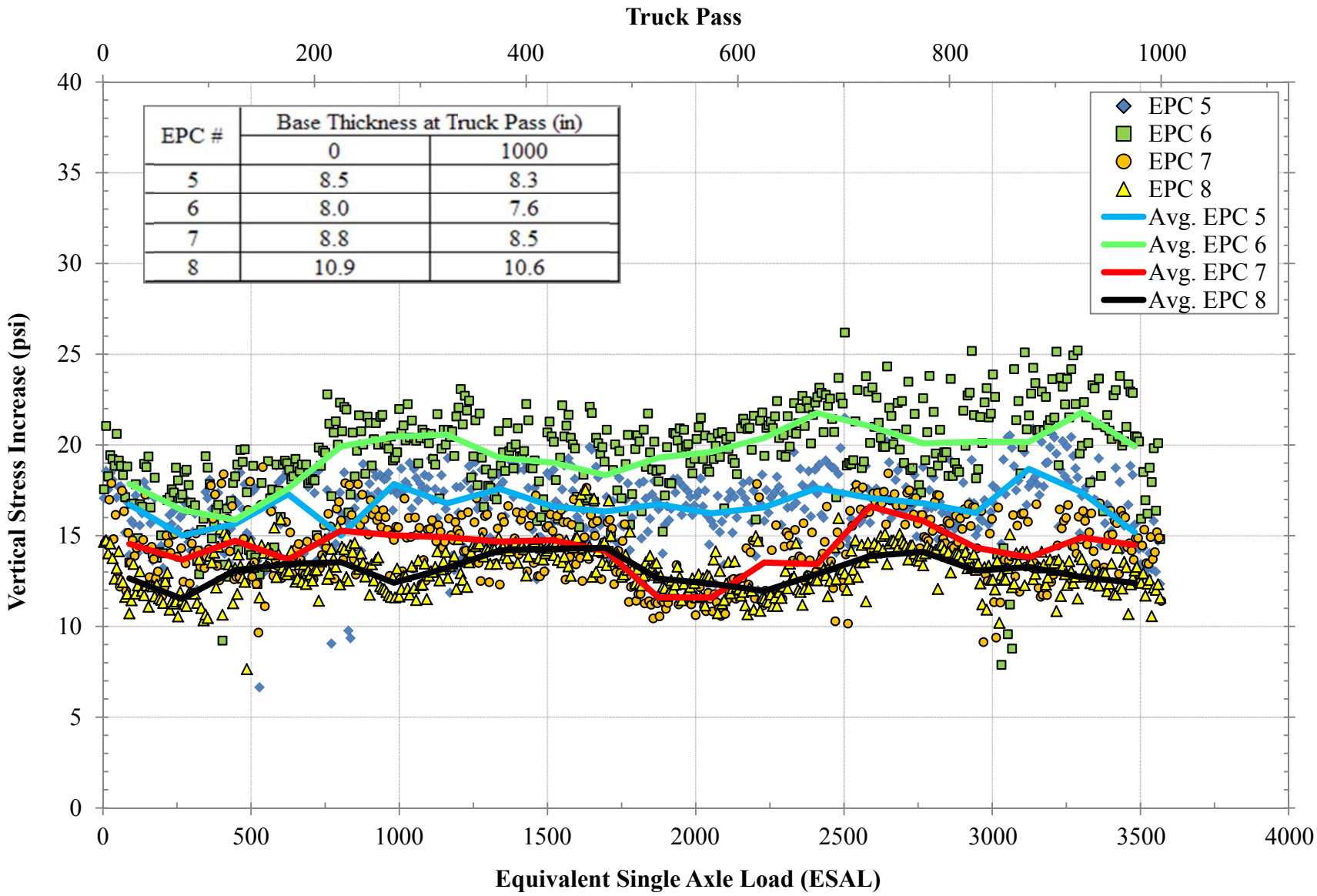

EPC #	Base Thickness at Truck Pass (in)	
	0	1000
5	8.5	8.3
6	8.0	7.6
7	8.8	8.5
8	10.9	10.6

Figure H143: Vertical stress increase three inches below the base/subgrade interface for Test Section 2

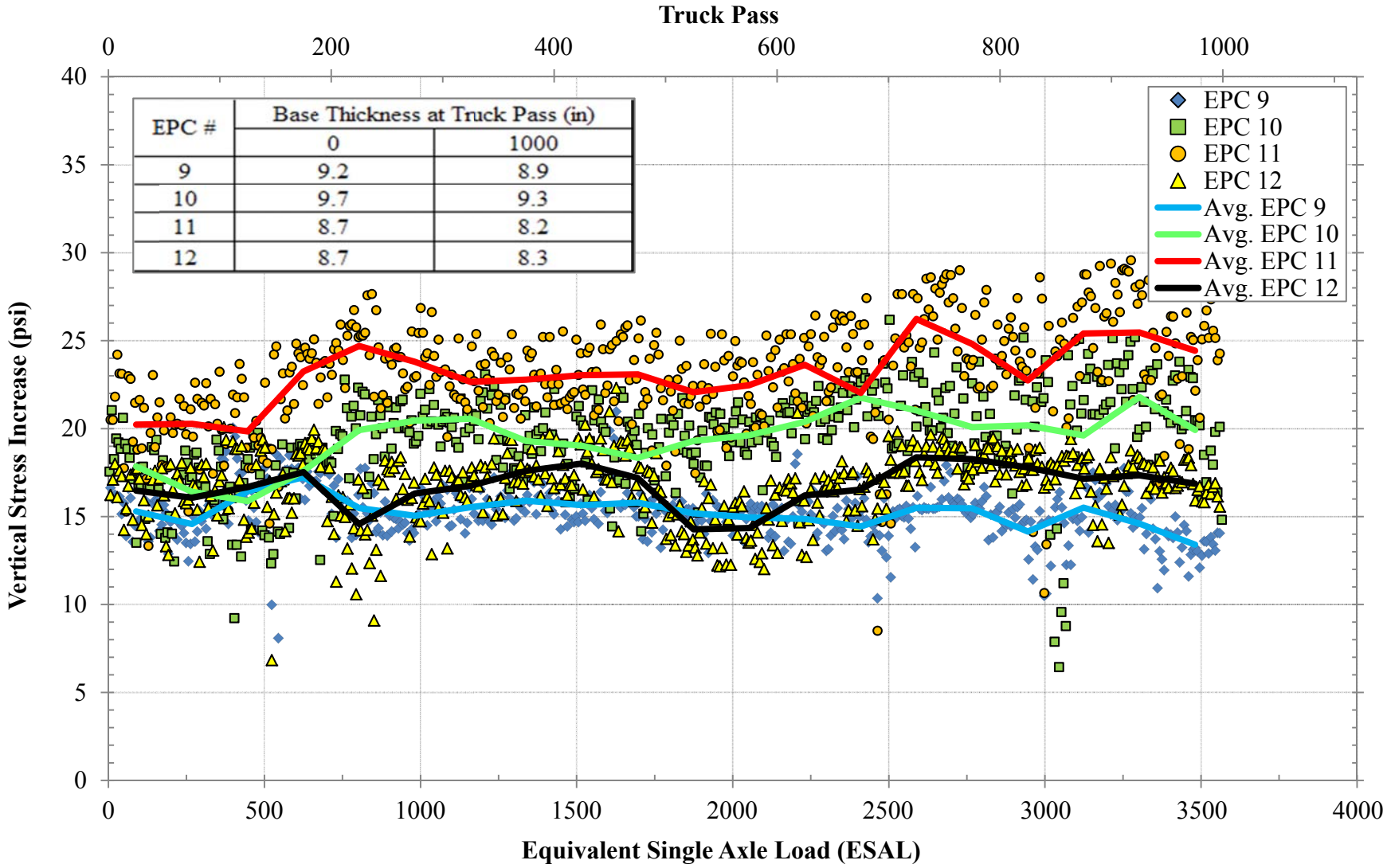

EPC #	Base Thickness at Truck Pass (in)	
	0	1000
9	9.2	8.9
10	9.7	9.3
11	8.7	8.2
12	8.7	8.3

Figure H144: Vertical stress increase three inches below the base/subgrade interface for Test Section 3

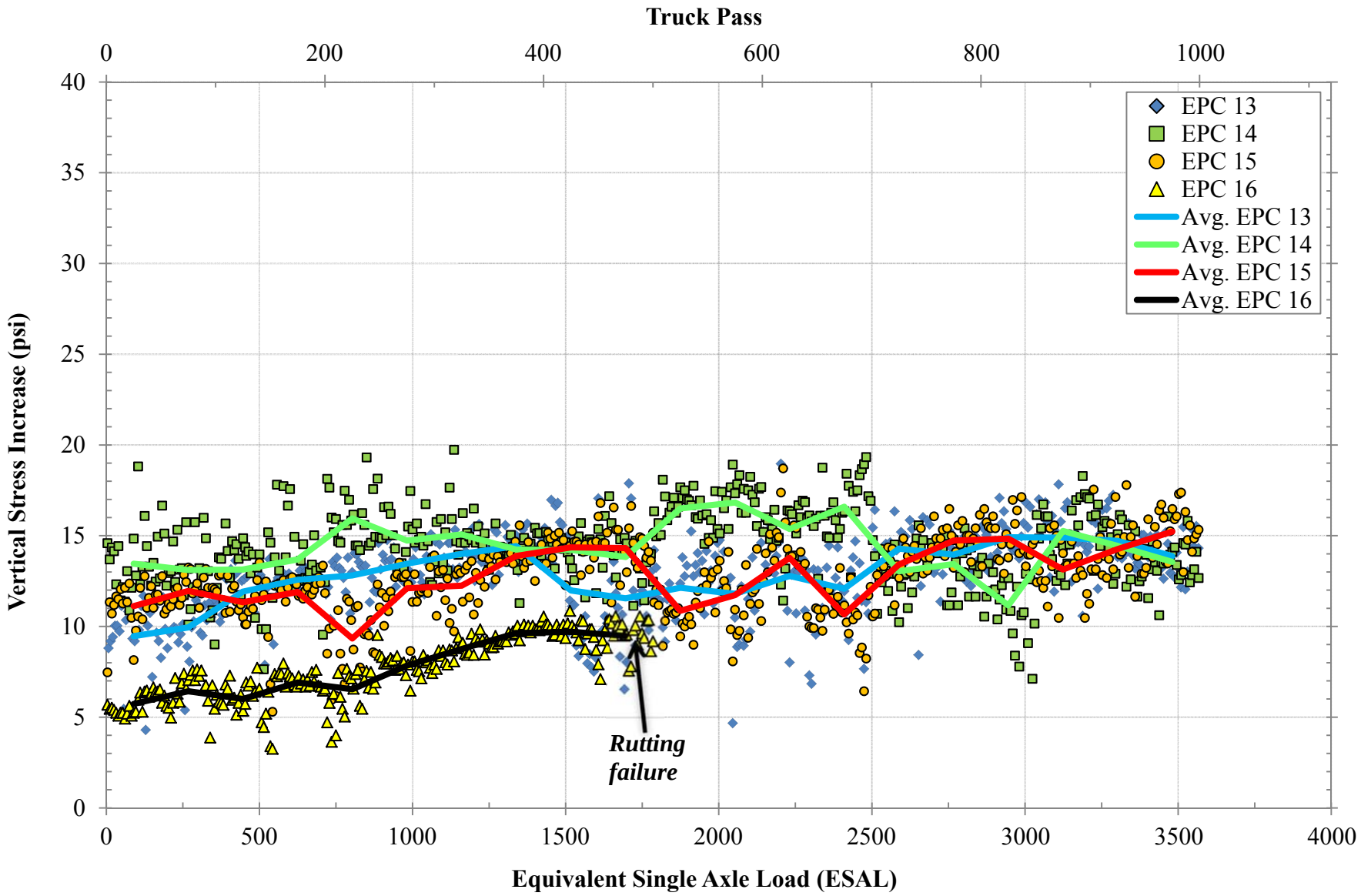

Figure H145: Vertical stress increase six inches below the base/subgrade interface for Test Section 4